UNIVERSITY OF OKLAHOMA

GRADUATE COLLEGE

MOLYBDENUM(VI) BIS(AMIDATE) COMPLEXES FOR GROUP TRANSFER REACTIONS AND CATALYSIS

A DISSERTATION

SUBMITTED TO THE GRADUATE FACULTY

in partial fulfillment of the requirements for the

Degree of

DOCTOR OF PHILOSOPHY

By

JOSHUA MILES SMITH
Norman, Oklahoma
2019

MOLYBDENUM(VI) BIS(AMIDATE) COMPLEXES FOR GROUP TRANSFER REACTIONS AND CATALYSIS

A DISSERTATION APPROVED FOR THE
DEPARTMENT OF CHEMISTRY AND BIOCHEMISTRY

BY

Dr. Robert Thomson, Advisor

Dr. Daniel Glatzhofer, Chair

Dr. Michael Ashby

Dr. Wai Tak Yip

Dr. Ian Sellers

Acknowledgements

First, I would like to thank my high school chemistry teacher Mrs. Smith, for making chemistry seem so simple. I never thought I would be pursuing a Ph.D. in chemistry 10 years later, but here I am and she was the one that started it all. Even more importantly, I would like to thank my undergraduate mentor, Dr. Dwight Myers. I was fortunate enough to work with Dr. Myers for four years at East Central University, making superconductors, playing with liquid N_2, and melting metals in a microwave (literally my senior thesis). Without Dr. Myers' inspiration I would never have given graduate school a second thought, and for that I'll always be grateful.

Secondly, I would like to thank Dr. Thomson for opening my eyes to the vastness of chemistry. I couldn't have asked for a better scientist to help me sharpen my understanding of metal chemistry than Dr. Thomson. Coming into graduate school, I had never heard of organometallic synthesis or Schlenk lines and had never touched a glovebox or worked with anything more dangerous than a strong acid. Rob showed me the ropes my first week and made sure I knew what I was doing. Throughout my time at the University of Oklahoma, Rob has pushed me to be a better scientist, while also allowing me to be creative, which has kept research fresh and exciting.

I want to thank the support I have received from the Chemistry Department as a whole, Dr. Glatzhofer and Dr. Ashby advice and guidance over the years, Dr. Yip and Dr. Halterman, for making sure I was taken care of, and a major thanks to Dr. Susan Nimmo (NMR), Dr. Doug Powell (XRD), and Dr. Steven Foster (MS), for teaching me so much over the years!

Finally, I would like to thank my friends and family. My parents (Mike and Crystal) and siblings (Felicia, Sean, and Jen) have been so supportive since I started college and I can't thank them enough. Especially my dad, for always being there for me and giving me the advice I needed (even when I don't know I need it). I'm very lucky to have such a supportive family. I've made so many great friends over these few years, Sammie, Nate, Curt, Matt, Christopher…just to name a few, and I never would have made it this far without them!

Table of Contents

List of Tables

List of Figures

Abbreviations

ATR	Attenuated Total Reflectance
Bn	Benzyl
DCE	Dichloroethane
DCM	Dichloromethane
DFT	Density Functional Theory
DIPP	2,6-diisopropylphenyl
DME	Dimethoxyethane
DMP	2,6-dimethylphenyl
DMS	Dimethyl Sulfide
DMSO	Dimethyl Sulfoxide
DMSOR	Dimethyl Sulfoxide Reductase
DODH	Deoxydehydration
EI	Electron Impact
Et_2O	Diethyl Ether
FeMoco	Nitrogenase Iron-Molybdenum Cofactor
FTIR	Fourier-Transform Infrared
GC	Gas Chromatography
HOMO	Highest Occupied Molecular Orbital
IR	Infrared
LDA	Lithium Dimethylamide
LUMO	Lowest Unoccupied Molecular Orbital
^{m}DMP	3,5-dimethylphenyl
Me	Methyl
Mes*	2,4,6-tri-*tert*-butylphenyl
MS	Mass Spectrometry
NMR	Nuclear Magnetic Resonance
OAT	Oxygen Atom Transfer
^{o}DMP	2,6-dimethylphenyl
$OPMe_3$	Trimethylphosphine Oxide
OSCER	OU Supercomputing for Education and Research
PFP	Perfluorophenyl
Ph	Phenyl
PMe_3	Trimethylphosphine
ROMP	Ring-Opening Metathesis Polymerization
TBHP	*tert*-butylhydrogenperoxide
^{t}Bu	*tert*-butyl
THF	Tetrahydrofuran
XRD	X-Ray Diffraction

Abstract

Molybdenum complexes bearing bidentate amidate ligands have been synthesized and characterized using nuclear magnetic resonance spectroscopy (NMR), infrared spectroscopy (FTIR), and in most cases, single crystal X-ray diffraction (XRD). Three classes of bis(amidate) complexes are presented herein; dioxo, oxo/imido, and bis(imido) species. The tight bite-angle of the amidate ligand generates Mo complexes that exhibit distorted octahedral geometries. Density functional theory (DFT) calculations were employed to investigate the potential for isomerization and hemilability of the amidate ligand. A feature of the amidate complexes bearing imido groups, is a general *trans*-influence on the amidate ligand. This manifests as long Mo-O bonds for the amidate *trans* to the imido fragment in the case of the oxo/imido class. Hemilability is observed structurally with the $[^{tBu}NO^{tBu}]_2MoON^tBu$-THF complex **3.9**. These complexes were utilized for various group transfer reactions. The dioxo class exhibits catalytic activity in oxygen atom transfer and epoxidation of various alkenes. The oxo/imido class demonstrates oxygen atom transfer capability, as well as catalytic epoxidation of *cis*-cyclooctene. The bis(imido) class enables some activity toward the cross metathesis of imines. Future directions of this work includes expansion of the amidate ligand set to alternative electron-withdrawing ligands, incorporation of sulfur to make thioamidate ligands, synthesis of new Mo-element multiple bonds via group transfer reactions, expansion of the reaction scope for epoxidation and imine metathesis, and the full investigation into deoxydehydration reactions of the Mo-oxo complexes.

Chapter 1: Introduction

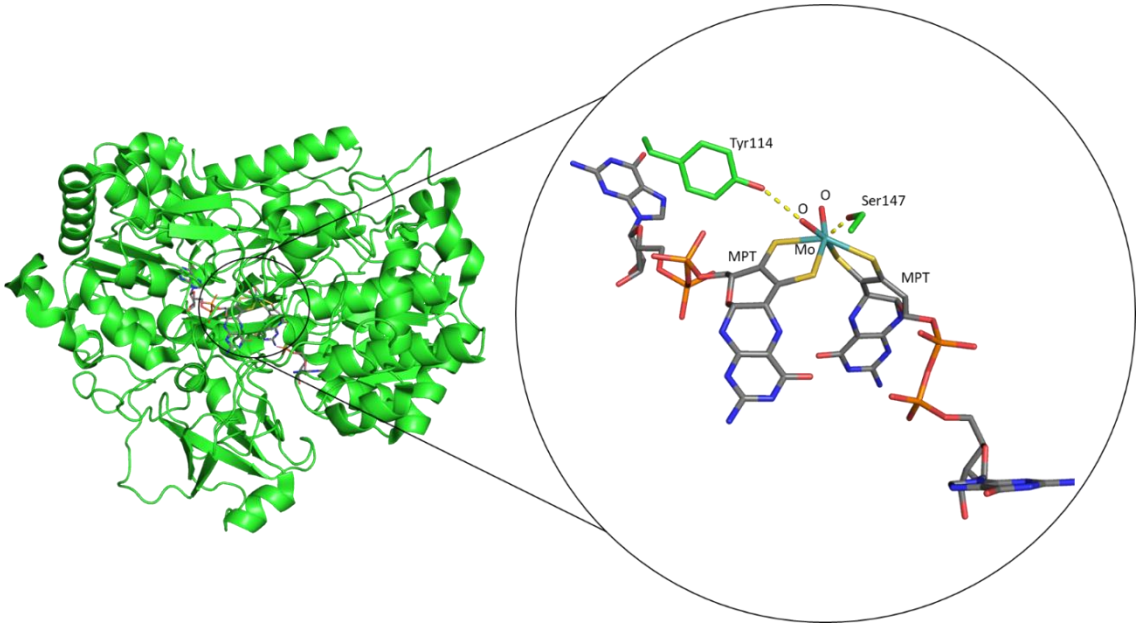

Figure 1.1 The structure of dimethyl sulfoxide reductase (DMSOR) from *Rhodobacter capsulatus* (PDB id: 1E5V).[1]

1.1 Chemistry Inspired by Nature

Nature has been using chemistry since the beginning of the universe. The success of life in all areas on Earth, including even the harshest environments on the planet, is owed to the ability of transition metals to move atoms around, providing the energy needed for life.[2] Nature has been using complex organometallic chemistry for millennia, so it is only logical for us learn from what nature has discovered. Not only is metal chemistry important for the health of organisms, but the overall health of the environment as well.[2]

For example, dimethyl sulfoxide (DMSO) in the ocean serves as an oxygen (ultimately energy) source for phytobacteria.[2-3] This phytobacteria converts the DMSO to dimethyl sulfide (DMS) using enzymes to remove the oxygen atom, which is then used in anaerobic respiration.[2-3] The DMS is then slowly pulled into the atmosphere around large plumes of these bacteria, which serves to seed clouds over the ocean.[2-3] The clouds formed from this process help to cover the ocean often shielding reefs from bleaching, since the bacteria are often found in large reefs.[2-3] Furthermore, the increase of DMS in the atmosphere attracts birds to the area, where they eat the bacteria affecting bird migration patterns.[2-3] It is remarkable that all of these large-scale effects are due to a simple oxygen atom transfer (OAT) reaction that occurs at a molybdoenzyme, DMSO reductase (DMSOR; Figure 1.1).[2-3]

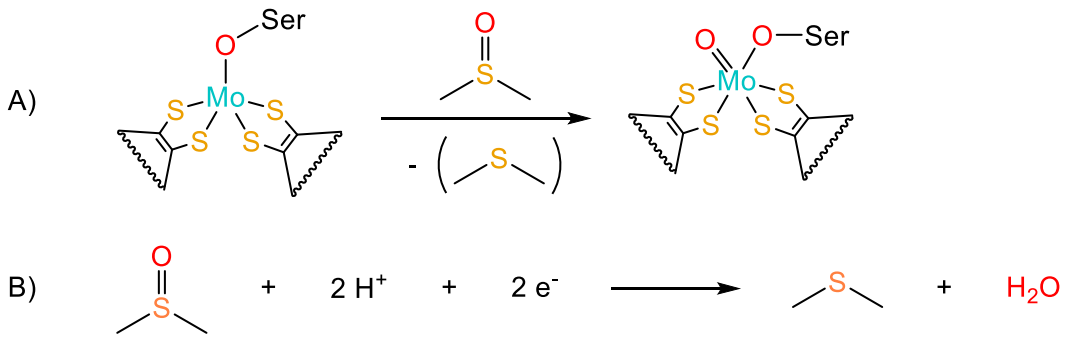

Scheme 1.1 (A) Reduction of dimethylsulfoxide by DMSOR and (B) the net reaction.

The OAT reaction that DMSOR performs is a simple oxygen abstraction and concomitant oxidation of a secondary substrate, as shown in Scheme 1.1. The concept that we are interested in harnessing is the controlled transfer of atoms to substrates using appropriate metal complexes. An industrial example of this is the epoxidation of

propylene. Propylene is epoxidized to generate propylene oxide on the scale of over 8 million tons per year.[4] This is a highly important reaction as propylene oxide is used to make polyols which can be polymerized into polyurethane polymers for various applications, such as sponges and paint products.[4] A leading industrial method for the production of the propylene oxide uses a heterogeneous molybdenum salt as the catalyst.[4] The epoxidation of other alkenes has been demonstrated by many Mo complexes that are functional analogues to the DMSO reductase active site.[5]

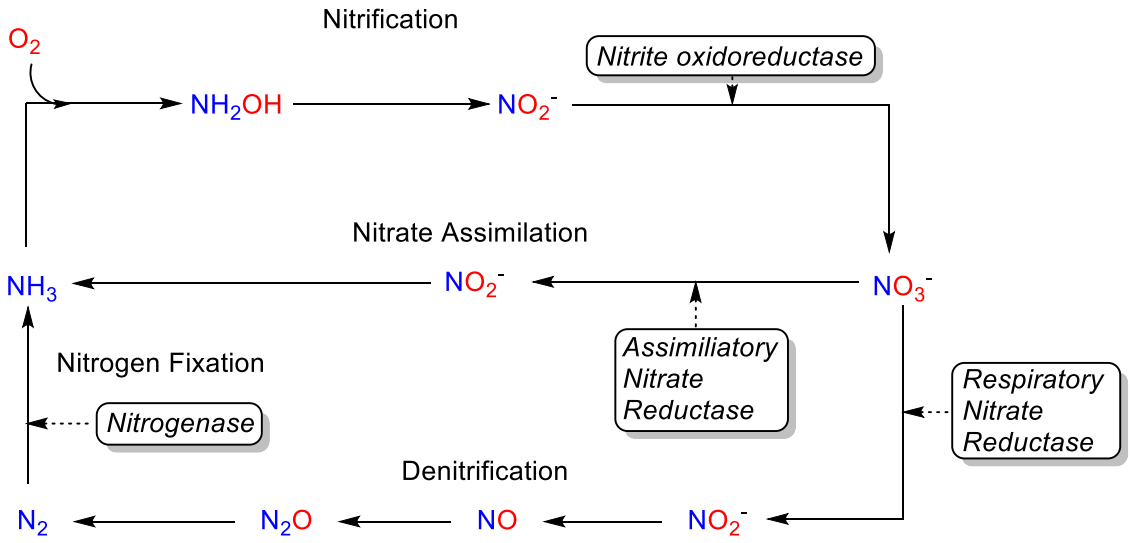

Figure 1.2 Simplified depiction of the global nitrogen cycle showing the application of Mo-containing enzymes in nature.

Molybdenum is found in nature at the active sites of over 30 distinct enzymes, and found in low abundance throughout every living organism.[6-10] These enzymes are responsible for the growth and health of organisms, and cycling carbon, nitrogen, and sulfur in the atmosphere. In the global nitrogen cycle, molybdenum's role in the iron-molybdenum cofactor (FeMoco) found in nitrogenase enzymes that fix N_2 to NH_3,

has been extensively studied.[11-13] However, molybdenum also plays a role in many other steps of the nitrogen cycle, and is found in the nitrite oxidoreductase, respiratory nitrate reductase, and assimilatory nitrate reductase enzymes (Figure 1.2). Molybdenum-containing enzymes are also key parts of almost every step of the inorganic sulfur cycle. [6-10, 14] As mentioned earlier, DMSOR enzymes catalyze the reduction of DMSO to DMS, a key step in the inorganic sulfur cycle.[13]

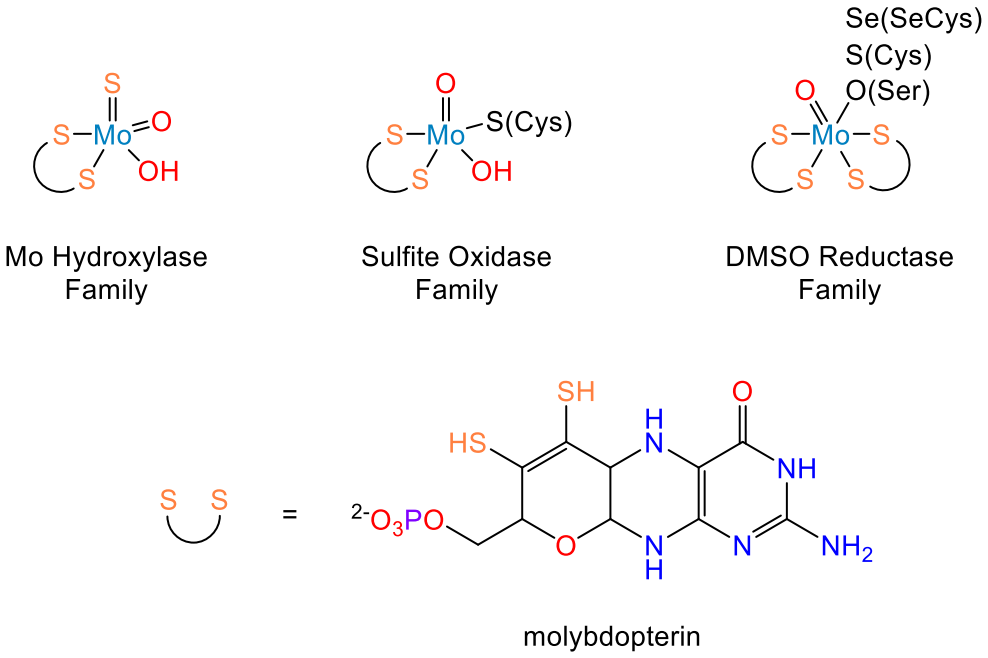

Figure 1.3 Active site structure of the three major families of Mo-containing enzymes and the molybdopterin cofactor.

The versatility of molybdenum is interesting, but what is even more important is that all the active sites of these seemingly different enzyme families are remarkably similar.[6, 15] There are three families of molybdenum-containing enzymes: molybdenum hydroxylase, DMSOR, and sulfite oxidase, as seen in Figure 1.3.[2-3, 8, 15-16] All Mo containing enzymes, other than FeMoco, have at least one molybdopterin ligand bound

bidentate to the metal center.[2-3, 8, 14-16] Also, there are one or two doubly bound chalcogens to the Mo-center of these enzymes.[2-3, 8, 14-16]

Considering the structure of the active sites of molybdoenzymes featuring a bidentate chelating ligand molybdopterin, it is not surprising that much of the investigation into mimicking the enzyme reactivity has focused on bidentate dithiolene type ligands.[13-15] These dithiolene complexes are great structural analogues to the DMSOR active site.[17] The dithiolene ligands have been studied on transition metals since the 1960s and have presented as "non-innocent" ligands exhibiting redox chemistry, valence tautomerization, and geometric isomerization as shown in Figure 1.4.[17-19] Consequently, to our knowledge complexes bearing dithiolene ligands have not exhibited activity in the epoxidation reaction of alkenes.

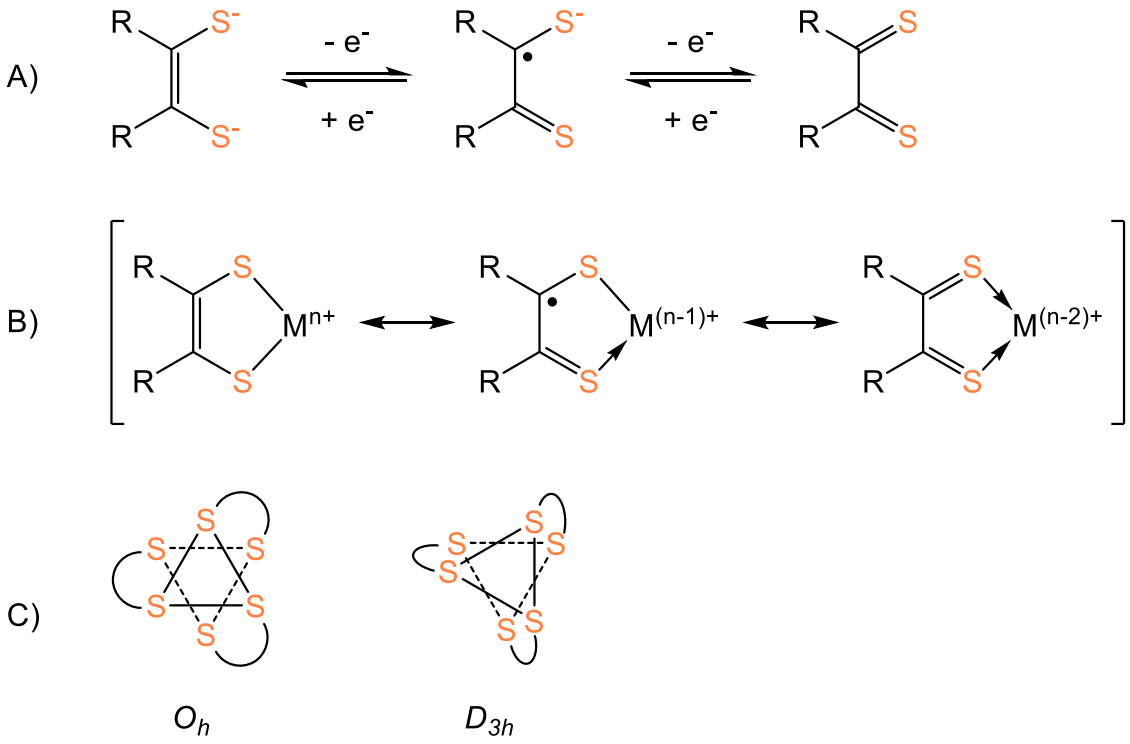

Figure 1.4 (A) Redox chemistry of dithiolenes, (B) valence tautomerization of dithiolene metal complexes, and (C) geometric isomers of tris(dithiolene) complexes.

1.2 Molybdenum and Catalysis

In addition to dithiolene complexes, researchers have made several non-dithiolene contributions to the area of Mo dioxo complexes that react analogously to DMSOR.[20-24] Generally, complexes that are active in OAT reactions are also active for epoxidation processes.[20-24] Theoretical investigations have found that a key intermediate in the DMSOR mechanism is approximately trigonal-prismatic.[25] Only a handful of $[MoO_2]^{2+}$ complexes have been synthesized that distort the metal center significantly enough to approach trigonal-prismatic geometry.[26-27] While reduction of DMSO to DMS isn't of major importance to industry, the ability of complexes, featuring $[MoO_2]^{2+}$ cores, to perform epoxidation reactions is of great significance, and epoxidation of a number of alkenes is performed on an industrial-scale by Mo dioxo species.[28-29] Several complexes have been made to study the oxo transfer reaction of DMSO to DMS. Many of these complexes utilize bidentate and tridentate N,O chelating ligands.[22-23, 30-36]

Transition metals have advantageous properties that allow for reactivity not observed for nearly any other elements on the periodic table. The *d*-orbitals allow for expanded coordination and the multiple oxidation states available to the metals allow for interaction with many different types of molecules and bonds. The *d*-orbitals in the middle of the transitions metal block often have vacancies allowing for various π-bond interactions. These interactions, whether it be back donation into ligand orbitals or π-electron donation from the ligand into empty *d*-orbitals, can have a drastic effect on the electronics of the metal and surrounding ligands.

Molybdenum, a Group 6 transition metal, is stable in many oxidation states from II to VI making it optimum for redox reactions, and it can accommodate coordination numbers ranging from 4 to 8.[10] This versatility is illustrated by the breadth of chemistry already demonstrated by natural molybdoenzymes and synthetic molybdenum complexes.

Molybdenum compounds are used in industrial catalysis, for example, in alkene metathesis and epoxidation.[37] These reactions generate value-added feedstock chemicals on the order of millions of tons for use in industrial materials synthesis.[4] The epoxidation of propylene yields propylene oxide which is easily converted to polyether polyols used in the synthesis of polyurethane plastics. [4] Olefin metathesis by molybdenum catalysts is used for the conversion of propylene to ethylene and 2-butenes (Scheme 1.2B), as well as, the reverse process to generate propylene.[4] The metathesis reaction is also applied selectively in the total synthesis of complex drug targets, and in the ring-opening polymerization of strained cyclic alkenes, such as norbornene (Scheme 1.2C).[38-39]

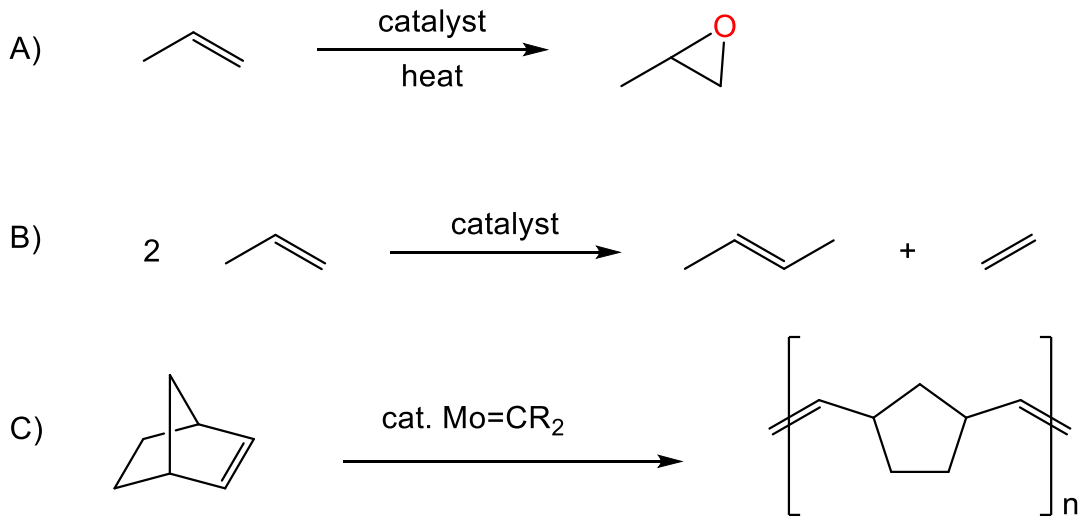

Scheme 1.2 (A) Epoxidation of propylene to propylene oxide, (B) cross metathesis of propylene to form ethylene and 2-butene, and (C) the ring-opening metathesis polymerization (ROMP) of norbornene.

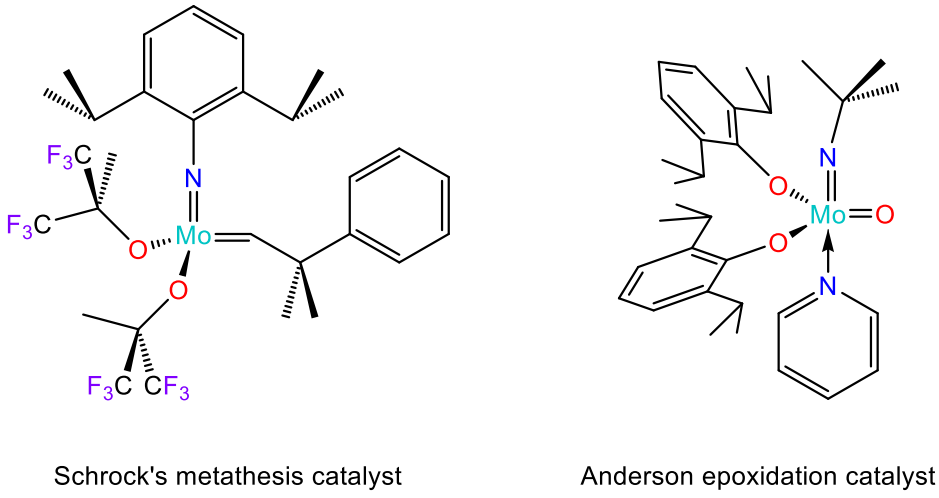

Schrock's metathesis catalyst

Anderson epoxidation catalyst

Figure 1.5 Representation of an early olefin metathesis catalyst by Schrock and coworkers and a mixed oxo-imido complex for alkene epoxidation by Anderson and coworkers.

Dioxo species featuring the unusual η^2-pyrazolate ligands have been used to generate distorted Mo(VI) complexes and applied to OAT reactions.[26, 40-41] These complexes exhibit improved catalytic activity towards OAT due to their pseudo-trigonal prismatic

geometry, when compared to similar octahedral Mo dioxo species.[26, 35, 40] The analogous oxo-imido complex featuring η^2-pyrazolate ligands has also been prepared and its capacity for OAT reactivity was studied for comparison to the dioxo systems, but these molecules were prone to hydrolysis during catalysis.[40] However, other Mo(VI) oxo-imido complexes have been reported that exhibit OAT and epoxidation reactivity (Figure 1.5).[22, 30-32, 42] Interestingly, oxo-imido species of molybdenum are rare when compared to the dioxo and bis(imido) complexes that have been reported and the reactivity of these complexes has been poorly studied.[33]

Many imido ligands featured on Mo complexes are used as ancillary ligands to affect the metal center and not participate directly in reactivity. This can be observed with the Schrock metathesis catalyst family (Figure 1.5), which features an imido group as an ancillary ligand. The imido fragment serves to influence the steric environment and control the electronic properties of the metal center, instead of being directly involved in the metathesis reactions occurring at the metal center. Thus, an important area of inquiry is whether the imido group can have an impact on the epoxidation reaction.

It has also been shown with bis(imido) complexes of Mo that the imido ligand can participate in metathesis reactions of imines. This reaction is useful for general cross-metathesis purposes as shown in Scheme 1.3A, but also has the potential for ring-opening metathesis polymerization (ROMP) of imines for the generation of new materials (Scheme 1.3B).[43] While the cross-metathesis reactivity of Mo-imido complexes has been known for about 20 years, there have been surprisingly few reports in the area.[43-48] The ring-opening of a cyclic imine was first reported in 2000, but progress towards ROMP of imines has not been made with Mo-imido complexes. It is of interest

to explore this imine metathesis reaction with a new ligand system on Mo(VI) bis(imido)complexes, as well as oxo-imido complexes, which have yet to exhibit this type of reactivity.

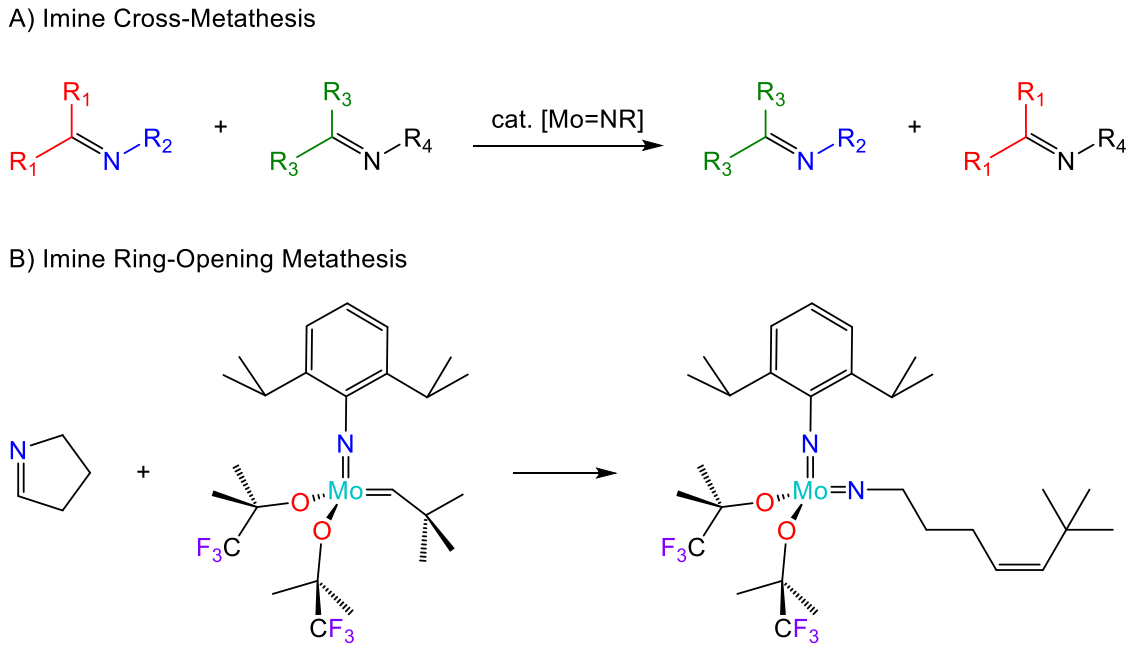

Scheme 1.3 (A) General cross-metathesis reactions of imines. (B) First example of ring-opening metathesis of a cyclic imine.

1.3 Amidate Ligands

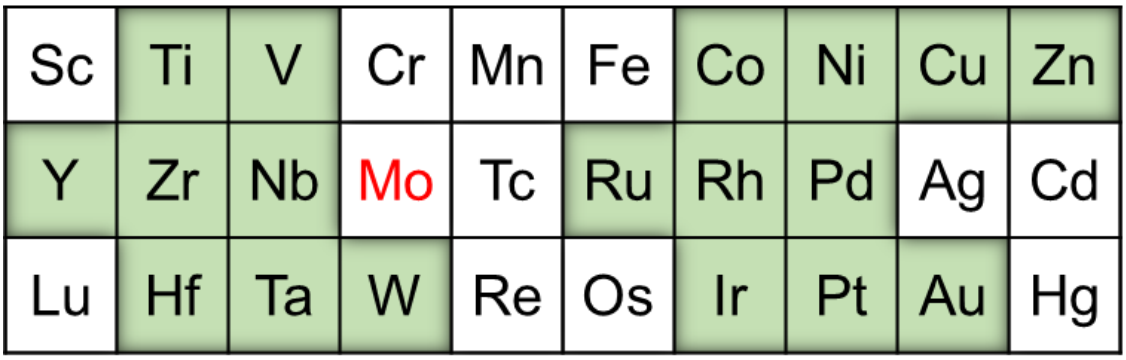

Figure 1.6 Section of periodic table to illustrate the use of amidate ligands in transition metal coordination chemistry. The green elements are those that have amidate complexes reported.

The use of amidate ligands on transition metals has seen substantial growth in recent years, with complexes of over 17 different transition metals (Figure 1.6). This increase in interest is partly due to the success of Group 4 amidate complexes for hydrofunctionalization reactions such as the hydroamination of alkynes (Figure 1.7).[49] Since this early work, the amidate ligand has been applied to almost every transition metal group and just recently expanded into actinides with the synthesis of the first uranium amidate complexes.[50] Recently, bis(imido) W(VI) bis(amidate) complexes were reported as the first of Group 6 species, while the complexes presented in this work are the first Mo(VI) bis(amidate) complexes.[51] The other more practical reasoning for the increased use of amidate ligands is that the ligand has many advantageous properties starting with their preparation.

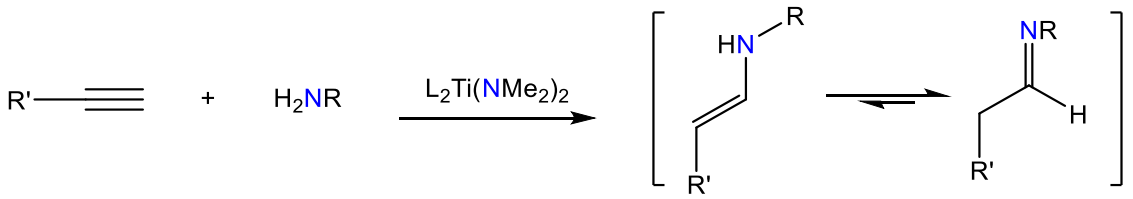

Figure 1.7 The catalytic hydroamination of alkynes by a bis(amido) Ti(IV) bis(amidate) complex.

Amide syntheses require one synthetic step in most cases, can be made in large quantities, and use cheap simple starting feedstocks namely anilines/amines and acyl chlorides. This modular synthesis allows for greater ligand design control, easily varying steric and electronic characteristics of the amides themselves. The amidate ligand features two points of control in this respect at R and R′ as seen in Scheme 1.4. Starting with steric control, consider the change in the R group. If this is a bulkier group it will crowd the metal center, and influence the auxiliary bonds to the metal center, such as a Mo=O bond. If this group is less bulky, then the effect is reversed, and more room is allowed for reactivity at the metal center. The electronics of the ligand can be tuned at both R and R′ by using electron donating or withdrawing groups. The stronger the withdrawing effect, the more electron density will be pulled from the metal center, making the molybdenum center more electrophilic. More electron withdrawing ligands have been shown to increase OAT reactivity.[52] The variance in amide characteristics leads to varied structural and electronic characteristics when the ligand is coordinated to a metal.

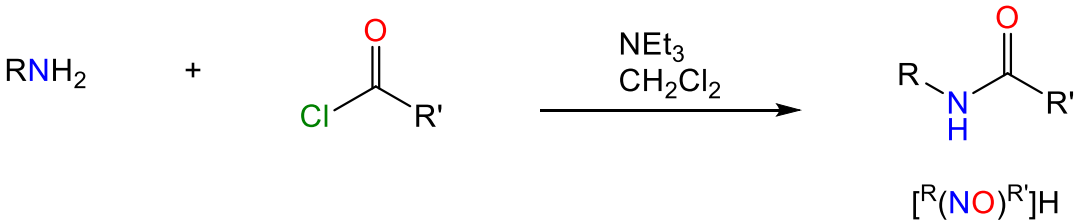

Scheme 1.4. General synthetic procedure for amide proligands of the form $[^{R}(NO)^{R'}]H$.

The amidate ligand can exhibit varied binding modes (κ^1, κ^2, μ^2, etc.) when coordinated to a metal as seen in Scheme 1.5. When the ligand is bound κ^2, it creates a 4-membered metallocycle with a tight bite angle, providing distorted octahedral geometry at the metal center. For Mo complexes, this distortion of geometry means that the bonds of the molybdenum center are contorted in strained angles. These strained bonds can be advantageous if the goal is to make and break bonds, as is the case in catalysis. Some dioxo and oxo-imido complexes have been synthesized with distorted geometries, showing the utility of this in ligand design. The amidate ligand can also exhibit hemilability which can be very useful when performing reactions that require open sites at the metal center.[53-54] Hemilability is the ability of the κ^2-bound ligand to disengage from the metal center and become κ^1-bound as shown in Scheme 1.5. This ligand now still provides an electronic effect, but also has opened a vacancy at the metal center for coordination of an incoming substrate.

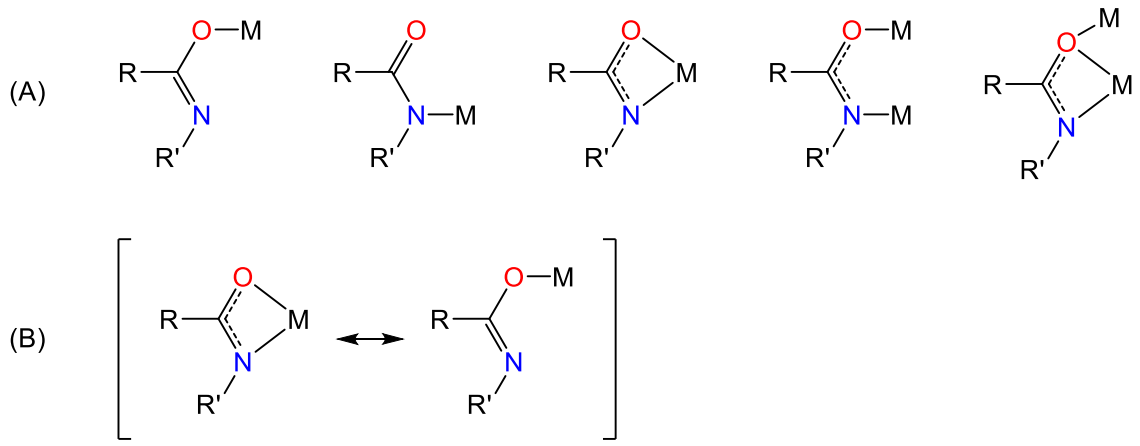

Scheme 1.5 (A) Possible amidate binding modes and (B) hemilability.

It is the goal of this research to exploit all these advantageous traits of the amidate ligand while trying to improve or develop new processes that Mo(VI) complexes can perform. The amidate ligand binds in such a tight bite angle, the metal center deviates significantly from octahedral geometry. The amidate ligands used in this study display the desired control at the metal center, as verified by single crystal X-ray crystallographic studies, and the electronic properties have been varied to affect the reactivity of the metal centers towards catalysis. Chapter 2 introduces a series of the first dioxo Mo(VI) bis(amidate) complexes and presents reactivity studies of these complexes towards OAT and alkene epoxidation. Chapter 3 introduces a series of the first oxo-imido Mo(VI) bis(amidate) complexes, solid-state structural evidence of hemilability, and their ability to promote epoxidation reactions as well as OAT. Chapter 4 introduces a series of the first bis(imido) Mo(VI) bis(amidate) complexes, including the synthesis of two complexes featuring amidate ligands that have not been reported for any system, and initial imine metathesis results. Chapter 5 discusses the future directions of this work,

including the targeted variations of the amidate ligands, reactivity studies, and some preliminary results for different group transfer reactions.

1.4 References

1. Bray, R. C.; Adams, B.; Smith, A. T.; Bennett, B.; Bailey, S., Reversible dissociation of thiolate ligands from molybdenum in an enzyme of the dimethyl sulfoxide reductase family. *Biochemistry* **2000,** *39* (37), 11258-11269.
2. Reedijk, J. E.; Bouwman, E. E., *Bioinorganic Catalysis*. 2nd ed.; CRC Press: Boca Raton, 1999.
3. Stiefel, E. I., Molybdenum bolsters the bioinorganic brigade. *Science* **1996,** *272*, 1599-1600.
4. Baer, H.; Bergamo, M.; Forlin, A.; Pottenger, L. H.; Lindner, J., Propylene Oxide. In *Ullmann's Encyclopedia of Industrial Chemistry*, 2012.
5. Hossain, M. K.; Schachner, J. A.; Haukka, M.; Lehtonen, A.; Mösch-Zanetti, N. C.; Nordlander, E., Dioxidomolybdenum(VI) and -tungsten(VI) complexes with tripodal amino bisphenolate ligands as epoxidation and oxo-transfer catalysts. *Polyhedron* **2017,** *134*, 275-281.
6. Coughlan, M. P., *Molybdenum and Molybdenum-Containing Enzymes*. Elsevier Science: Kent, 1980.
7. Hille, R., The molybdenum oxotransferases and related enzymes. *Dalton Trans.* **2013,** *42* (9), 3029-3042.
8. Hille, R.; Hall, J.; Basu, P., The mononuclear molybdenum enzymes. *Chem. Rev.* **2014,** *114* (7), 3963-4038.
9. Hille, R.; Nishino, T.; Bittner, F., Molybdenum enzymes in higher organisms. *Coord. Chem. Rev.* **2011,** *255* (9-10), 1179-1205.

10. Stiefel, E. I., Molybdenum Compounds. In *Kirk-Othmer Encyclopedia of Chemical Technology*, 2011.

11. Fryzuk, M. D., Activation and functionalization of molecular nitrogen by metal complexes. *Chem. Rec.* **2003,** *3* (1), 2-11.

12. Fryzuk, M. D.; Johnson, S. A., The continuing story of dinitrogen activation. *Coord. Chem. Rev.* **2000,** *200-202*, 379-409.

13. Pierpont, A. W.; Cundari, T. R., Dinitrogen activation by low-coordinate transition metal complexes. *J. Coord. Chem.* **2011,** *64* (18), 3123-3135.

14. Holm, R. H., The biologically relevant oxygen atom transfer chemistry of molybdenum: from synthetic analogue systems to enzymes. *Coord. Chem. Rev.* **1990,** *100*, 183-221.

15. Dobbek, H., Structural aspects of mononuclear Mo/W-enzymes. *Coord. Chem. Rev.* **2011,** *255* (9-10), 1104-1116.

16. Majumdar, A.; Sarkar, S., Bioinorganic chemistry of molybdenum and tungsten enzymes: A structural-functional modeling approach. *Coord. Chem. Rev.* **2011,** *255* (9-10), 1039-1054.

17. Sugimoto, H.; Tsukube, H., Chemical analogues relevant to molybdenum and tungsten enzyme reaction centres toward structural dynamics and reaction diversity. *Chem. Soc. Rev.* **2008,** *37* (12), 2609-2619.

18. Holm, R. H.; Solomon, E. I.; Majumdar, A.; Tenderholt, A., Comparative molecular chemistry of molybdenum and tungsten and its relation to hydroxylase and oxotransferase enzymes. *Coord. Chem. Rev.* **2011,** *255* (9-10), 993-1015.

19. McCleverty, J. A., Molybdenum: Inorganic & Coordination Chemistry. *Eur. J. Inorg. Chem.* **2006**, 1-28.

20. Enemark, J. H.; Cooney, J. J. A.; Wang, J. J.; Holm, R. H., Synthetic analogues and reaction systems relevant to the molybdenum and tungsten oxotransferases. *Chem. Rev.* **2004,** *104* (2), 1175-1200.

21. Dupé, A.; Judmaier, M. E.; Belaj, F.; Zangger, K.; Mösch-Zanetti, N. C., Activation of molecular oxygen by a molybdenum complex for catalytic oxidation. *Dalton Trans.* **2015,** *44* (47), 20514-20522.

22. Volpe, M.; Mösch-Zanetti, N. C., Molybdenum(VI) dioxo and oxo-imido complexes of fluorinated β-ketiminato ligands and their use in OAT reactions. *Inorg. Chem.* **2012,** *51* (3), 1440-1449.

23. Arumuganathan, T.; Mayilmurugan, R.; Volpe, M.; Mösch-Zanetti, N. C., Faster oxygen atom transfer catalysis with a tungsten dioxo complex than with its molybdenum analog. *Dalton Trans.* **2011,** *40* (31), 7850-7857.

24. Mayilmurugan, R.; Harum Bastian, N.; Volpe, M.; Sax Alexander, F.; Palaniandavar, M.; Mösch-Zanetti Nadia, C., Mechanistic insight into the reactivity of oxotransferases by novel asymmetric dioxomolybdenum(VI) model complexes. *Chem. Eur. J.* **2011,** *17* (2), 704-713.

25. Kaupp, M., Trigonal prismatic or not trigonal prismatic? On the mechanisms of oxygen-atom transfer in molybdopterin-based enzymes. *Angew. Chem. Int. Ed.* **2004,** *43* (5), 546-549.

26. Most, K.; Hoßbach, J.; Vidović, D.; Magull, J.; Mösch-Zanetti, N. C., Oxygen-transfer reactions of molybdenum- and tungstendioxo complexes containing η2-pyrazolate ligands. *Adv. Synth. Catal.* **2005,** *347* (2-3), 463-472.

27. Arumuganathan, T.; Volpe, M.; Harum, B.; Wurm, D.; Belaj, F.; Mösch-Zanetti, N. C., Unusual nonoctahedral geometry with molybdenum oxoimido complexes containing η2-pyrazolate ligands. *Inorg. Chem.* **2012,** *51* (1), 150-156.

28. Hauser, S. A.; Cokoja, M.; Khn, F. E., Epoxidation of olefins with homogeneous catalysts-*quo vadis*? *Catal. Sci. Technol.* **2013,** *3* (3), 552-561.

29. Kück, J. W.; Reich, R. M.; Kühn, F. E., Molecular epoxidation reactions catalyzed by rhenium, molybdenum, and iron complexes. *Chem. Rec.* **2016,** *16* (1), 349-364.

30. Zwettler, N.; Grover, N.; Belaj, F.; Kirchner, K.; Mösch-Zanetti, N. C., Activation of molecular oxygen by a molybdenum(IV) imido compound. *Inorg. Chem.* **2017,** *56* (17), 10147-10150.

31. Msch-Zanetti, N. C.; Wurm, D.; Volpe, M.; Lyashenko, G.; Harum, B.; Belaj, F.; Baumgartner, J., Replacement of an oxo by an imido group in oxotransferase model compounds: Influence on the oxygen atom transfer. *Inorg. Chem.* **2010,** *49* (19), 8914-8921.

32. Hüttinger, K.; Förster, C.; Bund, T.; Hinderberger, D.; Heinze, K., Stereochemical consequences of oxygen atom transfer and electron transfer in imido/oxido molybdenum(IV, V, VI) complexes with two unsymmetric bidentate ligands. *Inorg. Chem.* **2012,** *51* (7), 4180-4192.

33. Pastor, A.; Montilla, F.; Galindo, A., Oxido- versus imido-transfer reactions in oxido–imido molybdenum(VI) complexes: A combined experimental and theoretical study. *Polyhedron* **2015,** *90*, 233-238.

34. Saswati; Roy, S.; Dash, S. P.; Acharyya, R.; Kaminsky, W.; Ugone, V.; Garribba, E.; Harris, C.; Lowe, J. M.; Dinda, R., Chemistry of oxidomolybdenum(IV) and -(VI) complexes with ONS donor ligands: Synthesis, computational evaluation and oxo-transfer reactions. *Polyhedron* **2018,** *141*, 322-336.

35. Schulzke, C., Molybdenum and tungsten oxidoreductase models. *Eur. J. Inorg. Chem.* **2011**, 1189-1199.

36. Judmaier, M. E.; Wallner, A.; Stipicic, G. N.; Kirchner, K.; Baumgartner, J.; Belaj, F.; Mösch-Zanetti, N. C., Molybdenum(VI) dioxo complexes with tridentate phenolate ligands. *Inorg. Chem.* **2009,** *48*, 10211-10221.

37. Huber, S.; Cokoja, M.; Kühn, F. E., Historical landmarks of the application of molecular transition metal catalysts for olefin epoxidation. *J. Organomet. Chem.* **2014,** *751*, 25-32.

38. Grubbs, R. H.; Miller, S. J.; Fu, G. C., Ring-closing metathesis and related processes in organic synthesis. *Acc. Chem. Res.* **1995,** *28* (11), 446-452.

39. Nicolaou, K. C.; Bulger, P. G.; Sarlah, D., Metathesis reactions in total synthesis. *Angew. Chem. Int. Ed.* **2005,** *44* (29), 4490-4527.

40. T. Arumuganathan, M. V., Bastian Harum, Dietmar Wurm, Ferdinand Belaj,; Mösch-Zanetti, a. N. C., Unusual nonoctahedral geometry with molybdenum oxoimido complexes containing η2-pyrazolate ligands. *Inorg. Chem.* **2012,** *51*, 150-156.

41. El-Kadri, O. M.; Siddique, A. A.; Eaton, M. D.; Nath, N. K., Synthesis and characterization of two dioxidomolybdenum(VI) complexes bearing amidinato and pyrazolato ligands and their use in thin film growth and oxygen atom transfer reactions. *Polyhedron* **2018,** *147*, 36-41.

42. Anderson, J. C.; Smith, N. M.; Robertson, M.; Scott, M. S., An investigation into oxo analogues of molybdenum olefin metathesis complexes as epoxidation catalysts for alkenes. *Tetrahedron Lett.* **2009,** *50* (38), 5344-5346.

43. Cantrell, G. K.; Geib, S. J.; Meyer, T. Y., Ring-opening metathesis of a cyclic imine. *Organomet.* **2000,** *19* (18), 3562-3568.

44. Cantrell, G. K.; Meyer, T. Y., Transition-metal-catalyzed imine metathesis. *Organomet.* **1997,** *16* (25), 5381-5383.

45. Cantrell, G. K.; Meyer, T. Y., Catalytic C=N bond formation by metal-imide-mediated imine metathesis. *J. Am. Chem. Soc.* **1998,** *120* (32), 8035-8042.

46. McInnes, J. M., Transition metal imide/organic imine metathesis reactions: unexpected observations. *Chem. Commun.* **1998,** (16), 1669-1670.

47. Hamzaoui, B.; Pelletier, J. D. A.; Abou-Hamad, E.; Basset, J. M., Well-defined silica-supported zirconium-imido complexes mediated heterogeneous imine metathesis. *Chem. Commun.* **2016,** *52* (25), 4617-4620.

48. Barman, S.; Merle, N.; Minenkov, Y. a., Well-defined silica grafted molybdenum bis(imido) catalysts for imine metathesis reactions. *Organomet.* **2017,** *36* (8), 1550-1556.

49. Ryken, S. A.; Schafer, L. L., N,O-chelating four-membered metallacyclic titanium(IV) complexes for atom-economic catalytic reactions. *Acc. Chem. Res.* **2015,** *48* (9), 2576-2586.

50. Straub, M. D.; Hohloch, S.; Minasian, S. G.; Arnold, J., Homoleptic U(III) and U(IV) amidate complexes. *Dalton Trans.* **2018,** *47* (6), 1772-1776.

51. Clarkson, J. M.; Schafer, L. L., Bis(tert-butylimido)bis(N,O-chelate)tungsten(VI) complexes: Probing amidate and pyridonate hemilability. *Inorg. Chem.* **2017,** *56* (10), 5553-5566.

52. Mayilmurugan, R.; Harum, B.; Volpe, M.; Sax, A. F.; Palaniandavar, M.; Mosch-Zanetti, N. C., Mechanistic Insight into the Reactivity of Oxotransferases by Novel Asymmetric Dioxomolybdenum(VI) Model Complexes. *Chem. Eur. J.* **2011,** *17*, 704-713.

53. Comas-Vives, A.; Lledós, A.; Poli, R., A computational study of the olefin epoxidation mechanism catalyzed by cyclopentadienyloxidomolybdenum(VI) complexes. *Chem. Eur. J.* **2010,** *16* (7), 2147-2158.

54. Bagherzadeh, M.; Haghdoost, M. M.; Ghanbarpour, A.; Amini, M.; Khavasi, H. R.; Payab, E.; Ellern, A.; Woo, L. K., New molybdenum (VI) catalyst for the epoxidation of alkenes and oxidation of sulfides: An experimental and theoretical study. *Inorg. Chim. Acta* **2014,** *411*, 61-66.

Chapter 2: Dioxo Amidate Complexes: Synthesis, Characterization and Group Transfer Applications

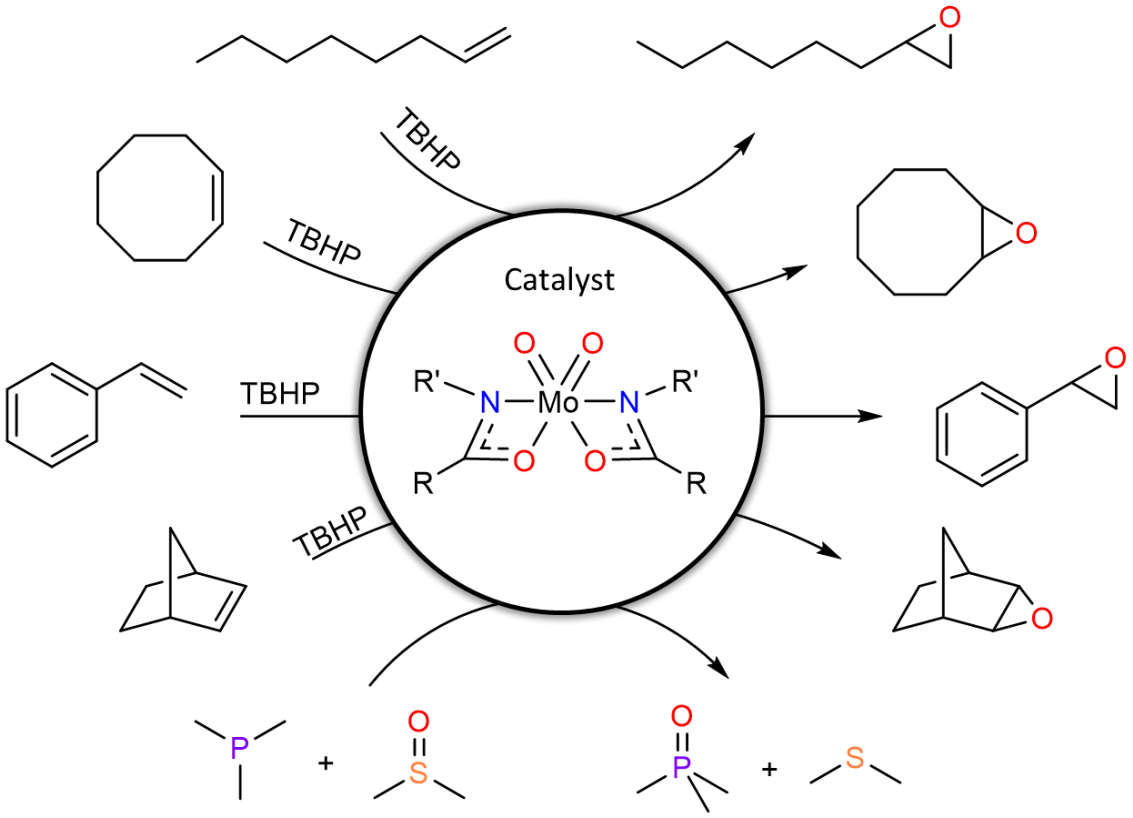

2.1 Introduction

Oxygen atom transfer reactions performed by molybdenum (VI) dioxo metal complexes have importance in both industrial processes and biological transformations.[1-5] Whether it is the removal of oxygen in bioderived materials via deoxydehydration (DODH),[6-8] or the addition of oxygen to alkenes to create value added epoxides,[9-12] metal

complexes capable of catalyzing these processes are of interest to large-scale industrial applications. Molybdoenzymes found in nature contain at least one doubly bonded oxo unit, and are involved in various degradation pathways of metabolites,[1-2, 5, 13-18] while industrial catalysts for epoxidation feature molybdenum oxide materials.[19] Many examples of Mo-oxo species acting as effective catalysts for oxygen transfer chemistry are known,[20-21] as well as a few examples of distorted geometry having an effect on catalytic reactivity.[22-24]

The molybdenum dioxo moiety found at the active site of many enzymes provides a natural starting point for oxygen atom transfer catalyst design. The simplest OAT reaction to study is the dimethylsulfoxide reductase (DMSOR) reaction, where an oxygen atom is transferred from dimethylsulfoxide (DMSO) to a receptor substrate. In the case of the test reactions, trimethylphosphine (PMe_3) is typically the phosphine of choice. Conveniently, the progress of this reaction can be monitored using ^{31}P NMR spectroscopy, which makes it an ideal candidate for assessing the catalytic reactivity of metal complexes.[25]

Amidate complexes of many main group elements and transition metals have been utilized for a wealth of purposes.[26-44] The amide proligand is desirable for the ease of its modular synthesis and the wide range of steric and electronic variation possible.[26] Amides are prepared by the reaction of an acyl chloride and a primary amine in the presence of a base. [26] A general scheme for the synthesis of the amide proligands used in this work is shown in Scheme 2.1, where R and R′ can be changed by using the appropriate acyl chloride and amine starting materials, respectively.

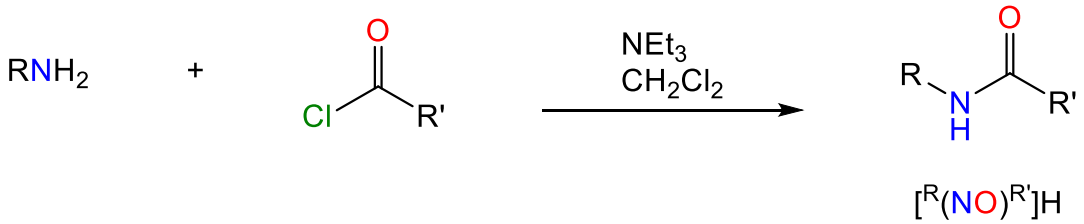

Scheme 2.1. General synthetic procedure for amide proligands of the form $[^{R}(NO)^{R'}]H$.

The primary ligands used in this research are shown in Figure 2.1. Likewise, the abbreviated notation used throughout for these ligands is illustrated in Scheme 2.1, where R is the substituent on the N of the ligand and R′ is the substituent on the carbonyl group.

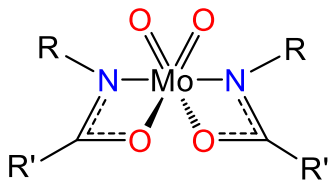

R = phenyl (Ph), 2,6-dimethylphenyl (DMP), or 2,6-diisopropylphenyl (DIPP)
R' = tBu, Ph, or pentafluorophenyl (PFP)

Figure 2.1 Varied functional groups used in this work.

While amidate complexes of many transition metals have been well studied as illustrated in Figure 2.2, [26-51] to our knowledge the use of the amidate ligand with Mo(VI) metal centers has not yet been reported. This chapter will focus on the synthesis, characterization, and reactivity of Mo(VI) dioxo bis(amidate) complexes. Nuclear magnetic resonance (NMR) spectroscopy, Fourier transform infrared (FTIR) spectroscopy, single crystal X-ray diffraction (XRD), and density functional theory (DFT) have all been employed to understand the bonding of amidate ligands to the Mo metal centers.

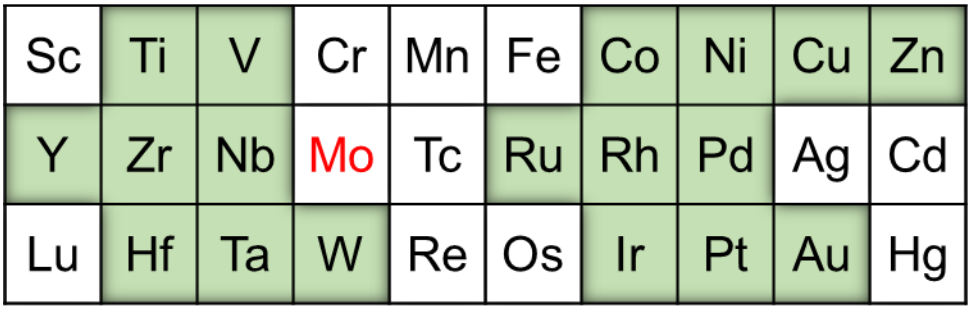

Figure 2.2 Section of the transition metals to illustrate the use of bidentate amidate ligands in metal chemistry.

The extensive use of molybdenum as catalysts for group transfer reactions[11-12, 52-54] is largely due to its ability to readily change oxidation states by ± 2 during reactions.[55] One of the most famous Mo catalytic reactions is the metathesis of C=C double bonds,[52, 56-57] which afforded Robert H. Grubbs (Ru[56]), Yves Chauvin (Ni, Ti, W[58]), and Richard R. Schrock (Mo[59]) the Nobel prize in chemistry in 2005, for their work on the metathesis reaction using various metal complexes. Molybdenum has also been observed to perform group transfer reactions in nature, as in the case of molybdoenzymes. [52, 56-59]

Amidate ligands have been shown to stabilize hard d^0 metal centers, like high oxidation state Group 4 metals,[33] thus Mo(VI)-amidate complexes are legitimate targets. The addition of amidate ligands to transition metals can proceed by either protonolysis[33] or salt metathesis.[33, 43] Many of the Group 4 complexes are prepared through protonolysis methods, as with the tungsten amidate complexes recently reported by Schafer and coworkers.[41] We have found that Mo(VI) amidate complexes can be generated using salt metathesis by employing readily available Cl_2MoE_2(DME) type starting materials.[60]

This work reports the first complexes of Mo(VI) bearing amidate ligands, and our investigations into the ability of these complexes to perform oxygen atom transfer (OAT)

reactions. The tight bite angles of the amidate ligands result in dioxo species that exhibit heavily distorted 6-coordinate geometries, which can have an effect on OAT activity.[22-23, 61] Here we discuss the scope of reactivity of this family of complexes, and the effect of varied steric and electronic changes to the amidate ligand framework on reactivity patterns towards oxygen atom transfer reactions.

2.2 Results and Discussion

2.2.1 Mo(VI) Bis-Amidate Syntheses

Group 4 amidate complexes have been extensively studied,[33] and synthetic routes to these complexes often use protonolysis with starting materials such as $Ti(NMe_2)_4$[33] or $Zr(CH_2Ph)_4$[33], which allow for the easy removal of volatile byproducts like $HNMe_2$ or $PhCH_3$. However, the analogous protonolysis materials for Mo(VI) are not as accessible so initially we focused on salt metathesis methods. Fortunately, in the case of Mo(VI) amidate complexes, salt metathesis methods are sufficient to cleanly generate the desired products, which can be easily separated from salt byproducts.

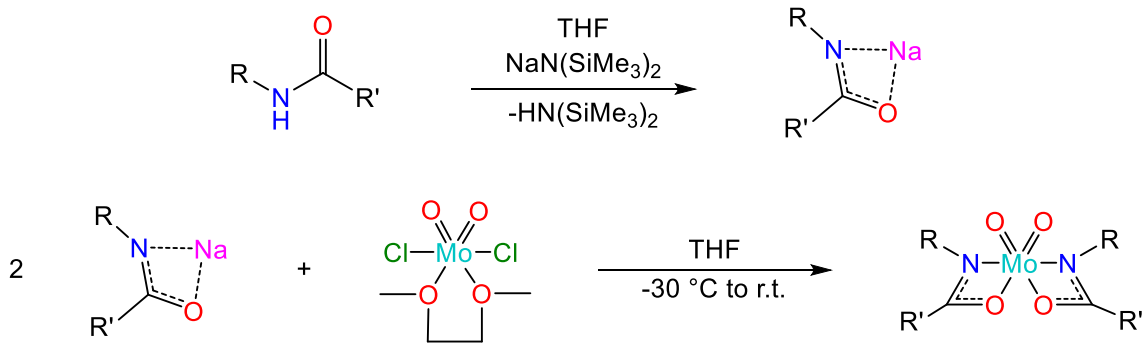

Scheme 2.2 General reaction scheme for the deprotonation of amides to generate the corresponding Na-amidate salts and dioxo Mo(VI) bis-amidate complexes.

To generate the Na salt of the amidate ligand, 1 equivalent of $Na\text{-}N(SiMe_3)_2$ is used to deprotonate $[^{R}(NO)^{R'}]H$ as shown in Scheme 2.2. The easily prepared precursor $Cl_2MoO_2(DME)$ is then treated with $[^{R}(NO)^{R'}]Na$ in a 1:2 stoichiometric ratio in dry THF at -30 ºC. The mixture is stirred while slowly warming to room temperature, leading to

the formation of complexes of the type L_2MoO_2. The crude reaction mixture is then isolated by evaporation of volatiles, and the desired complexes are successfully separated from salt byproducts by filtration of a suspension of the reaction mixture in toluene over a celite plug. The isolated complexes are stable in air in the solid state for short periods and are sensitive to moisture when in solution. The complexes can be stored for extended periods of time in a glovebox. Dioxo complexes of amidate ligands **2.1-2.7** have been synthesized and isolated in yields ranging from 60 - 97%, and have been characterized in the solution phase by NMR spectroscopy, and in the solid-state by single crystal XRD and FTIR.

2.2.2 Alternative Deprotonation Protocols

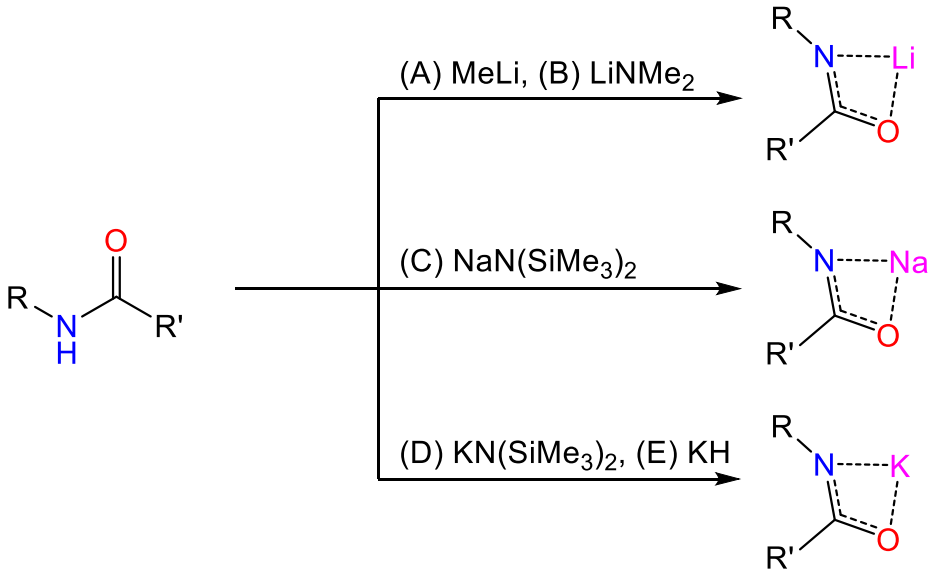

Scheme 2.3 General synthetic routes to ligand salts.

Multiple alkali metal bases [MeLi, $LiNMe_2$ (LDA), $NaN(SiMe_3)_2$, KH, and $KN(SiMe_3)_2$] have been used in the deprotonation of the amidate proligand [$^{DMP}(NO)^{tBu}$]H (**2.2**) as shown in Scheme 2.3. Due to some of the alkali metal bases requiring special handling, the protocols vary. Experimental details for these experiments are in Section 2.4.4. Deprotonation using MeLi yields the lithium salt of the ligand (L-Li). The salt metathesis of L-Li with Cl_2MoO_2(DME) yields pure product, but in poor yield (34%). The deprotonation of the amidate ligand using LDA is incomplete leading to a significant free ligand impurity in the product. It should be noted that attempts to use NaH as a deprotonating agent yielded insoluble blue products upon Mo addition. Using KH as a deprotonating agent required an elevated temperature during deprotonation and an extra filtration step. The best results still yielded an impure product and very low yield (18 mg, 17%). Using $KN(SiMe_3)_2$ as a deprotonating reagent led to multiple unknown byproducts. ^{1}H NMR spectra for these reactions are given in Figure 2.3.

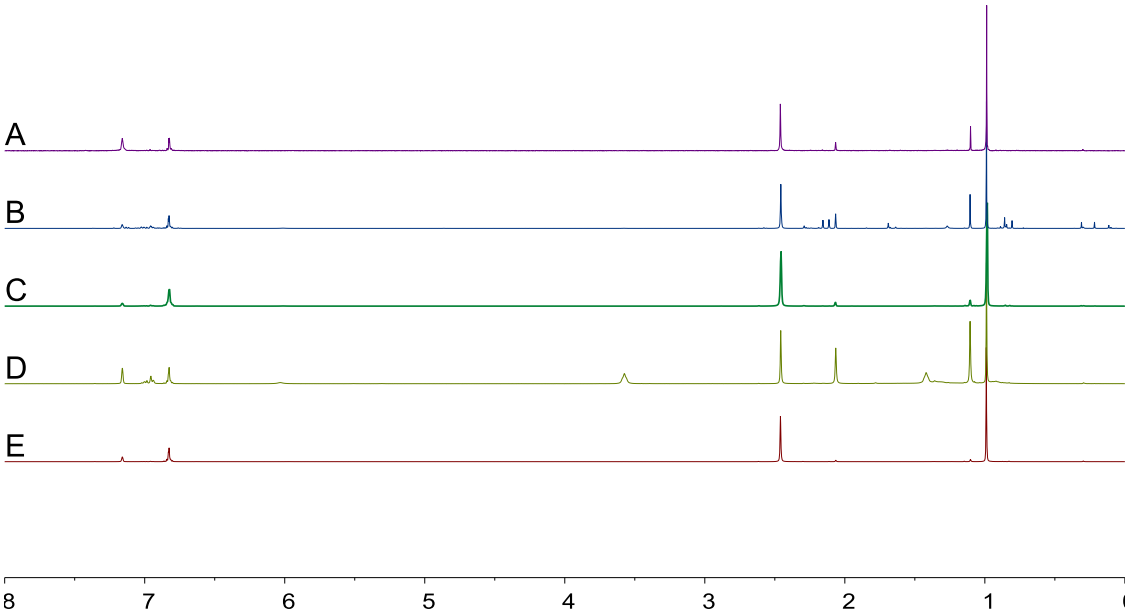

Figure 2.3 ^{1}H NMR spectra for complex **2.9** via different salt metathesis routes (A) K-H, (B) $KN(SiMe_3)_2$, (C) $NaN(SiMe_3)_2$, (D) LDA, (E) MeLi.

A route to the L_2MoO_2 complexes using Cl-$SiMe_3$ elimination has also been shown to afford clean product as illustrated in Scheme 2.4. The deprotonation of the amidate ligand using MeLi followed by reaction with Cl-$SiMe_3$ affords L-$SiMe_3$ as shown in Figure 2.4C. Reaction of L-$SiMe_3$ with Cl_2MoO_2(DME) at 90 °C in toluene selectively yields L_2MoO_2 with no evidence of formation of L_2MoCl_2O, indicating the elimination of Cl-$SiMe_3$, rather than $O(SiMe_3)_2$. The ^{1}H NMR spectra of complex **2.9** synthesized by both salt metathesis and Cl-$SiMe_3$ elimination are presented in Figure 2.4A-B.

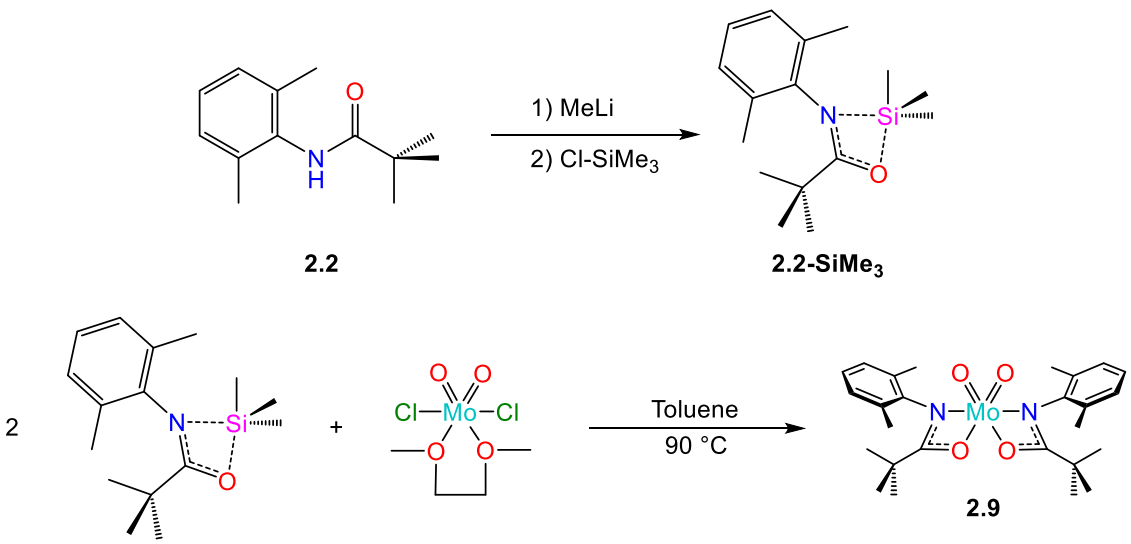

Scheme 2.4 Synthetic scheme for the Cl-$SiMe_3$ elimination route to Mo(VI) bis-amidate complex **2.9**.

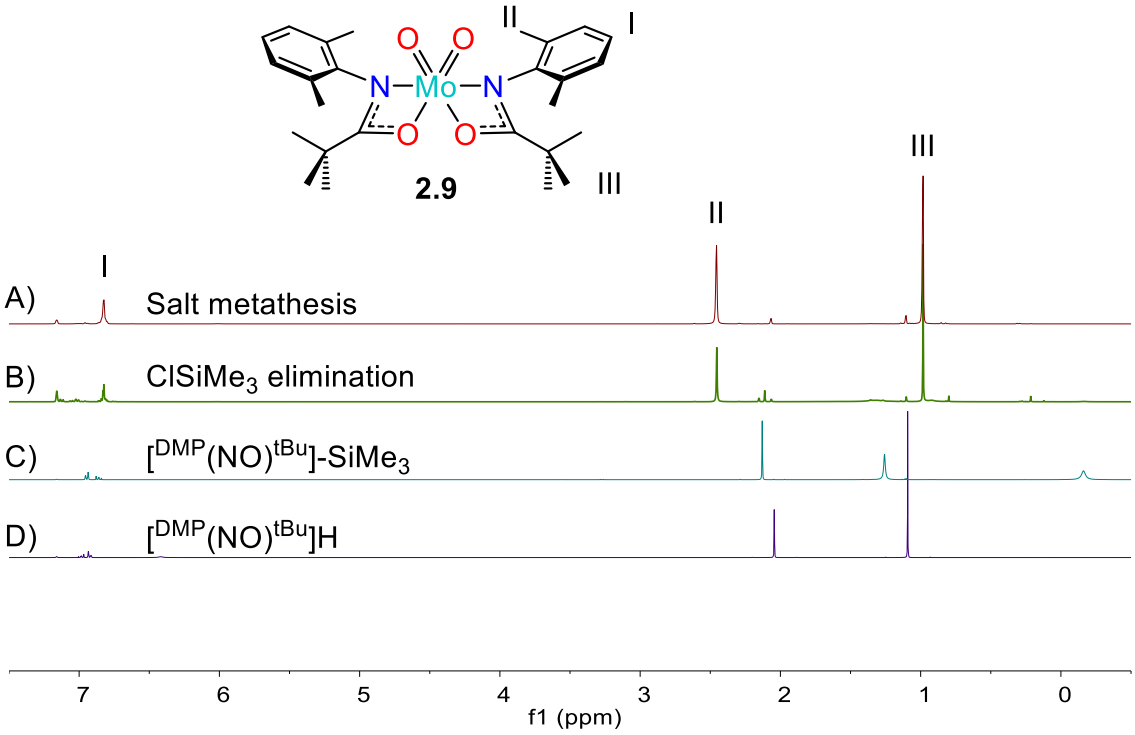

Figure 2.4 ^{1}H NMR spectra for (A) complex **2.9** synthesized by salt metathesis and (B) $ClSiMe_3$ elimination, (C) **2.2**-$SiMe_3$, and (D) **2.2**.

2.2.3 Characterization

The family of bis(amidate) dioxo Mo(VI) complexes are soluble in many non-polar (pentane, hexane, benzene, toluene) and polar (THF, DCM, DCE, diethyl ether, DME, DMSO) solvents. The complexes were all characterized by ^{1}H and ^{13}C NMR spectroscopy in D_6-benzene. For the DMP derivatives **2.9-2.11**, the methyl groups appear as one singlet in the ^{1}H NMR spectra, indicating free rotation about the C-N bond, and C_2 symmetry about the metal center. The ^{1}H NMR spectrum of complex **2.9** is presented in Figure 2.5, showing the ^{t}Bu groups at 0.98 ppm (A), the aryl methyl groups at 2.46 ppm (B), and the aryl protons as a large peak at 6.83 ppm (C).

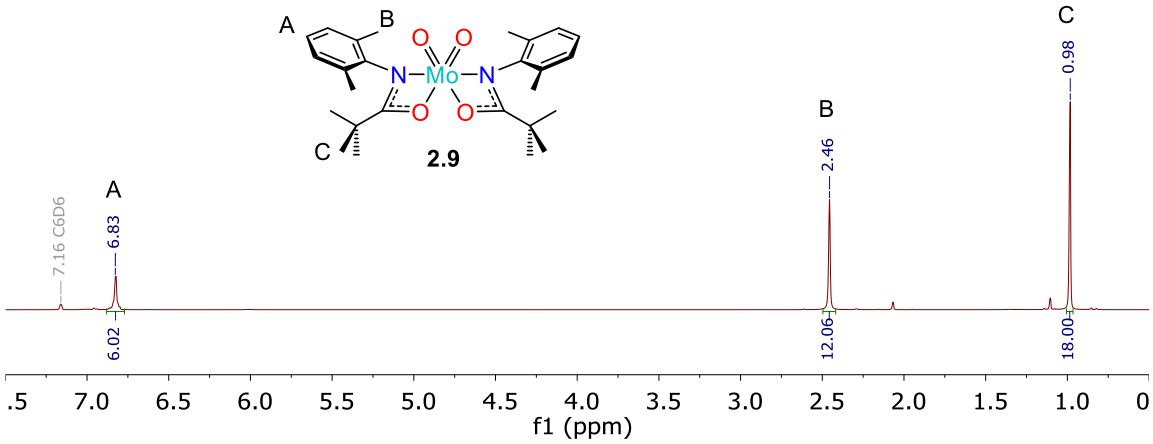

Figure 2.5 ^{1}H NMR spectrum of complex **2.9**.

For the DIPP derivatives **2.12-2.14**, the methine proton signal is broad as shown in peak B in the spectrum of complex **2.12** (Figure 2.6), and the isopropyl methyl protons appear as a set of 2 doublets, indicating rotational strain about the C-N bond. This strain is expected with the added bulk around the metal center in these complexes.

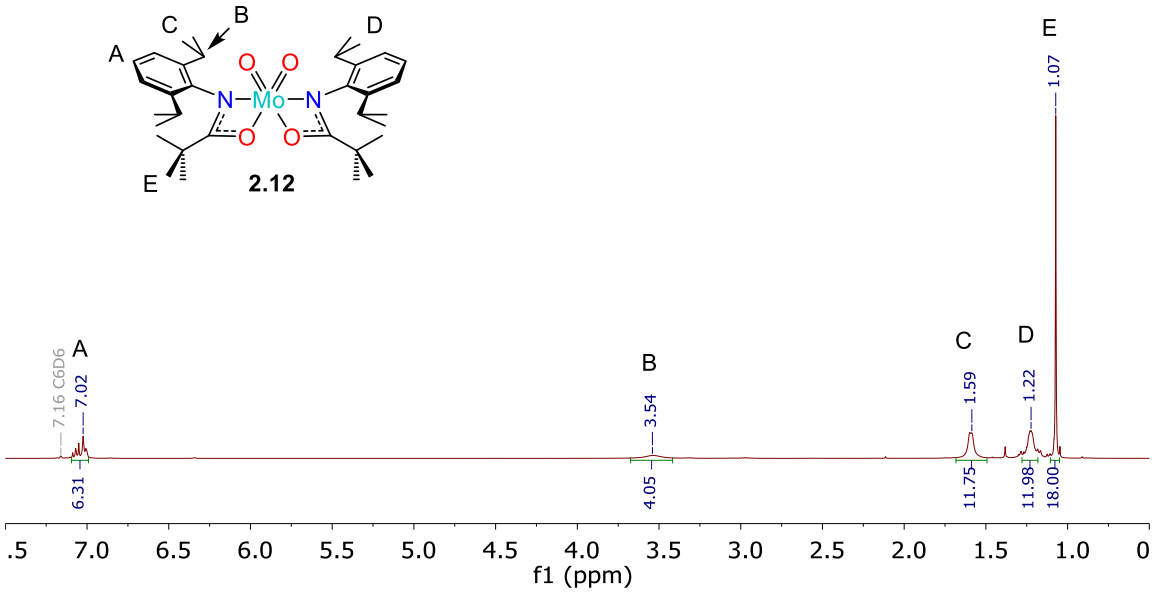

Figure 2.6 ^{1}H NMR spectrum for complex **2.12**.

The IR spectra of all complexes show two strong bands (Table 2.1) that are characteristic of the asymmetric and symmetric $\nu_{(M=O)}$ stretches in the $[MoO_2]^{2+}$ moiety.[55, 62-63] The frequencies for complexes **2.11** and **2.14** are notably closer to those of the Cl_2MoO_2(DME) starting material than the other complexes, likely due to the more anionic character of the amidate ligands in **2.11** and **2.14** resulting from the electron withdrawing nature of the perfluorophenyl group. In general, these frequencies are consistent with reported similar Mo-dioxo compounds. [60, 66-67]

Table 2.1. IR frequencies for **2.8-2.14** symmetric and asymmetric M=O vibrations.

	$\nu_{(Mo=O)}$	
Complex	**Asym.**	**Sym.**
2.8	916.62	947.06
2.9	912.16	941.15
2.10	913.46	940.39
2.11	**920.74**	**959.08**
2.12	915.89	942.12
2.13	918.02	942.88
2.14	**931.40**	**962.12**
Cl_2MoO_2(DME)	**921.39**	**958.34**

2.2.4 X-ray Crystallography

Molecular structures of complexes **2.8**-**2.12** and **2.14** were determined by single-crystal X-ray diffraction analysis. Crystals suitable for X-ray crystallography of complexes **2.8**, **2.11**, and **2.14** were grown from slow evaporation of 1:1 DCM/hexane solutions at room temperature. Crystals of complexes **2.9** and **2.12** were grown from slow evaporation of toluene solutions at room temperature. Crystals of complex **2.10** were grown from a 1:1 solution of Et_2O/toluene at room temperature. The solid-state structures show that all of the complexes have *cis*-dioxo ligands with two κ^2-amidate ligands bound with their N donors in a pseudo-*trans* arrangement. Relevant crystallographic information for these complexes is collated in Appendix A.

The X-ray crystal structure for complex **2.8** is presented in Figure 2.7. The Mo oxo bond distances are 1.685(5) Å. The amidate bond distances Mo(1)-O(1) and Mo(1)-N(1) are 2.237(5) and 2.098(5) Å, respectively. The amidate ligand backbone bond lengths, O(1)-C(7) and N(1)-C(7) are 1.275(7) and 1.317(8) Å, respectively. The

metal oxygen bond lengths for the amidate ligands again indicate an amido-ketone bonding character in the amidate ligands. This is consistent with the shorter C-O bonds, which indicate more double bond character than the ligand C-N bonds.

The *trans* bond angles N(1)-Mo(1)-N(1)#1 and O(2)-Mo(1)-O(1)#1 are 144.3(3)º and 152.1(2)º respectively. These all deviate heavily from a traditional octahedral complex, where the *trans* ligands should be 180º apart. The bond angle between the *cis* oxo ligands, O(2)-Mo(1)-O(2)#1, is 104.6(4)º, while the *cis* amidate O(1)-Mo(1)-O(1)#1 bond angle is 81.7(3)º. The amidate bite-angle is 59.38(17)°. These angles are typical for amidate complexes of transition metals. The selected bond angles and distances are presented in Table 2.2 for complex **2.8**.

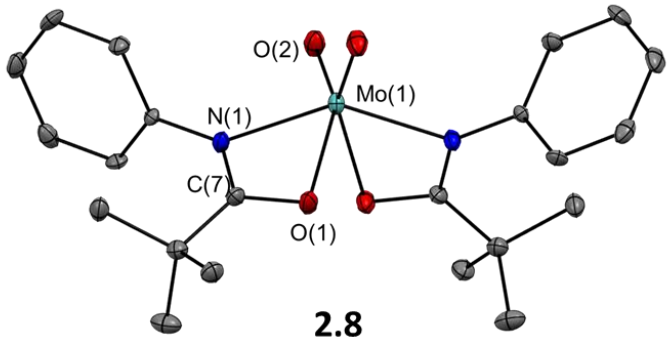

Figure 2.7. X-ray crystal structure of complex **2.8** shown at 50% probability with hydrogen atoms omitted for clarity.

Table 2.2 Selected Bond Distances (Å) and Angles (°) for $[^{Ph}(NO)^{tBu}]_2MoO_2$, **2.8**.

	Lengths (Å)		Angles (°)
Mo(1)-O(2)	1.685(5)	O(2)-Mo(1)-O(2)#1	104.6(4)
Mo(1)-N(1)	2.098(5)	O(2)-Mo(1)-N(1)#1	94.0(2)
Mo(1)-O(1)	2.237(5)	O(2)-Mo(1)-N(1)	107.8(2)
O(1)-C(7)	1.275(7)	N(1)-Mo(1)-N(1)#1	144.3(3)
N(1)-C(7)	1.317(8)	O(2)-Mo(1)-O(1)#1	152.1(2)
		N(1)-Mo(1)-O(1)#1	92.60(18)
		O(2)-Mo(1)-O(1)	92.3(2)
		N(1)-Mo(1)-O(1)	59.38(17)
		O(1)-Mo(1)-O(1)#1	81.7(3)

The X-ray crystal structure for complex **2.9** is presented in Figure 2.8. The Mo oxo bond distances are 1.6955(10)) and 1.6992(10) Å. The amidate bond distances Mo(1)-O(3A), Mo(1)-O(3B), Mo(1)-N(1A), and Mo(1)-N(1B) are 2.2353(10), 2.2500(9), 2.0958(11), and 2.0944(11) Å, respectively. The amidate ligand backbone bond lengths, O(3A)-C(1A), O(3B)-C(1B), N(1A)-C(1A), and N(1B)-C(1B) are 1.2801(16), 1.2759(16), 1.3277(17), and 1.3322(17) Å, respectively.

The *trans* bond angles N(1A)-Mo(1)-N(1B), O(1)-Mo(1)-O(3A), and O(2)-Mo(1)-O(3B) are 144.45(4)º, 152.01(4)º, and 151.26(4)º, respectively. The bond angle between the *cis* oxo ligands, O(1)-Mo(1)-O(2), is 105.78(5)º, while the *cis* amidate O(3A)-Mo(1)-O(3B) bond angle is 75.78(4)º. The amidate bite angles, N(1A)-Mo(1)-O(3A) and N(1B)-Mo(1)-O(3B), are 59.86(4)º and 59.57(4)º, respectively. The selected bond angles and distances are presented in Table 2.3 for complex **2.9**.

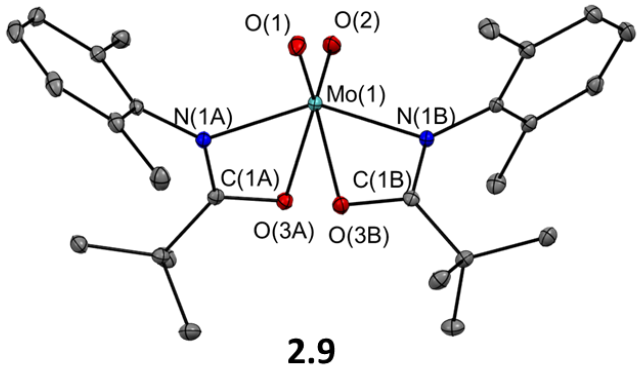

2.9

Figure 2.8. X-ray crystal structure of complex **2.9** shown at 50% probability with hydrogen atoms omitted for clarity.

Table 2.3 Selected Bond Distances (Å) and Angles (°) for $[^{DMP}(NO)^{tBu}]_2MoO_2$, **2.9**

	Lengths (Å)		Angles (°)
Mo(1)-O(2)	1.6955(10)	O(2)-Mo(1)-O(1)	105.78(5)
Mo(1)-O(1)	1.6992(10)	O(2)-Mo(1)-N(1B)	93.49(5)
Mo(1)-N(1B)	2.0944(11)	O(1)-Mo(1)-N(1B)	107.41(5)
Mo(1)-N(1A)	2.0958(11)	O(2)-Mo(1)-N(1A)	105.25(5)
Mo(1)-O(3A)	2.2353(10)	O(1)-Mo(1)-N(1A)	96.35(5)
Mo(1)-O(3B)	2.2500(9)	N(1B)-Mo(1)-N(1A)	144.45(4)
O(3A)-C(1A)	1.2801(16)	O(2)-Mo(1)-O(3A)	95.39(5)
N(1A)-C(1A)	1.3277(17)	O(1)-Mo(1)-O(3A)	152.01(4)
O(3B)-C(1B)	1.2759(16)	N(1B)-Mo(1)-O(3A)	88.97(4)
N(1B)-C(1B)	1.3322(17)	N(1A)-Mo(1)-O(3A)	59.86(4)
		O(2)-Mo(1)-O(3B)	151.26(4)
		O(1)-Mo(1)-O(3B)	92.82(4)
		N(1B)-Mo(1)-O(3B)	59.57(4)
		N(1A)-Mo(1)-O(3B)	93.96(4)
		O(3A)-Mo(1)-O(3B)	75.78(4)

The X-ray crystal structure for complex **2.10** is presented in Figure 2.9. The Mo oxo bond distances are 1.6928(10) and 1.7016(10) Å. The amidate bond distances Mo(1)-O(1), Mo(1)-O(2), Mo(1)-N(1), and Mo(1)-N(2) are 2.2708(10), 2.2723(10), 2.0953(11), and 2.0838(10) Å, respectively. The amidate ligand backbone bond lengths,

O(1)-C(1), O(2)-C(16), N(1)-C(1), and N(2)-C(16) are 1.2786(16), 1.2759(15), 1.2252(16), and 1.3378(16) Å, respectively.

The *trans* bond angles N(1)-Mo(1)-N(2), O(1)-Mo(1)-O(3), and O(2)-Mo(1)-O(4) are 142.37(4)º, 152.51(4)º, and 153.70(4)º respectively. The bond angle between the *cis* oxo ligands, O(3)-Mo(1)-O(4), is 105.27(5)º, while the *cis* amidate O(1)-Mo(1)-O(2) bond angle is 74.34(4)º. The amidate bite angles, N(1)-Mo(1)-O(1) and N(2)-Mo(1)-O(2), are 59.93(4)º and 59.95(4)º, respectively. The selected bond angles and distances are presented in Table 2.4 for complex **2.10**.

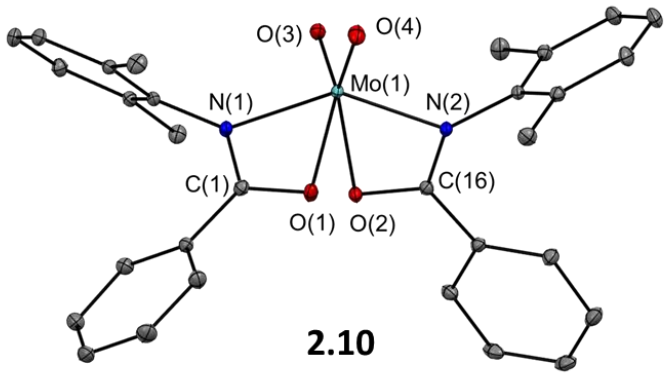

Figure 2.9. X-ray crystal structure of complex **2.10** shown at 50% probability with hydrogen atoms omitted for clarity.

Table 2.4 Selected Bond Distances (Å) and Angles (°) for $[^{DMP}(NO)^{Ph}]_2MoO_2$, **2.10**

	Lengths (Å)		Angles (°)
Mo(1)-O(4)	1.6928(10)	O(4)-Mo(1)-O(3)	105.27(5)
Mo(1)-O(3)	1.7016(10)	O(4)-Mo(1)-N(2)	98.64(5)
Mo(1)-N(2)	2.0838(10)	O(3)-Mo(1)-N(2)	104.08(4)
Mo(1)-N(1)	2.0935(11)	O(4)-Mo(1)-N(1)	107.67(5)
Mo(1)-O(1)	2.2708(10)	O(3)-Mo(1)-N(1)	94.55(4)
Mo(1)-O(2)	2.2723(10)	N(2)-Mo(1)-N(1)	142.37(4)
O(1)-C(1)	1.2786(16)	O(4)-Mo(1)-O(1)	93.13(5)
O(2)-C(16)	1.2759(15)	O(3)-Mo(1)-O(1)	152.51(4)
N(1)-C(1)	1.3352(16)	N(2)-Mo(1)-O(1)	92.87(4)
N(2)-C(16)	1.3378(16)	N(1)-Mo(1)-O(1)	59.93(4)
		O(4)-Mo(1)-O(2)	153.70(4)
		O(3)-Mo(1)-O(2)	95.41(4)
		N(2)-Mo(1)-O(2)	59.95(4)
		N(1)-Mo(1)-O(2)	86.29(4)
		O(1)-Mo(1)-O(2)	74.34(4)

The X-ray crystal structure for complex **2.11** is presented in Figure 2.10. The Mo oxo bond distances are 1.6880(15) and 1.6908(16) Å. The amidate bond distances Mo(1)-O(1A), Mo(1)-O(1B), Mo(1)-N(1A), and Mo(1)-N(1B) are 2.2662(16), 2.2834(15), 2.0904(18), and 2.0983(18) Å, respectively. The amidate ligand backbone bond lengths, O(1A)-C(9A), O(1B)-C(9B), N(1A)-C(9A), and N(1B)-C(9B) are 1.269(3), 1.262(3), 1.320(3), and 1.326(3) Å, respectively.

The *trans* bond angles N(1A)-Mo(1)-N(1B), O(1)-Mo(1)-O(1A), and O(2)-Mo(1)-O(1B) are 138.11(7)º, 154.72(7)º, and 154.94(7)º respectively. The bond angle between the *cis* oxo ligands, O(1)-Mo(1)-O(2), is 105.51(8)º, while the *cis* amidate O(1A)-Mo(1)-O(1B) bond angle is 77.25(6)º. The amidate bite angles, N(1A)-Mo(1)-O(1A) and N(1B)-Mo(1)-O(1B), are 60.01(6)º and 59.76(6)º, respectively. The selected bond angles and distances are presented in Table 2.5 for complex **2.11**.

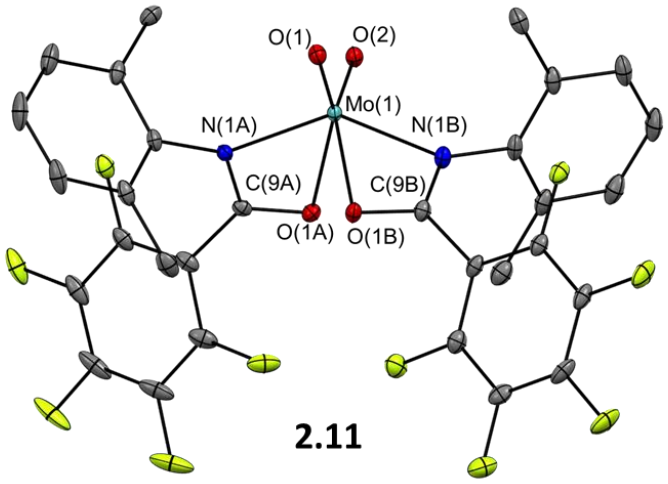

Figure 2.10 X-ray crystal structure of complex **2.11** shown at 50% probability with hydrogen atoms omitted for clarity.

Table 2.5 Selected Bond Distances (Å) and Angles (°) for $[^{DMP}(NO)^{PFP}]_2MoO_2$, **2.11**.

	Lengths (Å)		Angles (°)
Mo(1)-O(2)	1.6880(15)	O(2)-Mo(1)-O(1)	105.51(8)
Mo(1)-O(1)	1.6908(16)	O(2)-Mo(1)-N(1A)	108.29(7)
Mo(1)-N(1A	2.0904(18)	O(1)-Mo(1)-N(1A)	96.95(7)
Mo(1)-N(1B	2.0983(18)	O(2)-Mo(1)-N(1B)	97.30(7)
Mo(1)-O(1A	2.2662(16)	O(1)-Mo(1)-N(1B)	107.67(8)
Mo(1)-O(1B	2.2834(15)	N(1A)-Mo(1)-N(1B)	138.11(7)
O(1A)-C(9A	1.269(3)	O(2)-Mo(1)-O(1A)	92.56(7)
N(1A)-C(9A	1.320(3)	O(1)-Mo(1)-O(1A)	154.72(7)
O(1B)-C(9B	1.262(3)	N(1A)-Mo(1)-O(1A)	60.01(6)
N(1B)-C(9B	1.326(3)	N(1B)-Mo(1)-O(1A)	86.89(7)
		O(2)-Mo(1)-O(1B)	154.94(7)
		O(1)-Mo(1)-O(1B)	92.09(7)
		N(1A)-Mo(1)-O(1B)	86.60(6)
		N(1B)-Mo(1)-O(1B)	59.76(6)
		O(1A)-Mo(1)-O(1B)	77.25(6)

The X-ray crystal structure for complex **2.12** is presented in Figure 2.11. The Mo oxo bond distances are 1.690(2) and 1.699(2) Å. The amidate bond distances Mo(1)-O(1), Mo(1)-O(2), Mo(1)-N(1), and Mo(1)-N(2) are 2.229(2), 2.231(3), 2.100(3), and 2.084(3)

Å, respectively. The amidate ligand backbone bond lengths, O(1)-C(1), O(2)-C(18), N(1)-C(1), and N(2)-C(18) are 1.287(4), 1.278(4), 1.327(4), and 1.332(4) Å, respectively.

The *trans* bond angles N(1)-Mo(1)-N(2), O(1)-Mo(1)-O(3), and O(2)-Mo(1)-O(4) are 140.74(11)º, 152.95(11)º, and 153.16(11)º respectively. The bond angle between the *cis* oxo ligands, O(3)-Mo(1)-O(4), is 106.05(12)º, while the *cis* amidate O(1)-Mo(1)-O(2) bond angle is 75.52(9)º. The amidate bite angles, N(1)-Mo(1)-O(1) and N(2)-Mo(1)-O(2), are 59.99(9)º and 60.03(10)º, respectively. The selected bond angles and distances are presented in Table 2.6 for complex **2.12**.

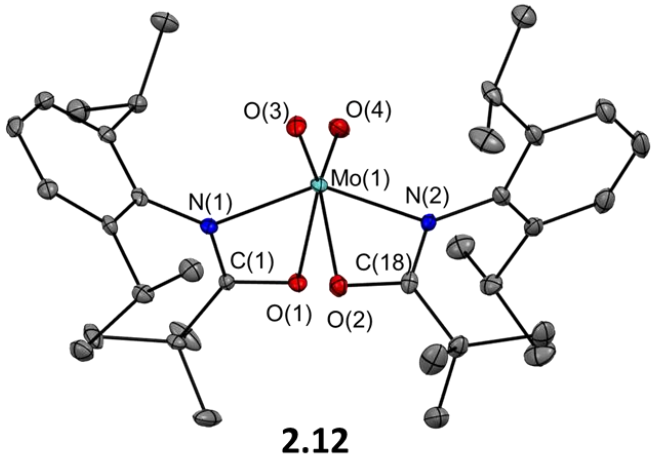

Figure 2.11. X-ray crystal structure of complex **2.12** shown at 50% probability with hydrogen atoms omitted for clarity.

Table 2.6 Selected Bond Distances (Å) and Angles (°) for $[^{DIPP}(NO)^{tBu}]_2MoO_2$, **2.12**.

	Lengths (Å)		Angles (°)
Mo(1)-O(4)	1.690(2)	O(4)-Mo(1)-O(3)	106.05(12)
Mo(1)-O(3)	1.699(2)	O(4)-Mo(1)-N(2)	97.37(12)
Mo(1)-N(2)	2.084(3)	O(3)-Mo(1)-N(2)	106.50(11)
Mo(1)-N(1)	2.100(3)	O(4)-Mo(1)-N(1)	108.32(11)
Mo(1)-O(1)	2.229(2)	O(3)-Mo(1)-N(1)	94.56(11)
Mo(1)-O(2)	2.231(3)	N(2)-Mo(1)-N(1)	140.74(11)
O(1)-C(1)	1.287(4)	O(4)-Mo(1)-O(1)	91.74(10)
O(2)-C(18)	1.278(4)	O(3)-Mo(1)-O(1)	152.95(11)
N(1)-C(1)	1.327(4)	N(2)-Mo(1)-O(1)	90.81(10)
N(2)-C(18)	1.332(4)	N(1)-Mo(1)-O(1)	59.99(9)
		O(4)-Mo(1)-O(2)	153.16(11)
		O(3)-Mo(1)-O(2)	94.98(11)
		N(2)-Mo(1)-O(2)	60.03(10)
		N(1)-Mo(1)-O(2)	85.93(10)
		O(1)-Mo(1)-O(2)	75.52(9)

The X-ray crystal structure for complex **2.14** is presented in Figure 2.12. The Mo oxo bond distances are 1.6854(11) and 1.6877(11) Å. The amidate bond distances Mo(1)-O(1), Mo(1)-O(2), Mo(1)-N(1), and Mo(1)-N(2) are 2.3189(13), 2.2611(11), 2.0906(11), and 2.0983(13) Å, respectively. The amidate ligand backbone bond lengths, O(1)-C(13), O(2)-C(32), N(1)-C(13), and N(2)-C(32) are 1.2626(15), 1.2692(15), 1.3259(16), and 1.3207(16) Å, respectively.

The *trans* bond angles N(1)-Mo(1)-N(2), O(1)-Mo(1)-O(4), and O(2)-Mo(1)-O(3) are 143.20(4)º, 153.11(4)º, and 151.53(4)º respectively. The bond angle between the *cis* oxo ligands, O(3)-Mo(1)-O(4), is 105.91(5)º, while the *cis* amidate O(1)-Mo(1)-O(2) bond angle is 73.87(3)º. The amidate bite angles, N(1)-Mo(1)-O(1) and N(2)-Mo(1)-O(2), are 59.30(4)º and 59.91(4)º, respectively. The selected bond angles and distances are presented in Table 2.7 for complex **2.14**.

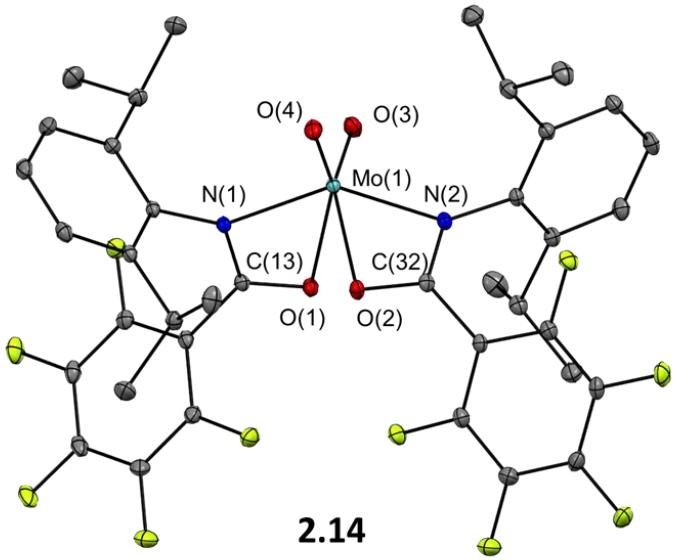

Figure 2.12. X-ray crystal structure of complex **2.14** shown at 50% probability, with hydrogen atoms omitted for clarity.

Table 2.7 Selected Bond Distances (Å) and Angles (°) for $[^{DIPP}(NO)^{PFP}]_2MoO_2$, **2.14**.

	Lengths (Å)		Angles (°)
Mo(1)-O(4)	1.6854(11)	O(4)-Mo(1)-O(3)	105.91(5)
Mo(1)-O(3)	1.6877(11)	O(4)-Mo(1)-N(1)	96.64(5)
Mo(1)-N(1)	2.0906(11)	O(3)-Mo(1)-N(1)	106.43(5)
Mo(1)-N(2)	2.0983(13)	O(4)-Mo(1)-N(2)	105.03(4)
Mo(1)-O(2)	2.2611(11)	O(3)-Mo(1)-N(2)	95.89(4)
Mo(1)-O(1)	2.3189(13)	N(1)-Mo(1)-N(2)	143.20(4)
O(1)-C(13)	1.2626(15)	O(4)-Mo(1)-O(2)	95.53(5)
N(1)-C(13)	1.3259(16)	O(3)-Mo(1)-O(2)	151.53(4)
O(2)-C(32)	1.2692(15)	N(1)-Mo(1)-O(2)	89.06(4)
N(2)-C(32)	1.3207(16)	N(2)-Mo(1)-O(2)	59.91(4)
		O(4)-Mo(1)-O(1)	153.11(4)
		O(3)-Mo(1)-O(1)	93.36(4)
		N(1)-Mo(1)-O(1)	59.30(4)
		N(2)-Mo(1)-O(1)	91.13(4)
		O(2)-Mo(1)-O(1)	73.87(3)

The crystal structures indicate pseudo C_2 symmetry, which is also observed in solution by ^{1}H NMR spectroscopy. The complexes exhibit identical connectivity about the Mo-center leading to very similar bond lengths and angles. The amidate ligands are coordinated to the Mo-center with the N donors *trans* to each other and the amidate O donors *trans* to the Mo=O fragments. The Mo-N_{amid} bond lengths are between 2.084(3) and 2.100(3) Å for all complexes. These bond lengths are very similar due to the highly ionic nature of the bonding in the amidate ligands.[64] The Mo-O_{amid} bonds are longer, ranging between 2.229(2) Å and 2.3189(13) Å. The longer bond for the amidate oxygen atoms is likely due to the *trans* influence of the Mo=O moieties, which have very strong π-donating properties. The amidate N-C backbone bond lengths are also consistently longer (Avg. 1.33 Å) than the corresponding amidate O-C backbone bond lengths (Avg. 1.28 Å). These deviations together with the longer Mo-O and shorter Mo-N bonds for the amidate ligands indicate an amido-ketone bonding character in these complexes (Fig. 2.3). This is in contrast to well-studied Group 4 systems, where the amidate ligand binding is more consistent with the alkoxy-imine description.[26, 33, 65]

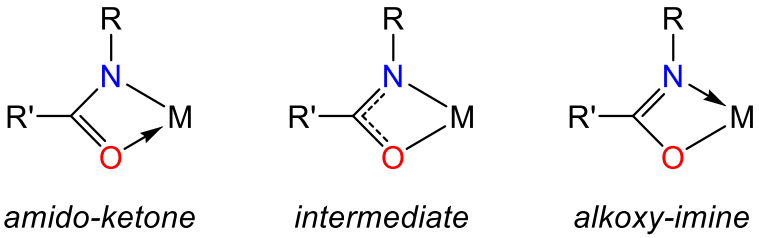

Figure 2.13. Resonance forms of amidate ligand illustrating amido-ketone vs. alkoxy-imine forms.

The amidate ligands have characteristic tight bite angles, with an average N-Mo-O bond angle of 59.7°. This deviation from octahedral geometry is observed with the majority of bond angles about the metal center. For example, the average N_{amid}-Mo-N_{amid} bond angle is 143.01°, while the *trans* arranged oxygen atoms have an average bond angle of 152.44°. The *cis*-oxo angles for the complexes are from 104.6(4)°-106.05(12)°.

The goal of using various R groups for the N-substituent of the amidate ligand to control the access to the reactive metal center is realized as shown in Figure 2.14. The partial spacefill models illustrate the increase in bulk about the metal center where Ph < DMP < DIPP.

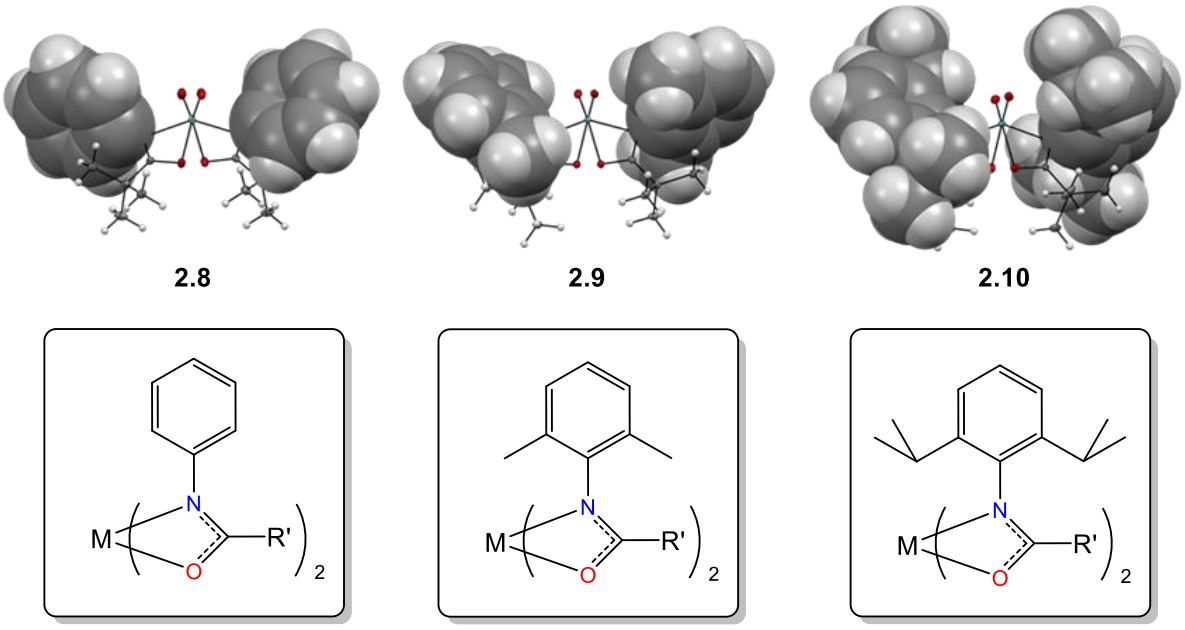

Figure 2.14 Changes in N-bound R group affects steric bulk around the metal center, as seen in the partial spacefill models of complexes **2.8**, **2.9**, and **2.12** (top) and illustrated representations (bottom).

2.2.5 Density Functional Theory Studies

Given the variable binding nature of the amidate ligands, computational studies were undertaken to investigate the potential for isomerization and ligand hemilability. The hemilabile ligand would allow for the opening of a coordination site at the Mo metal center. These open coordination site are important for a variety of catalytic reactions including epoxidation.[9, 66-67] To better understand the capability of the amidate ligand to isomerize in solution, density functional theory (DFT) calculations were performed on the three possible isomers, where the variation in the binding of the amidate ligands leads to complexes that are C_1 symmetric, or C_2 symmetric with either the O-donors pseudo-*trans* or the N-donors pseudo-*trans*. These relative geometries were labeled C_1, *O-trans* and *N-trans*. The relative energies of these isomers are the most obvious starting point for the analysis of bonding in this family of Mo(VI) bis(amidate) complexes. The relative energy diagram for complex **2.8** is shown in Figure 2.15. The *O-trans* isomer is the highest energy at 0.35 eV above the ground state *N-trans* isomer. This result is expected considering the steric bulk at the N-donors of the amidate ligands. The C_1 isomer has an intermediate degree of steric congestion, and is 0.16 eV higher in energy than the *N-trans* isomer. This energy gap is significant, but is still sufficiently low that it could be accessible at higher temperatures.

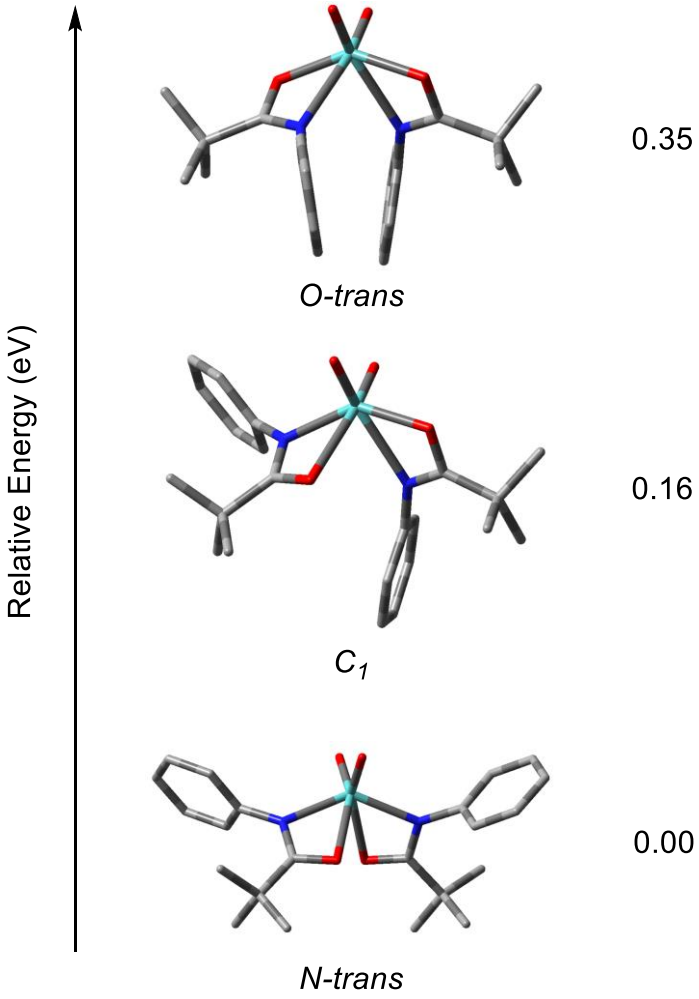

Figure 2.15 Relative energy diagram for complex **2.8**.

The calculated structures for the isomers of the dimethylphenyl series **2.9**-**2.11** are shown in Figure 2.16. Not surprisingly, the differences in the relative energies of the isomers are higher than those seen for the less sterically encumbered complex **2.8**. The steric demand causes a larger effect especially on the O-*trans* species, leading to a relative energy difference nearly double that observed for complex **2.9** at 0.64 eV. The more electron withdrawing amidate ligands [$^{DMP}(NO)^{Ph}$] and [$^{DMP}(NO)^{PFP}$] are not coordinated strongly enough, and the [$^{DMP}(NO)^{PFP}$] (**2.11**) complex becomes hemilabile when forced

into the O-*trans* configuration as shown in Figure 2.16. The C_1 isomers of the DMP series are all relatively close in energy at 0.26, 0.23, and 0.27 eV for complexes **2.9**, **2.10**, and **2.11**, respectively. The relative energies of the calculated isomers are summarized in Table 2.8.

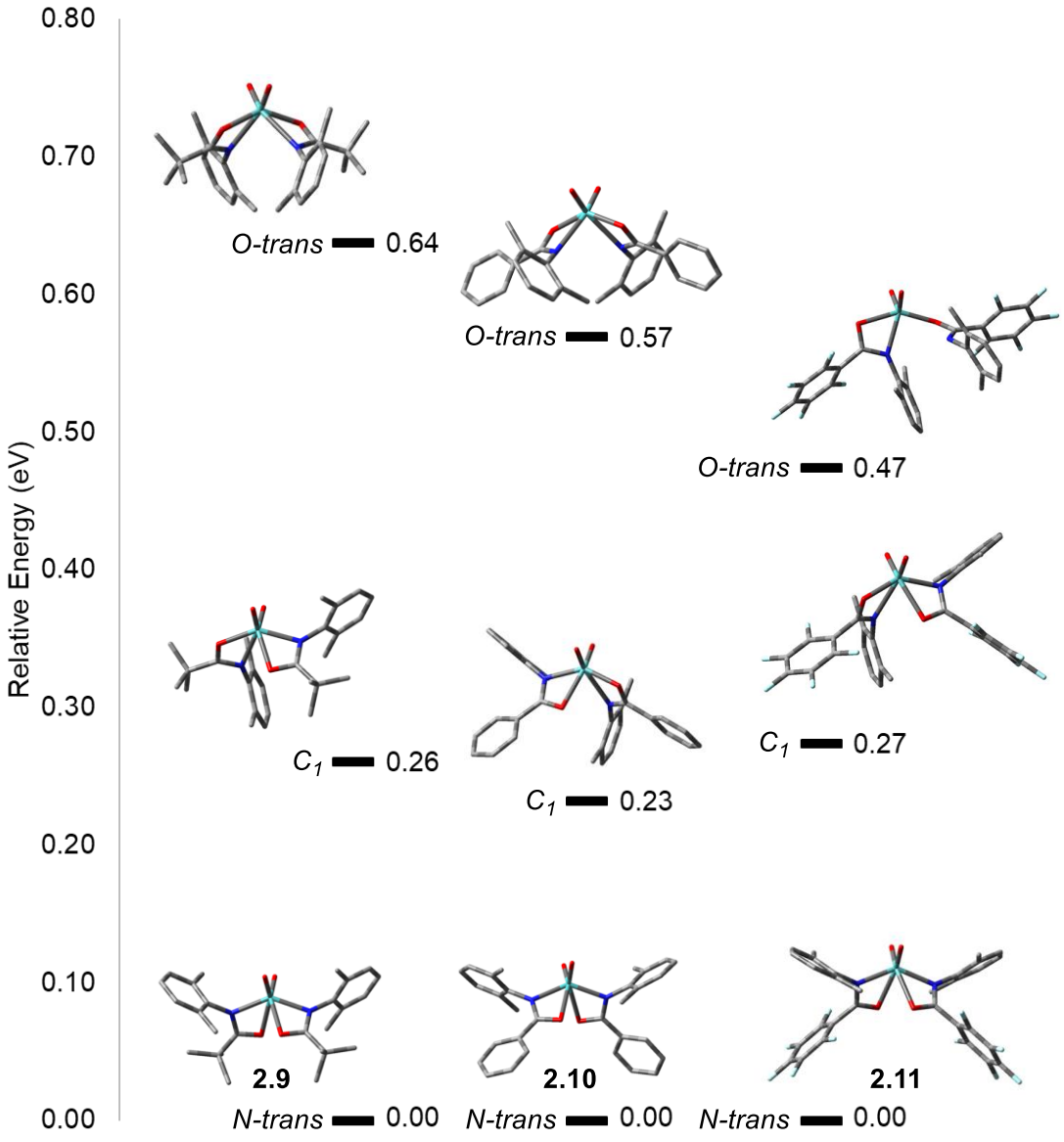

Figure 2.16 Relative energies and calculated structures for the DMP series.

Table 2.8 Relative energies (eV) of isomers for the DMP series.

2.9	*N-trans*	0.00
	C_1	0.26
	O-trans	0.64
2.10	*N-trans*	0.00
	C_1	0.23
	O-trans	0.57
2.11	*N-trans*	0.00
	C_1	0.27
	O-trans	0.47

In the case of the DIPP series of complexes **2.12-2.14**, the steric effects are more pronounced for the calculated structures as shown in Figure 2.17. The C_1 isomer of complex **2.12** exhibits a hemilabile amidate ligand. This is likely purely due to steric bulk, however the C_1 isomer of complex **2.13** manages to maintain 2 bidentate ligands, albeit with longer bond lengths. The C_1 isomer of complex **2.14** is κ^1 likely due to both extreme steric interactions, and the very low donating capability imparted by the perfluorophenyl substituted ligand. All O-*trans* isomers for the DIPP series exhibit 1 monodentate amidate ligand and one bidentate amidate ligand. The relative energies for the structures are 0.77, 0.70, and 0.87 eV for complexes **2.12**, **2.13**, and **2.14**, respectively. The relative energies for the DIPP calculated structures are shown in Table 2.9.

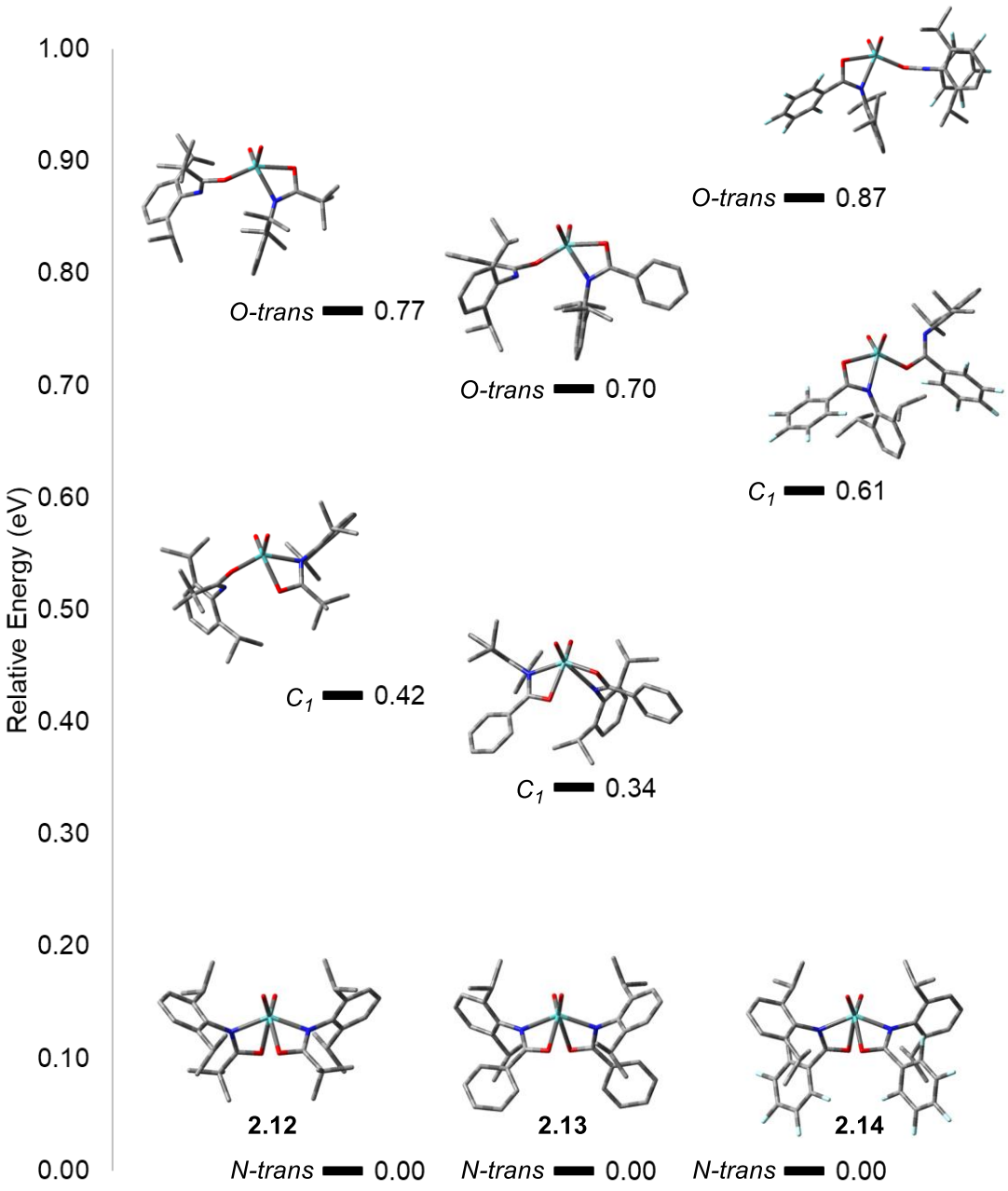

Figure 2.17 Relative energies and calculated structures of isomers for DIPP series.

Table 2.9 Relative energies (eV) of isomers for the DIPP series.

2.12	*N-trans*	0.00
	C_1	0.42
	O-trans	0.77
2.13	*N-trans*	0.00
	C_1	0.34
	O-trans	0.70
2.14	*N-trans*	0.00
	C_1	0.61
	O-trans	0.87

There are some obvious trends in the HOMO-LUMO gap shown in Table 2.10, with the complexes bearing more electron withdrawing ligands having smaller gaps than the complexes with more electron donating ligands. Interestingly, the HOMO-LUMO gap significantly drops when one ligand is κ^1 to the metal center. The farther away the amidate ligand is from the metal center, the lower the HOMO-LUMO gap. This is observed with C_1 isomers of complexes **2.9** and **2.10**, where the N atom of one ligand is *trans* to an oxo fragment. In these cases, the Mo-N bond is significantly longer, to the point of nearly being unconnected. For the complexes bearing large DIPP groups on the N of the ligand, some isomers are not stable, presumably due to steric hindrance, optimizing to κ^1 isomers instead.

Table 2.10. HOMO/LUMO gap in eV for all calculated isomers in order of relative energy from **2.8**-**2.14**

	HOMO-LUMO Gap for Isomers (eV)		
Complex	*N-trans*	C_1	*O-trans*
2.8	4.1629	3.9291	3.7044
2.9	3.7969	3.3384	3.2263
2.10	3.7177	3.3389	3.2779
2.11	3.5985	3.1906	2.7632
2.12	3.7436	2.8834	2.5289
2.13	3.7133	3.2769	2.7022
2.14	3.4919	2.4864	2.6201

2.2.6 Catalytic DMSO Reduction

The $[MoO_2]^{+2}$ moiety has been extensively studied with many ligand systems and it can be stated there are a few key features that are desirable. The ligands should be able to stabilize the Mo metal center during redox reactions, the ligands should sufficiently protect the metal center from side reactivity, and the metal center should deviate from octahedral geometry to some degree.[22-23] As discussed herein, the amidate ligand is capable of stabilizing Mo(VI), varied ligand structures offer the opportunity to tune the steric bulk about the metal center, and the tight bite-angle of the amidate ligand causes a significant deviation from octahedral geometry. In order to study the overall effects of these complexes we investigated their capabilities in the catalytic reduction of DMSO (Scheme 2.5), a biologically relevant process.

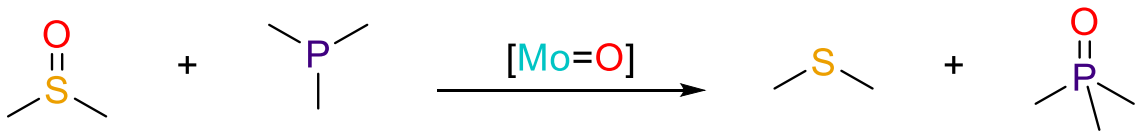

Scheme 2.5 Reduction of DMSO to DMS, using PMe_3 and a Mo=O catalyst.

The reduction of dimethylsulfoxide to dimethyl sulfide via oxygen atom transfer in molybdoenzymes can be modeled using trimethylphosphine as the oxygen-receiving molecule. The dioxo complexes presented here were screened at 5% and 10% catalyst loading for the catalytic reduction of DMSO. The precatalysts **2.8**-**2.14** (Figure 2.18) were dissolved in D_6-DMSO, and an appropriate amount of trimethylphosphine was added. This solution was stirred at 85°C for 3 hours with aliquots being taken at 1 and 3 hours. Using ^{31}P NMR spectroscopy, the ratio of $OPMe_3$:PMe_3 can be determined and converted to % conversion. The data for these catalytic runs is presented in Figure 2.19.

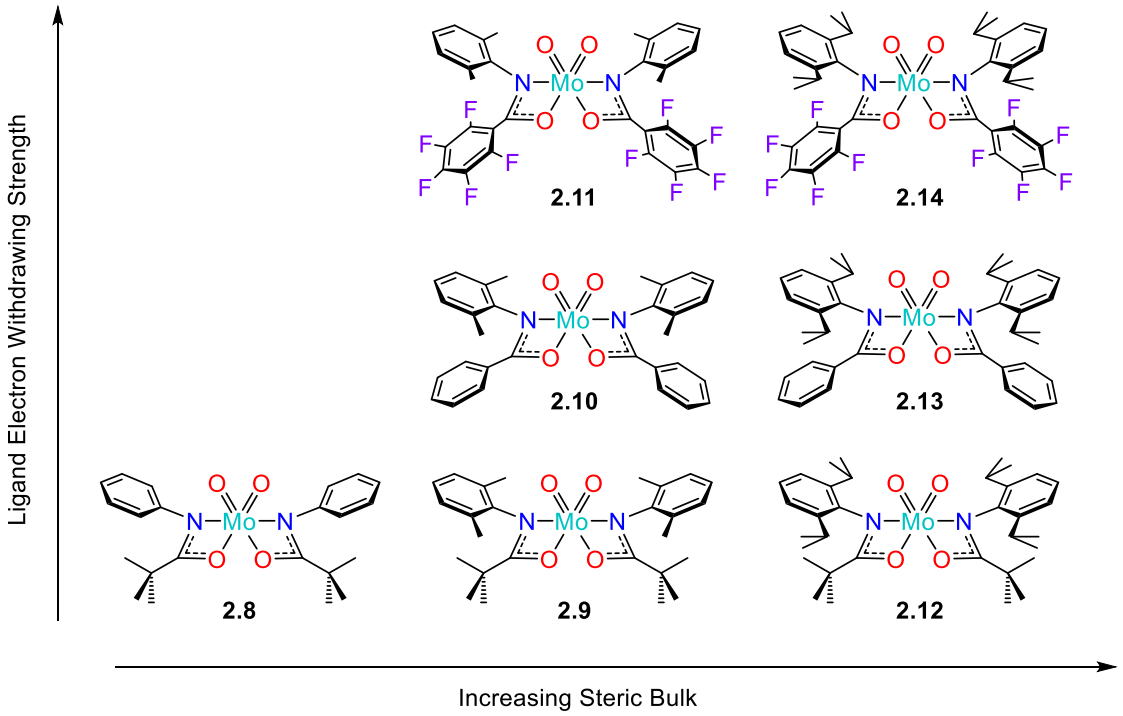

Figure 2.18 Complexes **2.8**-**2.14** illustrating the progression in steric bulk and electron withdrawing properties of the ligands.

Looking at the 5% catalyst loading data, there is a clear progression of speed of conversion in precatalysts **2.9**-**2.11** at the 1 hour timepoint, and this trend is also observed for the precatalysts **2.13**-**2.14**. This can be attributed to the electronic changes in the backbone of the ligand where we expected a trend in overall reaction rates where ^{t}Bu < Ph < PFP. This trend is observed, however, complex **2.12** appears to be the most effective in the OAT reaction based on overall yields at 5% catalyst loading. This is possibly due to the electron donating ability of the ligand, however the other r.t. data suggests the reaction rates increases with the increasing electron withdrawing character of the amidate ligand. It is likely that the steric bulk around the reactive metal center controls this reactivity. The active site of the molybdoenzymes feature thiolate-type ligands, which

have softer S donors, and dimerization of metal centers in the active site is not a problem, due to the complex pocket created by the protein's structure. The $[^{DIPP}(NO)^{tBu}]^-$ ligand is bulky enough to prevent the dimerization of two Mo centers, maintaining the monometallic catalyst species in solution. While $[^{DIPP}(NO)^{Ph}]_2MoO_2$ (**2.13**) and $[^{DIPP}(NO)^{PFP}]_2MoO_2$ (**2.14**) both perform more slowly than their less bulky analogues $[^{DMP}(NO)^{Ph}]_2MoO_2$ (**2.10**) and $[^{DMP}(NO)^{PFP}]_2MoO_2$ (**2.11**), $[^{DIPP}(NO)^{tBu}]_2MoO_2$ (**2.12**) outperforms the less bulky $[^{DMP}(NO)^{tBu}]_2MoO_2$ (**2.9**) at 5% catalyst loading. This is likely due to the bulkier aryl groups on the amidate ligand preventing the dimer formation observed as a catalyst end point for complex **2.9** (*vide infra*). At 10% catalyst loading for all precatalysts, the reaction proceeds similarly for 1 hour and almost quantitatively after 3 hours.

Overall for the OAT reaction it appears the backbone group (R′ = ^{t}Bu, Ph, or PFP) is not completely controlling the electronics, thus the reactivity, of the metal centers as evidenced with the complexes **2.11** and **2.12** having very similar yield at 5% loading. It appears that there is a 'sweet spot' for reactivity where the ligand is donating and bulky, complex **2.12**.

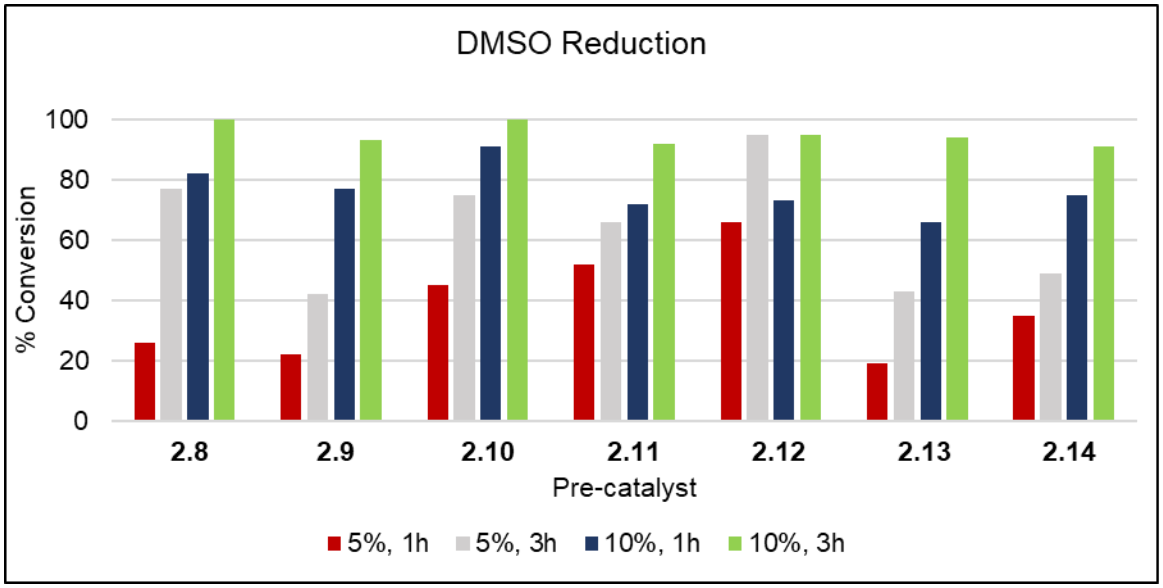

Figure 2.19 Catalytic oxygen atom transfer from DMSO to PMe_3 using precatalysts **2.8**-**2.14** at 5% and 10% catalyst loading. Percent conversion is calculated from the ratio of $OPMe_3$:PMe_3 determined by ^{31}P NMR spectroscopy.

2.2.7 Catalyst Decomposition

The oxygen atom transfer reaction from dimethylsulfoxide to a substrate requires an initial reduction of the Mo(VI) center to Mo(IV).[68] This reduction occurs readily with trimethylphosphine as the reductant. The reaction is easily recognized by a color change of the metal complex solution from a pale-yellow color to a deep red color. This reaction was investigated crystallographically, because the products formed could not be observed by ^1H NMR spectroscopy. Mo complex **2.9** was dissolved in D_6-benzene, and 1.6 eq of trimethylphosphine was added while the solution was stirred. The reaction occurs over the course of an hour, as evidenced by the observed color change from yellow to red. The single red crystals obtained for X-ray diffraction analysis precipitated from the solution over the course of 24 hours.

The solid-state structure, determined by X-ray diffraction, indicated the formation of a bridged oxo dimer species, ([^{DMP}(NO)^{tBu}]$_2$Mo(O)])$_2$(μ-O) (**2.15**), and is shown in Figure 2.20. The structure clearly shows that two amidate ligands are still attached to each Mo center after the reduction reaction occurs. This key result shows that the amidate ligands are capable of surviving redox-type reactivity at a metal center. The bond between the Mo centers and the bridging O, Mo(1)-O(1) and Mo(2)-O(1) are 1.8688(18) and 1.8711(18) Å, respectively. These bonds are consistent with a Mo-O single bond, indicating the Mo centers are both in the +5 oxidation state. Selected bond distances and angles for the complex are presented in Table 2.11.

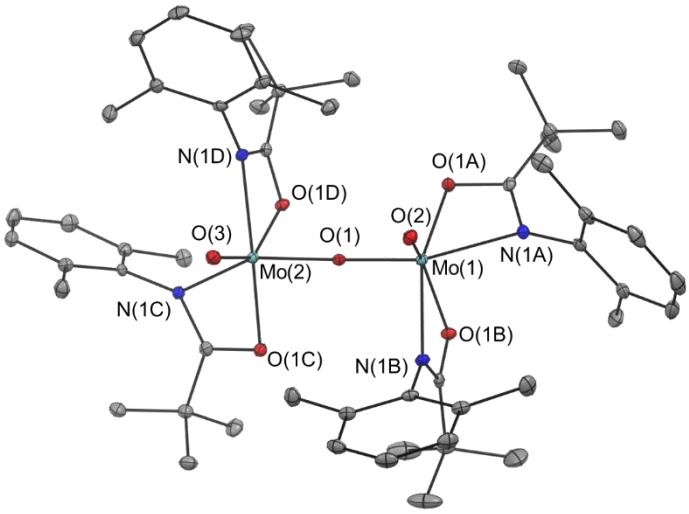

Figure 2.20 X-ray crystal structure of complex **2.15** shown at 50% probability with hydrogen atoms omitted for clarity.

Table 2.11. Selected Bond Distances (Å) and Angles (°) for ([^{DMP}(NO)^{tBu}]$_2$Mo(O))$_2$(μ-O), **2.15**

O(1B)-C(1B)	1.295(3)	N(1B)-Mo(1)-O(1B)	59.28(8)	O(3)-Mo(2)-O(1)	104.43(9)
O(1D)-C(1D)	1.297(3)	N(1D)-Mo(2)-O(1D)	59.40(8)	O(2)-Mo(1)-C(1A)	104.61(9)
C(1A)-N(1A)	1.307(3)	O(1A)-Mo(1)-N(1A)	61.03(8)	N(1B)-Mo(1)-N(1A)	105.04(8)
N(1C)-C(1C)	1.314(4)	O(1C)-Mo(2)-N(1C)	61.20(7)	O(3)-Mo(2)-C(1C)	107.11(9)
N(1D)-C(1D)	1.317(3)	N(1C)-Mo(2)-O(1D)	82.25(7)	O(3)-Mo(2)-O(1C)	110.72(8)
N(1B)-C(1B)	1.318(4)	O(1B)-Mo(1)-N(1A)	85.07(8)	N(1A)-C(1A)-O(1A)	111.7(2)
O(1C)-C(1C)	1.319(3)	O(1)-Mo(2)-O(1D)	87.28(7)	N(1C)-C(1C)-O(1C)	111.7(2)
C(1A)-O(1A)	1.327(3)	O(3)-Mo(2)-N(1D)	89.21(9)	O(1B)-C(1B)-N(1B)	112.0(2)
Mo(1)-O(2)	1.6812(19)	O(1)-Mo(1)-O(1B)	89.59(7)	O(1D)-C(1D)-N(1D)	112.0(2)
Mo(2)-O(3)	1.685(2)	O(1)-Mo(2)-O(1C)	89.92(7)	O(2)-Mo(1)-O(1A)	112.99(9)
Mo(1)-O(1)	1.8688(18)	O(1B)-Mo(1)-C(1A)	91.35(8)	O(1)-Mo(2)-C(1C)	119.50(8)
Mo(2)-O(1)	1.8711(18)	O(2)-Mo(1)-N(1B)	91.65(9)	O(1)-Mo(1)-C(1A)	122.35(8)
Mo(1)-O(1A)	2.0805(19)	O(1)-Mo(1)-O(1A)	91.70(7)	N(1D)-Mo(2)-C(1C)	132.34(8)
Mo(2)-O(1C)	2.086(2)	O(1D)-Mo(2)-C(1C)	91.82(8)	N(1B)-Mo(1)-C(1A)	132.49(8)
Mo(2)-N(1D)	2.171(2)	O(1A)-Mo(1)-O(1B)	93.92(8)	O(1)-Mo(2)-N(1C)	147.00(8)
Mo(1)-N(1B)	2.176(2)	O(2)-Mo(1)-N(1A)	95.74(9)	O(3)-Mo(2)-O(1D)	147.98(8)
Mo(2)-N(1C)	2.193(2)	O(1)-Mo(1)-N(1B)	95.91(8)	O(2)-Mo(1)-O(1B)	149.74(8)
Mo(2)-O(1D)	2.2018(19)	O(1)-Mo(2)-N(1D)	97.81(8)	O(1)-Mo(1)-N(1A)	151.66(8)
Mo(1)-O(1B)	2.2044(19)	O(1C)-Mo(2)-O(1D)	98.78(7)	O(1A)-Mo(1)-N(1B)	151.94(8)
Mo(1)-N(1A)	2.208(2)	O(3)-Mo(2)-N(1C)	100.88(8)	O(1C)-Mo(2)-N(1D)	156.18(8)
		O(2)-Mo(1)-O(1)	102.61(9)	Mo(1)-O(1)-Mo(2)	173.12(11)
		N(1D)-Mo(2)-N(1C)	103.41(8)		

A possible mechanism for the formation of dimeric complex **2.15** is given in Figure 2.21. Initial reduction of **2.9** by trimethylphosphine is proposed to give a putative Mo(IV) species **2.9$_{red}$**, with concomitant elimination of $OPMe_3$. Nucleophilic attack on **2.9$_{red}$** by another molecule of **2.9** results in the formation of the stable dimeric complex **2.15**. While magnetic susceptibility studies were not performed on **2.15**, the absence of ^{1}H NMR resonances for this complex suggests a d^1-d^1 electronic configuration with no magnetic coupling present between the two metal centers. Initial tests show that once the dimer is formed it is irreversible, as has been reported with similar complexes.[69-70]

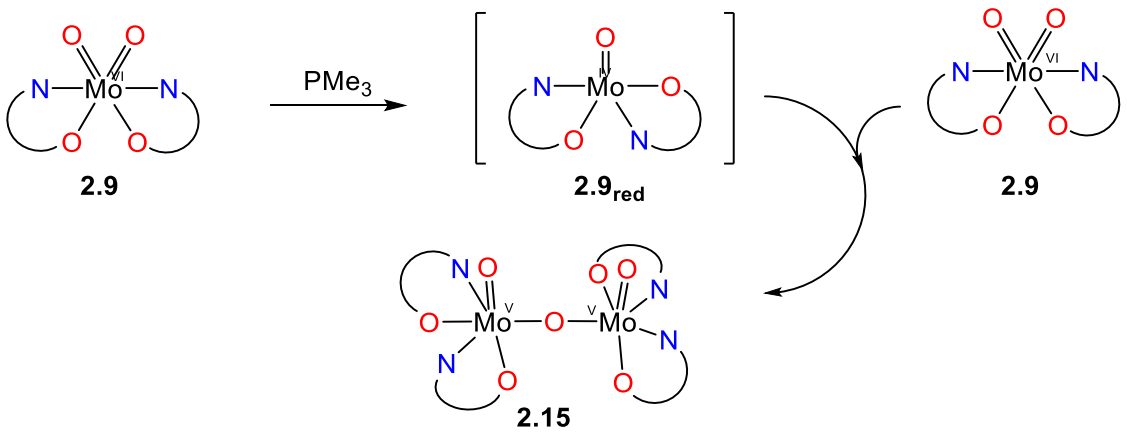

Figure 2.21 Proposed mechanism for dimer formation.

2.2.8 C=C Epoxidation

The biomimetic reduction of DMSO is useful to gauge the complexes ability to undergo redox reactions and maintain solution stability, but a more impactful reaction is the epoxidation of alkenes. The current industrial epoxidation reactions by Mo complexes require the use of heat and pressure.[19] The use of distorted metal centers and electronically tunable amidate ligands could allow for the development of an effective epoxidation catalyst that can operate at room temperature.

To probe the efficacy of the amidate ligand framework towards alkene epoxidation, complexes **2.8**-**2.14** were screened for the catalytic epoxidation of four different alkene substrates: *cis*-cyclooctene (**S1**), norbornene (**S2**), styrene (**S3**), and 1-octene (**S4**) (Scheme 2.6). Tertbutylhydroperoxide (TBHP) was chosen as the oxidant for these catalyst studies. Stock solutions of olefin (0.15 M), mesitylene standard (0.075 M), and TBHP (0.30 M) in DCE were prepared. To an aliquot of solution was added the precatalyst at 1 mol% loading, and the resulting solution was heated for 1 h. The reaction

was quenched by adding an excess of MnO_2 powder. The % conversion results are based on the disappearance of the starting olefin peak in the GC-MS spectrum.

The epoxidation of cis-cyclooctene is well-studied as an initial benchmark substrate for epoxidation catalysts.[11-12] Mo precatalysts featuring multidentate chelates, bridged metal centers, and various oxidation states have been shown to be catalytically active in this epoxidation reaction. [11-12] Our system features a distorted metal center, hemilabile ligand capability, and an electron deficient metal center, which we sought to exploit for the epoxidation reaction.

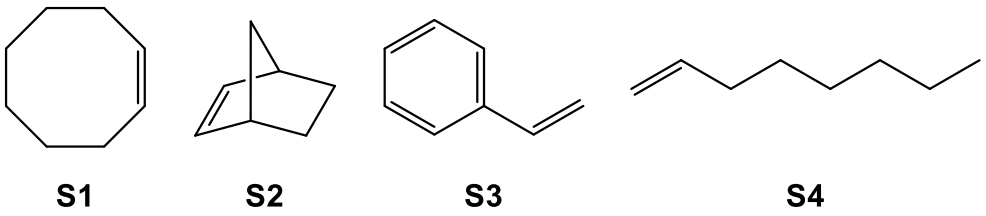

Scheme 2.6 Substrates for epoxidation studies.

The epoxidation of *cis*-cyclooctene (**S1**) by complexes **2.8**-**2.14** proceeds to quantitative completion at 80°C for all precatalysts, except **2.11**, with chemospecific formation of the epoxide, with no other products generated. These results are comparable to other reported bidentate ligand systems.[62, 71-74] For the series of *N*-diisopropylphenyl substituted complexes **2.12**-**2.14**, the catalytic activity at room temperature decreases as the ligands become more electron withdrawing. For the series of complexes bearing the ^{t}Bu substituted backbone, **2.8**, **2.9**, and **2.12**, the reactivity is highest with the least bulky of the series. This is likely due to the ability of complex **2.8** to accommodate a higher coordination number, or the ease of hemilability of the amidate ligands in this case.

For the epoxidation of norbornene, trends in reactivity are less noticeable. The reaction proceeds at room temperature, reaching up to 64% completion in one hour (**2.9**), while at 80 °C the reaction nears completion (91% completion, complex **2.12**). All of the dioxo complexes exhibit 100% selectivity for the epoxide product, with no evidence of alternate product formation. As was observed for *cis*-cyclooctene, the precatalysts with ^{t}Bu groups in the backbone of the amidate lead to higher yields, but the differences are small.

For the more challenging epoxidation of styrene (**S3**), all catalysts perform essentially the same regardless of temperature or ligand, with the exception that complex **2.8** is notably worse than the others. There are 2 products formed during the reaction of styrene and TBHP in the presence of the bis(amidate) dioxo precatalysts, the anticipated epoxide and the alcohol as determined by the mass spectrum. The selectivity could not be determined.

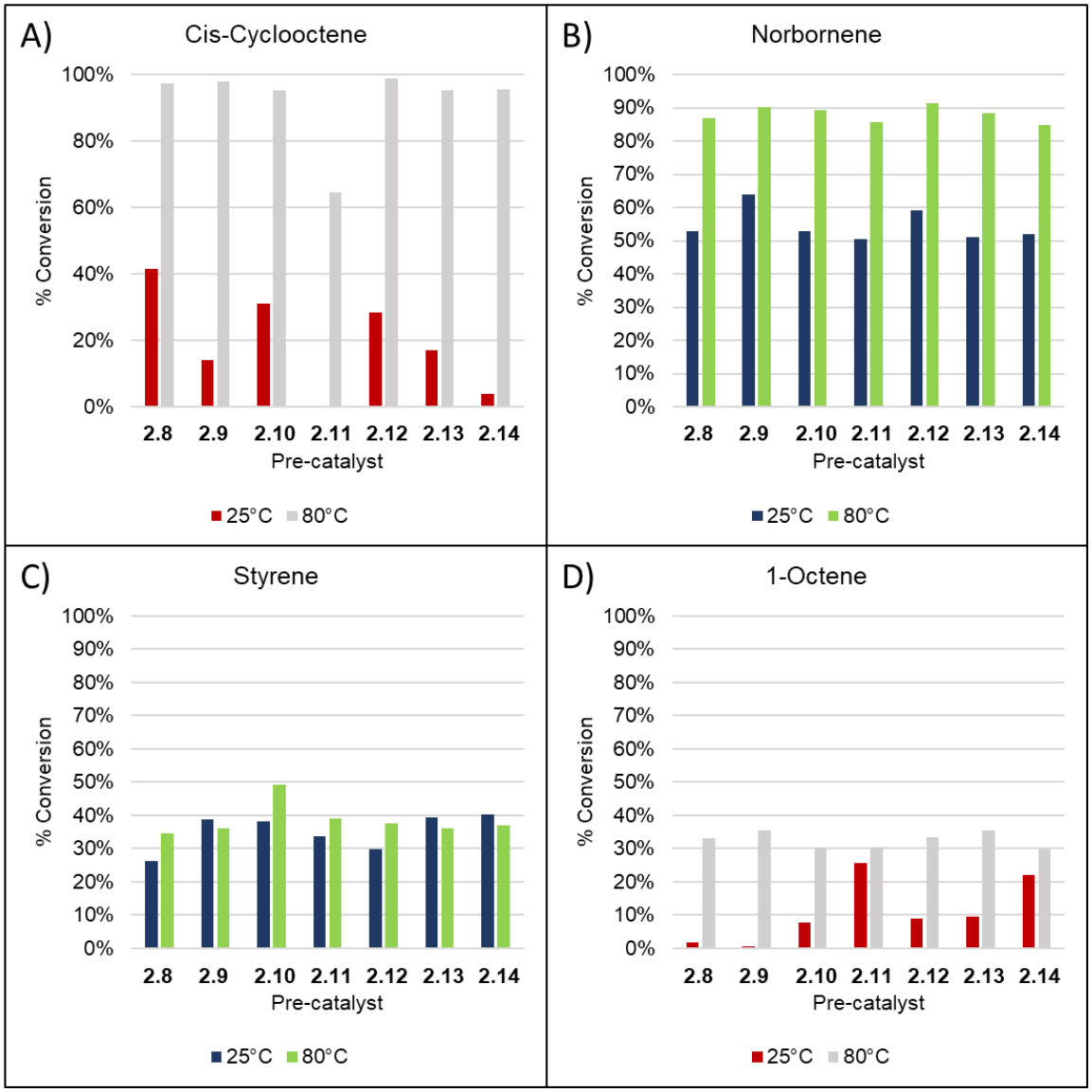

Figure 2.22. Epoxidation of cis-cylcooctene (**A**), norbornene (**B**), styrene (**C**), and 1-octene (**D**) in 1,2 dichloroethane at 25 °C and 80 °C by Mo(VI) dioxo bis-amidate precatalysts at 1% catalyst loading.

The most difficult substrate 1-octene (S4) was epoxidized at 80°C by all of the precatalysts, with approximately 30-35% conversion after 1 hour. However, at room temperature the more electron deficient metal centers (**2.11** and **2.14**) perform the best, and are almost as effective as they are 80°C, with 22-26% conversion after 1 hour. The

complexes **2.10**, **2.12**, and **2.13** also enable catalytic epoxidation at room temperature, converting S4 to the epoxide, but in only 8-9% conversion. The increased electron withdrawing nature of the ligand can be considered as the cause of this increased reactivity, but it somehow negatively impacts the epoxidation of *cis*-cyclooctene. The reasoning for the contrast in reactivity results could be partly due to loss of the amidate ligand during reaction. The *cis*-cyclooctene substrate is bulkier and could be forcing an amidate ligand to become labile, while the 1-octene molecule is less bulky allowing for the amidate ligand to remain bound in some fashion. The PFP derivatives are observed to have the weakest interaction with the Mo center due to their electron withdrawing character, so it is feasible that these ligands are the easiest to displace. It is also of note that the bulkier complex **2.12** reacts more quickly than the less bulky DMP and DIPP systems. This can be an example of the steric bulk of the ligand protecting the active catalyst from decomposition *in situ*. The epoxide is detected along with multiple other byproducts of the epoxidation reaction, thus selectivity cannot be determined for these reactions.

Table 2.12. Tabulated % conversion values for epoxidation reactions by dioxo precatalysts.

	Cis-cyclooctene		Norbornene		Styrene		1-Octene	
Precatalyst	25°C	80°C	25°C	80°C	25°C	80°C	25°C	80°C
2.8	**41%**	97%	53%	87%	26%	35%	2%	33%
2.9	14%	98%	**64%**	90%	**39%**	36%	1%	35%
2.10	31%	95%	53%	89%	**38%**	49%	8%	30%
2.11	0%	65%	51%	86%	34%	39%	**26%**	30%
2.12	**28%**	99%	**59%**	91%	30%	38%	9%	33%
2.13	17%	95%	51%	89%	**39%**	36%	9%	35%
2.14	4%	96%	52%	85%	**40%**	37%	**22%**	30%

2.3 Summary and Conclusions

Bis(amidate) complexes of Mo(VI) featuring two oxo ligands can be synthesized readily by salt metathesis, using Cl_2MoO_2(DME) as a starting material. These complexes exhibit solubility in a variety of solvents, and have been characterized in both the solid-state and in solution. These dioxo amidate complexes of Mo are stable under inert conditions for long periods of time, and have demonstrated applications in oxo group transfer reactions, and are suitable for the epoxidation of a range of reactive alkenes (*cis*-cyclooctene and norbornene); however, they do not perform well with more challenging substrates such as 1-octene and styrene.

Density functional theory calculations have been applied to the expected isomers of the bis(amidate) complexes to better understand the bonding in the complexes. Computational studies have shown that the ligands have the potential to become hemilabile under the right conditions, thus indicating the possibility of exploiting the reactivity of the Mo complexes using higher temperatures, coordinating solvents, etc.

2.4 Experimental

2.4.1 General Considerations

All synthetic procedures were carried out under dry N_2 using a VAC Atmospheres Nexus II glovebox. All solvents were purified using a VAC Atmospheres solvent purification system and stored in a glovebox over 4Å molecular sieves prior to use. Benzene-d_6 and toluene-d_8 were dried over 4Å molecular sieves and stored in a glovebox until use. All other reagents were purchased from commercial sources and used as received. ^{1}H, $^{13}C\{^{1}H\}$, ^{31}P and ^{19}F nuclear magnetic resonance (NMR) spectroscopic data were collected on a Varian Mercury VX 300 MHz NMR spectrometer or a Varian VNMRS 400 MHz spectrometer at ambient temperature unless otherwise stated. Chemical shifts are all referenced against residual protio solvent peaks. Infrared spectra were collected using attenuated total reflectance (ATR) on a Thermo Scientific Nicolet 6700 FT-IR spectrophotometer. Amide proligands[4] were prepared using literature procedures. Elemental analyses were performed by Midwest Microlab, LLC. GCMS data were collected on an Agilent 7890A Gas Chromatograph, an Agilent 5975C MSD with an Electron Impact (EI) ionization source, and a Chem Station instrument control and data handling system with a NIST 2008 database library (Agilent Technologies, Inc. Santa Clara, CA, USA).

Starting reagents and materials were used as received from Sigma Aldrich or Strem Chemicals. The molybdenum starting material, Cl_2MoO_2(DME) was prepared according to published procedures.[60] The amide proligands were prepared using literature

procedures.[26] The ^{1}H NMR spectral data for the proligands is provided for comparative purposes to the Mo complexes in this work.

[^{Ph}(NO)^{tBu}]H (2.1).

^{1}H NMR (400 MHz, Benzene-d_6) δ 1.04 (s, 9H, C-(CH_3)$_3$), 6.90 (s, 1H, N-*H*), 6.99 (s, 1H, Ar-*H*), 7.09 – 7.15 (m, 2H, Ar-*H*), 7.55 – 7.62 (m, 2H, Ar-*H*).

[^{DMP}(NO)^{tBu}]H (2.2)

^{1}H NMR (400 MHz, Benzene-d_6) δ 1.09 (s, 9H, C-(CH_3)$_3$), 2.04 (s, 6H, Ar-(CH_3)$_2$), 6.42 (s, 1H, N-*H*), 6.91 (s, 1H, Ar-*H*), 6.93 (s, 1H, Ar-*H*), 6.99 (d, *J* = 14.8 Hz, 1H, Ar-*H*).

[^{DMP}(NO)^{Ph}]H (2.3)

^{1}H NMR (400 MHz, Benzene-d_6) δ 2.12 (s, 6H, Ar-(CH_3)$_2$), 6.62 (s, 1H, N-*H*), 6.99 (s, 3H, Ar-*H*), 7.04 (dd, *J* = 8.6, 6.2 Hz, 1H, Ar-*H*), 7.10 (s, 3H, Ar-*H*), 7.73 (dd, *J* = 7.4, 1.9 Hz, 2H, Ar-*H*).

[^{DMP}(NO)^{PFP}]H (2.4)

^{1}H NMR (400 MHz, Benzene-d_6) δ 2.15 (s, 6H, Ar-(CH_3)$_2$), 5.93 (s, 1H, N-*H*), 6.91 (d, *J* = 7.5 Hz, 2H, Ar-*H*), 6.99 (t, *J* = 8.4 Hz, 1H, Ar-*H*). ^{19}F NMR (376 MHz, Benzene-d_6) δ -161.17 – -160.83 (m, 2F), -152.99 (t, *J* = 21.4 Hz, 1F), -141.46 – -141.28 (m, 2F).

[^{DIPP}(NO)^{tBu}]H (2.5)

^{1}H NMR (400 MHz, Benzene-d_6) δ 1.13 (s, 9H, C-(CH_3)$_3$), 1.21 (d, J = 6.9 Hz, 12H, CH-(CH_3)$_3$), 3.08 (s, 2H, CH-(CH$_3$)$_3$), 6.24 (s, 1H, N-H), 7.11 (d, J = 7.6 Hz, 2H, Ar-H), 7.21 (t, J = 7.8 Hz, 1H, Ar-H).

[^{DIPP}(NO)^{Ph}]H (2.6)

^{1}H NMR (400 MHz, Benzene-d_6) δ 1.20 (d, J = 6.9 Hz, 12H, CH-(CH_3)$_3$), 3.15 (s, 2H, CH-(CH$_3$)$_3$), 6.81 (s, 1H, N-H), 7.07 (dd, J = 8.5, 6.5, 1.6 Hz, 2H, Ar-H), 7.13 (d, J = 9.8 Hz, 2H, Ar-H), 7.24 (d, J = 7.6 Hz, 1H, Ar-H), 7.73 (d, J = 6.8 Hz, 2H, Ar-H).

[^{DIPP}(NO)^{PFP}]H (2.7)

^{1}H NMR (400 MHz, Benzene-d_6) δ 1.26 (d, J = 6.9 Hz, 12H, CH-(CH_3)$_3$), 3.17 (sept., J = 7.0 Hz, 2H, CH-(CH$_3$)$_3$), 5.99 (s, 1H, N-H), 7.09 (s, 2H, Ar-H), 7.21 (d, J = 15.4 Hz, 1H, Ar-H). ^{19}F NMR (376 MHz, Benzene-d_6) δ -160.76 (td, J = 21.8, 6.7 Hz, 2F), -152.84 (t, J = 21.3 Hz, 1F), -141.50 (d, J = 15.1 Hz, 2F).

2.4.2 Synthesis

Standard deprotonation protocol. [^{R}(NO)$^{R'}$]H is dissolved in an appropriate amount of THF. A vial is charged with 1 eq of NaN(SiMe$_3$)$_2$. The sodium amide is dissolved in THF. The two solutions are mixed and stirred at ambient temperature for 2 hours. The volatiles are removed *in vacuo* and the resulting [^{R}(NO)$^{R'}$]Na salt is used immediately without further purification.

Synthesis of $[^{Ph}(NO)^{tBu}]_2MoO_2$ (2.8)

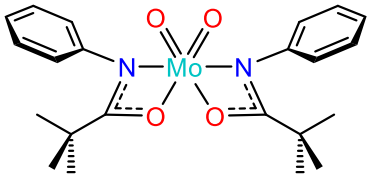

$[^{Ph}(NO)^{tBu}]Na$ (3.76 mmol, 2 eq.) was dissolved in ca. 20 mL of THF and cooled to -100 °C. In a scintillation vial 0.544 g (1.88 mmol, 1 eq.) of $O_2MoCl_2(DME)$ was dissolved in ca. 5 mL of THF and cooled to -100°C. After both solutions were at -100°C, the metal starting material solution was added to the flask containing the stirring solution of the amidate salt. The solution was allowed to warm to r.t. and react for 2 h. After 2 h the solvent was removed *in vacuo* from the pale green suspension. The pale green/tan solid was suspended in toluene and filtered over celite yielding a transparent tan solution. The solvent was removed to afford 71% (0.644 g) of tan product. Crystals were grown from slow evaporation from a 1:1 DCM/hexane solution. FTIR(ATR) (cm^{-1}): 3310.6, 3064.4, 2966.1, 2869.5, 1654.9, 1594.5, 1480.9, 1435.3, 1362.1, 1316.8, 1244.2, 1186.2, 1070.9, 1027.6, 947.06, 916.62, 844.55, 783.89, 751.06, 695.54, 590.21, 533.24. ^{1}H NMR (400 MHz, C_6D_6, 25°C): δ 1.01 (s, 18H, C(C*H*$_3$)$_3$), 6.85 (t, 2H, *p*-Ar-*H*), 6.96 (m, 4H, *m*-Ar-*H*), 7.14 (d, 4H, *o*-Ar-*H*). ^{13}C{^{1}H} NMR (101 MHz, C_6D_6, 25°C): δ 27.33, 40.88, 126.03, 129.49, 128.59, 144.77, 193.28.

Synthesis of $[^{DMP}(NO)^{tBu}]_2MoO_2$ (2.9)

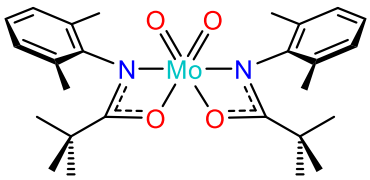

$[^{DMP}(NO)^{tBu}]Na$ (2.4 mmol, 2 eq.) was dissolved in 40 mL of THF and cooled to -35°C. In a scintillation vial 0.352 g (1.2 mmol, 1 eq.) of $O_2MoCl_2(DME)$ was dissolved in 15 mL of THF and cooled to -35°C. After both solutions were at -35°C the metal starting material solution was added to the flask containing the stirred solution of

ligand salt. The solution was allowed to warm to r.t. and react for 24 h. After 24 h the solvent was removed *in vacuo* from the pale green suspension. The pale green/tan solid was suspended in toluene and filtered through celite yielding a transparent tan solution. The solvent was removed to afford 87% (0.567 g) of tan product. Crystals were grown from slow evaporation of a toluene solution. FTIR(ATR) (cm^{-1}): 3271.1, 3023.8, 2956.2, 2920.4, 2868.4, 2736.2, 1648.5, 1583.9, 1471.1, 1429.7, 1360.8, 1244.1, 1218.9, 1185.9, 1093.5, 1058.3, 1029.3, 941.15, 912.16, 837.56, 774.69, 674.16, 607.13, 575.91, 532.68. *).* ^{1}H NMR (400 MHz, C_6D_6, 25°C): δ 0.99 (s, 18H, C(C*H*$_3$)$_3$), 2.46 (s, 12H, Ar(C*H*$_3$)$_2$), 6.82 (br s, 6H, Ar-*H).* ^{13}C{^{1}H} NMR (101 MHz, C_6D_6, 25°C) δ 19.19, 27.17, 41.25, 127.20, 128.48, 134.04, 142.90, 193.85. Anal. Calcd. for $C_{26}H_{36}MoN_2O_4$: C, 58.20; H, 6.76: N, 5.22. Found: C, 58.42; H, 7.01; N, 5.22.

Synthesis of [^{DMP}(NO)^{Ph}]$_2$MoO$_2$ (2.10)

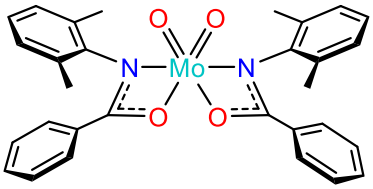

[^{DMP}(NO)^{Ph}]Na (3.95 mmol, 2 eq.) was dissolved in ca. 20 mL of THF. In a scintillation vial 0.570 g (1.974 mmol, 1 eq.) of O_2MoCl_2(DME) was dissolved in ca. 5 mL of THF. The metal starting material solution was added to the flask containing the stirred solution of sodium amidate salt at r.t. and stirred for 2 h. After 2 h the solvent was removed *in vacuo* from the pale green suspension. The pale green/tan solid was suspended in toluene and filtered over celite yielding a transparent tan solution. The solvent was removed to afford 60% (0.684 g) of tan product. Crystals were grown from slow evaporation of a 1:1 Et_2O/toluene solution. FTIR(ATR) (cm^{-1}): 3898, 3851.5, 3800.1, 3731.6, 3709.1, 3673.9, 3647.1, 3585.7, 3564.6, 3273.1, 3058, 3020, 2953, 2920.5, 2858,

2742.1, 2627.5, 2595.6, 2330.7, 2182.2, 2028, 1992.8, 1960.5, 1930, 1856.2, 1808.7, 1773.7, 1643.8, 1599.2, 1469.9, 1299.5, 1262.1, 1233.3, 1179.5, 1123, 1090.8, 1026.3, 990.41, 940.39, 913.46, 840.36, 802.14, 765.3, 708.63, 636.63, 591.42, 555.14. ^{1}H NMR (400 MHz, C_6D_6, 25°C): δ 2.51 (s, 12H, Ar(CH_3)$_2$), 6.74 (t, 4H, *p*-Ar-*H*), 6.90 (br s, 8H, *m*-Ar-*H*, 7.62 (d, 4H, *o*-Ar-*H*). ^{13}C{^{1}H} NMR (101 MHz, C_6D_6) δ 18.59, 127.17, 128.18, 128.76, 128.90, 130.65, 132.92, 133.55, 142.48, 181.40.

Synthesis of [^{DMP}(NO)^{PFP}]$_2$MoO$_2$ (2.11)

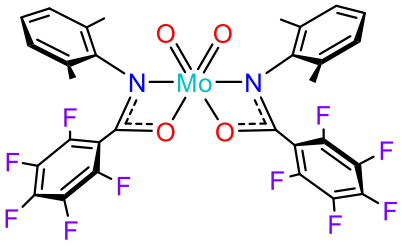

[^{DMP}(NO)^{PFP}]Na (2.34 mmol, 2 eq.) was dissolved in ca. 20 mL of THF and cooled to -35 °C. In a scintillation vial 0.338 g (2.17 mmol, 1 eq.) of O_2MoCl_2(DME) was dissolved in ca. 5 mL of THF and cooled to -35°C. After both solutions were at -35°C the metal starting material solution was added to the flask containing the stirred solution of amidate salt. The solution was allowed to warm to r.t. and react for 13 h. After 13 h the solvent was removed *in vacuo* from the pale green suspension. The pale green/tan solid was suspended in toluene and filtered over celite yielding a transparent tan solution. The solvent was removed to afford 87% (0.770 g) of tan product. FTIR(ATR) (cm^{-1}): 3889.8, 3851.8, 3800.5, 3733.5, 3709.5, 3674.3, 3647.8, 3023.8, 2962.5, 2928.6, 2868.8, 2408.2, 1653.5, 1517.9, 1475.6, 1380.8, 1329.6, 1257.4, 1217.4, 1167.2, 1109.8, 993.01, 959.08, 920.74, 874.7, 812.71, 768.22, 732.41, 694.4, 637.82, 580.43, 521.09. ^{1}H NMR (400 MHz, C_6D_6, 25°C): δ 2.51 (s, 12H, Ar(CH_3)$_2$), 6.77 (br s, 6H, Ar-*H*). ^{19}F NMR (376 MHz, C_6D_6, 25°C): δ -159.61 (t, 2F, *p*-Ar-*F*), -146.53 (dd 4F, *m*-Ar-*F*), -136.62 (dd, 4F, *o*-Ar-*F*). ^{13}C{^{1}H} NMR (101

MHz, C_6D_6, 25°C): δ 17.95, 18.22, 21.01, 125.29, 128.71, 128.92, 133.88, 137.49, 139.39, 175.33.

Synthesis of $[^{DIPP}(NO)^{tBu}]_2MoO_2$ (2.12)

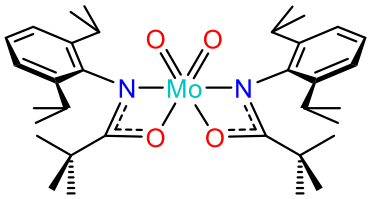

$[^{DIPP}(NO)^{tBu}]Na$ (4.87 mmol, 2 eq.) was dissolved in ca. 20 mL of THF. In a scintillation vial 0.703 g (2.43 mmol, 1 eq.) of $O_2MoCl_2(DME)$ was dissolved in ca. 5 mL of THF. The metal starting material solution was added to the flask containing the stirred solution of amidate ligand salt at r.t. and stirred for 12 h. After 12 h the solvent was removed *in vacuo* from the pale green suspension. The pale green/tan solid was suspended in toluene and filtered over celite yielding a transparent tan solution. The solvent was removed to afford 80% (1.260 g) of tan product. Crystals were grown by slow evaporation of a toluene solution. FTIR(ATR) (cm^{-1}): 3313.9, 2962.9, 2926.5, 2867.5, 1647.1, 1463.8, 1429.3, 1362.3, 1326.4, 1233.3, 1172.6, 1103.8, 1056.3, 942.12, 915.89, 846.56, 805.15, 770.88, 737.26, 681.76, 631.36, 590.72, 524.68. ^{1}H NMR (400 MHz, C_6D_6, 25°C): δ 1.07 (s, 18H, C(CH_3)$_3$), 1.22 (d, 12H, CH(CH_3)$_2$), 1.59 (d, 12H, CH(CH_3)$_2$), 3.54 (br s, 4H, C*H*(CH_3)$_2$), 7.02 (m, 6H, Ar-*H*). ^{13}C{^{1}H} NMR (101 MHz, c_6d_6) δ 22.24, 23.34, 25.69, 27.26, 28.28, 41.31, 123.43, 139.46, 143.99, 193.28.

Synthesis of $[^{DIPP}(NO)^{Ph}]_2MoO_2$ (2.13)

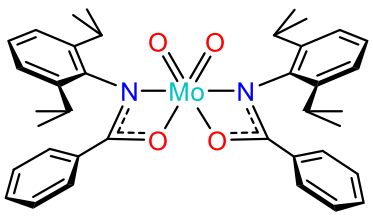

$[^{DIPP}(NO)^{Ph}]Na$ (3.71 mmol, 2 eq.) was dissolved in ca. 20 mL of THF. In a scintillation vial 0.535 g (1.85 mmol, 1 eq.) of $O_2MoCl_2(DME)$ was dissolved in ca. 5 mL of THF. The metal starting material solution was added to the flask containing the

stirred solution of ligand salt at r.t. and stirred for 12 h. After 12 h the solvent was removed *in vacuo* from the pale green suspension. The pale green/tan solid was suspended in toluene and filtered over celite yielding a transparent tan solution. The solvent was removed to afford 97% (1.234 g) of tan product. FTIR(ATR) (cm^{-1}): 3269.2, 3063.1, 2963, 2926.9, 2867.1, 1642.5, 1600.5, 1505, 1457.8, 1423.9, 1383, 1328, 1301.6, 1254, 1216.4, 1181.1, 1097.2, 1056, 1027.2, 942.88, 918.02, 844.77, 779.1, 746.22, 702.81, 623.19, 560.78. ^{1}H NMR (400 MHz, C_6D_6, 25°C): δ 0.96 (d, 12H, CH(CH_3)$_2$), 1.59 (d, 12H, CH(CH_3)$_2$), 3.83 (br s, 4H, CH(CH_3)$_2$), 6.76 (t, 4H, Ar-*H*), 6.90 (t, 2H, Ar-*H*), 7.12 (m, 6H, N-Ar-*H*), 7.75 (d, 4H, Ar-*H*). ^{13}C{^{1}H} NMR (101 MHz, c_6d_6) δ 23.06, 24.66, 28.47, 124.26, 128.26, 129.92, 130.24, 132.94, 139.76, 143.85, 181.70.

Synthesis of [^{DIPP}(NO)^{PFP}]$_2$MoO$_2$ (2.14)

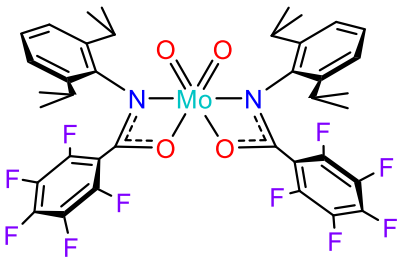

[^{DIPP}(NO)^{PFP}]Na (1.78 mmol, 2 eq.) was dissolved in ca. 20 mL of THF. In a scintillation vial 0.257 g (0.89 mmol, 1 eq.) of O_2MoCl_2(DME) was dissolved in ca. 5 mL of THF. The metal starting material solution was added to the flask containing stirred ligand salt at r.t. and stirred for 1 h. After 1 h the solvent was removed *in vacuo* from the pale green suspension. The pale green/tan solid was suspended in toluene and filtered over celite yielding a transparent tan solution. The solvent was removed to afford 91% (0.700 g) of tan product. Crystals were grown by slow evaporation from a 1:1 DCM/hexane solution. FTIR(ATR) (cm^{-1}): 3184.3, 3064.4, 3022.7, 2967.1, 2930.2, 2870.4, 2726.2, 1654.1, 1590.1, 1515.5, 1462.5, 1384.1, 1327.8, 1245.2, 1200.9, 1147.8, 1100.2, 1054.9, 991.92, 962.12, 931.4, 874.51,

801.49, 731.11, 693.67, 643.27, 584.29, 547.12. ^{1}H NMR (400 MHz, C_6D_6, 25°C): δ 1.11 (d, 12H, CH(CH_3)$_2$), 1.60 (d, 12H, CH(CH_3)$_2$), 3.64 (br s, 4H, CH(CH$_3$)$_2$), 6.95 (m, 6H, Ar-*H).* ^{19}F NMR (376 MHz, C_6D_6, 25°C): δ -159.87 (t, 2F, *p*-Ar-*F*), -147.67 (t, 4F, *m*-Ar-*F*), -136.74 (t, 4F, *o*-Ar-*F*). ^{13}C NMR (101 MHz, c_6d_6) δ 22.06, 23.42, 25.69, 28.30, 28.73, 123.51, 123.91, 129.26, 136.26, 144.80, 175.81.

Synthesis of ([^{DMP}(NO)^{tBu}]$_2$Mo(O))$_2$(μ-O) (2.15)

Complex **2.9** (35 mg, 1 eq) was dissolved in 2 mL of D_6-benzene. An excess of PMe_3 (8 mg, 1.6 eq) was added to the stirring solution. After about 30 mins the solution began to turn red. After 24 h the solution was a dark red brown slurry. A ^{1}H NMR spectrum was collected from an aliquot of the solution and was found to be NMR silent. Solvent was removed from the remainder of the reaction slurry affording a dark red residue. The red solid residue was recrystallized from a solution of THF/hexane in a 1:1 ratio.

Alternative Deprotonation Protocols

Amide deprotonation with MeLi. A vial was charged with 0.811 g (3.6 mmol) of [^{DMP}(NO)^{tBu}]H (**2.2**), which was dissolved in ca. 5 mL of THF. The solution was chilled in a freezer at -30 °C. To the cold ligand solution, 2.17 mL of MeLi solution (1.6M in Et_2O) was added quickly. The solution was stirred for 1 hour and the volatiles were removed *in vacuo*. The isolated salt [^{DMP}(NO)^{tBu}]Li was dissolved in THF and chilled to -30 °C. In another vial 0.520 g (0.67 mmol) of Cl_2MoO_2(DME) was added and dissolved in THF. The metal solution was added to the stirring salt solution and was

allowed to warm to room temperature. After 18 hours, the volatiles were removed from the tan solution. The isolated tan solid was suspended in toluene and filtered over celite, 0.073 g (20%) of tan solid (**2.9**) was isolated after removal of solvent.

Amide deprotonation with lithium dimethyl amide (LDA). A vial was charged with 0.104 g (0.46 mmol) of [^{DMP}(NO)^{tBu}]H (**2.2**), which was dissolved in ca. 4 mL of THF. To another vial 0.023 g (0.45 mmol) of $LiNMe_2$ was added and dissolved in ca. 4 mL of THF. The two solutions were mixed and stirred for 2 hours at ambient temperature and the volatiles were removed *in vacuo*. The isolated salt [^{DMP}(NO)^{tBu}]Li was dissolved in THF and chilled to -30 °C. In another vial 0.061 g (0.21 mmol) of Cl_2MoO_2(DME) was added and dissolved in THF. The metal solution was added to the salt solution and stirred, warming to room temperature, initially turning a light green color. After 24 hours, the volatiles were removed from the resultant red/brown solution. The brown solid isolated was suspended in toluene and filtered over celite in toluene. A brown solid (**2.9** + impurities) was isolated after removal of solvent.

Amide deprotonation with $KN(SiMe_3)_2$. A small flask was charged with 0.500 g (2.43 mmol) of [^{DMP}(NO)^{tBu}]H (**2.2**), which was dissolved in ca. 10 mL of THF. To a 20 mL vial 0.488 g (2.43 mmol) of $KN(SiMe_3)_2$ was added and dissolved in ca. 10 mL of THF. The two solutions were mixed and stirred for 2 hours at ambient temperature and the volatiles were removed *in vacuo*. The isolated salt [^{DMP}(NO)^{tBu}]K was dissolved in THF and chilled to -30 °C. In another vial 0.352 g (1.22 mmol) of Cl_2MoO_2(DME) was added and dissolved in THF. The metal solution was added to the stirring salt solution and allowed to warm to room temperature. After 18 hours, the volatiles were removed from the resultant red/brown solution. The brown solid isolated was suspended in toluene

and filtered over celite. A brown solid (**2.9** + impurities) was isolated after removal of solvent.

Amide deprotonation with KH. Many different variations of this reaction were attempted, but the following method yielded the purest product. A 100 mL Schlenk flask charged with 1.071 g (5.21 mmol) of [^{DMP}(NO)^{tBu}]H (**2.2**), 0.209 g (5.21 mmol) of KH, and 25 mL of THF was equipped with a condenser on the Schlenk line. The system was maintained under N_2 throughout the reaction. The mixture was stirred and refluxed at 73 °C for 18 hours. The solvent was removed *in vacuo* to isolate [^{DMP}(NO)^{tBu}]K. 0.100 g (0.41 mmol) of [^{DMP}(NO)^{tBu}]K was slurried in ca. 3 mL of toluene and stirred. A solution of 0.059 g (0.21 mmol) of Cl_2MoO_2(DME) in ca. 3 mL toluene was added slowly to the stirring mixture. 1 mL of THF was added to increase solubility. The reaction was stirred for 24 h and the volatiles were removed. The dark brown solid was suspended in hexanes and filtered over a celite plug. The solvent was removed to afford 0.019 g (17%) of tan product (**2.9**).

Preparation of **2.2-SiMe$_3$**. A 50 mL vacuum flask was charged with 1.00 g (4.80 mmol) of [^{DMP}(NO)^{tBu}]H (**2.2**) and 10 mL of diethyl ether. The solution was chilled to -100 °C. To the stirring solution, 3.04 mL (4.80 mmol) of 1.6 M MeLi solution was added quickly and stirred for 1 h. After 1 h, 0.61 mL (4.80 mmol) of $ClSiMe_3$ was added and the mixture was stirred for 18 h at r.t. After 18 h the volatiles were removed *in vacuo*. The off-white solid material was suspended in toluene and filtered through celite, 0.944 g (71%) of colorless product was obtained.

Synthesis of [^{DMP}(NO)^{tBu}]$_2$MoO$_2$ (**2.9**) *via ClSiMe$_3$ elimination.* A 20 mL vial was charged with 0.944 g (3.40 mmol) of [^{DMP}(NO)^{tBu}]SiMe$_3$ (**2.2-SiMe$_3$**), 0.492 g (1.70

mmol) of Cl_2MoO_2(DME), and ca. 10 mL of toluene. The solution was heated to 90 °C and stirred for 18 h. After 18 h the solution was cooled to r.t. and the solution was filtered over celite. The remaining volatiles were removed *in vacuo* yielding 0.352 g (39%) of $[^{DMP}(NO)^{tBu}]_2MoO_2$ (**2.9**).

2.4.3 Reactivity Studies

General Procedure for DMSO Reductions

A small vial was charged with a magnetic stir bar and precatalyst complex (0.05 or 0.10 eq). The catalyst was then dissolved in ca. 2 mL D_6-DMSO. Trimethylphosphine (1 eq) was added, and the solution was stirred and heated to 85°C, with aliquots taken after 1 h and 3 h of reaction. ^1H and ^{31}P NMR spectra of these aliquots were acquired as soon as the aliquots were collected.

General Procedure for the Epoxidation of Alkenes

A stock solution of olefin (0.15 M), mesitylene standard (0.075 M), and tertbutylhydroperoxide (TBHP) (0.30 M) in DCE was prepared. To an aliquot of solution was added the precatalyst at 1 mol% loading, and the resulting solution was heated for 1 h. The reaction was quenched by adding an excess of MnO_2 powder. Samples were analyzed by GCMS, with all mass spectra acquired in EI mode with full scan. Ultra-High Purity Helium carrier gas was set to a column head pressure of 12.5 psi maintaining a constant flow rate of 1.0 mL/min. Aliquots of 1 μL were injected into the instrument with

a 25:1 split and a detector delay of 3 min. GC separations were done with a Agilent Technologies HP-5 column (30 m, 0.25 mm i.d. and 0.25 μm thickness) programmed to start at 40°C with a 5 min hold, then linear ramp to 250°C at 20°C/min with a 10 min hold at 250°C. MS conditions were as follows: 230°C source, 150°C quadrupole, 150°C interface, 240°C injector and EM voltage of 1.04kV. Full scans were collected over the mass range of 25-500 at 2.86 scans/sec. Compound identification was verified by comparison of sample spectra to spectra available in the NIST08 library.

2.4.4 X-ray Crystallographic Studies

X-ray diffraction data were collected for complexes **2.8**, **2.9**, **2.10**, **2.12**, and **2.14** on a diffractometer with a Bruker APEX CCD area detector[75-76] with graphite-monochromated Mo Kα radiation (λ = 0.71073 Å). Selected crystals were mounted using high vacuum grease or Paratone oil onto a cryoloop and cooled to the data collection temperature of 100 K. Cell parameters were determined from a non-linear least squares fit. The data were corrected for absorption by the empirical method[77] giving minimum and maximum transmission factors. The space groups were determined by systematic absences and statistical tests and verified by subsequent refinement. The structure was solved by direct methods and refined by full-matrix least-squares methods on F2.[78=79] The positions of hydrogens were initially determined by geometry and were refined using a riding model. Non-hydrogen atoms were refined with anisotropic displacement parameters. Hydrogen atom displacement parameters were set to 1.2 (1.5 for methyl) times the isotropic equivalent displacement parameters of the bonded atoms.

2.4.5 Theoretical Calculations

Density functional theory (DFT) calculations were carried out on the OU Supercomputing for Education and Research (OSCER) high performance computing system on Intel Xeon "Haswell" processors using the Gaussian09 suite of programs. Computational input files for various complexes were generated from their crystallographic structures in Gaussview. Geometry optimization was performed using the hybrid density-functional/Hartree-Fock method RB3LYP. For the Mo center in each calculation the LANL2DZ basis set was employed. For all other atoms the 6-311G(D) basis set was utilized. Initial guesses for the geometric isomers were prepared in Gaussview by rotation of the amidate ligand about the dihedral angle illustrated in Figure 2.30.

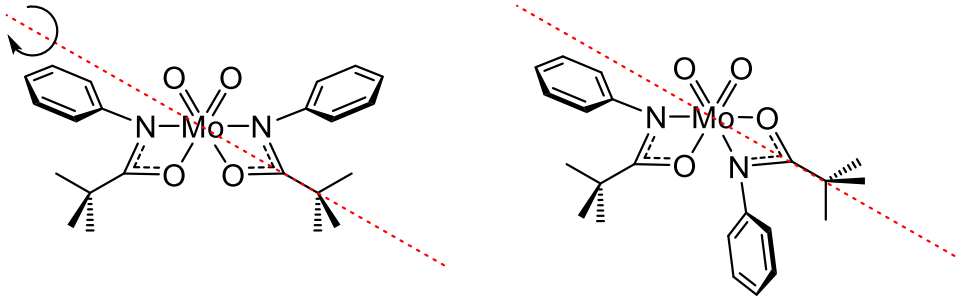

Figure 2.30 Illustration of the dihedral angle used to generate initial guesses for isomer calculations.

2.5 References

1. Holm, R. H., The biologically relevant oxygen atom transfer chemistry of molybdenum: from synthetic analogue systems to enzymes. *Coord. Chem. Rev.* **1990,** *100*, 183-221.
2. Sugimoto, H.; Tsukube, H., Chemical analogues relevant to molybdenum and tungsten enzyme reaction centres toward structural dynamics and reaction diversity. *Chem. Soc. Rev.* **2008,** *37* (12), 2609-2619.
3. Sanz, R.; Pedrosa, M. R., Applications of dioxomolybdenum(VI) complexes to organic synthesis. *Curr. Org. Chem.* **2009,** *6* (3), 239-263.
4. Majumdar, A.; Sarkar, S., Bioinorganic chemistry of molybdenum and tungsten enzymes: A structural-functional modeling approach. *Coord. Chem. Rev.* **2011,** *255* (9-10), 1039-1054.
5. Schulzke, C.; Ghosh, A. C., Molybdenum and tungsten oxidoreductase models. In *Bioinspired Catalysis: Metal-Sulfur Complexes*, 2014; pp 349-382.
6. Dethlefsen, J. R.; Lupp, D.; Teshome, A.; Nielsen, L. B.; Fristrup, P., Molybdenum-catalyzed conversion of diols and biomass-derived polyols to alkenes using isopropyl alcohol as reductant and solvent. *ACS Catal.* **2015,** *5* (6), 3638-3647.
7. Lupp, D.; Christensen, N. J.; Dethlefsen, J. R.; Fristrup, P., DFT study of the molybdenum-catalyzed deoxydehydration of vicinal diols. *Chem. Eur. J.* **2015,** *21* (8), 3435-3442.

8. Petersen, A. R.; Fristrup, P., New motifs in deoxydehydration: Beyond the realms of rhenium. *Chem. Eur. J.* **2017,** *23* (43), 10235-10243.

9. Jorgensen, K. A., Transition-metal-catalyzed epoxidations. *Chem. Rev.* **1989,** *89* (3), 431-458.

10. Pereira, C. C. L.; Balula, S. S.; Almeida Paz, F. A.; Valente, A. A.; Pillinger, M.; Klinowski, J.; Gonçalves, I. S., A highly efficient dioxo(μ-oxo)molybdenum(VI) dimer catalyst for olefin epoxidation. *Inorg. Chem.* **2007,** *46* (21), 8508-8510.

11. Hauser, S. A.; Cokoja, M.; Kühn, F. E., Epoxidation of olefins with homogeneous catalysts-*quo vadis*? *Catal. Sci. Technol.* **2013,** *3* (3), 552-561.

12. Kück, J. W.; Reich, R. M.; Kühn, F. E., Molecular epoxidation reactions catalyzed by rhenium, molybdenum, and iron complexes. *Chem. Rec.* **2016,** *16* (1), 349-364.

13. Berg, J. M.; Holm, R. H., A model for the active sites of oxo-transfer molybdoenzymes: Reactivity, kinetics, and catalysis. *J. Am. Chem. Soc.* **1985,** *107* (4), 925-932.

14. Magalon, A.; Fedor, J. G.; Walburger, A.; Weiner, J. H., Molybdenum enzymes in bacteria and their maturation. *Coord. Chem. Rev.* **2011,** *255* (9-10), 1159-1178.

15. Hille, R.; Nishino, T.; Bittner, F., Molybdenum enzymes in higher organisms. *Coord. Chem. Rev.* **2011,** *255* (9-10), 1179-1205.

16. Hille, R., The molybdenum oxotransferases and related enzymes. *Dalton Trans.* **2013,** *42* (9), 3029-3042.

17. Hille, R.; Hall, J.; Basu, P., The mononuclear molybdenum enzymes. *Chem. Rev.* **2014,** *114* (7), 3963-4038.

18. Coughlan, M. P., *Molybdenum and Molybdenum-Containing Enzymes*. Elsevier Science: Kent, 2014.

19. Baer, H.; Bergamo, M.; Forlin, A.; Pottenger, L. H.; Lindner, J., Propylene Oxide. In *Ullmann's Encyclopedia of Industrial Chemistry*, 2012.

20. Shylesh, S.; Jia, M.; Thiel, W. R., Recent progress in the heterogenization of complexes for single-site epoxidation catalysis. *Eur. J. Inorg. Chem.* **2010,** (28), 4395-4410.

21. Hossain, M. K.; Schachner, J. A.; Haukka, M.; Lehtonen, A.; Mösch-Zanetti, N. C.; Nordlander, E., Dioxidomolybdenum(VI) and -tungsten(VI) complexes with tripodal amino bisphenolate ligands as epoxidation and oxo-transfer catalysts. *Polyhedron* **2017,** *134*, 275-281.

22. Kaupp, M., Trigonal prismatic or not trigonal prismatic? On the mechanisms of oxygen-atom transfer in molybdopterin-based enzymes. *Angew. Chem. Int. Ed.* **2004,** *43* (5), 546-549.

23. Most, K.; Hoßbach, J.; Vidović, D.; Magull, J.; Mösch-Zanetti, N. C., Oxygen-transfer reactions of molybdenum- and tungstendioxo complexes containing η2-pyrazolate ligands. *Adv. Synth. Catal.* **2005,** *347* (2-3), 463-472.

24. Arumuganathan, T.; Volpe, M.; Harum, B.; Wurm, D.; Belaj, F.; Mösch-Zanetti, N. C., Unusual nonoctahedral geometry with molybdenum oxoimido complexes containing η2-pyrazolate ligands. *Inorg. Chem.* **2012,** *51* (1), 150-156.

25. Volpe, M.; Mösch-Zanetti, N. C., Molybdenum(VI) dioxo and oxo-imido complexes of fluorinated β-ketiminato ligands and their use in OAT reactions. *Inorg. Chem.* **2012,** *51* (3), 1440-1449.

26. Li, C.; Thomson, R. K.; Gillon, B.; Patrick, B. O.; Schafer, L. L., Amidate complexes of titanium and zirconium: a new class of tunable precatalysts for the hydroamination of alkynes. *Chem. Commun.* **2003,** (19), 2462-2463.

27. Thomson, R. K.; Patrick, B. O.; Schafer, L. L., Synthesis, characterization, and reactivity of the first hafnium alkyl complex stabilized by amidate ligands. *Can. J. Chem.* **2005,** *83* (6-7), 1037-1042.

28. Wood, M. C.; Leitch, D. C.; Yeung, C. S.; Kozak, J. A.; Schafer, L. L., Chiral neutral zirconium amidate complexes for the asymmetric hydroamination of alkenes. *Angew. Chem. Int. Ed.* **2006,** *46* (3), 354-358.

29. Fujita, K.-i.; Yamashita, M.; Puschmann, F.; Martinez Alvarez-Falcon, M.; Incarvito, C. D.; Hartwig, J. F., Organometallic chemistry of amidate complexes. Accelerating effect of bidentate ligands on the reductive elimination of N-aryl amidates from palladium(II). *J. Am. Chem. Soc.* **2006,** *128* (28), 9044-9045.

30. Gott, A. L.; Clarke, A. J.; Clarkson, G. J.; Scott, P., Structure-activity relationships for Group 4 biaryl amidate complexes in catalytic hydroamination/cyclization of aminoalkenes. *Organomet.* **2007,** *26* (7), 1729-1737.

31. Stanlake, L. J. E.; Beard, J. D.; Schafer, L. L., Rare-earth amidate complexes. Easily accessed initiators for ϵ-caprolactone ring-opening polymerization. *Inorg. Chem.* **2008,** *47* (18), 8062-8068.

32. Eisenberger, P.; Ayinla Rashidat , O.; Lauzon Jean Michel , P.; Schafer Laurel , L., Tantalum–amidate complexes for the hydroaminoalkylation of secondary

amines: Enhanced substrate scope and enantioselective chiral amine synthesis. *Angew. Chem. Int. Ed.* **2009,** *48* (44), 8361-8365.

33. Leitch, D. C.; Beard, J. D.; Thomson, R. K.; Wright, V. A.; Patrick, B. O.; Schafer, L. L., N,O-chelates of Group 4 metals: Contrasting the use of amidates and ureates in the synthesis of metal dichlorides. *Eur. J. Inorg. Chem.* **2009,** (18), 2691-2701.

34. Zhang, W.; Wang, Y.; Cao, J.; Wang, L.; Pan, Y.; Redshaw, C.; Sun, W.-H., Synthesis and characterization of dialkylaluminum amidates and their ring-opening polymerization of ε-caprolactone. *Organomet.* **2011,** *30* (22), 6253-6261.

35. Baker, R. T.; Gordon, J. C.; Hamilton, C. W.; Henson, N. J.; Lin, P.-H.; Maguire, S.; Murugesu, M.; Scott, B. L.; Smythe, N. C., Iron complex-catalyzed ammonia-borane dehydrogenation. A potential route toward B-N-containing polymer motifs using earth-abundant metal catalysts. *J. Am. Chem. Soc.* **2012,** *134* (12), 5598-5609.

36. Webster, R. L.; Noroozi, N.; Hatzikiriakos, S. G.; Thomson, J. A.; Schafer, L. L., Titanium pyridonates and amidates: novel catalysts for the synthesis of random copolymers. *Chem. Commun.* **2013,** *49* (1), 57-59.

37. Yang, W.; Wang, D.; Song, Q.; Zhang, S.; Wang, Q.; Ding, Y., Phosphorescent cyclometalated iridium(III) complexes based on amidate ancillary ligands: Their synthesis and photophysical properties. *Organomet.* **2013,** *32* (15), 4130-4135.

38. Bennett, S. D.; Core, B. A.; Blake, M. P.; Pope, S. J. A.; Mountford, P.; Ward, B. D., Chiral lanthanide complexes: coordination chemistry, spectroscopy, and catalysis. *Dalton Trans.* **2014,** *43* (15), 5871-5885.

39. Corona, T.; Pfaff, F. F.; Acuna-Pares, F.; Draksharapu, A.; Whiteoak, C. J.; Martin-Diaconescu, V.; Lloret-Fillol, J.; Browne, W. R.; Ray, K.; Company, A., Reactivity of a nickel(II) bis(amidate) complex with meta-chloroperbenzoic acid: formation of a potent oxidizing species. *Chem. Eur. J.* **2015,** *21* (42), 15029-15038.

40. Cheng, H.; Xiao, Y.; Lu, C.; Zhao, B.; Wang, Y.; Yao, Y., Synthesis and characterization of bis(amidate) rare-earth metal amides and their application in catalytic addition of amines to carbodiimides. *New J. Chem.* **2015,** *39* (10), 7667-7671.

41. Clarkson, J. M.; Schafer, L. L., Bis(tert-butylimido)bis(N,O-chelate)tungsten(VI) complexes: Probing amidate and pyridonate hemilability. *Inorg. Chem.* **2017,** *56* (10), 5553-5566.

42. Lauzon, J. M.; Eisenberger, P.; Roşca, S. C.; Schafer, L. L., Amidate complexes of tantalum and niobium for the hydroaminoalkylation of unactivated alkenes. *ACS Catal.* **2017,** *7* (9), 5921-5931.

43. Straub, M. D.; Hohloch, S.; Minasian, S. G.; Arnold, J., Homoleptic U(III) and U(IV) amidate complexes. *Dalton Trans.* **2018,** *47* (6), 1772-1776.

44. Beattie, D. D.; Lascoumettes, G.; Kennepohl, P.; Love, J. A.; Schafer, L. L., Disproportionation reactions of an organometallic Ni(I) amidate complex: Scope and mechanistic investigations. *Organomet.* **2018,** *37* (9), 1392-1399.

45. Barral, M. C.; de la Fuente, I.; Jimenez-Aparicio, R.; Priego, J. L.; Torres, M. R.; Urbanos, F. A., Synthesis of diruthenium(II,III) amidate compounds. Crystal

structure of [Ru2(μ-HNOCC4H3S)4(thf)2]SbF6·0.5cyclohexane. *Polyhedron* **2001,** *20* (19), 2537-2544.

46. Jimenez, C. A.; Belmar, J. B.; Alderete, J.; Delgado, F. S.; Lopez-Rodriguez, M.; Pena, O.; Julve, M.; Ruiz-Perez, C., New anionic cobalt complexes using highly hindered bis-amides with varying donor abilities as ligands. *Dalton Trans.* **2007,** (21), 2135-2144.

47. Drover, M. W.; Schafer, L. L.; Love, J. A., Amidate-ligated complexes of rhodium(I): A showcase of coordination flexibility. *Organomet.* **2015,** *34* (10), 1783-1786.

48. Liu, F.; Chen, W., Oxidative addition of Cl2, HClO to square-planar Pt(II) complexes: Synthesis and structural characterization of platinum(II) and platinum(IV) bis(amidate) complexes. *Eur. J. Inorg. Chem.* **2006,** (6), 1168-1173.

49. Schmidt, S.; Schaeper, R.; Schulz, S.; Blaeser, D.; Woelper, C., Insertion reactions of heterocumulenes into Zn-C bonds: Synthesis and structural characterization of multinuclear zinc amidate complexes. *Organomet.* **2011,** *30* (5), 1073-1078.

50. Lee, B.-W.; Sik Min, K.; Doh, M.-K., Copper(II) complexes with novel chiral amidate ligands. *Inorg. Chem. Comm.* **2002,** *5* (2), 163-165.

51. Kilpin, K. J.; Henderson, W.; Nicholson, B. K., Organogold(III) complexes containing chelating bis(amidate) ligands: Synthesis, characterization and biological activity. *Polyhedron* **2007,** *26* (2), 434-447.

52. Nicolaou, K. C.; Bulger, P. G.; Sarlah, D., Metathesis reactions in total synthesis. *Angew. Chem. Int. Ed.* **2005,** *44* (29), 4490-4527.

53. Berg, E.; Orthaber, A.; Santoni, M. P.; Howard, F.; Ott, S., Toward metathesis reactions on vinylphosphaalkenes. In *Phosphorus, Sulfur and Silicon and the Related Elements*, 2013; Vol. 188, pp 152-158.

54. Aljuhani, M. A.; Barman, S.; Abou-Hamad, E.; Gurinov, A.; Ould-Chikh, S.; Guan, E.; Jedidi, A.; Cavallo, L.; Gates, B. C.; Pelletier, J. D. A.; Basset, J.-M., Imine metathesis catalyzed by a silica-supported hafnium imido complex. *ACS Catal.* **2018,** *8* (10), 9440-9446.

55. Young, C. G., Molybdenum. *ChemInform* **2004,** *35* (40).

56. Grubbs, R. H.; Miller, S. J.; Fu, G. C., Ring-closing metathesis and related processes in organic synthesis. *Acc. Chem. Res.* **1995,** *28* (11), 446-452.

57. Schrock, R. R., Synthesis of stereoregular polymers through ring-opening metathesis polymerization. *Acc. Chem. Res.* **2014,** *47* (8), 2457-66.

58. Soufflet, J.-P.; Commereuc, D.; Chauvin, Y., Catalyse de transformation des olefines par les complexes du tengstene. Forme possible des intermediaires. *C. 'R. Acad. Sci. Paris, Ser. C* **1973,** *276*, 169-171.

59. Murdzek, J. S.; Schrock, R. R., Well-characterized olefin metathesis catalysts that contain molybdenum. *Organomet.* **1987,** *6* (6), 1373-1374.

60. Rufanov, K. A.; Zarubin, D. N.; Ustynyuk, N. A.; Gourevitch, D. N.; Sundermeyer, J.; Churakov, A. V.; Howard, J. A. K., Synthesis and structure of a series of new haloaryl imido complexes of molybdenum. *Polyhedron* **2001,** *20* (5), 379-385.

61. Minelli, M.; Hart-Cooper, W.; Sinnwell, J. G.; Blumberg, D. T.; Guzei, I. A.; Spencer, L. C.; Saucedo Vázquez, J. P.; Solano Peralta, A.; Sosa Torres, M., Synthesis, structure, and characterization of molybdenum(VI) imido complexes with N-salicylidene-2-aminothiophenol. *Polyhedron* **2018,** *146*, 26-34.

62. Nogueira, S. L.; Neves, P.; Gomes, C. A.; Amarante, A. T.; Paz, A. F.; Valente, A. A.; Gonçalves, S. I.; Pillinger, M., A comparative study of molybdenum carbonyl and oxomolybdenum derivatives bearing 1,2,3-triazole or 1,2,4-triazole in catalytic olefin epoxidation. *Molecules* **2018,** *24* (1).

63. Coelho, A. C.; Nolasco, M.; Balula, S. S.; Antunes, M. M.; Pereira, C. C. L.; Almeida Paz, F. A.; Valente, A. A.; Pillinger, M.; Ribeiro-Claro, P.; Klinowski, J.; Gonçalves, I. S., Chemistry and catalytic activity of molybdenum(VI)-pyrazolylpyridine complexes in olefin epoxidation. Crystal structures of monomeric dioxo, dioxo-μ-oxo, and oxodiperoxo derivatives. *Inorg. Chem.* **2011,** *50* (2), 525-538.

64. Thomson, R. K.; Zahariev, F. E.; Zhang, Z.; Patrick, B. O.; Wang, Y. A.; Schafer, L. L., Structure, bonding, and reactivity of Ti and Zr amidate complexes: DFT and X-ray crystallographic studies. *Inorg. Chem.* **2005,** *44* (24), 8680-8689.

65. Drover, M. W.; Love, J. A.; Schafer, L. L., 1,3-N,O-Complexes of late transition metals. Ligands with flexible bonding modes and reaction profiles. *Chem. Soc. Rev.* **2017,** *46* (10), 2913-2940.

66. Comas-Vives, A.; Lledós, A.; Poli, R., A computational study of the olefin epoxidation mechanism catalyzed by cyclopentadienyloxidomolybdenum(VI) complexes. *Chem. Eur. J.* **2010,** *16* (7), 2147-2158.

67. Huber, S.; Cokoja, M.; Kühn, F. E., Historical landmarks of the application of molecular transition metal catalysts for olefin epoxidation. *J. Organomet. Chem.* **2014,** *751*, 25-32.

68. Mayilmurugan, R.; Harum Bastian, N.; Volpe, M.; Sax Alexander, F.; Palaniandavar, M.; Mösch-Zanetti Nadia, C., Mechanistic insight into the reactivity of oxotransferases by novel asymmetric dioxomolybdenum(VI) model complexes. *Chem. Eur. J.* **2011,** *17* (2), 704-713.

69. Villata, L. S.; Fliz, M. R.; Capparelli, A. L., Photochemical and catalytic properties of dimeric species of molybdenum(V). *Coord. Chem. Rev.* **2000,** *196* (1), 65-84.

70. Sugimoto, H.; Sakurai, T.; Miyake, H.; Tanaka, K.; Tsukube, H., Mononuclear five-coordinate molybdenum(VI) and -(V) monosulfide complexes coordinated with dithiolene ligands: reversible redox of Mo(V)/Mo(IV) and irreversible dimerization of [MoVS]- cores to a dinuclear [MoV2(μ-S)2]2- core. *Inorg. Chem.* **2005,** *44* (20), 6927-6929.

71. Gnyar, A.; Betz, D.; Drees, M.; Herdtweck, E.; Kühn, F. E., Highly soluble dichloro, dibromo and dimethyl dioxomolybdenum(VI)- bipyridine complexes as catalysts for the epoxidation of olefins. *J. Mol. Catal. A: Chem.* **2010,** *331* (1-2), 117-124.

72. Schachner, J. A.; Traar, P.; Sala, C.; Melcher, M.; Harum, B. N.; Sax, A. F.; Volpe, M.; Belaj, F.; Msch-Zanetti, N. C., Dioxomolybdenum(VI) complexes with pyrazole based aryloxide ligands: Synthesis, characterization and application in epoxidation of olefins. *Inorg. Chem.* **2012,** *51* (14), 7642-7649.

73. Traar, P.; Schachner, J. A.; Stanje, B.; Belaj, F.; Msch-Zanetti, N. C., Dioxomolybdenum(VI) complexes with naphtholate-oxazoline ligands in catalytic epoxidation of olefins. *J. Mol. Catal. A: Chem.* **2014,** *385*, 54-60.

74. Nunes, C. D.; Calhorda, M. J., Molybdenum(II) catalyst precursors in olefin oxidation reactions. *Inorg. Chim. Acta* **2015,** *431*, 122-131.

75. *APEX2*, Bruker AXS Inc.: Madison, Wisconsin, USA, 2007.

76. *SAINT*, Bruker AXS Inc.: Madison, Wisconsin, USA, 2007.

77. Krause, L.; Herbst-Irmer, R.; Sheldrick, G. M.; Stalke, D., Comparison of silver and molybdenum microfocus X-ray sources for single-crystal structure determination. *J. Appl. Cryst.* **2015,** *48* (1), 3-10.

78. Sheldrick, G., SHELXT - Integrated space-group and crystal-structure determination. *Acta Crystallogr., Sect. A: Found. Crystallogr.* **2015,** *71* (1), 3-8.

79. Sheldrick, G., Crystal structure refinement with SHELXL. *Acta Crystallogr., Sect. C: Cryst. Struct. Commun.* **2015,** *71* (1), 3-8.

Chapter 3: Oxo-Imido Amidate Complexes: Synthesis, Characterization and Group Transfer Applications

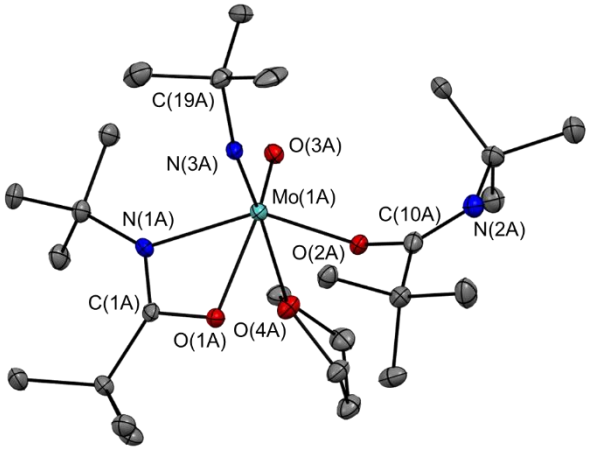

3.1 Introduction

Mixed oxo-imido complexes of Mo are relatively rare when compared to well-studied dioxo and bis-imido species, often being overlooked as unwanted byproducts.[1-10] These complexes are of interest for both the epoxidation and imine metathesis capabilities exhibited by dioxo and bis(imido) compounds, respectively, but we will focus on their biological relevance. The molybdoenzymes that inspire the dioxo research discussed in Chapter 2 feature a Mo=O moiety often accompanied by another fragment like a sulfide.[2, 11-14] Mixed oxo/sulfide species are difficult to generate, as they tend to dimerize through the sulfide ligands.[15-20] Thus, alternative functionalities like imido groups are useful to model the effect of the ancillary ligands on OAT reactions.[2, 21]

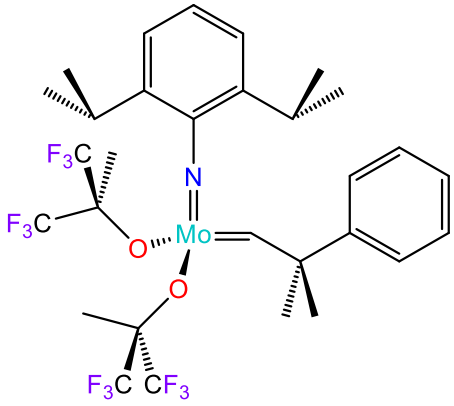

Schrock's metathesis catalyst

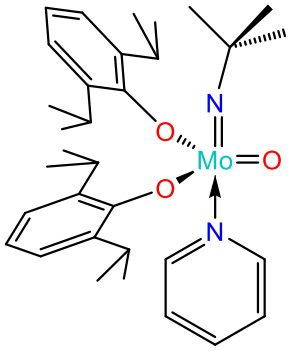

Anderson epoxidation catalyst

Figure 3.1 Representation of an early olefin metathesis catalyst by Schrock and a mixed oxo-imido complex for alkene epoxidation by Anderson and coworkers.

Mixed oxo-imido complexes could provide better reactivity towards oxygen atom transfer reactions due to the π-donating ability of the imido fragment. The R group of the imido fragment can also prevent the dimerization problem observed with many dioxo species.[22-25] Only a few examples of oxo-imido complexes are reported to perform the epoxidation reaction of alkenes, one example being Anderson's epoxidation catalyst is shown in Figure 3.1. Distorted trigonal prismatic oxo-imido derivatives reported by Mosch-Zanetti and coworkers have also been shown to exhibit OAT reactivity,[21, 26] but the observed reactivity of these species was inferior to the dioxo analogues, with steric congestion being the predominant reasoning.[2, 27] In addition to oxygen atom transfer processes, there have been examples of Mo(VI) oxo-imido complexes as intermediates in heterometathesis reactions of ketones and *N*-sulfinylimines.[28]

Other notable examples of Group 6 imido groups in catalysis are the Schrock olefin metathesis catalysts where the imido group is ancillary to the reactive alkylidene.[3, 29] The first generation of Schrock's metathesis catalysts featured simple bulky imido groups that

served as π-donors and provided steric protection for the reactive metal center (Figure 3.1).[3, 29-30] The pace of development of new oxo-imido complexes has increased since the development of a protocol to prepare $Cl_2MoON^tBu(DME)$ via disproportionation.[7-10, 31] This easy-to-isolate starting material, has allowed for much quicker access to mixed oxo-imido complexes, and provided a convenient entry point into oxo-imido complexes bearing amidate ligands. [7-10, 31]

3.2 Results and Discussion

3.2.1 Synthesis

Molybdenum bis(amidate) complexes featuring both an oxo and an imido ligand fragment have been generated in moderate to excellent yields (41-95%) by salt metathesis, as shown in Scheme 3.1. These mixed oxo-imido complexes are significantly less common in Mo(VI) chemistry when compared to dioxo and bis imido complexes.[32-33] These complexes have been characterized by NMR and FTIR spectroscopies, as well as by X-ray crystallography.

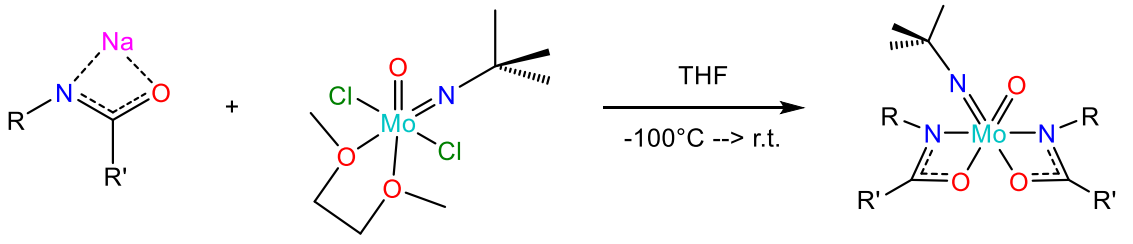

R = Ph, R' = ^{t}Bu (**3.2**)
R = DMP, R' = ^{t}Bu (**3.3**), Ph (**3.4**), PFP (**3.5**)
R = DIPP, R' = ^{t}Bu (**3.6**), Ph (**3.7**), PFP (**3.8**)
R = ^{t}Bu, R' = ^{t}Bu (**3.9**)

Scheme 3.1 General synthetic scheme for bis(amidate) Mo(VI) oxo-imido complexes and naming convention.

In contrast to the dioxo complexes, these species exhibit solution phase dynamic behavior and ligand hemilability confirmed by X-ray crystallography (*vide infra*). As presented in Figure 3.2, the ^{1}H NMR spectrum for complex **3.2** is simple, featuring only a singlet at 1.09 ppm for the ^{t}Bu imido fragment, a singlet at 1.13 ppm for the ^{t}Bu groups

of the amidate ligands, a triplet at 6.86 ppm (J = 7.5 Hz, 2H), a virt. triplet at 7.01 ppm (4H), and a doublet at 7.24 ppm (J = 7.5 Hz, 2H) for the ligand aromatic protons.

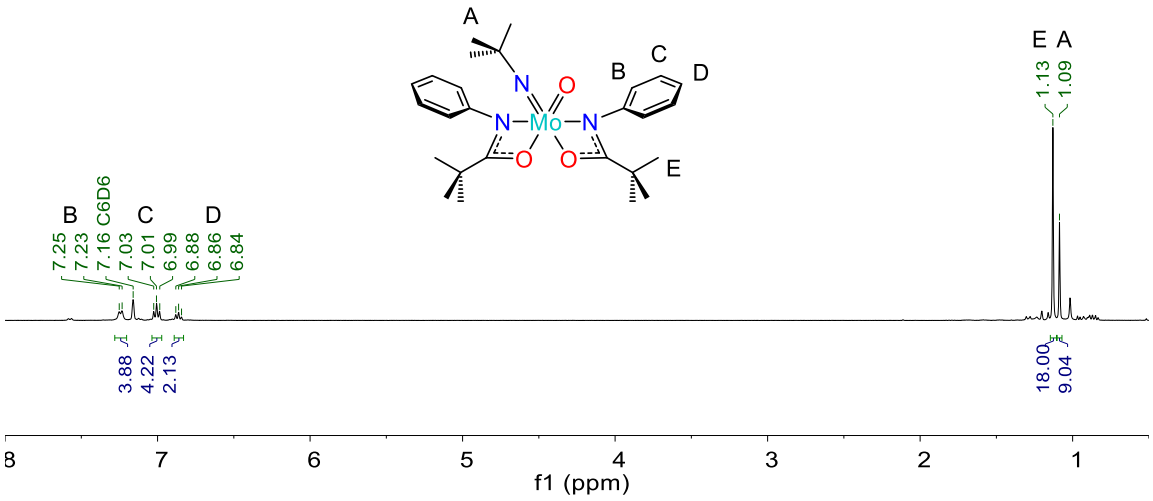

Figure 3.2 ^{1}H NMR spectrum of complex **3.2**.

The ^{1}H NMR spectra for complexes featuring DMP groups on the amidate N have distinctive broad peaks for the aryl methyl protons due to the asymmetry of the molecule, and steric interactions with the added bulk of the Mo=N^{t}Bu fragment as compared to the dioxo complexes, these described in Chapter 2. These broad peaks were investigated by variable-temperature ^{1}H NMR spectroscopy for complex **3.3** ([^{DMP}(NO)^{tBu}]$_2$MoON^{t}Bu) as shown in Figure 3.3. The data shows that when the solution is cool enough (about 0°C), the broad peak becomes 3 separate peaks. One peak is likely due to free rotation of the aryl group closest to the oxo group about its N-C_{ispo} bond, with the other two peaks corresponding to the rotation-restricted aryl group closest to the imido group. The peak for the aryl group closest to the oxo eventually separates into two peaks at about -20°C.

The broad peak observed at 20-30°C separates into two peaks at higher temperatures due to the C_1 symmetry of the molecule.

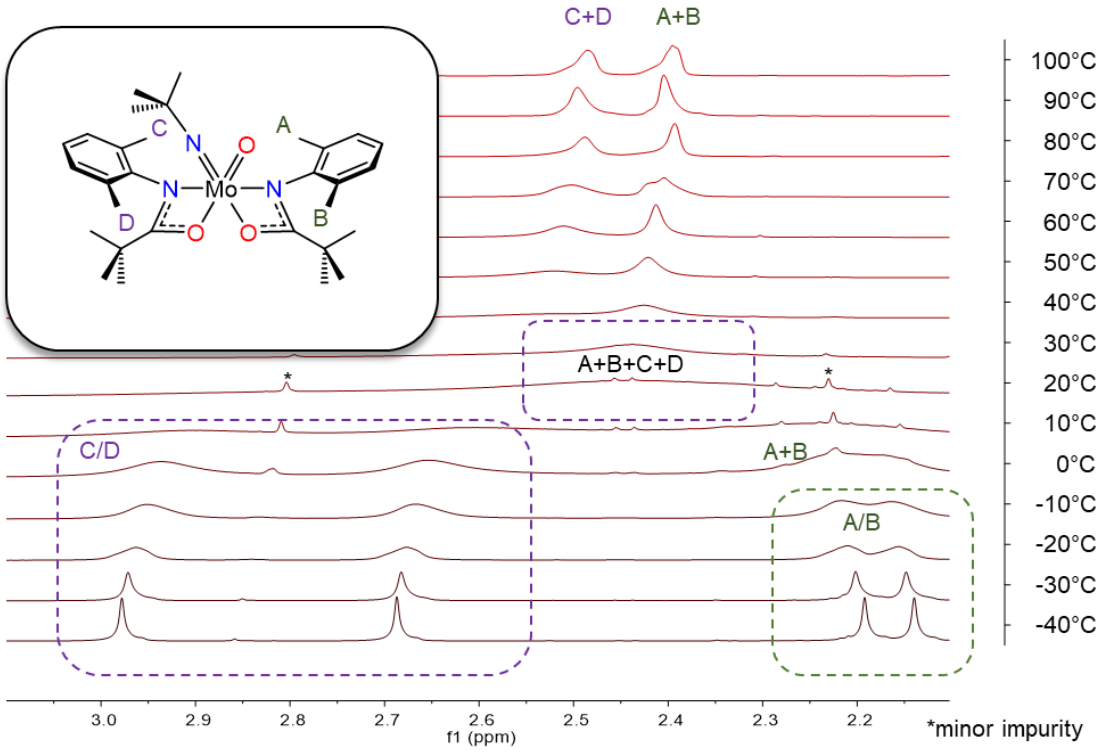

Figure 3.3. Variable temperature ^{1}H NMR spectra of complex **3.3** from -40°C to 100°C. The spectra between 0°C and 30°C have been enhanced to show the broad peak around 2.5 ppm.

Evaluation of the related complexes bearing *N*-2,6-dimethylphenyl substituents on the amidate ligands shows similar behavior to **3.3**. The ^{1}H NMR spectrum of complex **3.4** ($[^{DMP}(NO)^{Ph}]_2MoON^tBu$) exhibits a broad peak for the methyl groups at 2.50 ppm and the imido ^{t}Bu protons resonate at 0.98 ppm. The ^{1}H NMR spectrum of the perfluorophenyl derivative $[^{DMP}(NO)^{PFP}]_2MoON^tBu$ (**3.5**) exhibits a similar broad peak at

2.51 ppm for 2 of the methyl groups accompanied by a sharper peak at 2.36 for the other 2 methyl groups and the imido ^{t}Bu protons resonate at 1.08 ppm.

The oxo-imido complexes bearing *N*-2,6-diisopropylphenyl substituted amidate ligands feature very complex ^{1}H NMR spectra as expected, due to the asymmetry of the complexes and the steric bulk provided by the N-bound group. This complexity presents as 4 septets between 3-4.5 ppm, and 8 doublets between 0.5-2 ppm (often overlapping) for the isopropyl groups, and a sharp singlet for the imido protons at about 1 ppm. A representative example can be seen in the ^{1}H NMR spectrum of complex **3.6** ([^{DIPP}(NO)^{tBu}]$_2$MoON^{t}Bu) shown in Figure 3.4.

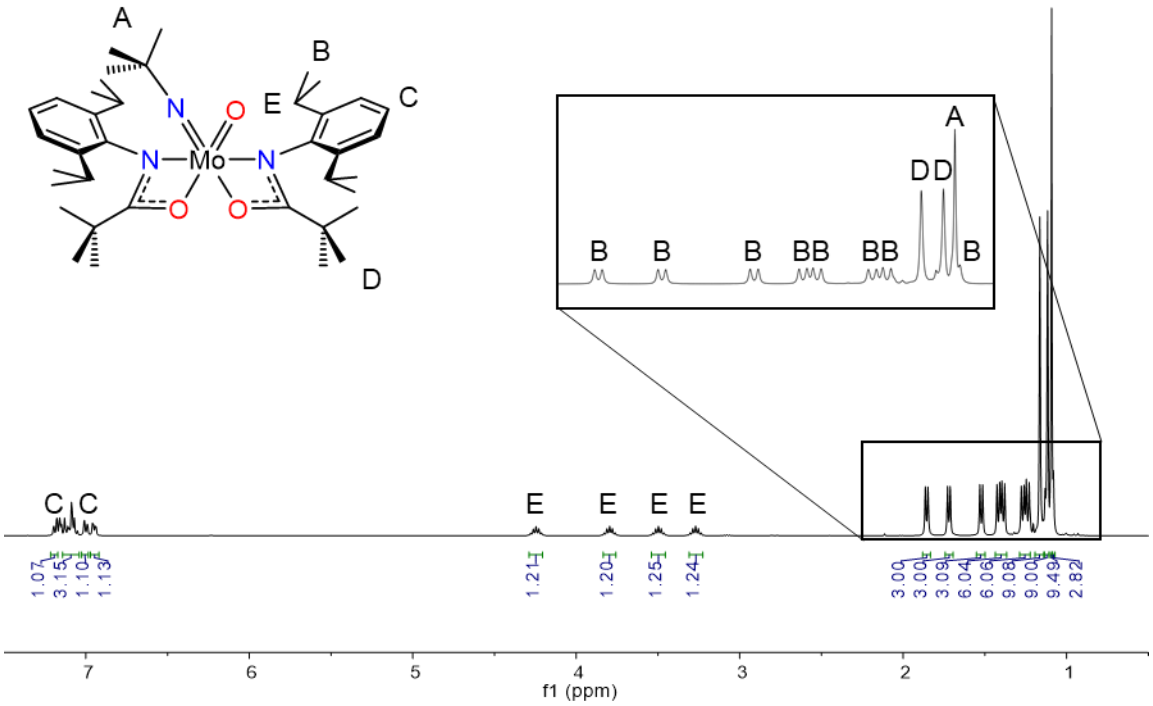

Figure 3.4 ^{1}H NMR spectrum of [^{DIPP}(NO)^{tBu}]$_2$MoON^{t}Bu (**3.6**).

3.2.2 X-ray Crystallography

Crystals of $[^{DMP}(NO)^{tBu}]_2MoON^tBu$ (**3.3**) were obtained from slow evaporation of a toluene solution at ambient temperature. A thermal ellipsoid plot of complex **3.3** is shown in Figure 3.5. The *trans* bond angles N(1A)-Mo(1)-N(1B), O(1)-Mo(1)-O(1B), and N(1C)-Mo(1)-O(1A) are 142.90(9)°, 150.89(9)° and 155.08(9)°, respectively. These are large deviations from the expected 180° for an octahedral complex. The *trans* nitrogen atoms of the amidate ligands deviate from linearity considerably, likely due to the bulky 2,6-dimethylphenyl substituents. The imido bond angle is 158.3(2) which is slightly bent, but suggests a high degree of π-donation to the Mo center.[34] The amidate bite angles N(1A)-Mo(1)-O(1A) and N(1B)-Mo(1)-O(1B) are tight at 59.03(8)° and 59.49(8)°, respectively, as expected. The oxo-imido N(1C)-Mo(1)-O(1) angle is 104.84° and the O(1A)-Mo(1)-O(1B) angle is 75.36(8)°.

The Mo=N^{t}Bu bond length is 1.733(3) Å and the Mo=O bond length is 1.710(2) Å, consistent with other Mo(VI)-oxo and Mo(VI)-imido species.[8-9, 27, 31, 33, 35-36] The Mo(1)-N(1A) and Mo(1)-N(1B) bond lengths are 2.099(2) and 2.142(2) Å, respectively, while the Mo(1)-O(1A) and Mo(1)-O(1B) bond lengths are 2.306(2) and 2.221(2) Å, respectively. The longer Mo-O bond for the amidate ligand A (2.306 Å) is compensated for by the shorter Mo-N bond (2.099 Å) and is likely due to the *trans*-influence of the imido ligand. This can be compared to the analogous dioxo complex (**2.9**) distances, which average 2.243 Å and 2.0951 Å for the Mo-O and Mo-N bonds, respectively. In the case of both amidate ligands on **3.3**, a shorter Mo-N bond is observed indicating amido-ketone type binding, as is the case for the dioxo species. This designation is further supported by the C-O and C-N bond lengths for the amidate ligands, O(1A)-C(9A),

O(1B)-C(9B), N(1A)-C(9A), and N(1B)-C(9B), which are 1.264(4), 1.288(3), 1.344(4) and 1.325(4) Å, respectively. These distances also show that the amidate ligand *trans* to the imido group has even greater amido-ketone character as the C-O bond is closer to a double bond. Selected bond distances and angles for complex **3.3** are shown in Table 3.1.

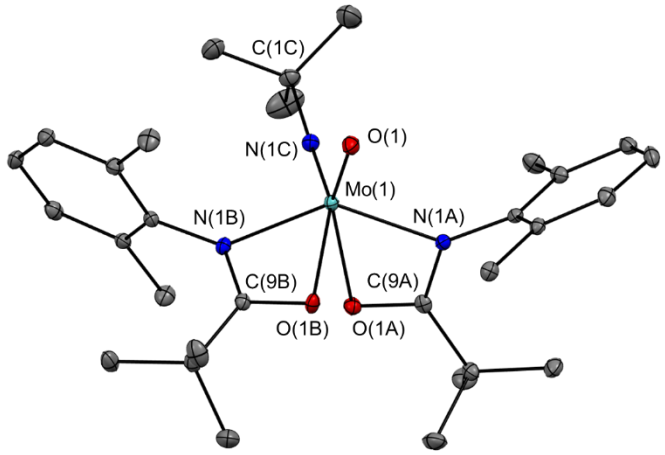

Figure 3.5 Thermal ellipsoid plot of $[^{DMP}(NO)^{tBu}]_2MoON^tBu$ (**3.3**) shown at 50% probability with hydrogen atoms omitted for clarity.

Table 3.1 Selected Bond Distances (Å) and Angles (°) for $[^{DMP}(NO)^{tBu}]_2MoON^tBu$, **3.3**.

	Lengths (Å)		Angles (°)
O(1A)-C(9A)	1.264(4)	N(1A)-Mo(1)-O(1A)	59.03(8)
O(1B)-C(9B)	1.288(3)	N(1B)-Mo(1)-O(1B)	59.49(8)
N(1B)-C(9B)	1.325(4)	O(1B)-Mo(1)-O(1A)	75.36(8)
N(1A)-C(9A)	1.344(4	N(1B)-Mo(1)-O(1A)	89.48(8)
N(1C)-C(1C)	1.460(4)	N(1A)-Mo(1)-O(1B)	91.48(8)
Mo(1)-O(1)	1.710(2)	O(1)-Mo(1)-O(1A)	92.18(9)
Mo(1)-N(1C)	1.733(3)	O(1)-Mo(1)-N(1B)	94.86(9)
Mo(1)-N(1A)	2.099(2)	N(1C)-Mo(1)-O(1B)	96.32(10)
Mo(1)-N(1B)	2.142(2)	N(1C)-Mo(1)-N(1A)	98.46(10)
Mo(1)-O(1B)	2.221(2)	O(1)-Mo(1)-N(1A)	104.67(10)
Mo(1)-O(1A)	2.306(2)	O(1)-Mo(1)-N(1C)	104.84(11)
		N(1C)-Mo(1)-N(1B)	106.71(10)
		N(1A)-Mo(1)-N(1B)	142.90(9)
		O(1)-Mo(1)-O(1B)	150.89(9)
		N(1C)-Mo(1)-O(1A)	155.08(9)
		C(1C)-N(1C)-Mo(1)	158.3(2)

X-ray quality single crystals for complexes **3.5**, **3.6**, and **3.7** were grown from 1:1 solutions of DCM/Hexanes at ambient temperature. A thermal ellipsoid plot of $[^{DMP}(NO)^{PFP}]_2MoON^tBu$ (**3.5**) is shown in Figure 3.6. The bond angles for the *trans* atoms N(1)-Mo(1)-N(2), O(2)-Mo(1)-O(3), and O(1)-Mo(1)-N(3) are 143.17(11), 151.53(11) and 155.32(11)°, respectively. The imido bond angle is 158.0(3), which is again slightly bent.[34] The amidate bite angles O(1)-Mo(1)-N(1) and O(2)-Mo(1)-N(2) are 58.45(10) and 59.49(9)°, respectively. The oxo-imido angle O(3)-Mo(1)-N(3) is 104.93(13)°, while the amidate oxo angle O(1)-Mo(1)-O(2) is 77.90(9)°. These angles are consistent with complex **3.3**, which is expected due to the similar steric properties of the ligands.

The Mo=N^{t}Bu bond length is 1.721(3) Å, and the Mo=O bond length is 1.697(3) Å, consistent with previously reported Mo(VI)=O and Mo(VI)=NR bond lengths.[8-9, 27, 31, 33, 35-36] The amidate Mo-N bond lengths are 2.088(3) and 2.147(3) Å for Mo(1)-N(1) and Mo(1)-N(2), respectively, while the amidate Mo-O bond lengths are 2.393(2) and 2.273(2) Å for Mo(1)-O(1) and Mo(1)-O(2), respectively. Again, the *trans* influence is observed with the amidate ligand *trans* to the imido group a having longer Mo-O bond, which is compensated for by a shorter Mo-N bond. The C-N and C-O bond lengths O(1)-C(9), O(2)-C(24), N(1)-C(9), and N(2)-C(24) are 1.262(4), 1.285(4), 1.328(4) and 1.305(4) Å, respectively. These bond lengths show that for the amidate ligand *trans* to the imido group, the C-O bond exhibits significant double bond character, thus the amidate resonance is more amido-ketone in character. Selected bond lengths and angles for complex **3.5** are presented in Table 3.2.

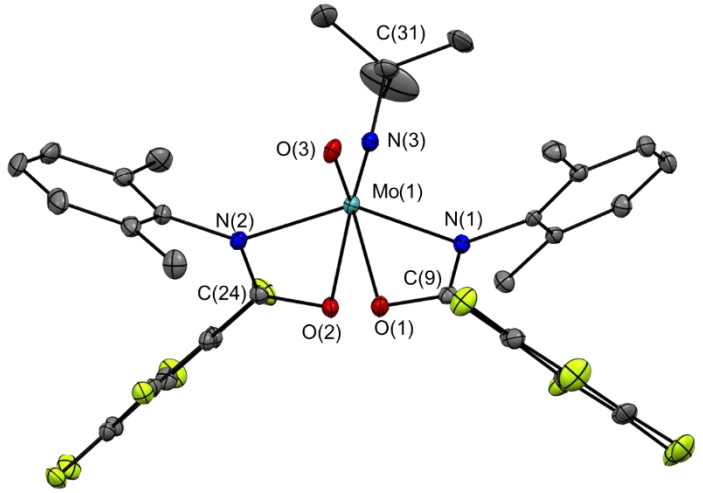

Figure 3.6 Thermal ellipsoid plot of [^{DMP}(NO)^{PFP}]$_2$MoON^{t}Bu (**3.5**) shown at 50% probability with hydrogen atoms omitted for clarity.

Table 3.2 Selected Bond Distances (Å) and Angles (°) for [^{DMP}(NO)^{PFP}]$_2$MoON^{t}Bu, **3.5**

	Lengths (Å)		Angles (°)
O(1)-C(9)	1.262(4)	N(1)-Mo(1)-O(1)	58.45(10)
O(2)-C(24)	1.285(4)	N(2)-Mo(1)-O(2)	59.49(9)
N(2)-C(24)	1.305(4)	O(2)-Mo(1)-O(1)	77.90(9)
N(1)-C(9)	1.328(4)	N(1)-Mo(1)-O(2)	87.74(10)
N(3)-C(31)	1.470(5)	O(3)-Mo(1)-O(1)	88.19(10)
Mo(1)-O(3)	1.697(3)	N(2)-Mo(1)-O(1)	95.73(10)
Mo(1)-N(3)	1.721(3)	N(3)-Mo(1)-N(1)	97.40(12)
Mo(1)-N(1)	2.088(3)	N(3)-Mo(1)-O(2)	97.57(12)
Mo(1)-N(2)	2.147(3)	O(3)-Mo(1)-N(2)	98.05(11)
Mo(1)-O(2)	2.273(2)	N(3)-Mo(1)-N(2)	102.82(12)
Mo(1)-O(1)	2.393(2)	O(3)-Mo(1)-N(3)	104.93(13)
		O(3)-Mo(1)-N(1)	106.09(11)
		N(1)-Mo(1)-N(2)	143.17(11)
		O(3)-Mo(1)-O(2)	151.53(11)
		N(3)-Mo(1)-O(1)	155.32(11)
		C(31)-N(3)-Mo(1)	158.0(3)

The X-ray crystal structure for [^{DIPP}(NO)^{tBu}]$_2$MoON^{t}Bu (**3.6**) is shown in Figure 3.7. The *trans* bond angles N(1)-Mo(1)-N(2), O(1)-Mo(1)-O(3), and O(2)-Mo(1)-N(3) are 140.6(4), 152.0(5), and 155.7(6)°, respectively. The *trans* nitrogen atoms of the amidate ligands show a larger degree of deviation from linearity than the previous complexes, likely due to larger isopropyl groups. The imido bond angle is 174.2(14), which is almost completely linear and more typical of a triply-bonded imido fragment.[34, 37-38] The amidate bite angles O(1)-Mo(1)-N(1) and O(2)-Mo(1)-N(2) are 59.1(4) and 59.5(4)°, respectively. The oxo-imido angle N(3)-Mo(1)-O(3) is 106.7(8)° and the amidate oxygen angle O(1)-Mo(1)-O(2) is 77.3(4)°.

The Mo=N^{t}Bu bond length is 1.718(16) Å and the Mo=O bond length is 1.692(12) Å. The imido bond length is consistent with an Mo≡N triple bond.[37-38] The amidate Mo-N bond lengths Mo(1)-N(1) and Mo(1)-N(2) are 2.140(11) Å and 2.082(11) Å, respectively, while the amidate Mo-O bond lengths Mo(1)-O(1) and Mo(1)-O(2) are 2.230(11) Å and 2.255(10) Å, respectively. The imido *trans* influence is again observed, but to a lesser extent with this complex. This could be due to the steric bulk of the 2,6-diisopropylphenyl group preventing the amidate nitrogen from moving closer to the metal center. The bond distances for O(1)-C(1), O(2)-C(18), N(1)-C(1), and N(2)-C(18) are 1.266(17), 1.236(17), 1.327(18), and 1.335(18) Å, respectively. These bond lengths again show that the ligand *trans* to the imido has a shorter C-O bond, but the effect is less obvious than the previous oxo-imido complexes. Selected bond angles and distances for complex **3.6** are presented in Table 3.3.

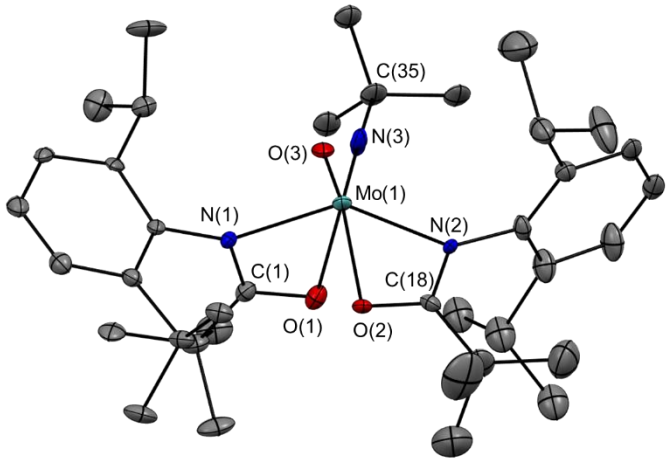

Figure 3.7 Thermal ellipsoid plot of [^{DIPP}(NO)^{tBu}]$_2$MoON^{t}Bu (**3.6**) shown at 50% probabilty with hydrogen atoms omitted for clarity.

Table 3.3 Selected Bond Distances (Å) and Angles (°) for [^{DIPP}(NO)^{tBu}]$_2$MoON^{t}Bu, **3.6**

	Lengths (Å)		Angles (°)
O(2)-C(18)	1.236(17)	N(1)-Mo(1)-O(1)	59.1(4)
O(1)-C(1)	1.266(17)	N(2)-Mo(1)-O(2)	59.5(4)
N(1)-C(1)	1.327(18)	O(1)-Mo(1)-O(2)	77.3(4)
N(2)-C(18)	1.335(18)	N(1)-Mo(1)-O(2)	88.9(4)
N(3)-C(35)	1.53(3)	N(2)-Mo(1)-O(1)	89.2(4)
Mo(1)-O(3)	1.692(12)	O(3)-Mo(1)-O(2)	91.9(5)
Mo(1)-N(3)	1.718(16)	N(3)-Mo(1)-O(1)	92.0(7)
Mo(1)-N(2)	2.082(11)	O(3)-Mo(1)-N(1)	95.4(5)
Mo(1)-N(1)	2.140(11)	N(3)-Mo(1)-N(2)	99.1(5)
Mo(1)-O(1)	2.230(11)	N(3)-Mo(1)-N(1)	104.3(6)
Mo(1)-O(2)	2.255(10)	O(3)-Mo(1)-N(3)	106.7(8)
		O(3)-Mo(1)-N(2)	107.6(5)
		N(2)-Mo(1)-N(1)	140.6(4)
		O(3)-Mo(1)-O(1)	152.0(5)
		N(3)-Mo(1)-O(2)	155.7(6)
		C(35)-N(3)-Mo(1)	174.2(14)

The X-ray crystal structure of $[^{DIPP}(NO)^{Ph}]_2MoON^tBu$ (**3.7**) is shown in Figure 3.8. The *trans* bond angles N(1)-Mo(1)-N(2), O(1)-Mo(1)-O(3), and O(2)-Mo(1)-N(3) are 140.58(9), 152.64(8), and 155.86(10)°, respectively. These angles are similar to the corresponding angles in the ^{t}Bu backbone complex **3.6**. The imido bond angle is 171.5(2)°, which is consistent with a linear triply bound imido group as mentioned for complex **3.6**. The amidate bite angles O(1)-Mo(1)-N(1) and O(2)-Mo(1)-N(2) are 59.37(8) and 59.82(8)°, respectively. The oxo-imido angle O(3)-Mo(1)-N(3) is 105.93(11)°, and the amidate oxygen ligand angle O(1)-Mo(1)-O(2) is 76.40(7)°.

The Mo=N^{t}Bu bond length is 1.733(2) Å and the Mo=O bond length is 1.705(2) Å. The amidate ligand Mo-N bonds Mo(1)-N(1) and Mo(1)-N(2) are 2.134(2) and 2.095(2) Å, respectively, while the amidate ligand Mo-O bonds Mo(1)-O(1) and Mo(1)-O(2) are 2.2725(19) Å and 2.2767(19) Å, respectively. This reduced *trans*-influence is likely due to the steric bulk of the ligand as was previously described for complex **3.6**. The reduced influence is observed with the amidate ligand bonds O(1)-C(1), O(2)-C(20), N(1)-C(1), and N(2)-C(20) which are 1.277(3), 1.275(3), 1.321(4), and 1.334(3) Å, respectively. These homologous bonds are essentially identical, except for the longer C-N bond for the *trans* ligand suggesting more single bond character for the C-N bond. Selected bond distances and angles of complex **3.7** are presented in Table 3.4.

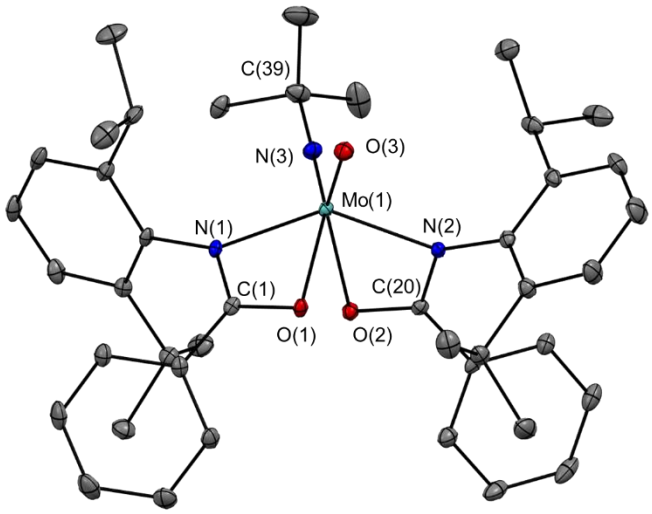

Figure 3.8 Thermal ellipsoid plot of $[^{DIPP}(NO)^{Ph}]_2MoON^tBu$ (**3.7**) shown at 50% probability with hydrogen atoms omitted for clarity.

Table 3.4 Selected Bond Distances (Å) and Angles (°) for $[^{DIPP}(NO)^{Ph}]_2MoON^tBu$, **3.7**.

	Lengths		Angles
O(2)-C(20)	1.275(3)	N(1)-Mo(1)-O(1)	59.37(8)
O(1)-C(1)	1.277(3)	N(2)-Mo(1)-O(2)	59.81(8)
N(1)-C(1)	1.321(4)	O(1)-Mo(1)-O(2)	76.40(7)
N(2)-C(20)	1.334(3)	N(2)-Mo(1)-O(1)	88.01(8)
N(3)-C(39)	1.454(4)	N(1)-Mo(1)-O(2)	89.29(8)
Mo(1)-O(3)	1.705(2)	O(3)-Mo(1)-O(2)	91.91(9)
Mo(1)-N(3)	1.733(2)	N(3)-Mo(1)-O(1)	93.32(10)
Mo(1)-N(2)	2.095(2)	O(3)-Mo(1)-N(1)	96.42(9)
Mo(1)-N(1)	2.134(2)	N(3)-Mo(1)-N(2)	98.60(10)
Mo(1)-O(1)	2.2725(19)	N(3)-Mo(1)-N(1)	104.36(10)
Mo(1)-O(2)	2.2767(19)	O(3)-Mo(1)-N(3)	105.93(11)
		O(3)-Mo(1)-N(2)	107.60(9)
		N(2)-Mo(1)-N(1)	140.58(9)
		O(3)-Mo(1)-O(1)	152.64(8)
		N(3)-Mo(1)-O(2)	155.86(10)
		C(39)-N(3)-Mo(1)	171.5(2)

Overall, bond lengths for the Mo=O fragments of all complexes featuring both amidate ligands bound in a κ^2 fashion are fairly consistent at 1.701 Å Avg., with 1.692(12) Å for **3.6** being the shortest and 1.711(3) Å for **3.3** as the longest. The Mo=N^{t}Bu bond was also consistent with an average length of 1.726 Å, with 1.718(16) Å being the shortest (**3.6**) and 1.733(3) Å (**3.3** and **3.7**) being the longest among the related complexes. A general *trans* influence is observed, where the amidate ligand *trans* to the imido group can be characterized as having more amido-ketone character. The stronger *trans* influence is also accompanied by more bent character of the imido ligand. The increased linearity of the imido fragment for complexes **3.6** and **3.7** might be due to the steric pressure of the N-DIPP groups of these complexes. The C-O bonds of amidate ligands are significantly shorter (1.269 Å Avg.) and the C-N bonds are longer (1.327 Å Avg.) in all complexes. The Mo-O and Mo-N bonds for the amidate ligands *trans* to the Mo=N^{t}Bu group are also observed to have longer Mo-O bonds and shorter Mo-N bonds. The average amidate Mo-O and Mo-N bond lengths for the oxo-imido complexes are 2.278 Å and 2.116 Å, respectively, compared to 2.258 Å and 2.094 Å for the dioxo series. This average increase in Mo-O bond length can be attributed to the *trans* influence of the imido fragments.

3.2.3 Hemilability

Synthesis of the analogous bis(amidate) complex bearing all tertbutyl substituents, [^{tBu}(NO)^{tBu}]$_2$MoON^{t}Bu, results in an unusual situation where on of the amidate ligands can readily become κ^1 in solution as shown in Figure 3.9, complex **3.9** ([^{tBu}(NO)^{tBu}]$_2$MoON^{t}Bu) exhibits a structure where a THF molecule occupies one

coordination site displacing a N-donor of an amidate ligand. The *trans* angles O(2A)-Mo(1A)-N(1A), O(1A)-Mo(1A)-O(3A), and N(3A)-Mo(1A)-O(4A) are 145.63(11), 147.05(11), and 175.21(12)°, respectively. These angles are once again distorted from octahedral, but the THF-Mo-imido bond angle (175.21°) is the closest to 180° of any Mo amidate complex reported thus far. This is likely due to the relieved steric pressure of the amidate ligand when it is bound κ^2 and the relieved torsion of the tight bite angle it forces on the metal center. This tight bite angle is observed with the κ^2 bound amidate ligand, where the bond angle O(1A)-Mo(1A)-N(1A) is 59.47(10)°, consistant with κ^2 amidate ligands in other related complexes. The imido bond angle is 175.21(12) which is consistent with a linear, triply-bound imido moiety. The oxo-imido angle O(3A)-Mo(1A)-N(3A) is 103.61(13)° and the bond angle of the amidate oxygen atoms O(1A)-Mo(1A)-O(2A) is 88.39(10)°, however this angle is not directly comparable to other complexes due to the κ^1-bound ligand.

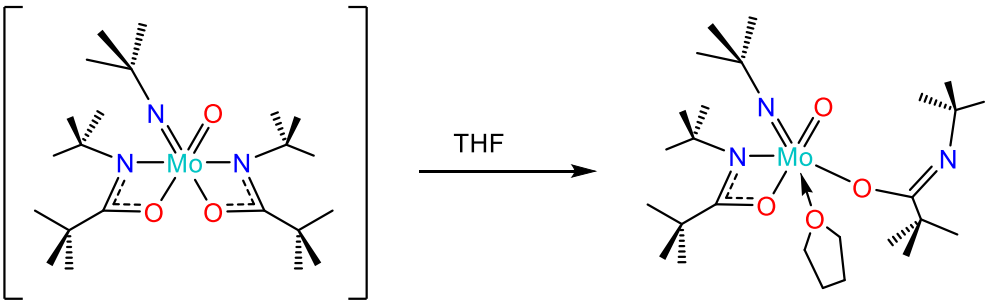

3.9

Figure 3.9 Formation of the THF coordinated complex **3.9** ([^{tBu}(NO)^{tBu}]$_2$MoON^{t}Bu-(THF)).

The Mo=N^{t}Bu bond length is 1.734(3) Å and the Mo=O bond length is 1.706(2) Å, which are both similar to the other oxo-imido Mo bis(amidate) complexes presented in this work. The amidate ligand bond lengths Mo(1A)-O(1A), Mo(1A)-O(2A), and Mo(1A)-N(1A) are 2.151(2), 1.949(2), and 2.192(3) Å, respectively. These bond lengths are a considerable deviation from the rest of the series, with the κ^1-bound amidate ligand exhibiting alkoxy-imine character instead of amido-ketone character. The Mo-O bond for the κ^1-bound amidate ligand is much shorter than any of the other Mo-N or Mo-O amidate bonds presented in this work. The intra-amidate bond lengths O(1A)-C(1A), O(2A)-C(10A), N(1A)-C(1A), and N(2A)-C(10A) are 1.295(4), 1.351(4), 1.314(4), and 1.257(5) Å, respectively. These bond lengths suggest that the κ^2 bound amidate has more amido-ketone character, while the κ^1-bound amidate ligand is bound more like an alkoxy-imine. The Mo-THF bond distance is 2.459(3) Å, which is characteristic of neutrally coordinated oxygen donors on Mo(VI).[39-40]

This complex is isolated as an orange oil and darkens over time (<24 h) with the ligand crystallizing as needles out of the material at room temperature in inert atmosphere. This instability suggests the ligand binding is weak and this is consitant with the structure bearing a hemilabile amidate ligand and a coordinated THF. Due to this instability, a ^{1}H NMR spectrum without contamination of free ligand has not been obtained. This observation is also consistant with attempted syntheses of the dioxo and bis(imido) complexes bearing the [^{tBu}(NO)^{tBu}]$^{-}$ ligand.

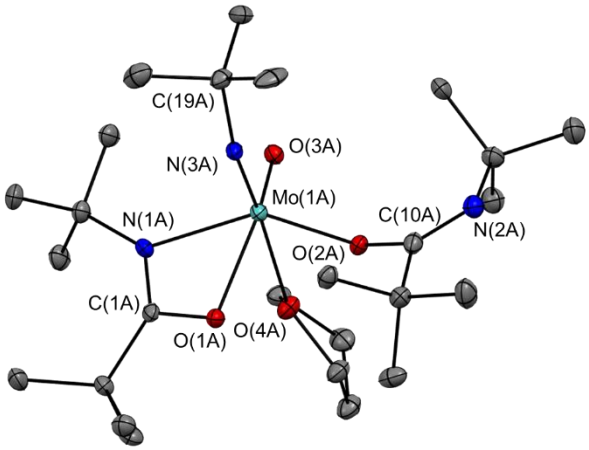

Figure 3.10 Thermal ellipsoid plot of [^{tBu}(NO)^{tBu}]$_2$MoON^{t}Bu-(THF) (**3.9**) shown at 50% probability with hydrogen atoms omitted for clarity.

Table 3.5 Selected Bond Distances (Å) and Angles (°) for [^{tBu}(NO)^{tBu}]$_2$MoON^{t}Bu-(THF), **3.9**.

Lengths (Å)			Angles (°)
N(2A)-C(10A)	1.257(5)	O(1A)-Mo(1A)-N(1A)	59.47(10)
O(1A)-C(1A)	1.295(4)	O(1A)-Mo(1A)-O(4A)	72.44(9)
N(1A)-C(1A)	1.314(4)	O(2A)-Mo(1A)-O(4A)	78.24(9)
O(2A)-C(10A)	1.351(4)	N(1A)-Mo(1A)-O(4A)	80.38(10)
N(3A)-C(19A)	1.458(5)	O(3A)-Mo(1A)-O(4A)	80.90(10)
Mo(1A)-O(3A)	1.706(2)	O(2A)-Mo(1A)-O(1A)	88.39(10)
Mo(1A)-N(3A)	1.734(3)	N(3A)-Mo(1A)-N(1A)	97.26(13)
Mo(1A)-O(2A)	1.949(2)	O(3A)-Mo(1A)-N(1A)	97.74(11)
Mo(1A)-O(1A)	2.151(2)	N(3A)-Mo(1A)-O(2A)	101.90(12)
Mo(1A)-N(1A)	2.192(3)	N(3A)-Mo(1A)-O(1A)	102.77(12)
Mo(1A)-O(4A)	2.459(3)	O(3A)-Mo(1A)-N(3A)	103.61(13)
		O(3A)-Mo(1A)-O(2A)	105.03(11)
		O(2A)-Mo(1A)-N(1A)	145.63(11)
		O(3A)-Mo(1A)-O(1A)	147.05(11)
		C(19A)-N(3A)-Mo(1A)	157.4(3)
		N(3A)-Mo(1A)-O(4A)	175.21(12)

3.2.4 Oxygen Atom Abstraction From an Oxo-imido Complex

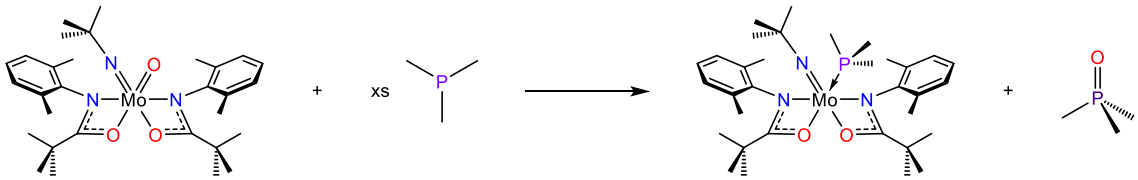

Scheme 3.2 Oxo abstraction from complex **3.3** using trimethylphosphine.

Oxo abstraction from an oxo-imido complex was investigated for comparison to the dioxo complexes studied in Chapter 2. The imido ligands have been used as a substitute for sulfides due to their stability as an alternative heteroligand for DMSO reductase model chemistry.[2, 21] It is of interest to observe the differences in oxygen atom abstraction from an oxo-imido complex versus the analogous dioxo complex. As shown in Scheme 3.2, the reaction of complex **3.3** with 4 equiv of PMe_3 generates $OPMe_3$, and a new Mo complex with coordinated PMe_3 based on the ^{31}P NMR. This reaction is evidence of a stable Mo(IV) bis(amidate) species. Access to a Mo(IV) bis(amidate) species allows for possible oxidation routes to new Mo(VI) bis(amidate) complexes.

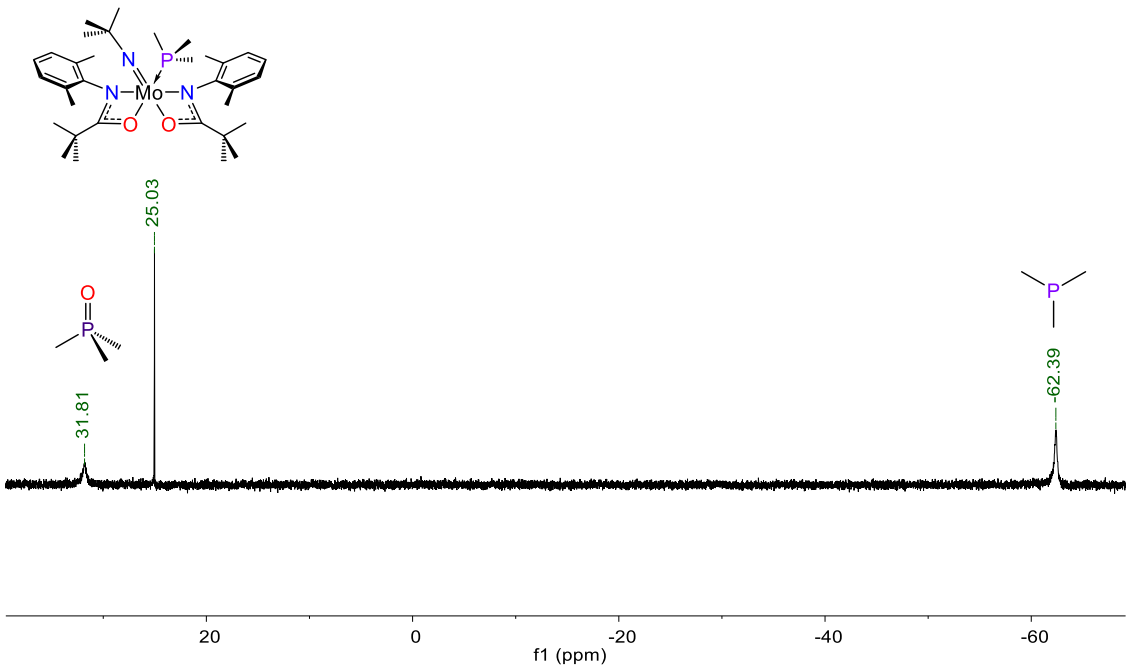

Figure 3.11 ^{31}P NMR spectrum for the reaction of complex **3.3** and PMe_3.

3.2.5 Epoxidation of *Cis*-Cyclooctene By Oxo-Imido Complexes

Epoxidation of *cis*-cyclooctene was studied with the series of oxo-imido complexes **3.2-3.8**. The results for the reactions at 1% catalyst loading, 80 °C, and 1 hour reaction times are presented in Figure 3.12. The results show that the bulkier N-DIPP-substituted oxo-imido complexes, and the more activated complex $[^{DMP}(NO)^{PFP}]_2Mo(O)N^tBu$ (**3.5**) were successful in quantitatively converting the *cis*-cyclooctene to its corresponding epoxide. The least effective complex featured the $[^{Ph}(NO)^{tBu}]$ ligand and is likely poor at this transformation due to instability. These results are comparable to the dioxo species in terms of yield and selectivity.

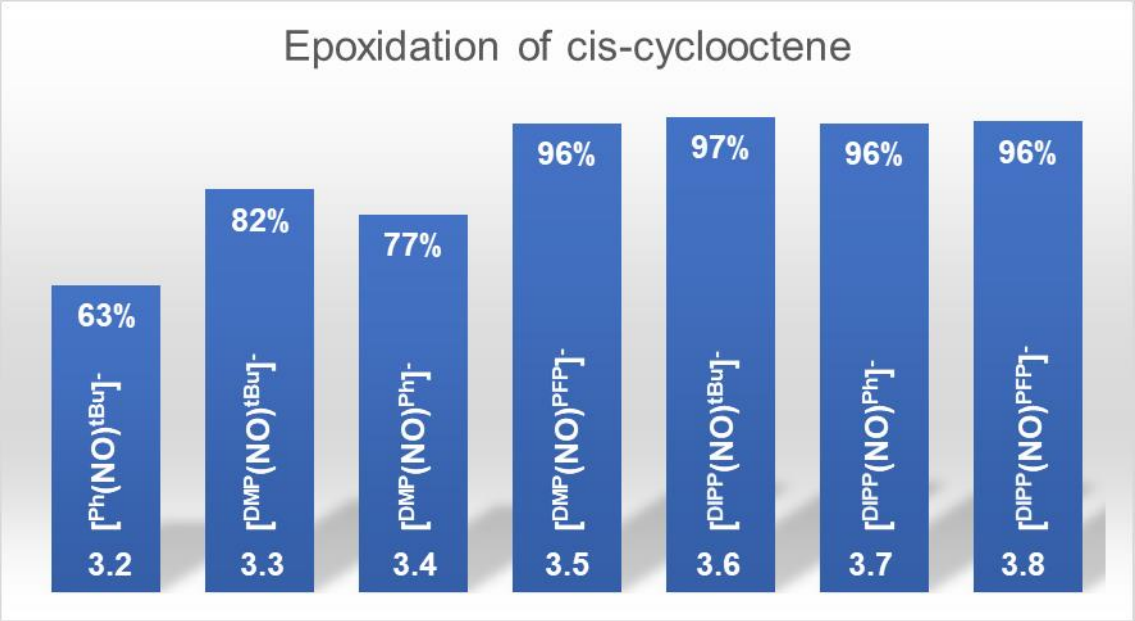

Figure 3.12 % conversion data for the epoxidation of *cis*-cyclooctene by oxo-imido Mo bis(amidate) complexes for 1 h at 80 °C.

3.3 Summary and Conclusions

Oxo-imido complexes of Mo featuring amidate ligands have been synthesized and fully characterized. These are an interesting addition to the relatively small family of Mo oxo-imido complexes. The amidate ligand, while stabilizing these Mo(VI) centers, exhibits a distorted octahedral coordination environment. The amidate ligand is affected by the *trans*-influence that results in a change in bond length of the amidate ligand *trans* to the imido fragment. This results in an overall increase of Mo-O bond length for the series versus the analogous dioxo complexes in Chapter 2. When using the more donating $[^{tBu}(NO)^{tBu}]^-$ ligand, we observe a hemilabile amidate coordination mode when one N-donor is displaced by a coordinated THF molecule. This provides evidence for the predicted hemilabile nature of the amidate ligand at a Mo center.

The utility of mixed oxo-imido Mo bis(amidate) complexes in oxygen atom transfer reactions, such as the epoxidation of alkenes, has been briefly explored, and the results are promising. It is observed that the oxo group can be abstracted by PMe_3 in solution to yield $OPMe_3$ and a PMe_3 coordinated Mo(IV) species similar to reported oxo-imido complexes.[2, 27] and the mixed oxo-imido complexes catalyze epoxidation reactions at 80 °C with quantitative conversion of *cis*-cyclooctene to the epoxide, which is similar to the dioxo analogues (Ch. 2).

3.4 Experimental

3.4.1 General Considerations

Refer to Chapter 2 for the general working conditions.

[^{tBu}(NO)^{tBu}]H (3.1)

This amide was synthesized using literature methods.[41] ^{1}H NMR (400 MHz, Benzene-D_6) δ 1.05 (s, 9H, C-(CH_3)$_3$), 1.26 (s, 9H, N-(CH_3)$_3$), 5.02 (s, 1H, N-*H*).

3.4.2 Synthesis

Synthesis of [^{Ph}(NO)^{tBu}]$_2$MoON^{t}Bu (3.2)

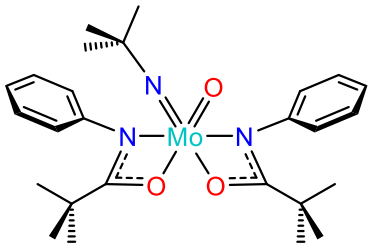

[^{Ph}(NO)^{tBu}]Na (0.699 mmol, 2 eq.) was dissolved in ca. 5 mL of THF and cooled to -30 °C. In a scintillation vial 0.344 g (0.350 mmol, 1 eq.) of [^{t}BuN]MoOCl$_2$(DME) was dissolved in ca. 5 mL of THF and cooled to -30°C. After both solutions were at -30°C the Mo starting material solution was added to the flask containing the stirred solution of ligand salt. The solution was allowed to warm to r.t. and react for 36 h. After 36 h the solvent was removed *in vacuo* from the pale green suspension. The pale green solid was suspended in toluene and filtered over celite yielding a transparent green solution. The solvent was removed to afford 91% (0.170 g) of green product. ^{1}H NMR (400 MHz, Benzene-D_6) δ 1.09 (s, 9H, N-C(CH_3)$_3$), 1.13 (s,

18H, C-C(C*H*$_3$)$_3$), 6.86 (t, *J* = 7.5 Hz, 2H, Ar-*H*), 7.01 (virt. t, 4H, Ar-*H*), 7.24 (d, *J* = 7.5 Hz, 4H, Ar-*H*). ^{13}C NMR (101 MHz, Benzene-*D*$_6$) δ 27.29, 27.82, 28.94, 41.03, 71.65, 119.86, 125.50, 126.39, 128.39, 139.44, 175.60.

Synthesis of [^{DMP}(NO)^{tBu}]$_2$MoON^{t}Bu (3.3)

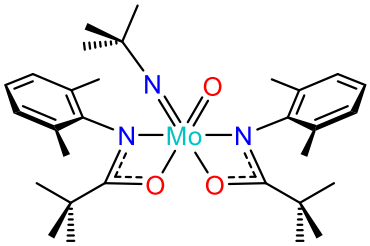

[^{DMP}(NO)^{tBu}]Na (5.8 mmol, 2 eq.) was dissolved in 40 mL of THF and cooled to -35°C. In a scintillation vial 1.000 g (2.9 mmol, 1 eq.) of [^{t}BuN]MoOCl$_2$(DME) was dissolved in 15 mL of THF and cooled to -35°C. After both solutions were at -35°C the Mo starting material solution was added to the flask containing the stirred solution of ligand salt. The solution was allowed to warm to r.t. and react for 24 h. After 24 h the solvent was removed *in vacuo* from the green suspension. The green solid was suspended in toluene and filtered through celite yielding a transparent green solution. The solvent was removed to afford 86.8% (0.567 g) of olive green product. Crystals were grown from slow evaporation of toluene solution. ^{1}H NMR (300 MHz, Benzene-*D*$_6$, 25°C): δ 1.00 (s, 9H, NC(C*H*$_3$)$_3$), δ 1.08 (s, 18H, CC(C*H*$_3$)$_3$), δ 2.49 (broad s, 12H, NC$_6$H$_3$(C*H*$_3$)$_2$), δ 6.88 (broad s, 6H, NC$_6$*H*$_3$(CH$_3$)$_2$). ^{13}C NMR (101 MHz, C$_6$D$_6$) δ 19.19, 27.26, 27.42, 29.08, 40.97, 71.56, 125.83, 127.42, 127.66, 127.91, 134.29. Anal. Calcd. for C$_{30}$H$_{45}$MoN$_3$O$_3$: C, 60.90; H, 7.67: N, 7.10. Found: C, 60.79; H, 7.79; N, 6.75.

Synthesis of [^{DMP}(NO)^{Ph}]$_2$MoON^{t}Bu (3.4)

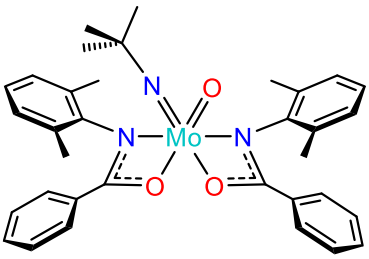

[^{DMP}(NO)^{Ph}]Na (0.89 mmol, 2 eq.) was dissolved in ca. 20 mL of THF and cooled to -100 °C. In a scintillation vial 0.153 g (0.44 mmol, 1 eq.) of [^{t}BuN]MoOCl$_2$(DME) was dissolved in ca. 5 mL of THF and cooled to -100°C. After both solutions were at -100°C the Mo starting material solution was added to the flask containing the stirred solution of ligand salt. The solution was allowed to warm to r.t. and react for 12 h. After 12 h the solvent was removed *in vacuo* from the pale green suspension. The green solid was suspended in toluene and filtered over celite yielding a transparent green solution. The solvent was removed to afford 42% (0.118 g) of olive green product. IR(ATR) (cm^{-1}): 3267, 3114, 3054.6, 3024.2, 2965.2, 2921.6, 2856.7, 1644, 1600, 1512.2, 1476.5, 1449.2, 1298.9, 1264.3, 1232.5, 1180.9, 1132.2, 1092.7, 1027.7, 941.63, 891.16, 842.08, 793.16, 765.9, 706.2, 630.67, 591.17, 539.04. ^{1}H NMR (400 MHz, Benzene-D_6) δ 0.98 (s, 9H), 2.08 – 2.50 (m, 12H), 6.94 (s, 6H), 7.13 (dd, J = 8.2, 7.4 Hz, 4H), 7.25 – 7.32 (m, 2H), 7.37 – 7.44 (m, 4H). ^{13}C NMR (101 MHz, Benzene-D_6) δ 19.05, 21.05, 29.12, 30.72, 72.40, 125.31, 126.24, 127.43, 127.67, 127.91, 127.95, 128.18, 128.26, 128.40, 128.63, 128.95, 130.80, 131.75, 132.51, 134.19.

Synthesis of [^{DMP}(NO)^{PFP}]$_2$MoON^{t}Bu (3.5)

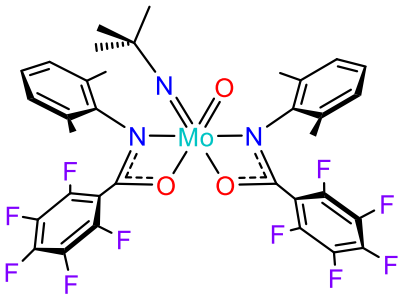

[^{DMP}(NO)^{PFP}]Na (0.78 mmol, 2 eq.) was dissolved in ca. 5 mL of THF and cooled to -100 °C. In a scintillation vial 0.134 g (0.39 mmol, 1 eq.) of [^{t}BuN]MoOCl$_2$(DME) was dissolved in ca. 2 mL of THF and cooled to -100°C. After both solutions were at -100°C, the Mo starting material solution was added to the stirring vial. The solution was allowed to warm to r.t. and react for 24 h. After 24 h the solvent was removed *in vacuo* from the green suspension. The pale green/tan solid was suspended in toluene and filtered over celite yielding a transparent tan solution. The solvent was removed to afford 38% (0.121 g) of light green product. Crystals were grown from slow evaporation of a 1:1 DCM/hexane solution. IR(ATR) (cm^{-1}): 3247.6, 3024, 2972.4, 2926.8, 2860.6, 1655.2, 1593.9, 1494.1, 1444.6, 1327.1, 1249.3, 1215.6, 1107.8, 990.27, 917.78, 871.48, 814.14, 768.14, 712.28, 686.15, 635.62, 580.72, 552.34, 521.01. ^{1}H NMR (400 MHz, Benzene-D_6) δ 1.08 (s, 9H), 2.36 (s, 6H), 2.51 (s, 6H), 6.82 (d, J = 3.5 Hz, 7H). ^{19}F NMR (376 MHz, Benzene-D_6) δ -160.47 (dd, J = 21.3, 15.5 Hz, 2F), -149.10 – -148.93 (m, 1F), -137.57 – -137.33 (m, 2F). ^{13}C{^{1}H} NMR (101 MHz, Benzene-D_6) δ 18.02, 18.69, 19.01, 28.82, 30.40, 71.26, 74.35, 126.53, 127.19, 128.71, 132.82, 134.78, 135.90, 138.38, 142.53, 143.12, 144.97.

Synthesis of [^{DIPP}(NO)^{tBu}]$_2$MoON^{t}Bu (3.6)

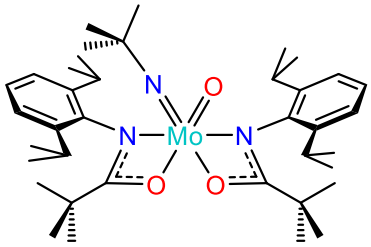

[^{DIPP}(NO)^{tBu}]Na (1.20 mmol, 2 eq.) was dissolved in ca. 10 mL of THF and cooled to -30 °C. In a scintillation vial 0.206 g (0.60 mmol, 1 eq.) of [^{t}BuN]MoOCl$_2$(DME)was dissolved in ca. 5 mL of THF and cooled to -30°C. After both solutions were at -30°C the Mo starting material solution was added to the flask containing the stirred solution of ligand salt. The solution was allowed to warm to r.t. and react for 18 h, after which the solvent was removed *in vacuo* from the green suspension. The green solid was suspended in toluene and filtered over celite yielding a light green solution. The solvent was removed to afford 95% (0.401 g) of light green product. Crystals were grown from slow evaporation of a 1:1 DCM/hexane solution. IR(ATR) (cm^{-1}): 3320.6, 3056.8, 2961, 2925.6, 2866.8, 2708.5, 1646.3, 1582.6, 1449.8, 1360.5, 1325.8, 1230.7, 1175.2, 1105.5, 1042.9, 954.43, 898.9, 847.38, 806.08, 772.98, 738.32, 677.64, 625.99, 587.33, 544.94. ^{1}H NMR (400 MHz, Benzene-D_6) δ 1.08 (s, 3H), 1.09 (s, 9H), 1.12 (s, 9H), 1.16 (s, 9H), 1.25 (dd, J = 12.5, 6.9 Hz, 6H), 1.40 (dd, J = 12.1, 6.8 Hz, 6H), 1.52 (d, J = 6.9 Hz, 3H), 1.72 (d, J = 6.6 Hz, 3H), 1.86 (d, J = 6.5 Hz, 3H), 3.27 (sept, J = 6.7 Hz, 1H), 3.50 (sept, J = 6.9 Hz, 1H), 3.80 (sept, J = 6.8 Hz, 1H), 4.25 (sept, J = 6.7 Hz, 1H), 6.95 (dd, J = 6.7, 2.5 Hz, 1H), 7.00 (dd, J = 7.5, 1.6 Hz, 1H), 7.04 – 7.15 (m, 3H), 7.19 (dd, J = 7.7, 1.7 Hz, 1H). ^{13}C NMR (101 MHz, Benzene-D_6) δ 192.18, 188.25, 145.31, 143.82, 143.27, 143.14, 143.05, 140.65, 127.94, 127.70, 127.46, 126.90, 126.81, 123.78, 123.61, 123.55, 122.96, 72.11, 41.88, 41.15, 28.29, 27.96, 27.92, 27.74, 27.43, 27.23, 25.66, 25.08, 24.30, 23.48, 23.01, 22.94.

Synthesis of [^{DIPP}(NO)^{Ph}]$_2$MoON^{t}Bu (3.7)

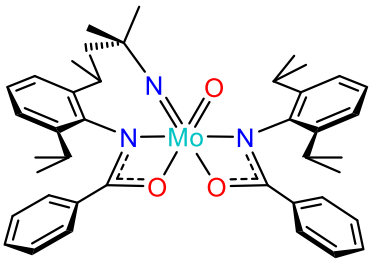

[^{DIPP}(NO)^{Ph}]Na (1.66 mmol, 2 eq.) was dissolved in ca. 20 mL of THF and cooled to -100 °C. In a scintillation vial 0.286 g (0.83 mmol, 1 eq.) of [^{t}BuN]MoOCl$_2$(DME) was dissolved in ca. 5 mL of THF and cooled to -100°C. After both solutions were at -100°C the Mo starting material solution was added to the flask containing the stirred solution of ligand salt. The solution was allowed to warm to r.t. and react for 18 h, after which the solvent was removed *in vacuo* from the dark green suspension. The green solid was suspended in toluene and filtered over celite yielding a light green solution. The solvent was removed to afford 59% (0.366 g) of light green product. Crystals were grown from slow evaporation of a 1:1 DCM/hexane solution. IR(ATR) (cm^{-1}): 3286.5, 3245, 3062, 3026.3, 2967, 2924.4, 2865.4, 1640.6, 1600.8, 1478.8, 1435.4, 1382.5, 1358.8, 1329.5, 1299.9, 1233.6, 1177.7, 1132.4, 1099.2, 1055.7, 1027.3, 944.28, 903.13, 841.22, 774.08, 745.35, 707.25, 637.29, 560.08. ^{1}H NMR (400 MHz, Benzene-D_6) δ 0.75 (d, J = 6.8 Hz, 3H), 1.03 (d, J = 6.6 Hz, 3H), 1.11 (d, J = 6.8 Hz, 3H), 1.18 (s, 3H), 1.20 (s, 9H), 1.36 (s, 6H), 1.71 (d, J = 6.7 Hz, 3H), 1.81 (d, J = 6.6 Hz, 3H), 3.35 – 3.49 (m, 1H), 3.71 – 3.83 (m, 1H), 4.22 (d, J = 8.2 Hz, 1H), 4.31 – 4.46 (m, 1H), 6.78 – 6.86 (m, 4H), 6.86 – 6.95 (m, 2H), 7.06 (d, J = 7.3 Hz, 2H), 7.20 (d, J = 4.0 Hz, 4H), 7.71 (d, J = 7.7 Hz, 2H), 7.84 (d, J = 7.8 Hz, 2H). ^{13}C NMR (101 MHz, Benzene-D_6) δ 137.54, 131.72, 129.88, 128.98, 128.22, 127.95, 127.80, 127.71, 127.47, 127.31, 125.35, 124.75, 124.20, 123.52, 72.68, 30.70, 28.76, 28.32, 28.08, 26.25, 24.51, 24.27, 23.80, 23.44, 22.99, 21.09.

Synthesis of [^{DIPP}(NO)^{PFP}]$_2$MoON^{t}Bu (3.8)

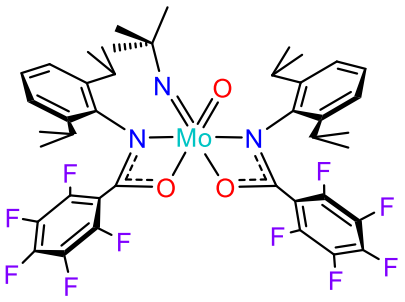

[^{DIPP}(NO)^{PFP}]Na (0.13 mmol, 2 eq.) was dissolved in ca. 5 mL of THF and cooled to -100 °C. In a scintillation vial 0.022 g (0.06 mmol, 1 eq.) of [^{t}BuN]MoOCl$_2$(DME) was dissolved in ca. 2 mL of THF and cooled to -100°C. After both solutions were at -100°C the Mo starting material solution was added to the vial containing the stirred solution of ligand salt. The solution was allowed to warm to r.t. and react for 24 h, after which the solvent was removed *in vacuo* from the pale green suspension. The pale green/tan solid was suspended in toluene and filtered over celite yielding a transparent tan solution. The solvent was removed to afford 85% (0.055 g) of light green product. IR(ATR) (cm^{-1}): 3181.6, 2967.9, 2930.4, 2871.8, 1654.9, 1504, 1463, 1434.9, 1383, 1337.6, 1203.3, 1151.9, 1098.5, 1055.4, 992.58, 909.26, 873.08, 800.88, 731.06, 695.2, 641.58, 573.92, 528.52. ^{1}H NMR (400 MHz, Benzene-D_6) δ 0.81 – 1.06 (m, 6H, CH-(CH_3)$_2$), 1.19 (s, 9H), 1.26 – 1.37 (m, 6H, CH-(CH_3)$_2$), 1.41 (d, J = 6.8 Hz, 3H, CH-(CH_3)$_2$), 1.52 (d, J = 6.7 Hz, 3H, CH-(CH_3)$_2$), 1.62 (d, J = 6.5 Hz, 3H, CH-(CH_3)$_2$), 1.73 (d, J = 6.5 Hz, 3H, CH-(CH_3)$_2$), 3.46 – 3.56 (m, 1H, CH-(CH$_3$)$_2$), 3.61 – 3.71 (m, 1H, CH-(CH$_3$)$_2$), 3.75 (m, 1H, CH-(CH$_3$)$_2$), 4.08 – 4.17 (m, 1H, CH-(CH$_3$)$_2$), 6.83 – 7.06 (m, 6H, Ar-H). ^{13}C NMR (101 MHz, Benzene-D_6) δ 13.91, 22.17, 22.35, 22.49, 23.10, 23.50, 24.90, 25.39, 26.48, 26.99, 27.49, 27.76, 28.45, 29.84, 74.97, 123.53, 124.13, 128.44.

Synthesis of [^{tBu}(NO)^{tBu}]$_2$MoON^{t}Bu-(THF) (3.9)

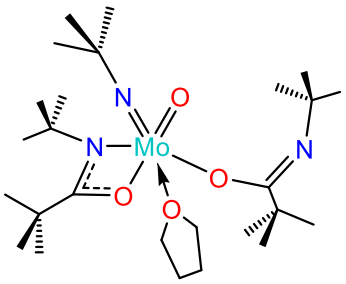

[^{tBu}(NO)^{tBu}]Na (1.27 mmol, 2 eq.) was dissolved in ca. 20 mL of THF and cooled to -100 °C. In a scintillation vial 0.219 g (0.64 mmol, 1 eq.) of [^{t}BuN]MoOCl$_2$(DME) was dissolved in ca. 5 mL of THF and cooled to -100°C. After both solutions were at -100°C, the Mo starting material solution was added to the flask containing the stirred solution of ligand salt. The solution was allowed to warm to r.t. and react for 24 h. After 24 h the solvent was removed *in vacuo* from the dark green suspension. The dark green oil was dissolved in toluene and filtered over celite yielding a transparent tan solution. The solvent was removed to afford 75% (0.238 g) of dark green oily product. Crystals were grown from slow evaporation of a THF solution. ^{1}H NMR (400 MHz, Benzene-D_6) δ 1.05 (s, 9H), 1.28 (s, 9H), 1.39 (s, 9H), 1.57 (s, 9H), 1.66 (s, 9H).

3.4.3 Reactivity Studies

Reaction of complex **3.3** *with PMe$_3$.* A small vial was charged with 100 mg (0.169 mmol) of [^{DMP}(NO)^{tBu}]$_2$MoON^{t}Bu (**3.3**). The complex was dissolved in ca. 2 mL D_6-benzene. To this solution, 51 mg (0.676 mmol, 4 eq) of PMe$_3$ was added and the solution was stirred for 24 h, during which time the pale green solution turned dark green. ^{1}H and ^{31}P NMR spectra were collected of the reaction mixture.

General procedure for epoxidation of *cis*-cyclooctene.

A stock solution of olefin (0.15 M), mesitylene standard (0.075 M), and tertbutylhydroperoxide (TBHP) (0.30 M) in DCE was prepared. To an aliquot of solution was added catalyst at 1 mol % loading, and the resulting solution was heated at 80 °C for 1 hour. The reaction was quenched by adding an excess of MnO_2 powder. Samples were analyzed using an Agilent 7890A Gas Chromatograph, an Agilent 5975C MSD with Electron Impact (EI) ion source, and a Chem Station instrument control and data handling system with a NIST 2008 database library (Agilent Technologies, Inc. Santa Clara, CA, USA). All mass spectra were acquired in EI mode with full scan. Ultra-High Purity Helium carrier gas was set to a column head pressure of 12.5 psi maintaining a constant flow rate of 1.0 mL/min. Aliquots of 1 μL were injected into the instrument with a 25:1 split and a detector delay of 3 min. GC separations were done with a Agilent Technologies HP-5 (30 m, 0.25 mm i.d. and 0.25 μm thickness) programmed to start at 40°C with a 5 min hold, then linear ramp to 250°C at 20°C/min with a 10 min hold at 250°C. MS conditions were as follows: 230°C source, 150°C quadrupole, 150°C interface, 240°C injector and EM voltage of 1.04kV. Full scans were collected over the mass range of 25-500 at 2.86 scans/sec. Data were analyzed using Chem Station software. Compound identification was verified by comparison of sample spectra to spectra available in the NIST08 library.

3.4.4 X-ray Crystallographic Studies

X-ray diffraction data were collected for complexes **3.2**, **3.5**-**3.7**, and **3.9** on a diffractometer with a Bruker APEX CCD area detector[42-43] with graphite-monochromated Mo Kα radiation (λ = 0.71073 Å). Selected crystals were mounted using high vacuum grease or Paratone oil onto a cryoloop and cooled to the data collection temperature of 100 K. Cell parameters were determined from a non-linear least squares fit. The data were corrected for absorption by the empirical method[44] giving minimum and maximum transmission factors. The space groups were determined by systematic absences and statistical tests and verified by subsequent refinement. The structure was solved by direct methods and refined by full-matrix least-squares methods on F2.[45-46] The positions of hydrogens were initially determined by geometry and were refined using a riding model. Non-hydrogen atoms were refined with anisotropic displacement parameters. Hydrogen atom displacement parameters were set to 1.2 (1.5 for methyl) times the isotropic equivalent displacement parameters of the bonded atoms.

3.5 References

1. Young, C. G., Molybdenum. *ChemInform* **2004,** *35* (40).
2. Mosch-Zanetti, N. C.; Wurm, D.; Volpe, M.; Lyashenko, G.; Harum, B.; Belaj, F.; Baumgartner, J., Replacement of an Oxo by an Imido Group in Oxotransferase Model Compounds: Influence on the Oxygen Atom Transfer. *Inorg. Chem.* **2010,** *49*, 8914-8921.
3. Murdzek, J. S.; Schrock, R. R., Well-characterized olefin metathesis catalysts that contain molybdenum. *Organomet.* **1987,** *6* (6), 1373-1374.
4. Takacs, J.; Cavell, R. G., Synthesis and characterization of new d0 tungsten and molybdenum imido complexes with heteroatomic bifunctional O-N chelate ligands. *Inorg. Chem.* **1994,** *33* (12), 2635-2638.
5. Vaughan, W. M.; Abboud, K. A.; Boncella, J. M., Synthesis of a tris(pyrazolyl) borate-stabilized molybdenum alkylidene and its hydrolysis products. Crystal structures of TpMo(CH2C(Me)2Ph) (NAr)(O) and [TpMo(NAr)(O)]2O. *J. Organomet. Chem.* **1995,** *485* (1), 37-43.
6. Cantrell, G. K.; Geib, S. J.; Meyer, T. Y., Ring-opening metathesis of a cyclic imine. *Organomet.* **2000,** *19* (18), 3562-3568.
7. Radius, U.; Wahl, G.; Sundermeyer, J., Diimido-, imido(oxo)-, dioxo- und imido(alkyliden)-halbsandwich-verbindungen über selektive hydrolyse und α—H-abstraktion an organylkomplexen des sechswertigen molybdäns und wolframs. *Z. Anorg. Allg. Chem.* **2004,** *630* (6), 848-857.

8. Merkoulov, A.; Harms, K.; Sundermeyer, J., Synthesis and investigations of the crystal structure of adinuclear diazadiene molybdenum oxo-imido complex with a unique N3Mo(μ-O)2MoN3 core. *Eur. J. Inorg. Chem.* **2005,** *2005* (24), 4902-4906.

9. Cross, W. B.; Anderson, J. C.; Wilson, C.; Blake, A. J., Molybdenum oxo−imido aryloxide complexes: Oxo analogues of olefin metathesis catalysts. *Inorg. Chem.* **2006,** *45* (11), 4556-4561.

10. Cross, W. B.; Anderson, J. C.; Wilson, C. S., Nucleophilic reactivity of a d0molybdenum oxo moiety. *Dalton Trans.* **2009,** (7), 1201-1205.

11. Schultz, B. E.; Hille, R.; Holm, R. H., Direct oxygen atom transfer in the mechanism of action of rhodobacter sphaeroides dimethyl sulfoxide reductase. *J. Am. Chem. Soc.* **1995,** *117* (2), 827--828.

12. Hille, R.; Nishino, T.; Bittner, F., Molybdenum enzymes in higher organisms. *Coord. Chem. Rev.* **2011,** *255* (9-10), 1179-1205.

13. Hille, R., The molybdenum oxotransferases and related enzymes. *Dalton Trans.* **2013,** *42* (9), 3029-3042.

14. Hille, R.; Hall, J.; Basu, P., The mononuclear molybdenum enzymes. *Chem. Rev.* **2014,** *114* (7), 3963-4038.

15. Thapper, A.; Donahue, J. P.; Musgrave, K. B.; Willer, M. W.; Nordlander, E.; Hedman, B.; Hodgson, K. O.; Holm, R. H., The unperturbed oxo−sulfido functional group cis-MoVIOS related to that in the xanthine oxidase family of molybdoenzymes: Synthesis, structural characterization, and reactivity aspects. *Inorg. Chem.* **1999,** *38* (18), 4104-4114.

16. Smith, P. D.; Slizys, D. A.; George, G. N.; Young, C. G., Toward a total model for the molybdenum hydroxylases: Synthesis, redox, and biomimetic chemistry of oxo-thio-Mo(VI) and -Mo(V) complexes. *J. Am. Chem. Soc.* **2000,** *122* (12), 2946-2947.

17. Partyka, D. V.; Staples, R. J.; Holm, R. H., Nucleophilic reactivity and oxo/sulfido substitution reactions of MVIO3 Groups (M = Mo, W). *Inorg. Chem.* **2003,** *42* (24), 7877-7886.

18. Doonan, C. J.; Millar, A. J.; Nielsen, D. J.; Young, C. G., cis-dioxomolybdenum(VI) and oxo(phosphine oxide)molybdenum(IV) complexes: Steric and electronic fine-tuning of cis-[MoOS]2+ precursors. *Inorg. Chem.* **2005,** *44* (13), 4506-4514.

19. Sugimoto, H.; Sakurai, T.; Miyake, H.; Tanaka, K.; Tsukube, H., Mononuclear Five-Coordinate Molybdenum(IV) and -(V) Monosulfide Complexes Coordinated with Dithiolene Ligands: Reversible Redox of Mo(V)/Mo(IV) and Irreversible Dimerization of [MoVS]- Cores to a Dinuclear [MoV2(μ-S)2]2- Core. *Inorganic Chemistry* **2005,** *44* (20), 6927-6929.

20. Laughlin, L. J.; Eagle, A. A.; George, G. N.; Tiekink, E. R. T.; Young, C. G., Synthesis, characterization, and biomimetic chemistry of cis-oxosulfidomolybdenum(VI) complexes stabilized by an intramolecular Mo(O)S···S interaction. *Inorg. Chem.* **2007,** *46* (3), 939-948.

21. Arumuganathan, T.; Volpe, M.; Harum, B.; Wurm, D.; Belaj, F.; Mösch-Zanetti, N. C., Unusual nonoctahedral geometry with molybdenum oxoimido complexes containing η2-pyrazolate ligands. *Inorg. Chem.* **2012,** *51* (1), 150-156.

22. Doonan, C. J.; Slizys, D. A.; Young, C. G., New insights into the Berg-Holm oxomolybdoenzyme model. *J. Am. Chem. Soc.* **1999,** *121* (27), 6430--6436.

23. Stelzig, L.; Kötte, S.; Krebs, B., Molybdenum complexes with tridentate NS2 ligands. Synthesis, crystal structures and spectroscopic properties. *J. Chem. Soc., Dalton Trans.* **1998,** (17), 2921-2926.

24. Subramanian, P.; Spence, J. T.; Ortega, R.; Enemark, J. H., Molybdenum(VI)-dioxo complexes with sterically bulky ligands. *Inorg. Chem.* **1984,** *23* (17), 2564-2572.

25. Craig, J. A.; Harlan, E. W.; Snyder, B. S.; Whitener, M. A.; Holm, R. H., Oxomolybdenum(IV,V,VI) complexes: structures, reactivities, and criteria of detection of binuclear (.mu.-oxo)molybdenum(V) products in oxygen atom transfer systems. *Inorg. Chem.* **1989,** *28* (11), 2082-2091.

26. Barr, M. E.; Smith, S. K.; Spencer, B.; Dahl, L. F., Photochemical synthesis and stereophysical characterization of W(CO), cyclo-(PW(CO)) : Experimental-theoretical bonding analysis of its unprecedented pentametal-coordinated cyclo -P, ligand. *Organomet.* **1991,** *10* (5), 3983--3991.

27. T. Arumuganathan, M. V., Bastian Harum, Dietmar Wurm, Ferdinand Belaj,; Mösch-Zanetti, a. N. C., Unusual nonoctahedral geometry with molybdenum oxoimido complexes containing η2-pyrazolate ligands. *Inorganic Chemistry* **2012,** *51*, 150-156.

28. Zhizhko, P. A.; Zhizhin, A. A.; Zarubin, D. N.; Ustynyuk, N. A., Oxo/imido heterometathesis between N-sulfinylamines and ketones catalyzed by a

silica-supported molybdenum imido complex. *Mendeleev Commun.* **2012,** *22* (2), 64-66.

29. Schrock, R. R.; Murdzek, J. S.; Bazan, G. C.; Robbins, J.; Dimare, M.; O'Regan, M., Synthesis of molybdenum imido alkylidene complexes and some reactions involving acyclic olefins. *J. Am. Chem. Soc.* **1990,** *112* (10), 3875-3886.

30. Schrock, R. R., High-oxidation-state molybdenum and tungsten alkylidyne complexes. *Acc. Chem. Res.* **1986,** *19* (11), 342-348.

31. Ramnauth, R.; Al-Juaid, S.; Motevalli, M.; Parkin, B. C.; Sullivan, A. C., Synthesis, structure, and catalytic oxidation chemistry from the first oxo−imido Schiff base metal complexes. *Inorg. Chem.* **2004,** *43* (13), 4072-4079.

32. Young, C. G., Molybdenum.

33. Mösch-Zanetti, N. C.; Wurm, D.; Volpe, M.; Lyashenko, G.; Harum, B.; Belaj, F.; Baumgartner, J., Replacement of an oxo by an imido group in oxotransferase model compounds: Influence on the oxygen atom transfer. *Inorg. Chem.* **2010,** *49* (19), 8914-8921.

34. Gibson, V. C.; Redshaw, C.; Clegg, W.; Elsegood, M. R. J.; Siemeling, U.; Türk, T., Bridged bis(imido)molybdenum complexes: isolobal analogues of ansa-zirconocenes and bizirconocenes. *J. Chem. Soc., Dalton Trans.* **1996,** (24), 4513-4515.

35. Anderson, J. C.; Smith, N. M.; Robertson, M.; Scott, M. S., An investigation into oxo analogues of molybdenum olefin metathesis complexes as epoxidation catalysts for alkenes. *Tetrahedron Lett.* **2009,** *50* (38), 5344-5346.

36. Volpe, M.; Mösch-Zanetti, N. C., Molybdenum(VI) dioxo and oxo-imido complexes of fluorinated β-ketiminato ligands and their use in OAT reactions. *Inorg. Chem.* **2012,** *51* (3), 1440-1449.

37. Barrie, P.; A. Coffey, T.; D. Forster, G.; Hogarth, G., Bent vs. linear imido ligation at the octahedral molybdenum(VI) dithiocarbamate stabilised centre. *J. Chem. Soc., Dalton Trans.* **1999,** (24), 4519-4528.

38. Chen, T.; Sorasaenee, K. R.; Wu, Z.; Diminnie, J. B.; Xue, Z., Synthesis, characterization and X-ray structures of new molybdenum bis(imide) amide and silyl complexes. *Inorg. Chim. Acta* **2003,** *345*, 113-120.

39. Fox, H. H.; Yap, K. B.; Robbins, J.; Cai, S.; Schrock, R. R., Simple, high yield syntheses of molybdenum(VI) bis(imido) complexes of the type Mo(NR)2Cl2(1,2-dimethoxyethane). *Inorg. Chem.* **1992,** *31* (11), 2287-2289.

40. Schrock, R. R.; Jamieson, J. Y.; Dolman, S. J.; Miller, S. A.; Bonitatebus, P. J.; Hoveyda, A. H., New chiral molybdenum catalysts for asymmetric olefin metathesis that contain 3,3′-disubstituted octahydrobinaphtholate or 2,6-dichlorophenylimido ligands. *Organomet.* **2002,** *21* (2), 409-417.

41. Li, C.; Thomson, R. K.; Gillon, B.; Patrick, B. O.; Schafer, L. L., Amidate complexes of titanium and zirconium: a new class of tunable precatalysts for the hydroamination of alkynes. *Chem. Commun.* **2003,** (19), 2462-2463.

42. *APEX2*, Bruker AXS Inc.: Madison, Wisconsin, USA, 2007.

43. *SAINT*, Bruker AXS Inc.: Madison, Wisconsin, USA, 2007.

44. Krause, L.; Herbst-Irmer, R.; Sheldrick, G. M.; Stalke, D., Comparison of silver and molybdenum microfocus X-ray sources for single-crystal structure determination. *J. Appl. Cryst.* **2015,** *48* (1), 3-10.

45. Sheldrick, G., SHELXT - Integrated space-group and crystal-structure determination. *Acta Crystallogr., Sect. A: Found. Crystallogr.* **2015,** *71* (1), 3-8.

46. Sheldrick, G., Crystal structure refinement with SHELXL. *Acta Crystallogr., Sect. C: Cryst. Struct. Commun.* **2015,** *71* (1), 3-8.

Chapter 4: Bis(Imido) Amidate Complexes: Synthesis, Characterization and Group Transfer Applications

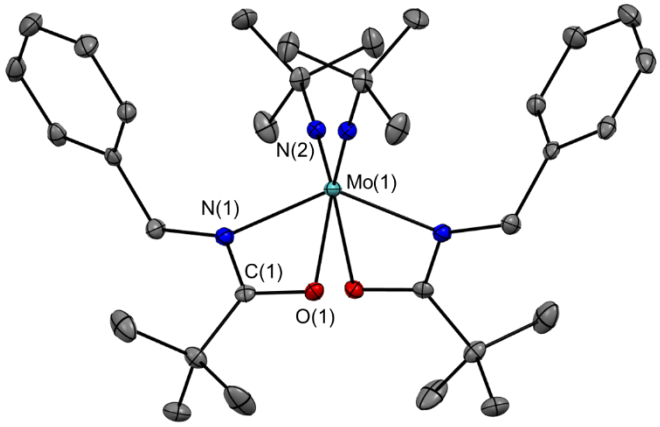

4.1 Introduction

Bis(imido) complexes of Mo(VI) are of interest to our group and others for their ability to perform the metathesis reaction with imines.[1-5] The cross-metathesis of imines is useful for the generation of new carbon-nitrogen bonds as shown in Scheme 4.1A. Considering the metathesis of alkenes as an analogous reaction, the metathesis of imines could also be applied to ring closing reactions to generate complex ring systems and ring-opening metathesis polymerization (ROMP) of cyclic imines, which would be a valuable reaction for the generation of new polymers.[5-6] Currently there are only a couple of examples of ring-opening metathesis of a cyclic imine[5-6], but without polymerization as shown in Scheme 4.1B. The potential advantages of metal-catalyzed metathesis of imines, over known mechanisms, e.g. acid catalyzed imine metathesis[7], are milder

reactions conditions, better selectivity, tolerance for functional groups, and faster reaction rates.[4-5]

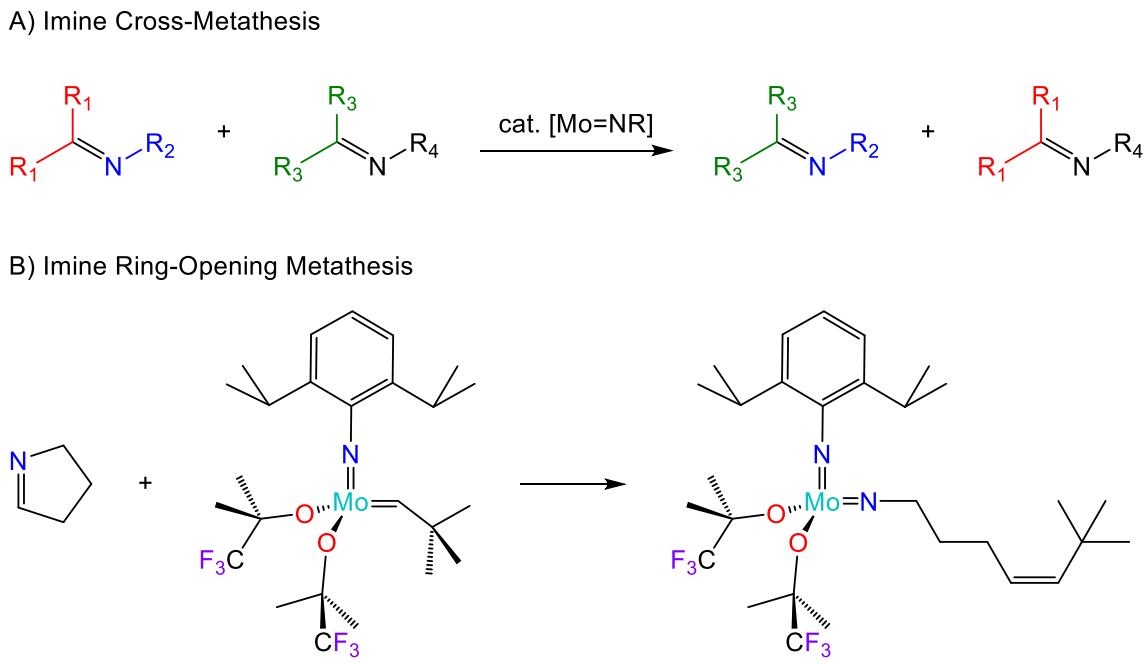

Scheme 4.1 (A) General cross-metathesis reactions of imines. (B) First example of a ring opening metathesis of a cyclic imine.

Bis(amidate) complexes of W featuring two imido groups are the only examples of Group 6 amidate complexes outside of this work.[8] In this chapter we will discuss the properties of bis(imido) complexes featuring the ligands previously described in chapters 2 and 3, as well as complexes featuring benzyl (Bn) (**4.1**), 3,5-dimethylphenyl (^{m}DMP) (**4.2**), and perfluorophenyl (PFP) (**4.3**) substituents bound to the N atom of the amidate ligands as shown in Figure 4.1. These ligands are an extension of the less bulky [^{Ph}(NO)^{tBu}]$_2$MoE$_2$ complexes studied in Chapters 2 and 3. To our knowledge this is the

first reported use of the N-Bn and N-PFP substituted amidate ligands on any metal system.

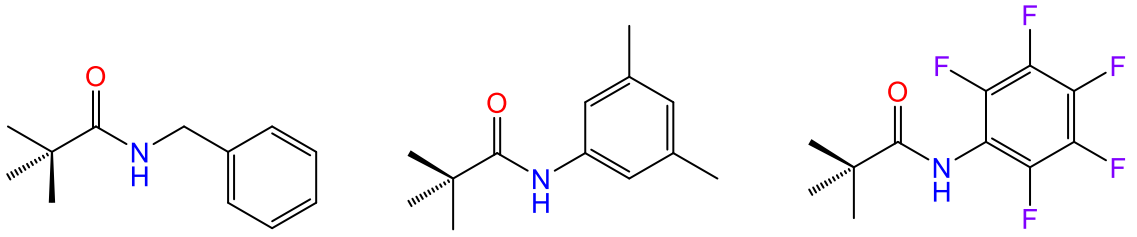

$[^{Bn}(NO)^{tBu}]H$ $[^{mDMP}(NO)^{tBu}]H$ $[^{PFP}(NO)^{tBu}]H$

4.1 **4.2** **4.3**

Figure 4.1 New amide proligands used in bis(imido) complex syntheses.

4.2 Results and Discussion

4.2.1 Synthesis

Bis(imido) complexes of molybdenum featuring amidate ligands can be obtained by salt metathesis methods. The proligand $[^{R}(NO)^{R'}]H$ was dissolved in THF and an equivalent of $NaN(SiMe_3)_2$ added, and the reaction mixture was stirred for 2 h. The volatiles were removed *in vacuo* leaving behind the sodium salt of the ligand. This salt was redissolved in THF and cooled to -30°C. The Mo starting material $Cl_2Mo(N^tBu)_2(DME)$ was dissolved in THF separately and cooled to -30°C. The Mo precursor solution was added quickly to the cooled ligand salt solution and stirred. The reaction solution was then slowly warmed to room temperature and stirred for another 2-24 h and the volatiles were removed *in vacuo*. The crude mixture was suspended in toluene and filtered over celite to removes salt byproducts. The solvent was removed *in vacuo* to yield the desired Mo-bis(amidate) complex. In most cases, no further purification was needed.

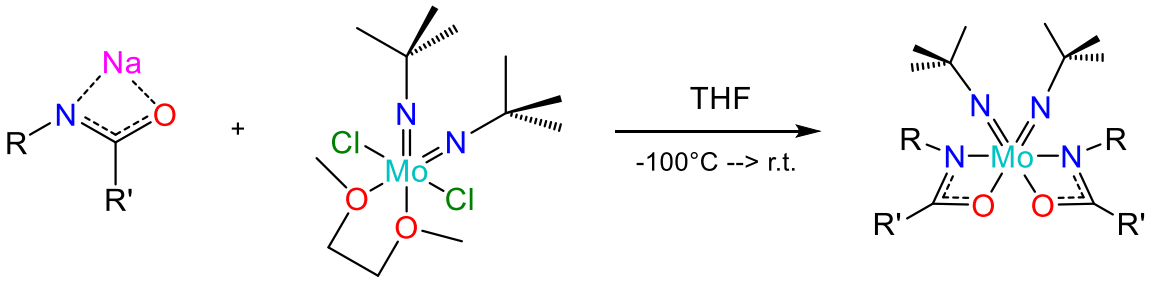

R' = ^{t}Bu and R = Ph (**4.4**), ^{o}DMP (**4.5**), DIPP (**4.8**), Bn (**4.11**), ^{m}DMP (**4.12**), or PFP (**4.13**)
R' = Ph and R = ^{o}DMP (**4.6**) or DIPP (**4.9**)
R' = PFP and R = ^{o}DMP (**4.7**) or DIPP (**4.10**)

Figure 4.2 General synthetic scheme for Mo(VI) bis(imido) bis(amidate) complexes.

4.2.2 Nuclear Magnetic Resonance Studies

The ^{1}H NMR spectra of the bis(imido) complexes prepared in this study were collected in D_6-benzene at 25 °C. All of the bis(imido) complexes exhibit C_2 axial symmetry in solution as expected. For all of the complexes, the Mo[=N^{t}Bu]$_2$ protons appear as a singlet between 1 and 1.3 ppm as illustrated for the ^{o}DMP series of complexes **4.5-4.7** in Figure 4.3. In these complexess, the protons of the aryl methyl groups resonate between 2 and 3 ppm, indicating hindered rotation about the N-C_{ispo} bonds of the aryl groups of the ligands, and C_2 symmetry about the metal center.

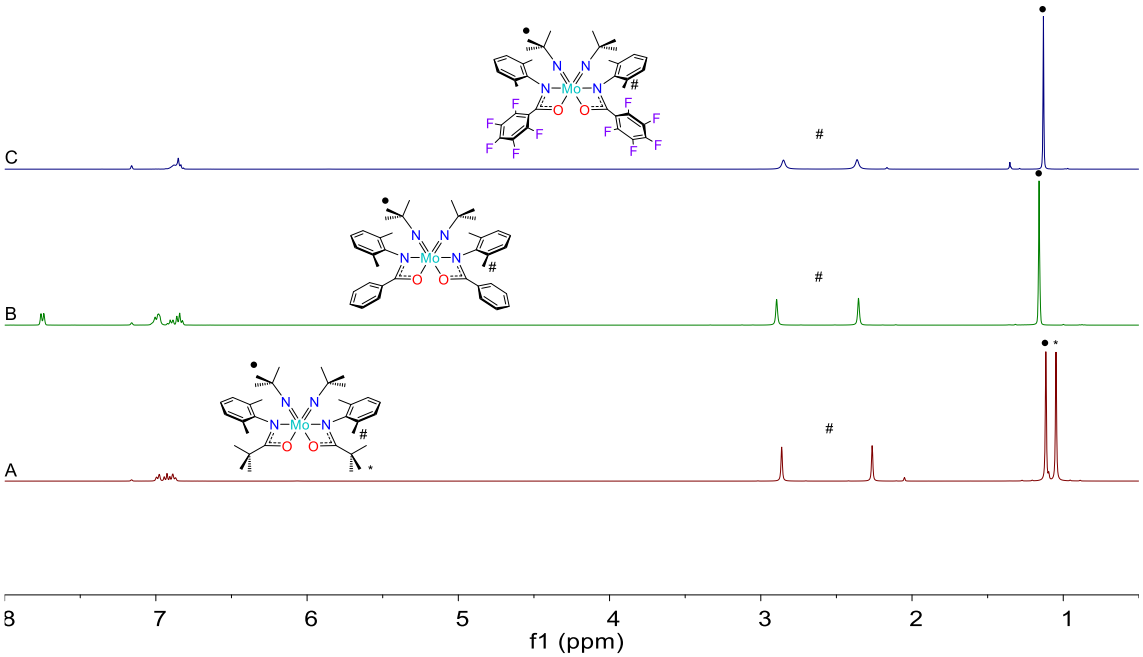

Figure 4.3 ^{1}H NMR spectra for complexes **4.5** (A), **4.6** (B), and **4.7** (C).

As seen in the DIPP series for the dioxo and oxo-imido complexes in Chapters 2 and 3, the ^{1}H NMR spectrum becomes more complicated due to steric hindrance. The isopropyl methyl groups typically present as 4 peaks between 1 and 2 ppm as demonstrated by the peaks labelled C in Figure 4.4. The methine protons are well-defined septets around 4 ppm (peaks B, Figure 4.4). This contrasts with the dioxo and oxo-imido complexes, which had less well-defined spectral features. The increased steric bulk in these bis(imido) species appears to enforce a more static structure in solution.

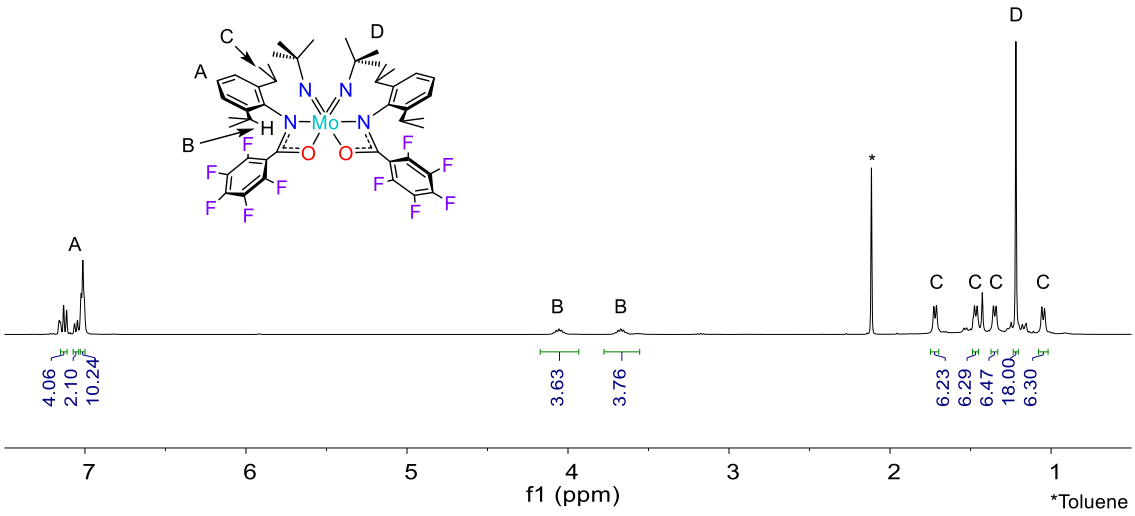

Figure 4.4 ^{1}H NMR spectrum for [^{DIPP}(NO)^{PFP}]$_2$Mo(N^{t}Bu)$_2$ (**4.10**).

The less bulky ligand systems, where R = Ph, Bn, ^{m}DMP, and PFP and R′ = ^{t}Bu, have simpler ^{1}H NMR spectra. For example, the ^{1}H NMR spectrum for [^{Bn}(NO)^{tBu}]$_2$Mo(N^{t}Bu)$_2$ (**4.11)** is presented in Figure 4.5. The aryl peaks of the benzyl groups are sharp, indicating free rotation of the phenyl rings. The ^{t}Bu peaks of the amidate ligands and imido fragments both appear as singlets at 1.20 ppm and 1.23 ppm. The benzylic protons appear as a doublet at about 5 ppm.

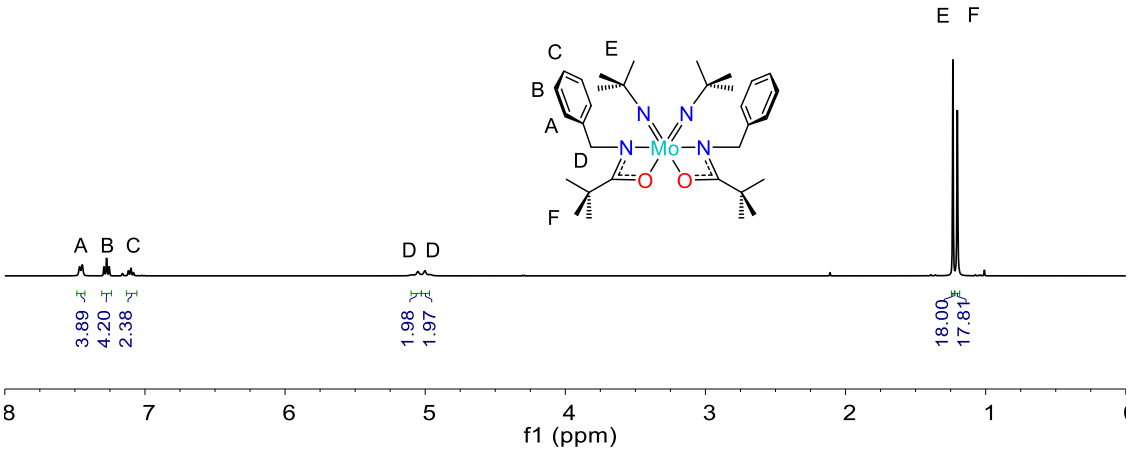

Figure 4.5 ^{1}H NMR of [^{Bn}(NO)^{tBu}]$_2$Mo(N^{t}Bu)$_2$ (**4.11**).

4.2.3 X-ray Crystallographic Studies

Crystals suitable for X-ray crystallographic analyses of complexes **4.4**, **4.7**, **4.9**, **4.11**, and **4.12** were grown from slow evaporation of 1:1 solutions of DCM/hexanes at room temperature. Single crystals of complexes **4.5** and **4.13** were grown from slow evaporation of toluene solutions at room temperature, and single crystals of complex **4.6** were afforded from slow evaporation of a hexane solution at room temperature.

The X-ray crystal structure of $[^{Ph}(NO)^{tBu}]_2Mo(N^tBu)_2$ (**4.4**) is shown in Figure 4.6. The *trans* bond angles N(1A)-Mo(1A)-N(2A), N(3A)-Mo(1A)-O(1A), and N(4A)-Mo(1A)-O(2A) are 140.01(5)°, 153.44(5)°, and 154.02(5)°, respectively. The imido bond angles Mo(1A)-N(3A)-C(23A) and Mo(1A)-N(4A)-C(27) are 178.12(11)° and 156.44(12)°, respectively. These bond angles show that one of the imido ligands are slightly bent, indicating less triple-bond character.[9] The amidate bite angles N(1A)-Mo(1A)-O(1A) and N(2A)-Mo(1A)-O(2A) are 59.43(5)° and 58.19(4)°, respectively. The *cis*-imido bond angle for N(3A)-Mo(1A)-N(4A) is 107.40(6)°, and the amidate O(1A)-Mo(1A)-O(2A) angle is 74.53(4)°.

The imido bond lengths Mo(1A)-N(3A), Mo(1A)-N(4A), N(3A)-C(23A), and N(4A)-C(27A) are 1.7393(14) Å, 1.7513(13) Å, 1.448(2) Å, and 1.453(2) Å, respectively. The longer Mo=N bond corresponds with the slightly bent bond angle. The amidate bond lengths Mo(1A)-N(1A), Mo(1A)-N(2A), Mo(1A)-O(1A), and Mo(1A)-O(2A) are 2.1114(12) Å, 2.1108(12) Å, 2.2670(11) Å, and 2.3569(11) Å, respectively. The Mo-O bond for the amidate ligand *trans* to the bent imido group [Mo(1A)-O(2A)] is longer indicating a *trans* influence similar to the affect described with the oxo-imido complexes in Chapter 3. The C-N and C-O bond lengths for the amidate ligands are 1.3298(19) Å,

1.3375(19) Å, 1.2770(17) Å, and 1.2687(17) Å for N(1A)-C(7A), N(2A)-C(18A), O(1A)-C(7), and O(2A)-C(18A) Å, respectively. These lengths indicate more double bond character with the amidate C-O bonds, indicating an amido-ketone ligand resonance structure. Selected bond angles and distances are presented in Table 4.1.

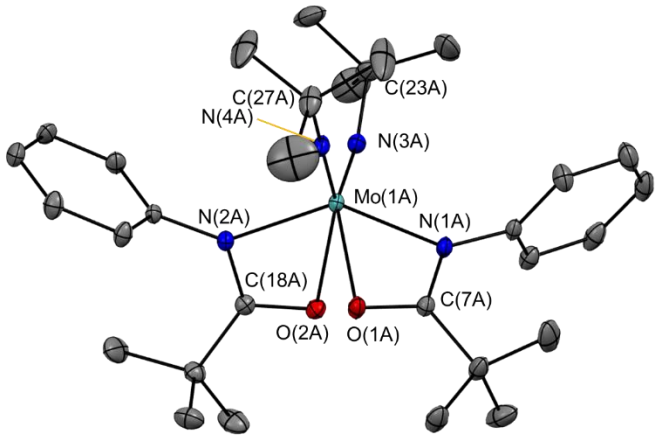

Figure 4.6 Thermal ellipsoid plot of $[^{Ph}(NO)^{tBu}]_2Mo(N^tBu)_2$ (**4.4**) shown at 50% probability with hydrogens omitted for clarity.

Table 4.1 Selected Bond Distances (Å) and Angles (°) for $[^{Ph}(NO)^{tBu}]_2Mo(N^tBu)_2$, **4.4**.

	Lengths (Å)		Angles (°)
O(2A)-C(18A)	1.2687(17)	N(2A)-Mo(1A)-O(2A)	58.19(4)
O(1A)-C(7A)	1.2770(17)	N(1A)-Mo(1A)-O(1A)	59.43(4)
N(1A)-C(7A)	1.3298(19)	O(1A)-Mo(1A)-O(2A)	74.53(4)
N(2A)-C(18A)	1.3375(19)	N(2A)-Mo(1A)-O(1A)	87.08(4)
N(3A)-C(23A)	1.448(2)	N(1A)-Mo(1A)-O(2A)	89.93(4)
N(4A)-C(27A)	1.453(2)	N(3A)-Mo(1A)-O(2A)	90.42(5)
Mo(1A)-N(3A)	1.7393(14)	N(4A)-Mo(1A)-O(1A)	94.66(5)
Mo(1A)-N(4A)	1.7513(13)	N(4A)-Mo(1A)-N(2A)	98.41(5)
Mo(1A)-N(2A)	2.1108(12)	N(3A)-Mo(1A)-N(1A)	99.67(5)
Mo(1A)-N(1A)	2.1114(12)	N(3A)-Mo(1A)-N(2A)	103.67(6)
Mo(1A)-O(1A)	2.2670(11)	N(4A)-Mo(1A)-N(1A)	105.02(6)
Mo(1A)-O(2A)	2.3569(11)	N(3A)-Mo(1A)-N(4A)	107.40(6)
		N(2A)-Mo(1A)-N(1A)	140.01(5)
		N(3A)-Mo(1A)-O(1A)	153.44(5)
		N(4A)-Mo(1A)-O(2A)	154.02(5)
		C(27A)-N(4A)-Mo(1A)	156.44(12)
		C(23A)-N(3A)-Mo(1A)	178.12(11)

The X-ray crystal structure for $[^{oDMP}(NO)^{tBu}]_2Mo(N^tBu)_2$ (**4.5**) is shown in **Figure 4.7**. The *trans* angles N(1A)-Mo(1)-N(1B), N(1D)-Mo(1)-O(1A), and N(1C)-Mo(1)-O(1B) are 139.69(14)°, 152.14(15)°, and 154.02(14)°, respectively. The imido bond angles Mo(1)-N(1C)-C(1C) and Mo(1)-N(1D)-C(1D) are 166.0(3)° and 166.1(3)°, respectively. These are within the typical linear range of 160-180° for a triply-bound imido moiety.[9] The amidate bite angles N(1A)-Mo(1)-O(1A) and N(1B)-Mo(1)-O(1B) are 58.71(12)° and 58.70(13)°, respectively. The *cis*-imido angle N(1C)-Mo(1)-N(1D) is 107.31(18)°, while the amidate angle O(1A)-Mo(1)-O(1B) is 74.76(11)°.

The imido bond lengths Mo(1)-N(1C), Mo(1)-N(1D), N(1C)-C(1C), and N(1D)-C(1D) are 1.741(4) Å, 1.743(4) Å, 1.464(5) Å, and 1.459(5) Å, respectively. The

amidate bond lengths Mo(1)-N(1A), Mo(1)-N(1B), Mo(1)-O(1A), and Mo(1)-O(1B) are 2.124(4) Å, 2.126(4) Å, 2.285(3) Å, and 2.292(3) Å, respectively. The C-N and C-O bond lengths N(1A)-C(9A), N(1B)-C(9B), O(1A)-C(9A), and O(1B)-C(9B) are 1.335(5) Å, 1.307(5) Å, 1.272(5) Å, and 1.293(5) Å, respectively. This again corresponds to the amido-ketone bonding character in the ligands. Selected bond angles and distances are presented in Table 4.2.

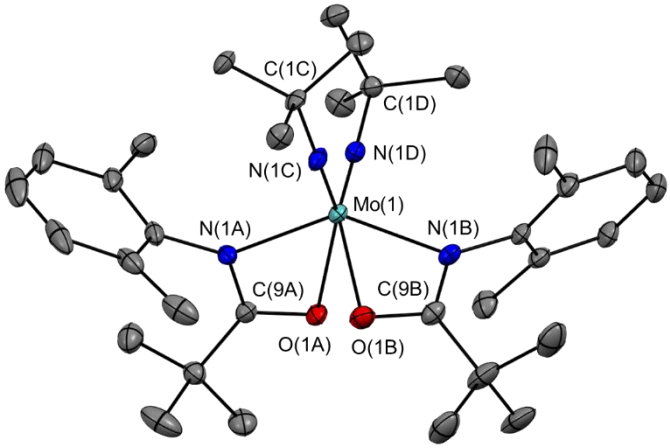

Figure 4.7 Thermal ellipsoid plot of $[^{oDMP}(NO)^{tBu}]_2Mo(N^tBu)_2$ (**4.5**) shown at 50% probability with hydrogens omitted for clarity.

Table 4.2 Selected Bond Distances (Å) and Angles (°) for $[^{oDMP}(NO)^{tBu}]_2Mo(N^tBu)_2$, **4.5**.

	Lengths (Å)		Angles (°)
O(1A)-C(9A)	1.272(5)	N(1B)-Mo(1)-O(1B)	58.70(13)
O(1B)-C(9B)	1.293(5)	N(1A)-Mo(1)-O(1A)	58.71(12)
N(1B)-C(9B)	1.307(5)	O(1B)-Mo(1)-O(1A)	74.76(11)
N(1A)-C(9A)	1.335(5)	N(1B)-Mo(1)-O(1A)	87.55(12)
N(1D)-C(1D)	1.459(5)	N(1A)-Mo(1)-O(1B)	89.27(13)
N(1C)-C(1C)	1.464(5)	N(1D)-Mo(1)-O(1B)	91.89(15)
Mo(1)-N(1C)	1.741(4)	N(1C)-Mo(1)-O(1A)	93.86(14)
Mo(1)-N(1D)	1.743(4)	N(1D)-Mo(1)-N(1A)	97.56(15)
Mo(1)-N(1A)	2.124(4)	N(1C)-Mo(1)-N(1B)	98.22(15)
Mo(1)-N(1B)	2.126(3)	N(1C)-Mo(1)-N(1A)	104.90(15)
Mo(1)-O(1B)	2.285(3)	N(1D)-Mo(1)-N(1B)	106.55(15)
Mo(1)-O(1A)	2.292(3)	N(1C)-Mo(1)-N(1D)	107.31(18)
		N(1A)-Mo(1)-N(1B)	139.69(14)
		N(1D)-Mo(1)-O(1A)	152.14(15)
		N(1C)-Mo(1)-O(1B)	154.02(14)
		C(1D)-N(1D)-Mo(1)	166.0(3)
		C(1C)-N(1C)-Mo(1)	166.1(3)

The X-ray crystal structure of the variant with the phenyl backbone $[^{oDMP}(NO)^{Ph}]_2Mo(N^tBu)_2$ (**4.6**) is shown in Figure 4.8. The *trans* angles N(1A)-Mo(1)-N(1B), N(1D)-Mo(1)-O(1B), and N(1C)-Mo(1)-O(1A) are 140.60(5)°, 150.99(6)°, and 151.44(6)°, respectively. The imido bond angles Mo(1)-N(1C)-C(1C) and Mo(1)-N(1D)-C(1D) are 154.03(12)° and 171.73(15)°, respectively. These bond angles show that one of the imido ligands are slightly bent, indicating less triple-bond character.[9] The amidate bite angles N(1A)-Mo(1)-O(1A) and N(1B)-Mo(1)-O(1B) are 58.41(5)° and 59.11(5)°, respectively. The *cis*-imido bond angle N(1D)-Mo(1)-N(1C) is 107.17(6), while the amidate angle O(1B)-Mo(1)-O(1A) is 73.41(4)°.

The imido bond distances for Mo(1)-N(1C), Mo(1)-N(1D), N(1C)-C(1C), and N(1D)-C(1D) are 1.7603(14) Å, 1.7400(13) Å, 1.460(2) Å, and 1.458(2) Å, respectively.

The amidate bond distances Mo(1)-N(1A), Mo(1)-N(1B), Mo(1)-O(1A), and Mo(1)-O(1B) are 2.1271(14) Å, 2.1402(15) Å, 2.3391(13) Å, and 2.2896(12) Å, respectively. The Mo-O bond for the amidate ligand *trans* to the bent imido group [Mo(1)-O(1A)] is longer indicating a *trans* influence. The The C-O and C-N bond lengths for the amidate ligands O(1A)-C(1A), O(1B)-C(1B), N(1A)-C(1A), and N(1B)-C(1B) are 1.271(2) Å, 1.279(2) Å, 1.332(2) Å, and 1.325(2) Å, respectively. Selected bond distances and angles are presented in Table 4.3.

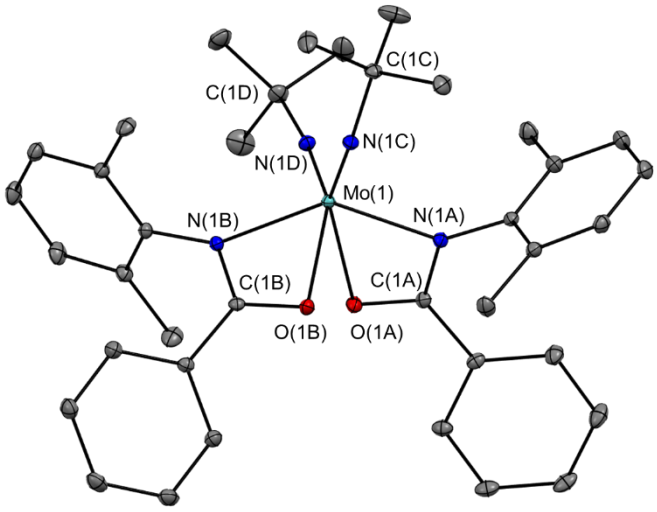

Figure 4.8 Thermal ellipsoid plot of [^{oDMP}(NO)^{Ph}]$_2$Mo(N^{t}Bu)$_2$ (**4.6**) shown at 50% probability with hydrogens omitted for clarity.

Table 4.3 Selected Bond Distances (Å) and Angles (°) for $[^{oDMP}(NO)^{Ph}]_2Mo(N^tBu)_2$, **4.6**.

	Lengths (Å)		Angles (°)
O(1A)-C(1A)	1.271(2)	N(1A)-Mo(1)-O(1A)	58.41(5)
O(1B)-C(1B)	1.279(2)	N(1B)-Mo(1)-O(1B)	59.11(5)
N(1B)-C(1B)	1.325(2)	O(1B)-Mo(1)-O(1A)	73.41(4)
N(1A)-C(1A)	1.332(2)	N(1A)-Mo(1)-O(1B)	88.47(5)
N(1D)-C(1D)	1.458(2)	N(1B)-Mo(1)-O(1A)	89.02(5)
N(1C)-C(1C)	1.460(2)	N(1D)-Mo(1)-O(1A)	92.85(6)
Mo(1)-N(1D)	1.7400(13)	N(1C)-Mo(1)-O(1B)	95.73(6)
Mo(1)-N(1C)	1.7603(14)	N(1C)-Mo(1)-N(1A)	95.75(6)
Mo(1)-N(1A)	2.1271(14)	N(1D)-Mo(1)-N(1B)	96.09(7)
Mo(1)-N(1B)	2.1402(15)	N(1D)-Mo(1)-N(1A)	106.24(7)
Mo(1)-O(1B)	2.2896(12)	N(1D)-Mo(1)-N(1C)	107.17(6)
Mo(1)-O(1A)	2.3391(13)	N(1C)-Mo(1)-N(1B)	108.29(6)
		N(1A)-Mo(1)-N(1B)	140.60(5)
		N(1D)-Mo(1)-O(1B)	150.99(6)
		N(1C)-Mo(1)-O(1A)	151.44(6)
		C(1C)-N(1C)-Mo(1)	154.03(12)
		C(1D)-N(1D)-Mo(1)	171.73(15)

The X-ray crystal structure of the perfluorophenyl variant $[^{oDMP}(NO)^{PFP}]_2Mo(N^tBu)_2$ (**4.7**) is shown in Figure 4.9. The *trans* angles N(2A)-Mo(1A)-N(1A), N(4A)-Mo(1A)-O(2A), and N(3A)-Mo(1A)-O(1A) are 141.4(4)°, 149.5(3)°, and 150.9(3)°, respectively. The imido bond angles Mo(1A)-N(3A)-C(31A) and Mo(1A)-N(4A)-C(35A) are 168.6(8)° and 162.8(7)°, respectively. The amidate bite angles N(1A)-Mo(1A)-O(1A) and N(2A)-Mo(1A)-O(2A) are 58.2(3)° and 58.6(3)°, respectively. The *cis*-imido angle N(4A)-Mo(1A)-N(3A) is 108.0(4), while the amidate angle O(2A)-Mo(1A)-O(1A) is 71.5(2)°.

The imido bond lengths Mo(1A)-N(4A), Mo(1A)-N(3A), N(3A)-C(31A), and N(4A)-C(35A) are 1.736(9) Å, 1.757(9) Å, 1.449(13) Å, and 1.500(13) Å, respectively. The amidate bond lengths Mo(1A)-N(1A), Mo(1A)-N(2A), Mo(1A)-O(1A), and

Mo(1A)-O(2A) are 2.126(9) Å, 2.108(9) Å, 2.357(7) Å, and 2.350(7) Å, respectively. The C-O and C-N bond lengths for the amidate ligands O(1A)-C(1A), O(2A)-C(16A), N(1A)-C(1A), and N(2A)-C(16A) are 1.270(12) Å, 1.278(12) Å, 1.307(13) Å, and 1.338(13) Å, respectively. These distances are consistent with amido-ketone binding character, where the N of the amidate ligand is more closely bound to the Mo and the C-O bond is more of a double bond, indicating more of a neutral coordination from the oxygen (O→Mo) and an anionic bond by the nitrogen atom (N-Mo). Selected bond distances and angles are presented in Table 4.4.

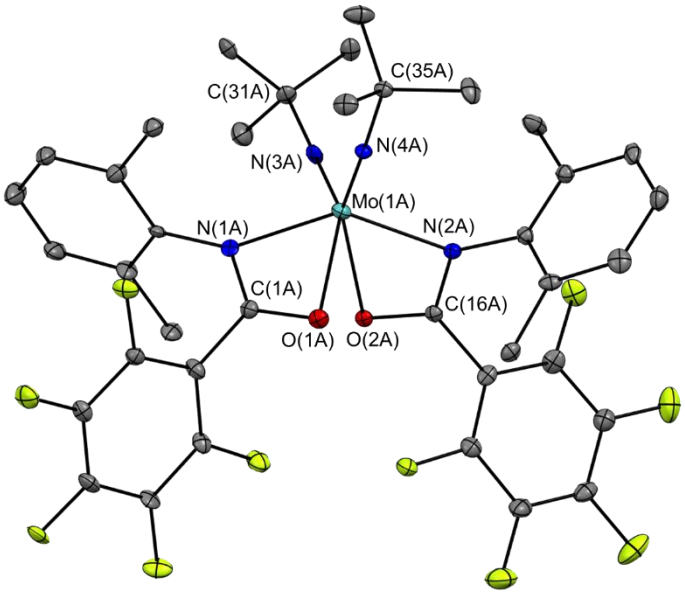

Figure 4.9 Thermal ellipsoid plot of [^{oDMP}(NO)^{PFP}]$_2$Mo(N^{t}Bu)$_2$ (**4.7**) shown at 50% probability with hydrogens omitted for clarity.

Table 4.4 Selected Bond Distances (Å) and Angles (°) for $[^{oDMP}(NO)^{PFP}]_2Mo(N^tBu)_2$, **4.7**.

Lengths (Å)			Angles (°)
O(1A)-C(1A)	1.270(12)	N(1A)-Mo(1A)-O(1A)	58.2(3)
O(2A)-C(16A)	1.278(12)	N(2A)-Mo(1A)-O(2A)	58.6(3)
N(1A)-C(1A)	1.307(13)	O(2A)-Mo(1A)-O(1A)	71.5(2)
N(2A)-C(16A)	1.338(13)	N(1A)-Mo(1A)-O(2A)	88.9(3)
N(3A)-C(31A)	1.449(13)	N(2A)-Mo(1A)-O(1A)	89.6(3)
N(4A)-C(35A)	1.500(13)	N(4A)-Mo(1A)-O(1A)	94.7(3)
Mo(1A)-N(4A)	1.736(9)	N(3A)-Mo(1A)-O(2A)	95.2(3)
Mo(1A)-N(3A)	1.757(9)	N(4A)-Mo(1A)-N(2A)	95.3(4)
Mo(1A)-N(2A)	2.108(9)	N(3A)-Mo(1A)-N(1A)	96.9(4)
Mo(1A)-N(1A)	2.126(9)	N(3A)-Mo(1A)-N(2A)	105.7(4)
Mo(1A)-O(2A)	2.350(7)	N(4A)-Mo(1A)-N(1A)	107.2(4)
Mo(1A)-O(1A)	2.357(7)	N(4A)-Mo(1A)-N(3A)	108.0(4)
		N(2A)-Mo(1A)-N(1A)	141.4(4)
		N(4A)-Mo(1A)-O(2A)	149.5(3)
		N(3A)-Mo(1A)-O(1A)	150.9(3)
		C(35A)-N(4A)-Mo(1A)	162.8(7)
		C(31A)-N(3A)-Mo(1A)	168.6(8)

The X-ray crystal structure of the bulkier DIPP derivative $[^{DIPP}(NO)^{Ph}]_2Mo(N^tBu)_2$ (**4.9**) is shown in Figure 4.10. The *trans* angles N(2A)-Mo(1A)-N(1A), N(4A)-Mo(1A)-O(2A), and N(3A)-Mo(1A)-O(1A) are 143.41(9)°, 152.72(10)°, and 151.61(10)°, respectively. The imido bond angles Mo(1A)-N(3A)-C(39A) and Mo(1A)-N(4A)-C(43A0 are 168.6(2)° and 170.0(2)°, respectively. The amidate bite angles N(1A)-Mo(1A)-O(1A) and N(2A)-Mo(1A)-O(2A) are 59.44(8)° and 58.20(8)°, respectively. The *cis*-imido angle N(4A)-Mo(1A)-N(3A) is 108.23(12)°, while the amidate angle O(2A)-Mo(1A)-O(1A) is 76.93(7)°.

The imido bond lengths Mo(1A)-N(4A), Mo(1A)-N(3A), N(3A)-C(39A), and N(4A)-C(43A) are 1.723(7) Å, 1.729(2) Å, 1.439(4) Å, and 1.445(4) Å, respectively. The amidate bond lengths Mo(1A)-N(1A), Mo(1A)-N(2A), Mo(1A)-O(1A), and

Mo(1A)-O(2A) are 2.125(2) Å, 2.115(2) Å, 2.242(2) Å, and 2.319(2) Å, respectively. The C-O and C-N bond lengths for the amidate ligands O(1A)-C(13A), O(2A)-C(32A), N(1A)-C(13A), and N(2A)-C(32A) are 1.258(3) Å, 1.253(3) Å, 1.321(3) Å, and 1.334(3) Å, respectively. Again, these distances are consistent with amido-ketone binding character. Selected bond distances and angles are presented in Table 4.5.

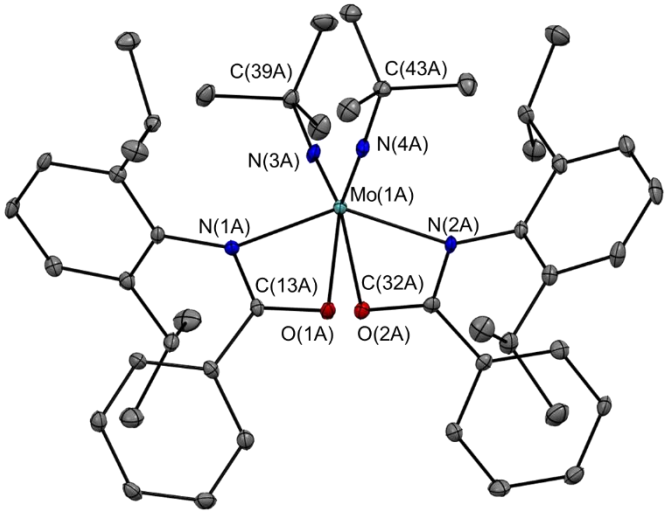

Figure 4.10 Thermal ellipsoid plot of $[^{DIPP}(NO)^{Ph}]_2Mo(N^tBu)_2$ (**4.9**) shown at 50% probability with hydrogens omitted for clarity.

Table 4.5 Selected Bond Distances (Å) and Angles (°) for $[^{DIPP}(NO)^{Ph}]_2Mo(N^tBu)_2$, **4.9**.

	Lengths (Å)		Angles (°)
O(2A)-C(32A)	1.253(3)	N(2A)-Mo(1A)-O(2A)	58.20(8)
O(1A)-C(13A)	1.258(3)	N(1A)-Mo(1A)-O(1A)	59.44(8)
N(1A)-C(13A)	1.321(3)	O(1A)-Mo(1A)-O(2A)	76.93(7)
N(2A)-C(32A)	1.334(3)	N(2A)-Mo(1A)-O(1A)	89.31(8)
N(3A)-C(39A)	1.439(4)	N(3A)-Mo(1A)-O(2A)	90.93(10)
N(4A)-C(43A)	1.445(4)	N(4A)-Mo(1A)-O(1A)	92.91(10)
Mo(1A)-N(4A)	1.723(3)	N(1A)-Mo(1A)-O(2A)	93.87(8)
Mo(1A)-N(3A)	1.729(2)	N(3A)-Mo(1A)-N(1A)	96.63(10)
Mo(1A)-N(2A)	2.115(2)	N(4A)-Mo(1A)-N(2A)	96.99(10)
Mo(1A)-N(1A)	2.125(2)	N(4A)-Mo(1A)-N(1A)	102.70(10)
Mo(1A)-O(1A)	2.242(2)	N(3A)-Mo(1A)-N(2A)	106.13(10)
Mo(1A)-O(2A)	2.319(2)	N(4A)-Mo(1A)-N(3A)	108.23(12)
		N(2A)-Mo(1A)-N(1A)	143.41(9)
		N(3A)-Mo(1A)-O(1A)	151.61(10)
		N(4A)-Mo(1A)-O(2A)	152.72(10)
		C(39A)-N(3A)-Mo(1A)	168.6(2)
		C(43A)-N(4A)-Mo(1A)	170.0(2)

The X-ray crystal structure of the sterically open N-benzyl derivative $[^{Bn}(NO)^{tBu}]_2Mo(N^tBu)_2$ (**4.11**) is shown in Figure 4.11. The *trans* angles N(1)-Mo(1)-N(1)#1 and N(2)-Mo(1)-O(1), are 134.72(7)°, and 156.26(5)°, respectively. The imido bond angles are nearly perfectly linear at 176.98°, indicating triply-bound imido moieties.[9] The amidate bite angle is 59.06(4)°. The *cis*-imido angle N(2)-Mo(1)-N(1)#1 is 106.27(6)°, while the amidate angle O(1)-Mo(1)-O(1)#1 is 76.39(5)°.

The imido bond lengths Mo(1)-N(2) and N(2)-C(13) are 1.7503(14) Å and 1.442(3) Å, respectively. The amidate bond lengths Mo(1)-N(1) and Mo(1)-O(1) are 2.1109(13) Å and 2.2904(11) Å, respectively. The C-O and C-N bond lengths for the amidate ligands O(1)-C(1) and N(1)-C(1) are 1.2716(19) Å and 1.327(2) Å, respectively.

Again, these distances are consistent with amido-ketone binding character. Selected bond distances and angles are presented in Table 4.6.

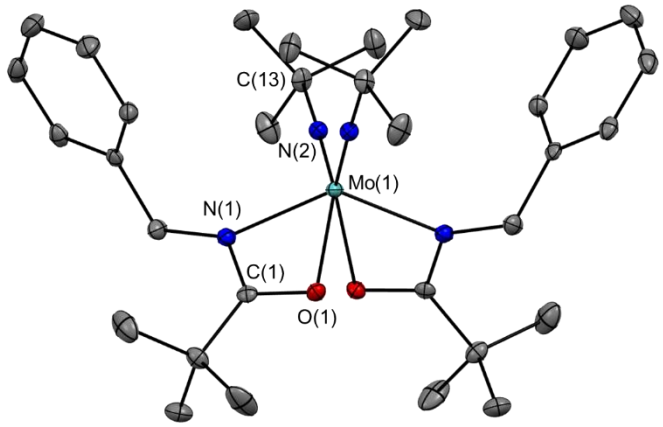

Figure 4.11 Thermal ellipsoid plot of $[^{Bn}(NO)^{tBu}]_2Mo(N^tBu)_2$ (**4.11**) shown at 50% probability with hydrogens omitted for clarity.

Table 4.6 Selected Bond Distances (Å) and Angles (°) for $[^{Bn}(NO)^{tBu}]_2Mo(N^tBu)_2$, **4.11**.

	Lengths (Å)		Angles (°)
O(1)-C(1)	1.2716(19)	N(1)-Mo(1)-O(1)	59.06(4)
N(1)-C(1)	1.327(2)	O(1)#1-Mo(1)-O(1)	76.39(5)
N(2)-C(13)	1.442(3)	N(1)-Mo(1)-O(1)#1	84.79(4)
Mo(1)-N(2)	1.7503(14)	N(2)-Mo(1)-O(1)#1	91.15(5)
Mo(1)-N(1)	2.1109(13)	N(2)-Mo(1)-N(1)	100.25(5)
Mo(1)-O(1)	2.2904(11)	N(2)-Mo(1)-N(1)#1	106.27(6)
O(1)-C(1)	1.2716(19)	N(1)-Mo(1)-N(1)#1	134.72(7)
		N(2)-Mo(1)-O(1)	156.26(5)
		C(13)-N(2)-Mo(1)	176.98(17)

The X-ray crystal structure of $[^{mDMP}(NO)^{tBu}]_2Mo(N^tBu)_2$ (**4.12**) is shown in Figure 4.12. The *trans* angles N(2)-Mo(1)-N(1), N(4)-Mo(1)-O(2), and N(3)-Mo(1)-O(1) are 143.04(10)°, 152.38(10)°, and 153.97(9)°, respectively. The imido bond angles Mo(1)-N(3)-C(27) and Mo(1)-N(4)-C(31) are 154.3(2)° and 175.9(2)°, respectively.

Again, this is indicating one bent and one linear imido group. The amidate bite angles N(1)-Mo(1)-O(1) and N(2)-Mo(1)-O(2) are 57.73(8)° and 59.55(8)°, respectively. The *cis*-imido angle N(4)-Mo(1)-N(3) is 106.33(12)°, while the amidate angle O(2)-Mo(1)-O(1) is 78.56(7)°.

The imido bond lengths Mo(1)-N(4), Mo(1)-N(3), N(3)-C(27), and N(4)-C(31) are 1.736(2) Å, 1.755(2) Å, 1.445(4) Å, and 1.443(4) Å, respectively. The amidate bond lengths Mo(1)-N(1), Mo(1)-N(2), Mo(1)-O(1), and Mo(1)-O(2) are 2.095.(2) Å, 2.109(2) Å, 2.3862(19) Å, and 2.3254(2) Å, respectively. As seen with complexes **4.4** and **4.6**, the longer Mo-O amidate bond corresponds to the increased *trans* influence of the bent imido fragment. The C-O and C-N bond lengths for the amidate ligands O(1)-C(1), O(2)-C(14), N(1)-C(1), and N(2)-C(14) are 1.259(3) Å, 1.277(3) Å, 1.333(3) Å, and 1.333(4) Å, respectively. Similar to previously described complexes, these distances are consistent with amido-ketone binding character. Selected bond distances and angles are presented in **Table 4.7**.

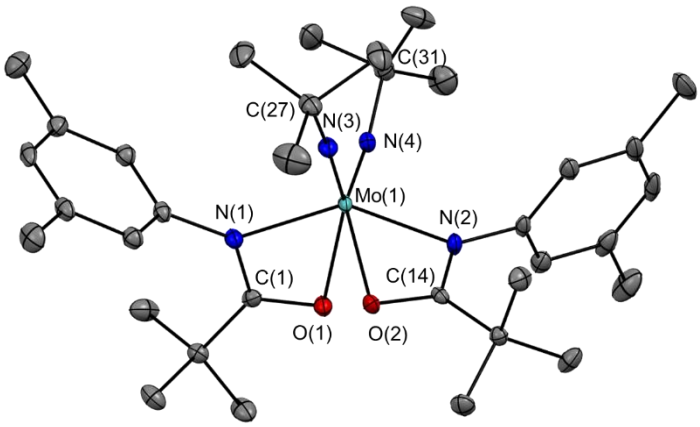

Figure 4.12 Thermal ellipsoid plot of [^{mDMP}(NO)^{tBu}]$_2$Mo(N^{t}Bu)$_2$ (**4.12**) shown at 50% probability with hydrogens omitted for clarity.

Table 4.7 Selected Bond Distances (Å) and Angles (°) for $[^{mDMP}(NO)^{tBu}]_2Mo(N^tBu)_2$, **4.12**.

	Lengths (Å)		Angles (°)
O(1)-C(1)	1.259(3)	N(1)-Mo(1)-O(1)	57.73(8)
O(2)-C(14)	1.277(3)	N(2)-Mo(1)-O(2)	59.55(8)
N(1)-C(1)	1.333(3)	O(2)-Mo(1)-O(1)	78.56(7)
N(2)-C(14)	1.333(4)	N(4)-Mo(1)-O(1)	87.18(10)
N(4)-C(31)	1.443(4)	N(1)-Mo(1)-O(2)	88.83(9)
N(3)-C(27)	1.445(4)	N(2)-Mo(1)-O(1)	94.83(8)
Mo(1)-N(4)	1.736(2)	N(3)-Mo(1)-O(2)	96.39(10)
Mo(1)-N(3)	1.755(2)	N(3)-Mo(1)-N(1)	96.96(10)
Mo(1)-N(1)	2.095(2)	N(4)-Mo(1)-N(2)	98.82(10)
Mo(1)-N(2)	2.109(2)	N(4)-Mo(1)-N(1)	103.46(11)
Mo(1)-O(2)	2.254(2)	N(3)-Mo(1)-N(2)	104.63(10)
Mo(1)-O(1)	2.3862(19)	N(4)-Mo(1)-N(3)	106.33(12)
		N(1)-Mo(1)-N(2)	143.04(10)
		N(4)-Mo(1)-O(2)	152.38(10)
		N(3)-Mo(1)-O(1)	153.97(9)
		C(27)-N(3)-Mo(1)	154.3(2)
		C(31)-N(4)-Mo(1)	175.9(2)

The X-ray crystal structure of the unusual N-perfluorophenyl species $[^{PFP}(NO)^{tBu}]_2Mo(N^tBu)_2$ (**4.13**) is shown in Figure 4.13. The *trans* angles N(2)-Mo(1)-N(1), N(4)-Mo(1)-O(2), and N(3)-Mo(1)-O(1) are 140.15(11)°, 154.24(11)°, and 152.17(12)°, respectively. The imido bond angles Mo(1)-N(3)-C(23) and Mo(1)-N(4)-C(27) are 179.0(3)° and 154.3(2)°, respectively. This is indicative of one bent and one linear imido group. The amidate bite angles N(1)-Mo(1)-O(1) and N(2)-Mo(1)-O(2) are 59.01(9)° and 57.76(10)°, respectively. The *cis*-imido angle N(4)-Mo(1)-N(3) is 107.49(14)°, while the amidate angle O(2)-Mo(1)-O(1) is 71.79(9)°.

The imido bond lengths Mo(1)-N(4), Mo(1)-N(3), N(3)-C(23), and N(4)-C(27) are 1.754(3) Å, 1.735(3) Å, 1.458(4) Å, and 1.456(5) Å, respectively. The amidate bond lengths Mo(1)-N(1), Mo(1)-N(2), Mo(1)-O(1), and Mo(1)-O(2) are 2.126(3) Å, 2.112(3)

Å, 2.275(2) Å, and 2.359(3) Å, respectively. Again, the longer Mo-O bond is coincident with a *trans* bent imido group. The C-O and C-N bond lengths for the amidate ligands O(1)-C(1), O(2)-C(16), N(1)-C(1), and N(2)-C(16) are 1.262(4) Å, 1.259(4) Å, 1.343(4) Å, and 1.341(5) Å, respectively. These distances are consistent with the series. Selected bond distances and angles are presented in Table 4.8.

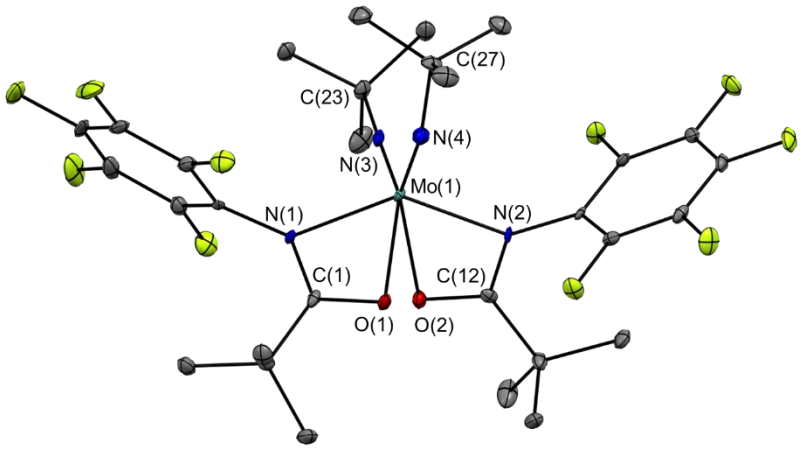

Figure 4.13 Thermal ellipsoid plot of $[^{PFP}(NO)^{tBu}]_2Mo(N^tBu)_2$ (**4.13**) shown at 50% probability with hydrogens omitted for clarity.

Table 4.8 Selected Bond Distances (Å) and Angles (°) for $[^{PFP}(NO)^{tBu}]_2Mo(N^tBu)_2$, **4.13**.

	Lengths (Å)		Angles (°)
O(2)-C(12)	1.259(4)	N(2)-Mo(1)-O(2)	57.76(10)
O(1)-C(1)	1.262(4)	N(1)-Mo(1)-O(1)	59.01(9)
N(2)-C(12)	1.341(5)	O(1)-Mo(1)-O(2)	71.79(9)
N(1)-C(1)	1.343(4)	N(2)-Mo(1)-O(1)	87.02(10)
N(4)-C(27)	1.456(5)	N(1)-Mo(1)-O(2)	89.83(10)
N(3)-C(23)	1.458(4)	N(3)-Mo(1)-O(2)	91.08(12)
Mo(1)-N(3)	1.735(3)	N(4)-Mo(1)-O(1)	96.28(12)
Mo(1)-N(4)	1.754(3)	N(4)-Mo(1)-N(2)	99.88(12)
Mo(1)-N(2)	2.112(3)	N(3)-Mo(1)-N(1)	100.41(12)
Mo(1)-N(1)	2.126(3)	N(3)-Mo(1)-N(2)	102.51(12)
Mo(1)-O(1)	2.275(2)	N(4)-Mo(1)-N(1)	103.71(13)
Mo(1)-O(2)	2.359(3)	N(3)-Mo(1)-N(4)	107.49(14)
		N(2)-Mo(1)-N(1)	140.15(11)
		N(3)-Mo(1)-O(1)	152.17(12)
		N(4)-Mo(1)-O(2)	154.24(11)
		C(27)-N(4)-Mo(1)	154.3(2)
		C(23)-N(3)-Mo(1)	179.0(3)

The average bond distances for the Mo(VI) bis(amidate) family is presented in Table 4.9 for comparative purposes. Overall, bond lengths for the Mo=N^{t}Bu fragments of all bis(imido) complexes are slightly varied with an average length of 1.744 Å, with 1.723(3) Å for **4.6** being the shortest and 1.7603(14) Å for **4.3** as the longest, which is longer than the overall average distance of 1.726 for the oxo-imido series. The longer Mo=N bonds coincide with a smaller Mo=N-C bond angles, which is indicative of less triple-bond character, as seen in $[^{oDMP}(NO)^{Ph}]_2Mo(N^tBu)_2$ (**4.3**) where Mo(1)-N(1C) is 1.7603(14) Å and the corresponding angle Mo(1)-N(1C)-C(1C) is 154.03(12)°.

In general, the C-O bonds of amidate ligands are significantly shorter (1.270 Å Avg.) and the C-N bonds are longer (1.329 Å Avg.) for the series of complexes. The average amidate Mo-O and Mo-N bond lengths for the bis(imido) complexes are 2.310 Å and 2.117 Å, respectively, compared to 2.278 Å and 2.116 Å for the oxo-imido series

and 2.258 Å and 2.094 Å for the dioxo series. A general *trans* influence is observed, where the amidate ligand *trans* to a more bent imido group can be characterized as having increased amido-ketone character. This is observed with longer Mo-O and C-N bonds, and shorter Mo-N and C-O bonds for the amidate ligands.

Table 4.9 Average bond distances for the Mo bis(amidate) series.

Bond	Oxo-Imido (Å)	Dioxo (Å)	Bis(Imido) (Å)	Overall Average (Å)
O-C (amidate)	1.269	1.274	1.270	1.271
N-C (amidate)	1.327	1.327	1.329	1.328
N-C (imido)	1.479		1.454	1.466
Mo=O (oxo)	1.701	1.692		1.696
Mo=N (imido)	1.726		1.744	1.735
Mo-N (amidate)	2.116	2.094	2.117	2.109
Mo-O (amidate)	2.278	2.258	2.310	2.282

4.2.4 Imine Metathesis Reactivity

Initial tests of imine metathesis using activated imines **4.14** (Figure 4.14) and **4.15** indicated some cross-metathesis product formation, however **4.14** was not very soluble in C_6D_6 making quantification of conversion difficult. The reaction was performed in C_6D_6 at 50 °C for 3 h using 10% loading of the complex $[^{oDMP}(NO)^{PFP}]_2Mo(N^tBu)_2$ (**4.7**). Upon addition of the precatalyst the solution became a dark purple color, and after 3 h the solution was lime green. The ^{1}H NMR spectra of the reaction and starting imines **4.14** and **4.15** are shown in Figure 4.14. There is clear formation of some other imine products indicated by the peaks between 8.0-8.3 ppm. The peaks at about 1.2 ppm indicate the formation of some ^{t}Bu byproducts from the reaction.

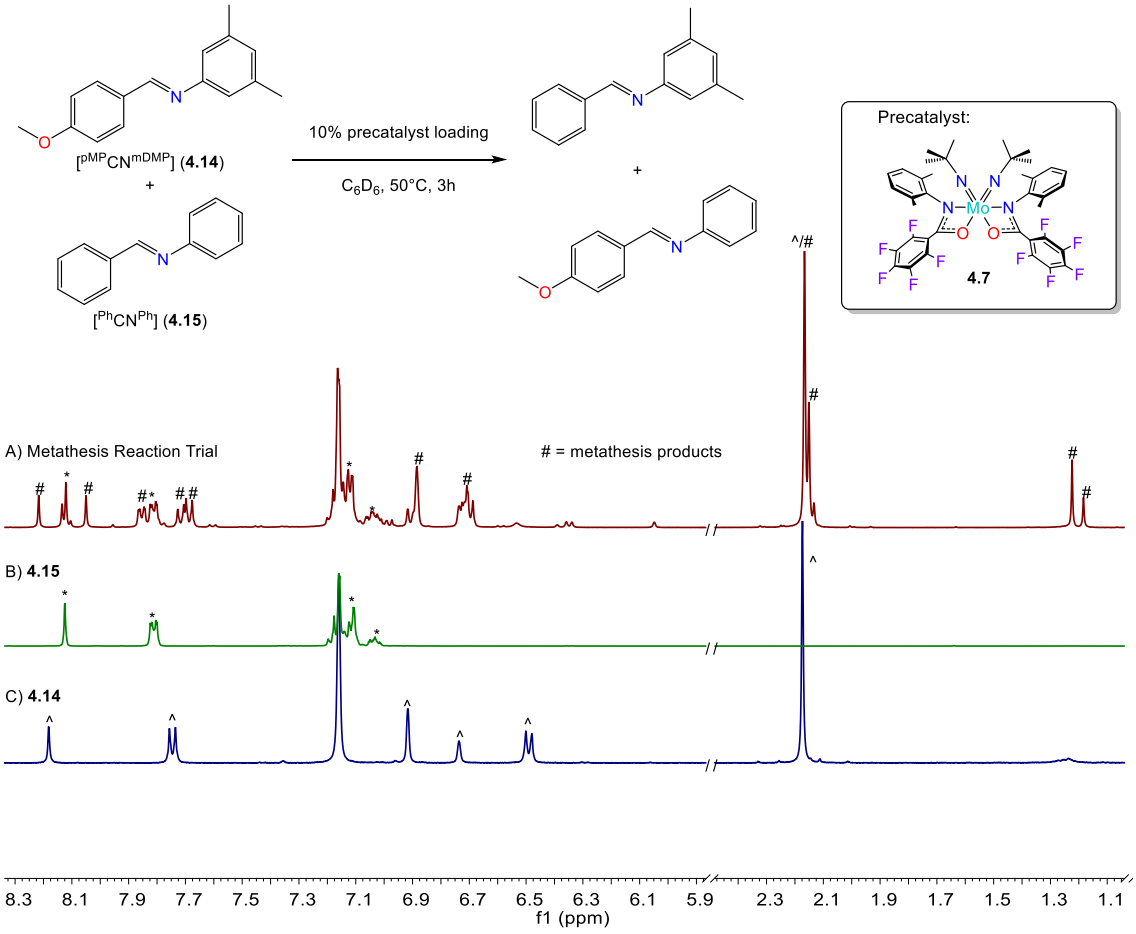

Figure 4.14 Imine metathesis reaction with activated substrate and relevant sections of the ^{1}H NMR spectra for (A) the catalyst test reaction (10% precatalyst loading (**4.7**), 50 °C, 3 h), (B) [^{Ph}CN^{Ph}] (**4.15**), and (C) [^{pMP}CN^{mDMP}] (**4.14**).

The quantification issue can be overcome by using a more soluble substrate **4.16** (Scheme 4.2B) however, the complexes **4.4-4.7** did not appear to produce any cross-metathesis products. This reaction needs to be further investigated using the full series of bis(imido) complexes and oxo-imido complexes presented in Chapter 3 to gauge the ability of the bis(amidate) complexes for this reactivity.

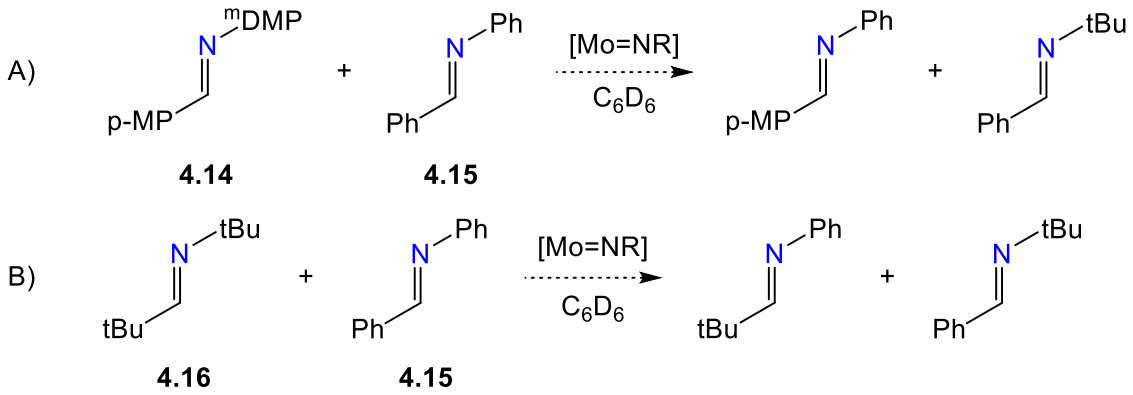

Scheme 4.2 The cross-metathesis reactions of [^{Ph}CN^{Ph}] (**4.15**) with (A) an "activated" imine, [^{pMP}CN^{mDMP}] (**4.14**), and (B) a simple imine, [^{tBu}CN^{tBu}] (**4.16**).

4.3 Conclusions

A series of bis(imido) Mo(VI) bis(amidate) complexes have been synthesized and characterized, including several species bearing amidate ligands that have not been previously reported. These bis(imido) complexes tend to be more stable toward moisture than the oxo-imido and dioxo analogues, presumably due to the added steric hindrance at the metal center induced by the ^{t}Bu imido moieties. The ^{1}H NMR spectra of these complexes suggest a C_2 symmetric Mo-center, with hindered rotation for the N-^{o}DMP and N-DIPP derivatives (**4.5**-**4.10**). The majority of these complexes have yielded crystals suitable for X-ray crystallography, and these structures show an amido-ketone binding motif for the amidate ligands as in the other complexes reported in Chapters 2 and 3. Multiple complexes feature non-linear imido ligands, which exhibit a strong *trans* influence on the amidate ligands, as observed with the oxo-imido complexes in Chapter 3.

The use of Mo bis(imido) as catalysts for the cross-metathesis of imines has been briefly investigated, indicating a more activated imine is required to drive the reaction forward. This reactivity should be expanded to include the full series of bis(imido) complexes, as well as the oxo-imido complexes presented in Chapter 3.

4.4 Experimental

4.4.1 General Considerations

Refer to Chapter 2 for general working conditions. Amidate proligands **4.1**-**4.3** were synthesized via previously reported literature protocols.[10] The ^{1}H NMR data is presented here as reference to compare with Mo-complex data.

[^{Bn}(NO)^{tBu}]H (4.1)

^{1}H NMR (400 MHz, Benzene-D_6) δ 1.04 (s, 9H, C-(CH_3)$_3$), 4.31 (d, J = 5.9 Hz, 2H, N-CH_2), 5.60 (s, 1H, N-H), 7.03 – 7.08 (m, 1H, Ar-H), 7.10 – 7.14 (m, 4H, Ar-H).

[^{mDMP}(NO)^{tBu}]H (4.2)

^{1}H NMR (400 MHz, Benzene-D_6) δ 1.06 (s, 9H, C-(CH_3)$_3$), 2.13 (s, 6H, Ar-(CH_3)$_2$), 6.60 (s, 1H, Ar-H), 6.81 (s, 1H, N-H), 7.29 (s, 2H, Ar-H).

[^{PFP}(NO)^{tBu}]H (4.3)

^{1}H NMR (400 MHz, Benzene-D_6) δ 1.00 (s, 9H, C-(CH_3)$_3$), 6.09 (s, 1H, N-H). ^{19}F NMR (376 MHz, Benzene-d_6) δ -163.91 – -163.46 (m, 2F, Ar-F), -157.42 (t, J = 22.0 Hz, 1F, Ar-F), -146.51 – -146.32 (m, 2H, Ar-F).

4.4.2 Synthesis

Synthesis of $[^{Ph}(NO)^{tBu}]_2Mo(N^tBu)_2$ (4.4)

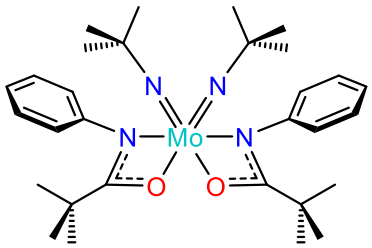

$[^{Ph}(NO)^{tBu}]Na$ (0.71 mmol, 2 eq.) was dissolved in ca. 20 mL of THF and cooled to -100 °C. In a scintillation vial 0.141 g (0.35 mmol, 1 eq.) of $[^tBuN]_2MoCl_2(DME)$ was dissolved in ca. 5 mL of THF and cooled to -100°C. After both solutions were at -100°C, the metal starting material solution was added to the flask containing the stirred solution of ligand salt. The solution was slowly warmed to r.t. and stirred for 24 h after which time the solvent was removed *in vacuo* from the yellow suspension. The yellow solid was suspended in toluene and filtered over celite to remove salts yielding a transparent yellow solution. The solvent was removed to afford 70% (0.145 g) of yellow product. Crystals were grown from slow evaporation of a 1:1 DCM/hexane solution. IR(ATR) (cm^{-1}): 2964.4, 2917.9, 1654.5, 1595.5, 1473.2, 1442.7, 1362.3, 1317.1, 1253.7, 1218.3, 1188.3, 1116.9, 1068.4, 1027.8, 954.4, 904.17, 843.97, 779.24, 749.25, 696.97, 587.32. ^{1}H NMR (400 MHz, Benzene-D_6) δ 1.16 (s, 18H, C-(CH_3)$_3$), 1.20 (s, 18H, N-(CH_3)$_3$), 6.89 (t, J = 7.4 Hz, 2H, Ar-*H*), 7.05 (t, J = 7.8 Hz, 4H, Ar-*H*), 7.27 (d, J = 7.7 Hz, 4H, Ar-*H*). ^{13}C NMR (101 MHz, Benzene-D_6) δ 128.80, 128.15, 127.96, 127.72, 127.48, 126.98, 124.56, 123.66, 119.55, 68.81, 41.23, 30.58, 28.27, 27.14.

Synthesis of [^{oDMP}(NO)^{tBu}]$_2$Mo(N^{t}Bu)$_2$ (4.5)

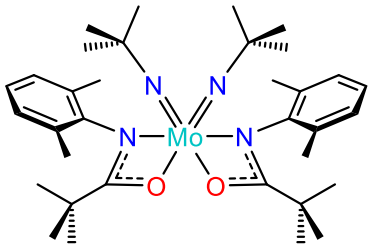

[^{DMP}(NO)^{tBu}]Na (3.4 mmol, 2 eq.) was dissolved in 40 mL of THF and cooled to -35°C. In a scintillation vial 0.675 g (1.7 mmol, 1 eq.) of [^{t}BuN]$_2$MoCl$_2$(DME) was dissolved in 15 mL of THF and cooled to -35°C. After both solutions were at -35°C, the metal starting material solution was added to the flask containing the stirred solution of ligand salt. The solution was slowly warmed to r.t. and stirred for 24 h after which time the solvent was removed *in vacuo* from the yellow suspension. The yellow solid was suspended in toluene and filtered through celite to remove salt byproducts yielding a transparent yellow solution. The solvent was removed to afford 78.6% (0.859 g) of yellow product. Crystals were grown from slow evaporation of a toluene solution. IR(ATR) (cm^{-1}): 3043.4, 2964.6, 2920.9, 2862.2, 1473.6, 1354, 1249.2, 1217.9, 1185.7, 1095.7, 1025.9, 949.49, 845.1, 802.18, 764.98, 669.78, 600.06, 575.97, 524.68. ^{1}H NMR (400 MHz, Benzene-D_6) δ 1.05 (s, 18H, C-(CH_3)$_3$), 1.12 (s, 18H, N-(CH_3)$_3$), 2.26 (s, 6H, Ar-(CH_3)$_2$), 2.86 (s, 6H, Ar-(CH_3)$_2$), 6.88 (d, J = 7.6 Hz, 2H, Ar-H), 6.93 (t, J = 7.4 Hz, 2H, Ar-H), 6.99 (d, J = 7.4 Hz, 2H, Ar-H). ^{13}C NMR (101 MHz, Benzene-D_6) δ 19.21, 19.99, 27.66, 30.69, 41.14, 69.23, 125.16, 127.22, 128.14, 133.06, 134.93, 147.01, 187.48. Anal. Calcd. for $C_{34}H_{54}MoN_4O_2$: C, 63.14; H, 8.42; N, 8.66. Found: C, 61.93; H, 8.20; N, 8.20.

Synthesis of [^{oDMP}(NO)^{Ph}]$_2$Mo(N^{t}Bu)$_2$ (4.6)

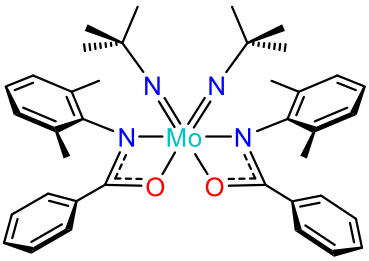

[^{oDMP}(NO)^{Ph}]Na (0.45 mmol, 2 eq.) was dissolved in ca. 20 mL of THF and cooled to -100 °C. In a scintillation vial 0.90 g (0.23 mmol, 1 eq.) of [^{t}BuN]$_2$MoCl$_2$(DME) was dissolved in ca. 5 mL of THF and cooled to -100°C. After both solutions were at -100°C the metal starting material solution was added to the flask containing the stirred solution of ligand salt. The solution was slowly warmed to r.t. and stirred for 24 h after which time the solvent was removed *in vacuo* from the gold colored suspension. The resultant yellow solid was suspended in toluene and filtered over celite to remove salts yielding a transparent yellow solution. The solvent was removed to afford 64% (0.100 g) of yellow product. Crystals were grown from slow evaporation of a hexane solution. IR(ATR) (cm^{-1}): 3269.9, 3059.7, 3028.9, 2971.1, 2920.5, 2860.5, 1642.5, 1580.5, 1486.8, 1454.8, 1377.7, 1354.9, 1298.6, 1265, 1234.9, 1203, 1131.2, 1091.7, 1026.3, 939.48, 890.1, 836.74, 799.53, 765.52, 702.33, 631.03, 591.6, 558.47, 533.7. ^{1}H NMR (400 MHz, Benzene-D_6) δ 1.16 (s, 18H, N-(CH_3)$_3$), 2.35 (s, 6H, Ar-(CH_3)$_2$), 2.90 (s, 6H, Ar-(CH_3)$_2$), 6.84 (s, 4H, Ar-*H*), 6.88 – 6.93 (m, 2H, Ar-*H*), 6.98 (d, J = 2.9 Hz, 6H, Ar-*H*), 7.72 – 7.77 (m, 4H, Ar-*H*). ^{13}C NMR (101 MHz, Benzene-D_6) δ 177.47, 146.63, 134.16, 130.77, 128.39, 127.73, 125.56, 69.91, 30.69, 19.57, 19.11.

Synthesis of [^{oDMP}(NO)^{PFP}]$_2$Mo(N^{t}Bu)$_2$ (4.7)

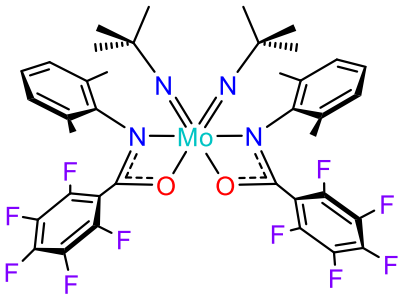

[^{oDMP}(NO)^{PFP}]Na (0.76 mmol, 2 eq.) was dissolved in ca. 5 mL of THF and cooled to -100 °C. In a scintillation vial 0.153 g (0.38 mmol, 1 eq.) of [^{t}BuN]$_2$MoCl$_2$(DME) was dissolved in ca. 5 mL of THF and cooled to -100°C. After both solutions were at -100°C the metal starting material solution was added to the vial containing the stirred solution of ligand salt. The solution was slowly warmed to r.t. and stirred for 24 h after which time the solvent was removed *in vacuo* from the orange suspension. The brown/yellow solid was suspended in toluene and filtered over celite to remove salts, yielding a transparent yellow solution. The solvent was removed to afford 48% (0.158 g) of yellow product. Crystals were grown from slow evaporation of a 1:1 DCM/hexane solution. IR(ATR) (cm^{-1}): 3023.6, 2974.7, 2922.9, 2860.8, 1652.2, 1594.8, 1525.5, 1478.4, 1452.9, 1357.1, 1305.3, 1217.1, 1108.7, 993.14, 870.26, 768.58, 685.91, 635.6, 582.65, 534.03. ^{1}H NMR (400 MHz, Benzene-D_6) δ 1.13 (s, 18H, N-(CH_3)$_3$), 2.36 (s, 6H, Ar-(CH_3)$_2$), 2.85 (s, 6H, Ar-(CH_3)$_2$), 6.87 (d, J = 11.3 Hz, 6H, Ar-H). ^{19}F NMR (376 MHz, Benzene-D_6) δ -137.75 (d, J = 21.9 Hz, 4F, Ar-F), -151.03 (t, J = 21.6 Hz, 2F, Ar-F), -161.29 (t, J = 20.7 Hz, 4F, Ar-F). ^{13}C NMR (101 MHz, Benzene-D_6) δ 169.80, 143.12, 134.93, 133.98, 128.61, 127.96, 127.94, 127.72, 127.70, 127.46, 126.51, 71.25, 31.89, 31.27, 30.40, 18.99, 1.74.

Synthesis of [^{DIPP}(NO)^{tBu}]$_2$Mo(N^{t}Bu)$_2$ (4.8)

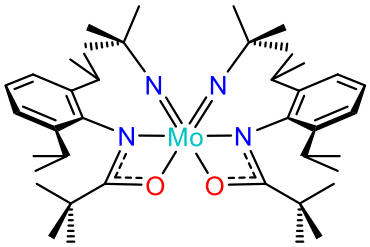

[^{DIPP}(NO)^{tBu}]Na (0.40 mmol, 2 eq.) was dissolved in ca. 20 mL of THF and cooled to -100 °C. In a scintillation vial 0.080 g (0.20 mmol, 1 eq.) of [^{t}BuN]$_2$MoCl$_2$(DME) was dissolved in ca. 5 mL of THF and cooled to -100°C. After both solutions were at -100°C the metal starting material solution was added to the flask containing the stirred solution of ligand salt. The solution was slowly warmed to r.t. and stirred for 24 h after which time the solvent was removed *in vacuo* from the golden suspension. The gold solid was suspended in toluene and filtered over celite yielding a transparent yellow solution. The solvent was removed to afford 98% (0.150 g) of yellow product. IR(ATR) (cm^{-1}): 3458.6, 3434.2, 3389.9, 3312.9, 3056.3, 2960.9, 2925.6, 2867.2, 1645.9, 1552.7, 1474.3, 1355, 1325.4, 1201.8, 1178, 1106.5, 1032.6, 950.82, 885, 844.5, 804.05, 768.77, 737.09, 674.17, 595.03, 524.41. ^{1}H NMR (400 MHz, Benzene-D_6) δ 1.10 (s, 18H, C-(CH_3)$_3$), 1.18 (s, 18H, N-(CH_3)$_3$), 1.25 (d, J = 6.8 Hz, 6H, CH-(CH_3)$_2$), 1.39 (d, J = 6.9 Hz, 6H, CH-(CH_3)$_2$), 1.49 (d, J = 7.1 Hz, 6H, CH-(CH_3)$_2$), 1.77 (d, J = 6.4 Hz, 6H, CH-(CH_3)$_2$), 3.59 (sept, J = 6.9 Hz, 2H, CH-(CH$_3$)$_2$), 3.99 (sept, J = 6.7 Hz, 2H, CH-(CH$_3$)$_2$), 7.02 (dd, J = 7.4, 1.5 Hz, 2H, Ar-H), 7.12 (m, 4H, Ar-H). ^{13}C NMR (101 MHz, Benzene-D_6) δ 23.35, 23.79, 24.04, 24.21, 27.05, 27.36, 27.46, 28.17, 30.09, 30.50, 41.72, 69.73, 122.98, 123.65, 125.99.

Synthesis of $[^{DIPP}(NO)^{Ph}]_2Mo(N^tBu)_2$ (4.9)

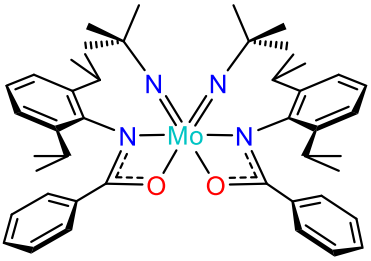

$[^{DIPP}(NO)^{Ph}]Na$ (1.59 mmol, 2 eq.) was dissolved in ca. 20 mL of THF and cooled to -100 °C. In a scintillation vial 0.317 g (0.80 mmol, 1 eq.) of $[^tBuN]_2MoCl_2(DME)$ was dissolved in ca. 5 mL of THF and cooled to -100°C. After both solutions were at -100°C the metal starting material solution was added to the flask containing the stirred solution of ligand salt. The solution was slowly warmed to r.t. and stirred for 24 h after which time the solvent was removed *in vacuo* from the golden suspension. The golden solid was suspended in toluene and filtered over celite to remove salts, yielding a transparent yellow solution. The solvent was removed to afford 75% (0.480 g) of yellow product. Crystals were grown from slow evaporation of a 1:1 DCM/hexane solution. IR(ATR) (cm^{-1}): 3203.6, 3062, 2961.5, 2922.4, 2866, 2721.4, 1779.3, 1731.8, 1584.5, 1484.7, 1427.3, 1381, 1355.5, 1329.3, 1245.7, 1202.8, 1121, 1095.9, 1030.3, 939.81, 848.51, 775.73, 746.29, 704.14, 633.29, 595.98, 565.04. ^{1}H NMR (400 MHz, Benzene-D_6) δ 0.95 (d, J = 6.9 Hz, 6H, CH-(CH_3)), 1.14 (d, J = 6.8 Hz, 6H, CH-(CH_3)), 1.18 (s, 18H, N-(CH_3)$_3$), 1.40 (d, J = 6.9 Hz, 6H, CH-(CH_3)), 1.73 (d, J = 6.6 Hz, 6H, CH-(CH_3)$_2$), 3.75 (sept, J = 6.9 Hz, 2H, CH-(CH$_3$)), 4.24 (sept, J = 6.8 Hz, 2H, CH-(CH$_3$)), 6.82 – 6.95 (m, 6H, Ar-H), 7.17 – 7.19 (m, 2H, Ar-H), 7.22 – 7.27 (m, 4H, Ar-H), 7.73 – 7.80 (m, 4H, Ar-H). ^{13}C{^{1}H} NMR (101 MHz, Benzene-D_6) δ 22.57, 23.34, 24.64, 25.82, 27.76, 27.82, 30.70, 70.21, 123.16, 124.78, 126.57, 127.63, 129.84, 131.00, 133.27, 142.49, 144.21, 144.73, 177.62.

Synthesis of $[^{DIPP}(NO)^{PFP}]_2Mo(N^tBu)_2$ (4.10)

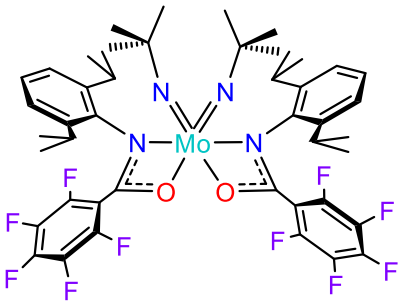

$[^{DIPP}(NO)^{PFP}]Na$ (0.16 mmol, 2 eq.) was dissolved in ca. 5 mL of THF and cooled to -100 °C. In a scintillation vial 0.032 g (0.08 mmol, 1 eq.) of $[^tBuN]_2MoCl_2(DME)$ was dissolved in ca. 2 mL of THF and cooled to -100°C. After both solutions were at -100°C the metal starting material solution was added to the flask containing the stirred solution of ligand salt. The solution was slowly warmed to r.t. and stirred for 2 h after which time the solvent was removed *in vacuo* from the golden suspension. The golden solid was suspended in toluene and filtered over celite to remove salts, yielding a transparent golden solution. The solvent was removed to afford 95% (0.075 g) of golden yellow product. IR(ATR) (cm^{-1}): 3286.9, 3179.3, 2972.5, 2869.9, 1757.9, 1654.1, 1592.2, 1503.3, 1464.5, 1434.2, 1383.6, 1359.9, 1329.9, 1239.3, 1197.8, 1097.3, 1056.9, 992.18, 869.42, 803.54, 731.91, 683, 636.61, 573.3, 533.69. ^{1}H NMR (400 MHz, Benzene-D_6) δ 1.08 (d, J = 6.9 Hz, 6H, CH-(CH_3)), 1.25 (s, 18H, N-(CH_3)$_3$), 1.38 (d, J = 6.8 Hz, 6H, CH-(CH_3)), 1.50 (d, J = 6.8 Hz, 6H, CH-(CH_3)), 1.75 (d, J = 6.5 Hz, 6H, CH-(CH_3)), 3.70 (sept, J = 13.1, 6.4 Hz, 2H, CH-(CH_3)), 4.08 (sept, J = 12.7, 6.3 Hz, 2H), 7.08 (d, J = 7.1 Hz, 2H, Ar-H), 7.14 (s, 2H, Ar-H), 7.18 (d, J = 3.6 Hz, 2H, Ar-H). ^{19}F NMR (376 MHz, Benzene-D_6) δ -161.54 – -161.32 (m, 4F, Ar-F), -151.48 (t, J = 21.7 Hz, 2F, Ar-F), -136.84 (d, J = 16.4 Hz, 4F, Ar-F). ^{13}C NMR (101 MHz, Benzene-D_6) δ 23.79, 23.95, 25.36, 26.20, 26.42, 27.41, 30.10, 30.51, 72.19, 123.60, 123.85, 124.65, 140.75, 144.08, 144.54.

Synthesis of $[^{Bn}(NO)^{tBu}]_2Mo(N^tBu)_2$ (4.11)

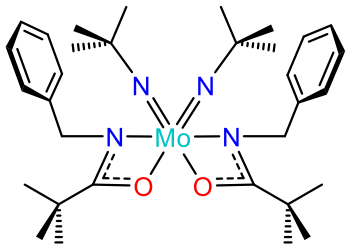

$[^{Bn}(NO)^{tBu}]Na$ (0.57 mmol, 2 eq.) was dissolved in ca. 5 mL of THF and cooled to -100 °C. In a scintillation vial 0.113 g (0.28 mmol, 1 eq.) of $[^tBuN]_2MoCl_2(DME)$ was dissolved in ca. 2 mL of THF and cooled to -100°C. After both solutions were at -100°C the metal starting material solution was added to the flask containing the stirred solution of ligand salt. The solution was slowly warmed to r.t. and stirred for 2 h after which time the solvent was removed *in vacuo* from the golden suspension. The golden solid was suspended in toluene and filtered over celite to remove salts, yielding a transparent yellow solution. The solvent was removed to afford 77% (0.135 g) of yellow product. Crystals were grown from slow evaporation of a 1:1 DCM/hexane solution. IR(ATR) (cm^{-1}): 3485.2, 3451, 3296.6, 3189.2, 3062, 3031.7, 2968.5, 2920.8, 2868.8, 1633.5, 1539, 1482.7, 1452, 1346.7, 1299.7, 1251.2, 1208.6, 1128.6, 1072.1, 1028.3, 984.49, 898.25, 840.48, 801.85, 735.22, 696.65, 632.48, 598.99, 555.49, 521.34. ^{1}H NMR (400 MHz, Benzene-D_6) δ 1.20 (s, 18H, C-(CH_3)$_3$), 1.23 (s, 18H, N-(CH_3)$_3$), 5.00 (s, 2H, N-CH_2), 5.05 (s, 2H, N-CH_2), 7.06 – 7.13 (m, 2H, Ar-*H*), 7.27 (t, J = 7.5 Hz, 4H, Ar-*H*), 7.46 (d, J = 7.5 Hz, 4H, Ar-*H*). ^{13}C NMR (101 MHz, Benzene-D_6) δ 27.52, 31.04, 39.45, 55.07, 68.55, 126.31, 126.81, 128.10, 129.01, 141.22.

Synthesis of [^{mDMP}(NO)^{tBu}]$_2$Mo(N^{t}Bu)$_2$ (4.12)

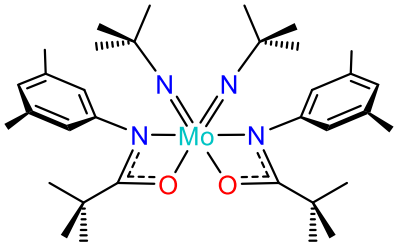

[^{mDMP}(NO)^{tBu}]Na (0.62 mmol, 2 eq.) was dissolved in ca. 5 mL of THF and cooled to -100 °C. In a scintillation vial 0.124 g (0.31 mmol, 1 eq.) of [^{t}BuN]$_2$MoCl$_2$(DME) was dissolved in ca. 2 mL of THF and cooled to -100°C. After both solutions were at -100°C the metal starting material solution was added to the flask containing the stirred solution of ligand salt. The solution was slowly warmed to r.t. and stirred for 24 h after which time the solvent was removed *in vacuo* from the golden suspension. The golden solid was suspended in toluene and filtered over celite yielding a transparent yellow solution. The solvent was removed to afford 98% (0.195 g) of yellow product. Crystals were grown from slow evaporation of a 1:1 DCM/hexane solution. IR(ATR) (cm^{-1}): 3283.9, 3005.4, 2963.1, 2916.5, 2859.9, 1651, 1600.3, 1548.9, 1475.1, 1352.9, 1305.1, 1257.4, 1219.3, 1154, 1126.2, 1053.6, 970.07, 900.89, 844.83, 797.9, 729.05, 679.5, 598.66. ^{1}H NMR (400 MHz, Benzene-D_6) δ 1.22 (s, 18H, C-(CH_3)$_3$), 1.27 (s, 19H, N-(CH_3)$_3$), 2.10 (s, 12H, Ar-(CH_3)$_2$), 6.55 – 6.60 (m, 2H, Ar-*H*), 6.98 (s, 4H, Ar-*H*). ^{13}C NMR (101 MHz, Benzene-D_6) δ 20.78, 27.23, 28.38, 30.59, 41.28, 68.76, 117.54, 124.74, 126.09, 137.40.

Synthesis of [^{PFP}(NO)^{tBu}]$_2$Mo(N^{t}Bu)$_2$ (4.13)

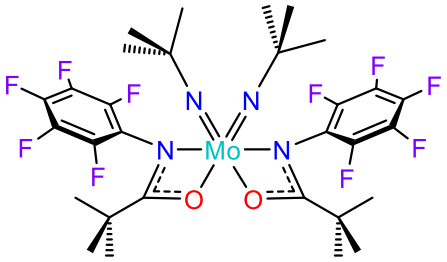

[^{PFP}(NO)^{tBu}]Na (0.46 mmol, 2 eq.) was dissolved in ca. 5 mL of THF and cooled to -30 °C. In a scintillation vial 0.92 g (1.23 mmol, 1 eq.) of [^{t}BuN]$_2$MoCl$_2$(DME) was dissolved in ca. 5 mL of THF and cooled to -30°C. After both solutions were at -30°C the metal starting material solution was added to the flask containing the stirred solution of ligand salt. The solution was slowly warmed to r.t. and stirred for 18 h after which time the solvent was removed *in vacuo* from the yellow suspension. The yellow solid was suspended in toluene and filtered over celite yielding a transparent yellow solution. The solvent was removed to afford 89% (0.157 g) of yellow product. Crystals were grown from slow evaporation of a toluene solution. ^{1}H NMR (400 MHz, Benzene-D_6) δ 1.04 (s, 18H C-(CH_3)$_3$), 1.05 (s, 18H, N-(CH_3)$_3$). ^{13}C NMR (101 MHz, Benzene-D_6) δ 1.76, 26.63, 26.84, 26.94, 30.07, 31.15, 31.90, 41.10, 70.14.

4.4.3 Reactivity Studies

The imines used in the metathesis test reactions, (E)-N-(3,5-dimethylphenyl)-1-(4-methoxyphenyl)methanimine (**4.14**), (E)-N,1diphenyl-methanimine (**4.15**), and (E)-N-(tert-butyl)-2,2-dimethylpropan-1-imine (**4.16**) were all synthesized via reported methods.[11] The imine metathesis test reactions were performed using the following example protocol.

Imine metathesis test reactions. The imines **4.14** (79 mg, 0.331 mmol, 1 equiv) and **4.15** (60 mg, 0.311 mmol, 1 equiv) were suspended in 2 mL C_6D_6 at r.t. and the precatalyst $[^{oDMP}(NO)^{PFP}]_2Mo(N^tBu)_2$ (**4.7**, 29 mg, 0.031 mmol, 0.1 equiv) was added. The stirring reaction mixture was heated to 50 °C. After 3 h an aliquot was taken for ^1H NMR. In the test reactions of **4.16**, the temperature was also increased to up to 90 °C with no difference in reactivity.

4.4.4 X-ray Crystallographic Studies

X-ray diffraction data were collected for complexes **4.4**-**4.7**, **4.9**, and **4.11**-**4.13** on a diffractometer with a Bruker APEX CCD area detector[12-13] with graphite-monochromated Mo Kα radiation (λ = 0.71073 Å). Selected crystals were mounted using high vacuum grease or Paratone oil onto a cryoloop and cooled to the data collection temperature of 100 K. Cell parameters were determined from a non-linear least squares fit. The data were corrected for absorption by the empirical method[14] giving minimum and maximum transmission factors. The space groups were determined by systematic absences and statistical tests and verified by subsequent refinement. The structure was solved by direct methods and refined by full-matrix least-squares methods on F2.[15-16] The positions of hydrogens were initially determined by geometry and were refined using a riding model. Non-hydrogen atoms were refined with anisotropic displacement parameters. Hydrogen atom displacement parameters were set to 1.2 (1.5 for methyl) times the isotropic equivalent displacement parameters of the bonded atoms.

4.5 References

1. Meyer, K. E.; Walsh, P. J.; Bergman, R. G., Zirconium-Mediated Imine Metathesis. Synthesis of 2,4-Diaza-1-zirconiacyclobutanes and the Mechanism of Their Reactions with Imines and Alkynes. *J. Am. Chem. Soc.* **1994,** *116* (6), 2669-2670.
2. Cantrell, G. K.; Meyer, T. Y., Azaheteroalkene metathesis: reactions of imines with Mo(VI) bis(imide) complexes. *Chem. Commun.* **1997**, 1551.
3. Cantrell, G. K.; Meyer, T. Y., Transition-metal-catalyzed imine metathesis. *Organomet.* **1997,** *16* (25), 5381-5383.
4. Cantrell, G. K.; Meyer, T. Y., Catalytic C=N bond formation by metal-imide-mediated imine metathesis. *J. Am. Chem. Soc.* **1998,** *120* (32), 8035-8042.
5. Cantrell, G. K.; Geib, S. J.; Meyer, T. Y., Ring-opening metathesis of a cyclic imine. *Organomet.* **2000,** *19* (18), 3562-3568.
6. Cantrell, G. K.; Geib, S. J.; Meyer, T. Y., Ring-opening of a cyclic imine: The first step of imine ROMP. *Organomet.* **1999,** *18* (21), 4250-4252.
7. Tóth, G.; Pintér, I.; Messmer, A., Mechanism of the exchmge reaction of aromatic scriff bases. *Tetrahedron Lett.* **1974,** *15* (9), 735-738.
8. Clarkson, J. M.; Schafer, L. L., Bis(tert-butylimido)bis(N,O-chelate)tungsten(VI) complexes: Probing amidate and pyridonate hemilability. *Inorg. Chem.* **2017,** *56* (10), 5553-5566.

9. Barrie, P.; A. Coffey, T.; D. Forster, G.; Hogarth, G., Bent vs. linear imido ligation at the octahedral molybdenum(VI) dithiocarbamate stabilised centre. *J. Chem. Soc., Dalton Trans.* **1999,** (24), 4519-4528.

10. Li, C.; Thomson, R. K.; Gillon, B.; Patrick, B. O.; Schafer, L. L., Amidate complexes of titanium and zirconium: a new class of tunable precatalysts for the hydroamination of alkynes. *Chem. Commun. (Cambridge, U. K.)* **2003,** (19), 2462-2463.

11. Xin, Z.; Kramer, S.; Overgaard, J.; Skrydstrup, T., Access to 1,2-Dihydroisoquinolines through Gold-Catalyzed Formal [4+2] Cycloaddition. *Chemistry – A European Journal* **2014,** *20* (26), 7926-7930.

12. *APEX2*, Bruker AXS Inc.: Madison, Wisconsin, USA, 2007.

13. *SAINT*, Bruker AXS Inc.: Madison, Wisconsin, USA, 2007.

14. Krause, L.; Herbst-Irmer, R.; Sheldrick, G. M.; Stalke, D., Comparison of silver and molybdenum microfocus X-ray sources for single-crystal structure determination. *J. Appl. Cryst.* **2015,** *48* (1), 3-10.

15. Sheldrick, G., SHELXT - Integrated space-group and crystal-structure determination. *Acta Crystallogr., Sect. A: Found. Crystallogr.* **2015,** *71* (1), 3-8.

16. Sheldrick, G., Crystal structure refinement with SHELXL. *Acta Crystallogr., Sect. C: Cryst. Struct. Commun.* **2015,** *71* (1), 3-8.

Chapter 5: Future Directions

5.1 Introduction

The first Mo(VI) amidate complexes have been presented in Chapters 2-4. The use of dioxo Mo(VI) bis(amidate) complexes for oxygen group transfer reactivity, including the catalytic epoxidation of various alkenes, has been demonstrated in Chapter 2. The ligands have exhibited the capability to stabilize Mo(VI) metal centers and maintain connectivity during changing oxidation states, as evidenced by the dimer formation upon reduction with trimethylphosphine. The application of these new dioxo Mo bis(amidate) complexes to the deoxydehydration (DODH) reaction of diols is of interest to our group, ultimately for the catalytic conversion of biomass derived diols to useful chemical feedstocks. Some initial results are presented *vide infra*.[1] These dioxo complexes also have the potential to be starting materials for new amidate complexes of Mo. The use of oxo fragments to generate new ligands via group transfer is of interest, *i.e.* the reaction of a metal oxo (M=O) with an isocyanate (RNCO) can eliminate CO_2 and generate a metal imido (M=NR).[2-6]

The Mo(VI) bis(amidate) complexes described in Chapter 3 represent an interesting addition to the relatively rare oxo-imido class of complexes and the complexes were successfully applied to the epoxidation of *cis*-cyclooctene. Investigation of the epoxidation reaction of different alkenes and reaction conditions are of interest to better understand the activity of these molecules under catalytic applications. These complexes, as with the dioxo species, could serve as precursors to new amidate complexes via group

transfer chemistry.[5-6] As discussed in previous chapters, Mo alkylidene complexes have proven be very valuable for the metathesis of alkenes, affording Richard Schrock a portion of the Nobel Prize in 2005.[7-8] The analogous metathesis reaction of imines has been explored to an extent by some researchers, but the reaction still needs to be improved in order to be useful.[9-13] The bis(imido) complexes presented in Chapter 4 were able to cross-metathesize select imines, but were not active with simple "non-activated" imines. Initial test reactions of the oxo-imido complexes as imine metathesis catalysts were equally ineffective. The metal-catalyzed ring-opening-metathesis-polymerization (ROMP) of cyclic imines has yet to be developed. The analogous metathesis of phosphaalkenes (P=C bonded materials) has not been demonstrated by any metal system to our knowledge. These reactions are all of interest to our group with the bis(amidate) complexes developed in this research.

Development of fine-tuned amidate ligands to increase the activity of Mo bis(amidate) complexes is of interest to our group. The expansion of the series to more donating amidate ligands and the use of softer thioamides are of use to explore the effect on the reactivity of the metal center. Also, exploring the effects of alternative electron withdrawing groups for different catalytic approaches is of interest due to the high cost of the PFP acyl chlorides. The use of ^{t}Bu imido groups was useful for ^{1}H NMR spectroscopy, but it could be useful to see the effects of less bulky and electronically varied imido groups, such as Ph imido. This chapter will discuss the targeted reactions with some initial results and the bis(amidate) synthetic targets. The synthesis of terminal phosphinidene complexes has been a goal of our group and some initial reactions indicating phosphinidene formation will also be discussed.

5.2 New Bis(Amidate) Complexes

The initial reactivity studies and complex characterization carried out in Chapters 2-4 have shown the ability of amidate ligands to stabilize Mo(VI) complexes, as well as confirmed the ligands stability during redox chemistry. It is of interest then to further expand the series of amidate complexes to explore the range of reactivity the complexes can perform. This includes utilizing new amidate ligands and installing new reactive fragments on the Mo metal center, such as new imido (Mo=NR), alkylidene ($Mo=CR_2$), and phosphinidene (Mo=PR) moieties.

5.2.1 Alternative Electron Withdrawing Amidate Ligands

Preliminary reactivity studies of the dioxo species support the notion that electron-withdrawing PFP groups can increase the reactivity of the Mo metal center. However, the cost of the starting materials for the PFP backbone can be prohibitive (~$8/g per Sigma-Aldrich). To address this cost the use of p-nitrophenyl ($0.23/g) in the backbone could prove to have the same electron-withdrawing characteristics, and dramatically reduce the cost of the starting materials and ultimately the catalysts. An initial proligand (**5.1**) using the DMP group on the N atom has been synthesized and the ^{1}H NMR is shown in Figure 5.1.

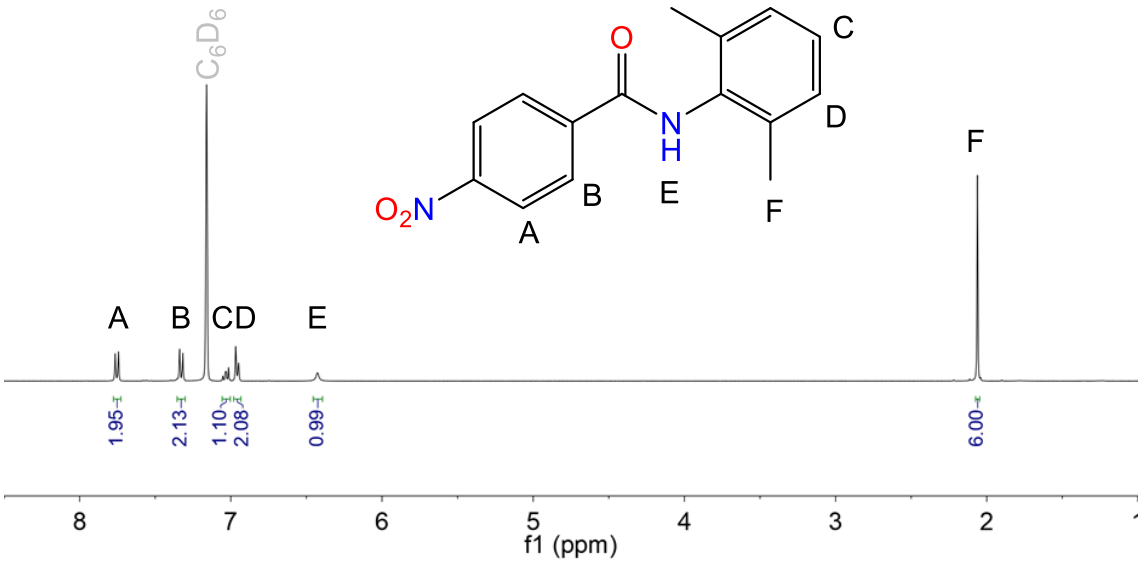

Figure 5.1 ^{1}H NMR spectrum for amidate proligand **5.1**.

5.2.2 Thioamidates

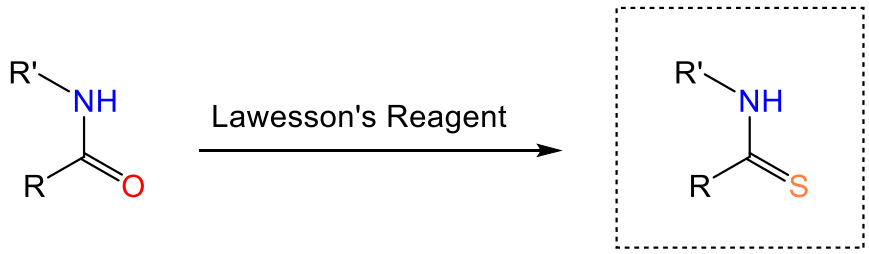

Scheme 5.1 Conversion of amidate proligand to thioimidate proligand using Lawesson's reagent.

The stability and reactivity of the Mo bis(amidate) complexes could be altered by changing the amidate ligand to a more biologically relevant thioamidate as shown in Scheme 5.1. The use of the softer sulfur atoms in the ligand could improve the binding strength of the ligand as well as help with maintaining coordination of the ligand at higher

temperatures. Initial attempts to generate the thioamides from amides have been inconsistent, but a general preparation of the thioamide using Lawesson's reagent is known.[14] Initial test reactions to use a commercially available thioamide, 2-mercaptothiazole (**5.2**), to generate a bis(thioamidate) Mo complex (**5.3**) as shown in Figure 5.2, have been unsuccessful.

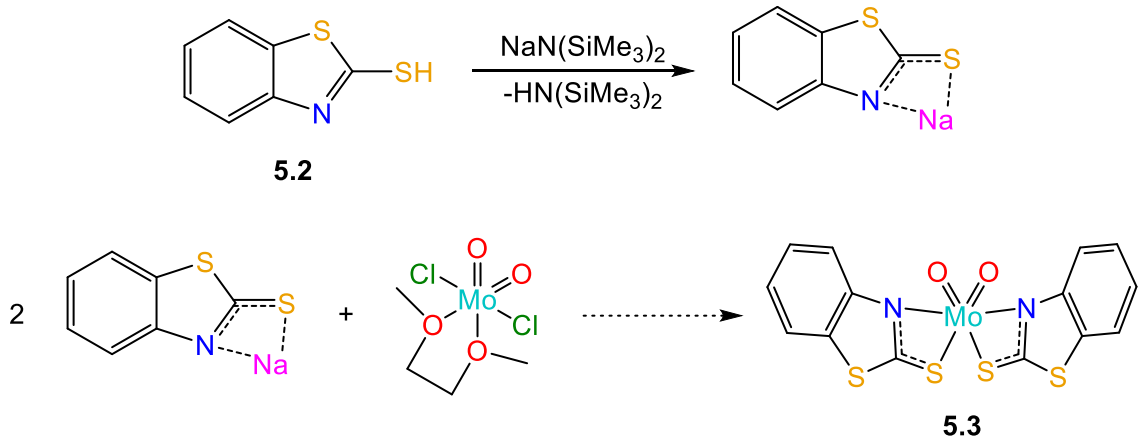

Figure 5.2 Attempted synthesis of a Mo bis(thioamidate) complex (**5.3**).

5.2.3 New Complexes via CO_2 Elimination

The ^{t}Bu imido group used in this work has a convenient ^{1}H NMR resonance, but it is bulky. It is of interest to change this group to a Ph to reduce bulk and use other groups to change the electronic characteristics. Use of a more electron-withdrawing imido fragment should in turn decrease the *trans* influence observed with the oxo-imido systems. It would also be interesting to substitute the ^{t}Bu imido group with a bulkier DMP or DIPP group to control reactivity of the oxo-imido complexes featuring less bulky amidate ligands. Reactions involving (R)NCO compounds with the Mo=O moiety under the right conditions could eliminate CO_2 and should generate the corresponding Mo=NR complex

as shown in Figure 5.3A. This type of reactivity is of interest to install alkylidenes using ketenes (Figure 5.3B) and ideally phosphinidenes from phosphaketenes (Figure 5.3C). It has been observed with other systems that the ketene reaction does not occur through the same pathway due to the lack of a lone pair on the carbon.[15] Reactions of phosphaketenes and oxo species have not been reported to our knowledge.

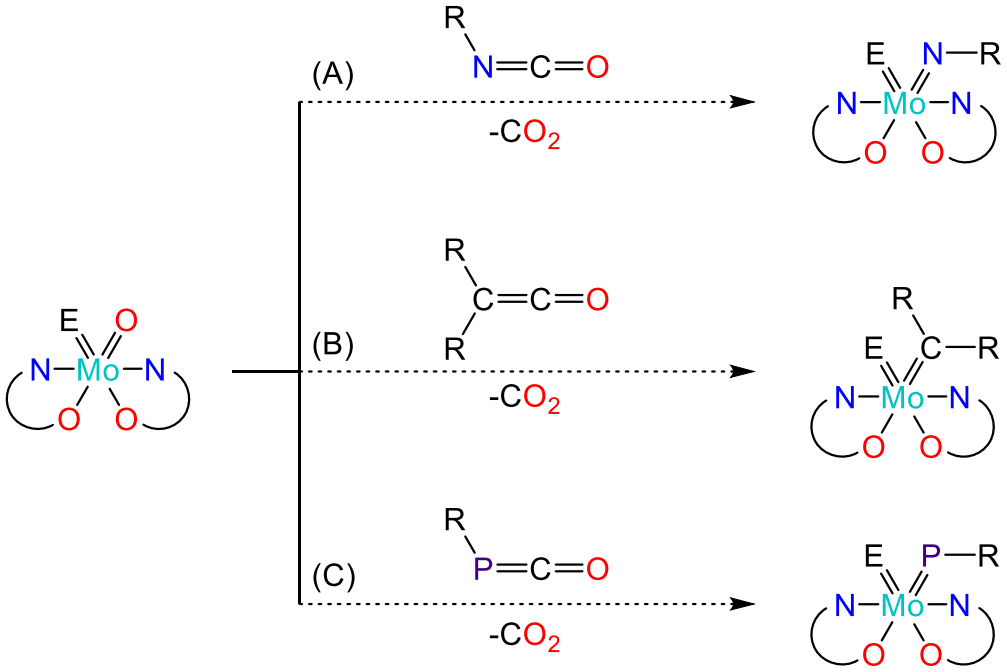

Figure 5.3 Targeted CO_2 elimination reactions of Mo=O complexes and (A) isocyanates, (B) ketenes, and (C) phosphaketenes.

Attempts to use isocyanates as a group transfer reagent to an oxo complex have had unclear results (Figure 5.4). The reaction of $[^{Ph}(NO)^{tBu}]_2MoO_2$ (**2.8**) and 4 eq. of (Ph)NCO produces a highly colored product that is either the oxo-imido species **5.4** or the bis(imido) complex **5.5** (Figure 5.4A). The reaction of **2.8** and 1 eq. of (DMP)NCO shows substantial conversion to the oxo-imido complex (**5.6**) as shown in Figure 5.4B. The

reaction of the bulkier dioxo compound $[^{DMP}(NO)^{tBu}]_2MoO_2$ (**2.9**) and 1 eq. of (Ph)NCO shows only a slight conversion of the dioxo to the oxo-imido complex **5.7 (**Figure 5.4C). The analogous reaction of 1 eq. of (Ph)NCO with $[^{DMP}(NO)^{tBu}]_2MoON^tBu$ (**3.3**) doesn't appear produce the desired bis(imido) species **5.8** (Figure 5.4D). The apparent differences in reactivity for these complexes are due to the steric bulk around the Mo=O moiety. For the $[^{DMP}(NO)^{tBu}]^-$ complexes, the N-2,6-dimethylphenyl group prevents easy access of the isocyanate in the proper orientation for reactivity. This is alleviated with the $[^{Ph}(NO)^{tBu}]^-$ system and we observe much quicker reactions (qualitatively) and better conversions, even with the bulkier DMP-isocyanate.

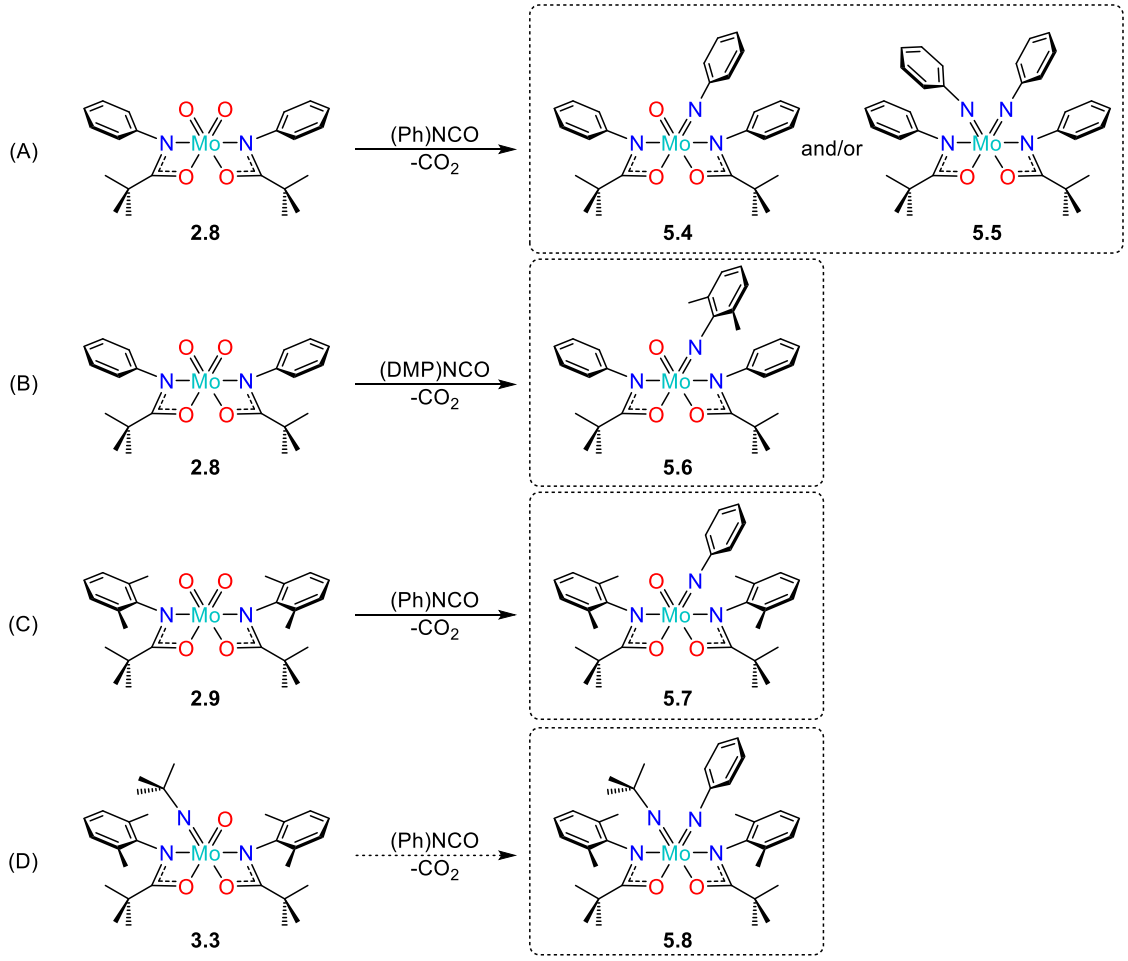

Figure 5.4 Attempted CO_2 elimination reactions using isocyanates.

Initial test reactions of diphenyl ketene with $[^{DMP}(NO)^{tBu}]_2MoON^tBu$ (**3.3**) and $[^{DIPP}(NO)^{tBu}]_2MoON^tBu$ (**3.6**) showed some reaction, but also loss of amidate ligand. The ^1H NMR spectra are very complicated, making assignments difficult. The C*H*-$(CH_3)_2$ region of the ^1H NMR spectrum for the reaction of diphenylketone with **3.6** is shown in Figure 5.5. The reaction of ketenes with dioxo species, as well as the other oxo-imido complexes, could provide the desired products if the proper conditions are determined.

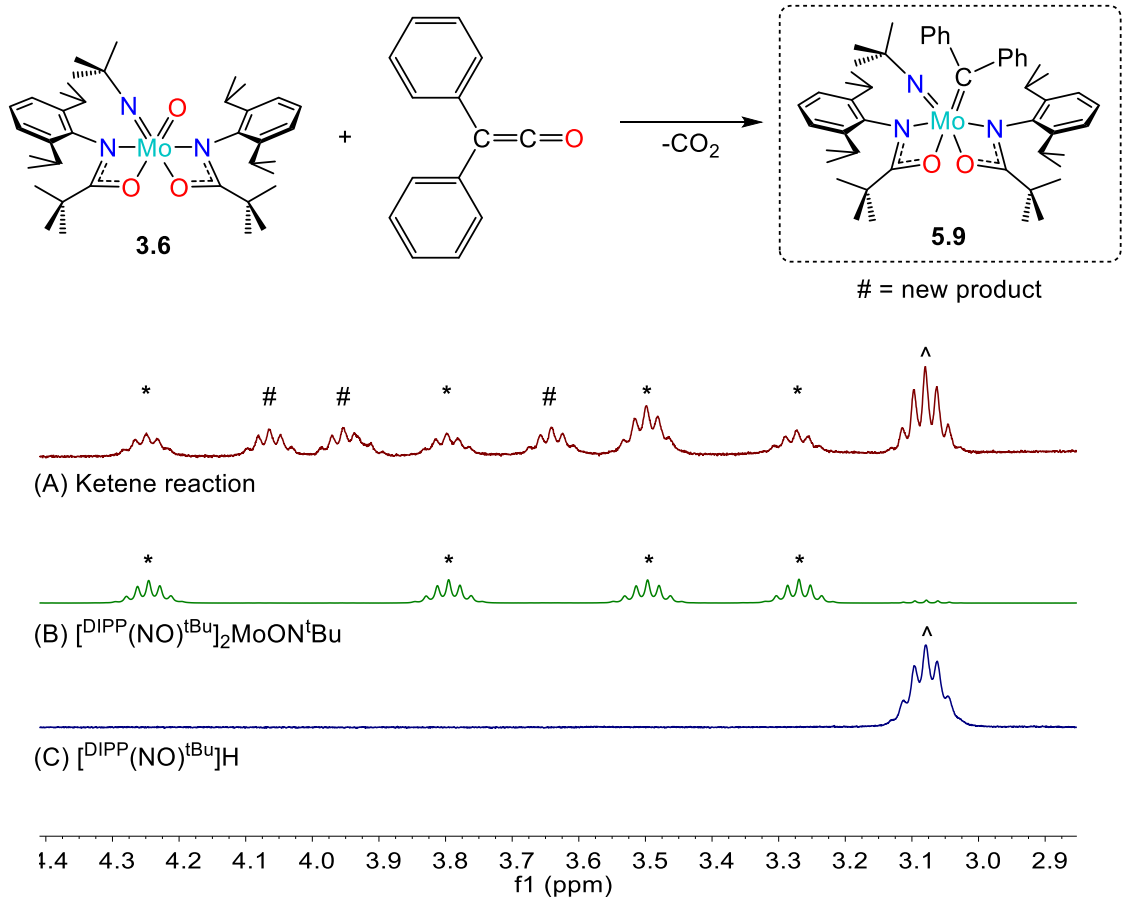

Figure 5.5 Reaction of $[^{DIPP}(NO)^{tBu}]_2MoON^tBu$ and diphenyl ketene. The C*H*-$(CH_3)_2$ region (~3-4.5 ppm) of the ^1H NMR for the reaction (A), the starting complex **3.6** (B), and the free ligand **2.5** (C), shown to highlight the generation of a new bis(amidate) product.

The group transfer of an isocyanate compound should be analogous to that of a phosphaketene (RPCO), thus the reaction of [Mo=O] and (R)PCO compounds could present a valuable pathway to the elusive Mo=PR fragment. There are only few examples of phosphaketenes in the literature and only one that is isolable at room temperature, (2,4,6-tri-*tert*-butylphenyl)PCO [(Mes*)PCO]. The reported synthesis of (Mes*)PCO uses phosgene as a starting material,[16] which is not available commercially. Consequently, we have developed a synthetic protocol using triphosgene (Scheme 5.2).

The reaction of (Mes*)PCO with Mo=O species has yet to be performed, as the development of this reaction is not complete.

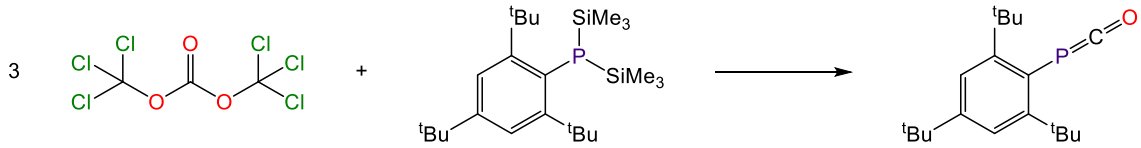

triphosgene | Mes*P(SiMe$_3$)$_2$ **5.10** | Mes*PCO **5.11**

Scheme 5.2 Alternative synthesis of (Mes*)PCO using triphosgene.

5.2.4 Isolated Mo(VI) Phosphinidene Complexes

The metathesis of P=C materials would be a major achievement in the area of catalysis and organometallics.[17] This transformation would allow for rapid access to new compounds and polymers that are currently too difficult or inefficient to generate in large quantities.[18-19] The metathesis of C=C bonds is well studied[7, 20-21] and the metathesis of P=P bonds has been shown in previous studies[22], but the P=C metathesis reaction has remained elusive. The diagonal relationship of carbon and phosphorus has led to the two elements sharing an impressive amount of analogous reactivity, best summarized in the book "Phosphorus: The Carbon Copy."[23] It is logical then, using this C-P analogy, to hypothesize that a Mo phosphinidene complex [Mo=P] should behave in a similar fashion as a Mo alkylidene complex[Mo=C].[19] However, the synthesis of terminal phosphinidenes of Mo are very rare.[24-29]

Our initial focus is the synthesis of a terminal phosphinidene complex of Mo(VI), analogous to the metathesis catalysts prepared by Schrock and coworkers. We have

attempted to use a phospha-Wittig reagent (**5.12**) as a oxidant to produce [Mo=PR] moieties as in Figure 5.6A. The dioxo complex $[^{DMP}(NO)^{tBu}]_2MoO_2$ (**2.9**) or the oxo-imido complex $[^{DMP}(NO)^{tBu}]_2MoO_2$ (**3.3**) was dissolved in C_6D_6 followed by addition of **5.12** at r.t. Both reactions become red/brown after addition, indicating possible generation of a Mo(V) species. Preliminary results indicate the possibility of a transient [Mo=PR] species, due to the formation of the diphosphine **5.13**, confirmed by $^{31}P\{^1H\}$ NMR spectroscopy (Figure 5.7).

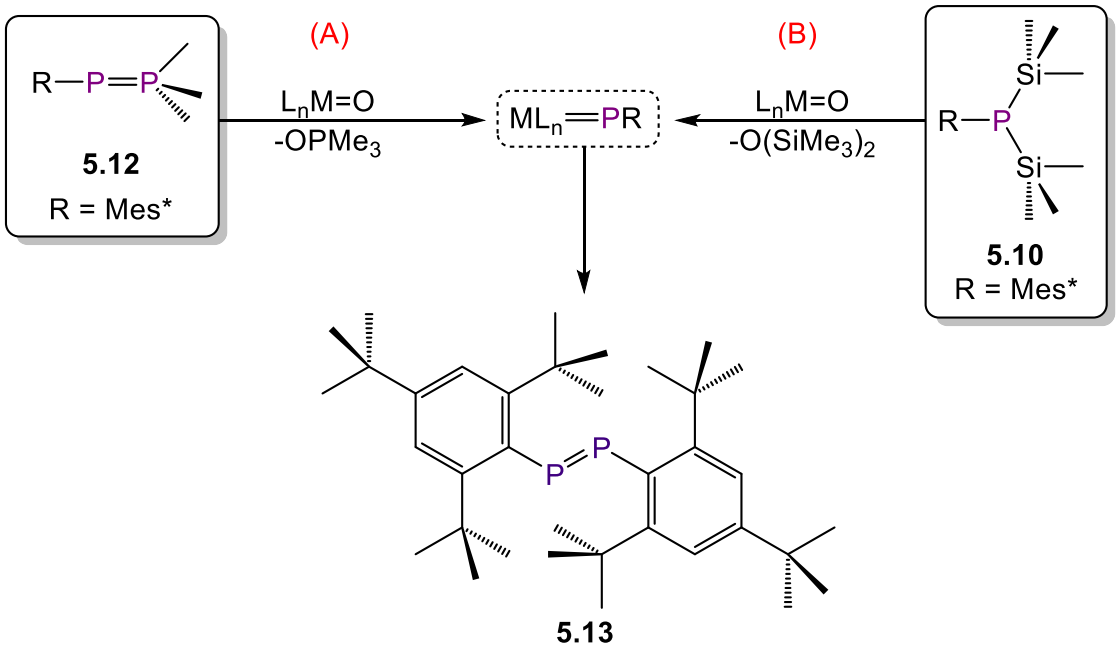

Figure 5.6 Potential pathways to a terminal Mo phosphinidene complex via (A) a phospha-Wittig reagent and (B) $O(SiMe_3)_2$ or Cl $SiMe_3$ elimination reaction.

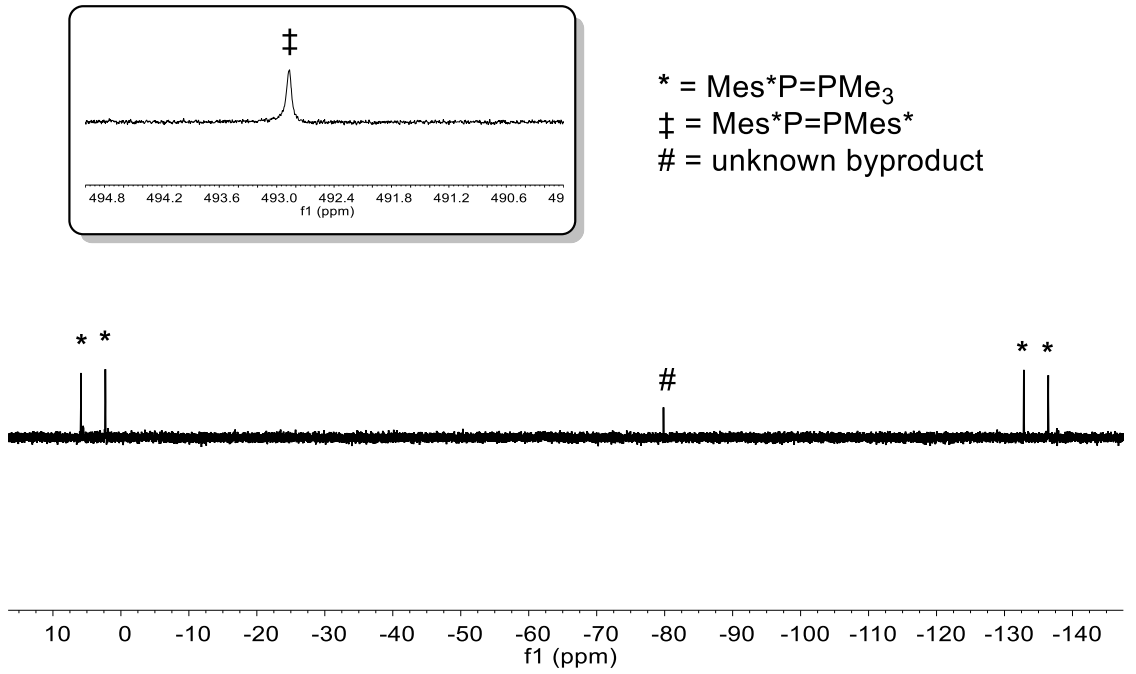

Figure 5.7 $^{31}P\{^{1}H\}$ NMR spectrum for the reaction of $[^{DMP}(NO)^{tBu}]_2MoO_2$ (**2.9**) and the Mes*P=PMe$_3$ (**5.12**). Inset: 490-495 ppm region.

An alternative pathway to a terminal phosphinidene complex is presented in Figure 5.6B, where the silylated phosphine Mes*P(SiMe$_3$)$_2$ (**5.10**) would react with an oxo fragment to eliminate volatile O(SiMe$_3$)$_2$ as a driving force. Initial test reactions of $[^{DMP}(NO)^{tBu}]_2MoO_2$ (**2.9**) and $[^{DMP}(NO)^{tBu}]_2MoON^tBu$ (**3.3**) with **5.10** indicated diminished reactivity and generation of Mes*PH$_2$, as confirmed by $^{31}P\{^{1}H\}$ NMR. However, the use of Cl$_2$MoO$_2$(DME) instead quickly converts **5.10** to the diphosphine **5.13**, indicating the amidate complexes tested might have been too sterically hindered at the Mo=O site to react. These reactions should be explored further using the extended series of Mo amidate complexes featuring an oxo moiety presented in this research.

5.3 Reactivity Targets

5.3.1 Ongoing Investigations

The reactivities presented in Chapters 2-4 are surface level investigations with very promising results. Further investigation of the OAT ability of complex **2.12** is needed to better understand why that complex is more effective than the rest of the series. The epoxidation reactions need to be fine-tuned with either different solvents, temperatures, reactions times, or modifications of the catalyst to find the optimum catalyst working conditions. The scope of epoxidation needs to be expanded for the oxo/imido complexes in Chapter 3, as well as the optimization of the reactions. The imine metathesis reaction of chemically different imines needs to be screened and optimized using the full suite of Mo-imido complexes presented in this work.

5.3.2 DODH Reactions

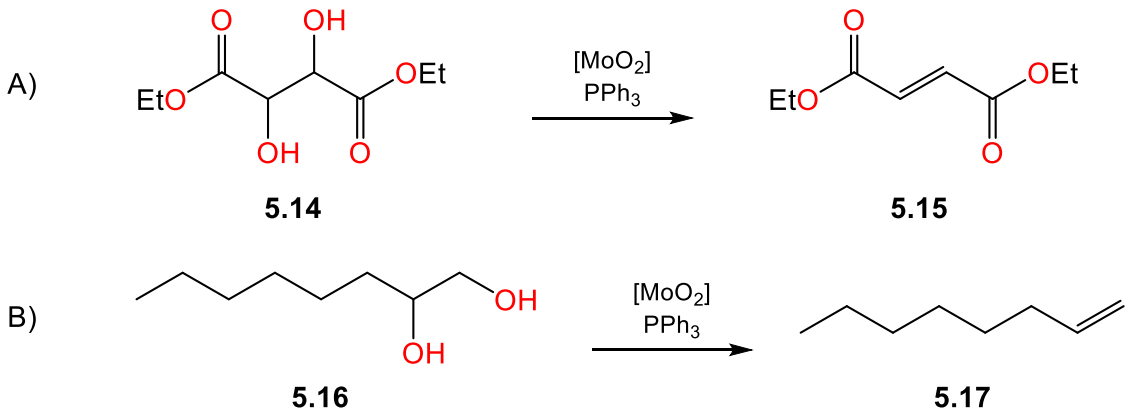

Scheme 5.3 General DODH reaction of (A) diethyl tartrate and (B) 1,2-octanediol.

Conversion of biomass to alkenes for synthetic use can help decrease our reliance on fossil fuels for fine chemical synthesis.[1, 30] Cheap Mo-oxo compounds have been used as catalysts for the conversion of diols to alkenes at high temperature (220-250 °C), but the application to the DODH of biomass-derived polyols has yet to be realized.[1, 30] Considering this area of research is quite new, we are interested in testing the ability of our amidate complexes during DODH reactions. The Mo dioxo complex $[^{DMP}(NO)^{tBu}]_2MoO_2$ (**2.9**) was used as a precatalyst at 5% loading for a test of this reaction. The substrates tested were the electrophilic diol, diethyl tartrate (**5.14**, Scheme 5.3A), and an aliphatic diol, 1,2-octanediol (**5.16**, Scheme 5.3B). For the DODH of **5.14**, complex **2.9** converts about 50% of the diol to alkene (**5.15**) over 24 h at 150 °C in benzene as determined by conversion of sacrificial reductant, PPh_3, to $OPPh_3$ by $^{31}P\{^1H\}$ NMR spectroscopy. There was no observed conversion of the **5.16** to **5.17** using 10% catalyst loading of **2.9** at 150 °C for 24 h in benzene. It is of interest to explore the reactivity of the full series of complexes, as well as the oxo-imido complexes, to see if the reactivity is improved by the varied electronics and steric environments of this suite of compounds.

5.4 Summary

It is of interest to generate new bis(amidate) complexes to increase the stability and reactivity of Mo(VI) complexes. This includes the synthesis of new amidate ligands and the utilization of thioamides as ligands. We are looking to further explore the installation of target groups (*i.e.* Mo=PR) using Mo(VI) bis(amidate) complexes as precursors. This could open the door to new reactions, and catalytic production of new materials (e. g. P=C metathesis).[19]

The use of the synthesized complexes in group transfer catalysis has been briefly explored, but the full extent of abilities of these complexes has yet to be explored. We are interested in further screening of substrates and conditions for the epoxidation of alkenes and the DODH of diols using the Mo-oxo complexes. We are also interested in the exploring the reactivity of the full series of Mo-imido complexes in imine metathesis reactions. The work presented here provides a foundation for design of new Mo(VI) catalysts bearing bidentate amidate ligands for a multitude of potential applications.

5.5 Experimental

5.5.1 General Considerations

Starting reagents were purchased from Sigma-Aldrich or Strem and used as received unless otherwise stated. Mes*P($SiMe_3$)$_2$ (**5.10**) and diphenyl ketene was prepared using literature methods.[31]

5.5.2 Synthesis

[^{DMP}(NO)^{PNP}]H (5.1)

A 125 mL Schlenk flask was charged with 4.926 (0.041 mol) of 2,6-dimethylaniline, 4.11 g (0.041 mol) of triethylamine, and 25 mL of DCM. In the glovebox, 6.858 g (0.037 mol) of 4-nitrobenzoyl chloride was dissolved in 10 mL of DCM in a Schlenk flask. The mixtures were chilled to -78 °C in a dry ice/ethanol bath. The acyl chloride solution was transferred via canula over the course of 10 minutes. The solution was warmed to room temperature and stirred for 18 h. After 18 h the volatiles were removed *in vacuo* and the remaining solid was recrystallized in toluene. The recrystallized material was filtered and washed with cold toluene yielding 4.30 g (43% yield) of orange solid product. ^{1}H NMR (400 MHz, Benzene-D_6) δ 2.06 (s, 6H, Ar-(CH_3)$_2$), 6.43 (s, 1H, N-*H*), 6.97 (s, 2H, Ar-*H*), 7.03 (dd, *J* = 8.4, 6.5 Hz, 1H, Ar-*H*), 7.33 (d, *J* = 8.7 Hz, 2H, Ar-*H*), 7.74 (s, 2H, Ar-*H*).

Attempted preparation of a Mo bis(thioamidate) complex (5.3).

The salt metathesis protocol used for amidate complexes syntheses in Ch 2-4 was followed. 0.269 g (1.609 mmol) of 2-mercaptobenzothiazole (**5.2**) was deprotonated with 0.275 g (1.609 mmol) of $NaN(SiMe_3)_2$ in THF at r.t. The isolated salt **5.2-Na** was redissolved in THF and chilled to -30 °C. 0.232 g (0.804 mmol) of $Cl_2MoO_2(DME)$ was dissolved in THF, chilled to -30 °C, and added to the stirring ligand salt solution. The reaction was stirred for 3 h, after which the volatiles were removed, and an orange solid was afforded. The solid was suspended in toluene making a purple-red solution, which was filtered over celite to remove salts. The solvent was removed to afford a sticky orange solid. ^{1}H NMR (400 MHz, Benzene-D_6) δ 0.05 (s, 4H), 0.09 (s, 3H), 0.23 (s, 10H), 0.29 (s, 5H), 2.11 (s, 1H), 6.20 (d, J = 8.0 Hz, 1H), 6.50 (s, 2H), 6.57 – 6.65 (m, 4H), 6.71 (t, J = 7.8 Hz, 2H), 6.82 – 6.91 (m, 4H), 7.01 (t, J = 1.1 Hz, 3H), 7.83 (d, J = 8.3 Hz, 2H), 8.01 (d, J = 8.3 Hz, 1H). **5.2**: ^{1}H NMR (400 MHz, Benzene-D_6) δ 6.42 (s, 1H), 6.52 (s, 1H), 6.62 (s, 1H), 6.71 (s, 1H), 10.03 (s, 1H).

Isocyanate CO_2 elimination reactions (Figure 5.4).

These reactions were performed on a small scale and products were not isolated.

(**A**) 42 mg (0.087 mmol) of $[^{Ph}(NO)^{tBu}]_2MoO_2$ (**2.8**) and 40 mg (0.348 mmol, 4 eq.) of (Ph)NCO stirred in 2 mL C_6D_6 at r.t for 10 h. Went dark red/orange quickly. ^{1}H NMR (400 MHz, Benzene-D_6) δ 0.93 (s, 11H), 1.01 (s, 18H, **2.8**), 1.03 (s, 5H, **2.1**), 1.20

(s, 1H), 6.58 (dd, *J* = 8.2, 1.3 Hz, 7H), 6.73 – 6.92 (m, 21H), 6.96 (s, 7H, **2.8**), 7.15 – 7.18 (m, 4H, **2.8**), 7.33 – 7.40 (m, 2H), 7.57 – 7.63 (m, 1H, **2.1**).

(**B**) 36 mg (0.075 mmol, 1 eq.) of $[^{Ph}(NO)^{tBu}]_2MoO_2$ (**2.8**) and 11 mg (0.075 mmol, 1 eq.) of (DMP)NCO stirred in 2 mL C_6D_6 at r.t for 10 h. Went to yellow slowly. ^{1}H NMR (400 MHz, Benzene-D_6) δ 1.01 (s, 18H, **2.8**), 1.02 (s, 4H, **2.1**), 1.97 (s, 11H), 6.67 – 6.73 (m, 3H), 6.73 – 6.79 (m, 2H), 6.82 – 6.88 (m, 3H, **2.8**), 6.96 (t, *J* = 7.7 Hz, 5H, **2.8**), 7.14 (d, *J* = 1.1 Hz, 4H, **2.8**), 7.54 – 7.61 (m, 1H, **2.1**).

(**C**) 40 mg (0.076 mmol, 1 eq.) of $[^{DMP}(NO)^{tBu}]_2MoO_2$ (**2.9**) was stirred in 2 mL C_6D_6, to this was added 9 mg (0.076 mmol, 1 eq.) of phenylisocyanate. No color change or NMR spectral change was noted after 24 h at r.t. The bright red orange solution was heated at 65°C for 24 h which produced some products confirmed by ^{1}H NMR spectroscopy.

24 h: ^{1}H NMR (400 MHz, Benzene-D_6) δ 0.98 (s, 18H), 1.10 (s, 2H), 1.96 (s, 1H), 2.06 (s, 1H), 2.16 (s, 1H), 2.46 (s, 12H), 6.56 (dd, *J* = 8.4, 1.4 Hz, 1H), 6.83 (d, *J* = 2.8 Hz, 6H).

48 h: ^{1}H NMR (400 MHz, Benzene-D_6) δ 0.99 (s, 18H), 0.99 – 1.02 (m, 12H), 1.08 (s, 6H), 1.97 (s, 9H), 2.06 (s, 1H), 2.16 (s, 1H), 2.46 (s, 12H), 6.71 (t, *J* = 9.5 Hz, 5H), 6.83 (s, 11H), 6.95 (s, 6H), 7.56 (d, *J* = 7.7 Hz, 1H).

(**D**) 50 mg (0.085 mmol) of $[^{DMP}(NO)^{tBu}]_2$MoONtBu (**3.3**) was dissolved in 2 mL C_6D_6. 10 mg (0.085 mmol) of (Ph)NCO added slowly to the solution, and the olive green

solution darkened. ^{1}H NMR (400 MHz, Benzene-D_6) δ 1.00 (s, 9H, **2.9**), 1.08 (s, 18H, **2.9**), 2.50 (s, 12H, **2.9**), 6.55 – 6.56 (m, 1H), 6.58 (s, 1H), 6.58 (d, *J* = 1.0 Hz, 1H), 6.75 – 6.76 (m, 1H), 6.77 (t, *J* = 1.4 Hz, 1H), 6.79 – 6.80 (m, 1H), 6.81 – 6.82 (m, 2H), 6.82 – 6.84 (m, 1H), 6.88 (t, *J* = 5.2 Hz, 6H, **2.9**).

Ketene CO_2 elimination reactions.

(**A**) $[^{DMP}(NO)^{tBu}]_2MoON^tBu$ (**3.3**) (0.076 g, 0.129 mmol) was dissolved in 2 mL of C_6D_6 then cooled to -30 °C before addition of the diphenyl ketene (0.025 g, 0.129 mmol), the reaction was stirred for 1 h and the ^{1}H NMR spectrum was collected. ^{1}H NMR spectrum contains mostly free ligand (**2.2**) and starting Mo complex (**3.3**). ^{1}H NMR (400 MHz, Benzene-D_6) δ 1.00 (s, 8H, **3.3**), 1.06 (s, 6H), 1.08 (s, 18H, **3.3**), 1.11 (s, 29H, **2.2**), 1.13 (s, 6H), 2.07 (s, 22H, **2.2**), 2.58 (s, 21H, **3.3**), 6.88 (d, *J* = 4.6 Hz, 9H), 6.96 (s, 13H), 7.05 (d, *J* = 4.3 Hz, 12H).

(**B**) $[^{DIPP}(NO)^{tBu}]_2MoON^tBu$ (**3.6**) (0.024 g, 0.034 mmol) was dissolved in 2 mL of C_6D_6 then cooled to -30 °C before addition of the diphenyl ketene (0.007 g, 0.034 mmol), the reaction was stirred for 1 h and the ^{1}H NMR spectrum was collected. ^{1}H NMR spectrum contains peaks for free ligand (**2.5**) and starting complex **3.6** as well as possible peaks for **5.9**. ^{1}H NMR (400 MHz, Benzene-D_6) δ 0.89 (s, 3H), 1.01 (d, *J* = 6.4 Hz, 1H), 1.06 (s, 3H), 1.09 (s, 4H), 1.13 (d, *J* = 5.6 Hz, 9H), 1.17 (s, 4H), 1.23 (dd, *J* = 13.5, 6.6 Hz, 10H), 1.31 – 1.46 (m, 8H), 1.54 (dd, *J* = 12.6, 6.7 Hz, 3H), 1.72 (d, *J* = 6.5 Hz, 1H), 1.86 (d, *J* = 6.5 Hz, 2H), 3.08 (p, *J* = 6.9 Hz, 2H), 3.22 – 3.35 (m, 1H), 3.50 (p, *J* = 7.0 Hz, 1H), 3.58 – 3.70 (m, 1H), 3.73 – 3.88 (m, 1H), 3.94 (q, *J* = 9.0, 7.9 Hz, 1H), 4.06 (q,

J = 6.7 Hz, 1H), 4.18 – 4.33 (m, 1H), 6.24 (s, 1H), 6.95 (d, *J* = 4.5 Hz, 2H), 7.00 (d, *J* = 7.1 Hz, 2H), 7.05 (d, *J* = 4.2 Hz, 7H), 7.08 – 7.12 (m, 3H), 7.12 (s, 1H), 7.23 (dd, *J* = 14.9, 7.6 Hz, 4H), 7.32 (d, *J* = 6.9 Hz, 1H), 7.37 (d, *J* = 7.0 Hz, 2H).

Synthesis of (Mes*)PCO (5.11).

A vial was charged with 0.361 g (1.146 mmol, 3 eq.) of triphosgene, 0.162 g (0.382 mmol, 1 eq.) of Mes*P($SiMe_3$)$_2$ (**5.10**), and 5 mL of toluene. The solution was stirred while heating to 40 °C for 16 h, after which the volatiles were removed *in vacuo*. The NMR spectra indicated some intermediates or byproducts present, but no starting phosphine **5.10**. ^{1}H NMR (400 MHz, Benzene-*D*$_6$) δ 1.18 (s, 9H), 1.22 (s, 6H), 1.35 (s, 9H), 1.51 (s, 18H), 1.60 (s, 9H), 6.96 – 7.08 (m, 2H), 7.12 (d, *J* = 7.7 Hz, 1H), 7.40 (s, 1H), 7.48 (d, *J* = 2.7 Hz, 1H), 7.54 (dq, *J* = 7.6, 4.3 Hz, 3H). ^{31}P{^{1}H} NMR (162 MHz, c_6d_6) δ -206.20 (**5.11**), 21.24, 21.36, 22.55, 22.68, 51.85.

Attempted phosphinidene syntheses (Figure 5.6).

The reactions were performed on a small scale in a vial at r.t. and the NMR spectral data were collected after stirring for 24 h.

(**A1**) [^{DMP}(NO)^{tBu}]$_2$$MoO_2$ (**2.9**) (0.050 g, 0.093 mmol, 1 eq.) and Mes*PMe_3 (**5.12**) (0.033 g, 0.093 mmol, 1 eq.) were combined in 2 mL of C_6D_6 at r.t. ^{1}H NMR (400 MHz, Benzene-*D*$_6$) δ 0.99 (s, 18H), 1.11 (s, 2H), 1.14 (s, 3H), 1.27 (s, 2H), 1.30 (s, 6H), 1.35 (s, 16H), 1.37 (s, 2H), 1.57 (d, *J* = 1.3 Hz, 12H), 1.91 (s, 4H), 2.07 (s, 1H), 2.37 (s, 1H), 2.46 (s, 12H), 2.62 (s, 1H), 2.77 (s, 1H), 6.81 (d, *J* = 4.7 Hz, 2H), 6.83 (d, *J* = 2.6 Hz, 4H), 6.84 – 6.88 (m, 3H), 6.92 – 6.97 (m, 2H), 7.43 (s, 2H), 7.53 (s, 1H), 7.60 (s,

1H). $^{31}P\{^{1}H\}$ NMR (162 MHz, Benzene-D_6) δ -136.44, -132.84, -79.83, 2.29, 5.88, 492.87.

(**A2**) $[^{DMP}(NO)^{tBu}]_2MoON^tBu$ (**3.3**) (0.100 g, 0.169 mmol, 1 eq.) and **5.12** (0.120 g, 0.338 mmol, 2 eq.) were combined in 2 mL of C_6D_6 at r.t. ^{1}H NMR (400 MHz, Benzene-D_6) δ 0.69 (d, J = 11.5 Hz, 6H), 1.00 (d, J = 1.7 Hz, 9H), 1.08 (d, J = 1.7 Hz, 18H), 1.33 – 1.39 (m, 27H), 1.57 (d, J = 1.8 Hz, 15H), 2.49 (s, 12H), 6.88 (d, J = 4.0 Hz, 6H), 7.39 – 7.45 (m, 4H), 7.61 (d, J = 1.6 Hz, 2H). $^{31}P\{^{1}H\}$ NMR (162 MHz, Benzene-D_6) δ -136.48, -132.88, -79.83, 2.27, 5.87, 492.87.

(**B1**) $[^{DMP}(NO)^{tBu}]_2MoO_2$ (**2.9**, 0.016 g, 0.030 mmol, 1 eq.) and **5.10** (0.013 g, 0.030 mmol, 1 eq.) were dissolved in toluene, and the reaction was followed by $^{31}P\{^{1}H\}$ NMR spectroscopy. $^{31}P\{^{1}H\}$ NMR (162 MHz, Benzene-D_6) δ -143.32.

(**B2**) **3.3** (0.025 g, 0.042 mmol, 1 eq.) and **5.10** (0.018 g, 0.042 mmol, 1 eq.) were dissolved in toluene, and the reaction was followed by $^{31}P\{^{1}H\}$ NMR spectroscopy. $^{31}P\{^{1}H\}$ NMR (162 MHz, Benzene-D_6) δ -143.14.

(**B3**) Cl_2MoO_2(DME) (0.025 g, 0.087 mmol, 1 eq.) and **5.10** (0.037 g, 0.087 mmol, 1 eq.) were combined in 2 mL of C_6D_6 at r.t. ^{1}H NMR (400 MHz, Benzene-d_6) δ 1.30 (s, 10H), 1.35 (s, 4H), 1.58 (s, 18H), 7.61 (s, 2H). $^{31}P\{^{1}H\}$ NMR (162 MHz, Benzene-D_6) δ 492.87.

DODH reactions (Scheme 5.3).

Reactants were dissolved in benzene in an NMR tube equipped with a Teflon stopcock. The reaction mixture was heated at 150 °C in an oil bath for 24 h after which a $^{31}P\{^{1}H\}$ NMR spectrum was obtained.

(**A**) Diethyl tartrate (**5.14**, 0.206 g, 1.0 mmol), PPh_3 (0.288 g, 1.1 mmol), and **2.9** (0.039 g, 0.1 mmol). $^{31}P\{^{1}H\}$ NMR (162 MHz, Chloroform-*D*) δ -5.05 (42%), 29.21 (58%).

(**B**) 1,2-octanediol (**5.16**, 0.146 g, 1.0 mmol), PPh_3 (0.288 g, 1.1 mmol), and **2.9** (0.039 g, 0.1 mmol). $^{31}P\{^{1}H\}$ NMR (162 MHz, Chloroform-*D*) δ -5.11 (95%), 29.16 (5%).

5.6 References

1. Sousa, S. C. A.; Fernandes, A. C., Efficient deoxygenation methodologies catalyzed by oxo-molybdenum and oxo-rhenium complexes. *Coord. Chem. Rev.* **2015,** *284*, 67-92.
2. Cross, W. B.; Anderson, J. C.; Wilson, C.; Blake, A. J., Molybdenum Oxo−Imido Aryloxide Complexes: Oxo Analogues of Olefin Metathesis Catalysts. *Inorg. Chem.* **2006,** *45* (11), 4556-4561.
3. Coffey, T. A.; Forster, G. D.; Hogarth, G., Synthesis and structural characterisation of dithiocarbamate-stabilised dimeric molybdenum(V) imido complexes via oxo substitution reactions with organic isocyanates. *J. Chem. Soc., Dalton Trans.* **1995,** (14), 2337-2349.
4. Green, M. L. H.; Hogarth, G.; Konidaris, P. C.; Mountford, P., Interconversion of oxo and imido ligands at a dimolybdenum centre: molecular and electronic structure of [{Mo(η-C5H4Me)(NPh)(μ-NPh)}2]. *J. Chem. Soc., Dalton Trans.* **1990,** (12), 3781-3787.
5. Kolomnikov, I. S.; Koreshkov, Y. D.; Lobeeva, T. S.; Volpin, M. E., Phenyl isocyanate as a source of phenylimido-ligand. *J. Chem. Soc. D* **1970,** (21), 1432-1432.
6. Nielson, A. J.; McCarley, R. E.; Laughlin, S. L.; Carlson, C. D., Phenylimido Complexes of Tungsten and Rhenium. *Inorg. Synth.* **1986**.
7. Murdzek, J. S.; Schrock, R. R., Well-characterized olefin metathesis catalysts that contain molybdenum. *Organomet.* **1987,** *6* (6), 1373-1374.

8. Schrock, R. R.; Murdzek, J. S.; Bazan, G. C.; Robbins, J.; Dimare, M.; O'Regan, M., Synthesis of Molybdenum Imido Alkylidene Complexes and Some Reactions Involving Acyclic Olefins. *J. Am. Chem. Soc.* **1990,** *112* (10), 3875--3886.

9. Cantrell, G. K.; Meyer, T. Y., Transition-metal-catalyzed imine metathesis. *Organomet.* **1997,** *16* (25), 5381-5383.

10. Cantrell, G. K.; Meyer, T. Y., Catalytic C=N bond formation by metal-imide-mediated imine metathesis. *J. Am. Chem. Soc.* **1998,** *120* (32), 8035-8042.

11. McInnes, J. M., Transition metal imide/organic imine metathesis reactions: unexpected observations. *Chem. Commun.* **1998,** (16), 1669-1670.

12. Cantrell, G. K.; Geib, S. J.; Meyer, T. Y., Ring-Opening of a Cyclic Imine: The First Step of Imine ROMP. *Organomet.* **1999,** *18* (21), 4250-4252.

13. Cantrell, G. K.; Geib, S. J.; Meyer, T. Y., Ring-opening metathesis of a cyclic imine. *Organomet.* **2000,** *19* (18), 3562-3568.

14. Jesberger, M.; Davis, T. P.; Barner, L., Applications of Lawesson's reagent in organic and organometallic syntheses. *Synthesis* **2003,** (13), 1929--1958.

15. Küsthardt, U.; Herrmann, W. A.; Ziegler, M. L.; Zahn, T.; Nuber, B., Mehrfachbindungen zwischen hauptgruppenelementen und übergangsmetallen XXVIII. Cycloaddition von heterokumulenen an oxorhenium-halbsandwich-komplexe: Synthese neuartiger metallacyclen. *J. Organomet. Chem.* **1986,** *311* (1), 163-175.

16. Appel, R.; Paulen, W., The First Stable Phosphaketene. *Angewandte Chemie International Edition in English* **1983,** *22* (10), 785-786.

17. Berg, E.; Orthaber, A.; Santoni, M. P.; Howard, F.; Ott, S., Toward metathesis reactions on vinylphosphaalkenes. In *Phosphorus, Sulfur and Silicon and the Related Elements*, 2013; Vol. 188, pp 152-158.

18. Baumgartner, T.; Réau, R., Organophosphorus π-Conjugated Materials. *Chem. Rev.* **2006,** *106* (11), 4681-4727.

19. Bates, J. I.; Dugal-Tessier, J.; Gates, D. P., Phospha-organic chemistry: from molecules to polymers. *Dalton Trans.* **2010,** *39* (13), 3151-3159.

20. Grubbs, R. H.; Miller, S. J.; Fu, G. C., Ring-closing metathesis and related processes in organic synthesis. *Acc. Chem. Res.* **1995,** *28* (11), 446-452.

21. Nicolaou, K. C.; Bulger, P. G.; Sarlah, D., Metathesis reactions in total synthesis. *Angew. Chem. Int. Ed.* **2005,** *44* (29), 4490-4527.

22. Dillon, K. B.; Gibson, V. C.; Sequeira, L. J., Transition-metal catalysed metathesis of phosphorus–phosphorus double bonds. *J. Chem. Soc., Chem. Commun.* **1995,** (23), 2429-2430.

23. Dillon, K. B.; Mathey, F.; Nixon, J. F., *Phosphorus : the carbon copy : from organophosphorus to phospha-organic chemistry*. Wiley: Chichester; New York, 1998.

24. Cowley, A. H.; Barron, A. R., The quest for terminal phosphinidene complexes. *Acc. Chem. Res.* **1988,** *21* (2), 81-87.

25. Scheer, M., Metal element triple bonds of the heavier group 15 elements. *Coord. Chem. Rev.* **1997,** *163*, 271-286.

26. Hopkins, A. D.; Wood, J. A.; Wright, D. S., Phosphinidine complexes of p block metals; new routes to cyclic ligands and Zintl phases. *Coord. Chem. Rev.* **2001,** *216-217*, 155-172.

27. Cummins, C. C., Terminal, Anionic Carbide, Nitride, and Phosphide Transition-Metal Complexes as Synthetic Entries to Low-Coordinate Phosphorus Derivatives. *Angew. Chem. Int. Ed.* **2006,** *45* (6), 862-870.

28. Johnson, B. P.; Balzs, G.; Scheer, M., Low-coordinate E1ligand complexes of Group 15 elements-A developing area. *Coord. Chem. Rev.* **2006,** *250* (9-10), 1178--1195.

29. Gardner, B. M.; Balzs, G.; Scheer, M.; Tuna, F.; McInnes, E. J. L.; McMaster, J.; Lewis, W.; Blake, A. J.; Liddle, S. T., Triamidoamine-uranium(IV)-stabilized terminal parent phosphide and phosphinidene complexes. *Angewandte Chemie - International Edition* **2014,** *53* (17), 4484--4488.

30. Dethlefsen, J. R.; Lupp, D.; Teshome, A.; Nielsen, L. B.; Fristrup, P., Molybdenum-catalyzed conversion of diols and biomass-derived polyols to alkenes using isopropyl alcohol as reductant and solvent. *ACS Catal.* **2015,** *5* (6), 3638-3647.

31. Becker, G.; Uhl, W.; Wessely, H.-J., Acyl- and Alkylidenephosphines. XVI. (Dimethylaminomethylidene)- and (Diphenylmethylidene) phosphines. *Z. Anorg. Allg. Chem.* **1981,** *479* (8), 41-56.

Appendix A: X-Ray Crystallographic Data

Table 5.1 Crystallographic Data and Refinement Details for $[^{Ph}(NO)^{tBu}]_2MoO_2$, **2.8.**

Formula	$C_{22}H_{28}MoN_2O_4$	V (Å^3)	2237.0(5)
M_r	480.4	Z, Z'	4, 0.5
Cell setting	monoclinic	D_x (Mg/m^{-3})	1.426
Space group	$C2/c$	m (mm^{-1})	0.615
a (Å)	17.243(3)	T_{min}, T_{max}	0.6948, 0.6341
b (Å)	8.2596(10)	$R1$[a]	0.0844
c (Å)	15.7476(19)	$wR2$[b]	0.2602
α (°)	90	Goodness-of-fit	1.081
β (°)	94.128(3)	Dr_{max}, Dr_{min} (e Å^{-3})	3.856, -4.245
γ (°)	90		

[a] $R1 = \Sigma \, ||F_o| - |F_c|| \, / \, \Sigma \, |F_o|$; [b] $wR2 = \{ \Sigma \, [w(F_o^2 - F_c^2)^2] \, / \, \Sigma \, [w(F_o^2)^2] \}^{1/2}$

Table 5.2 Crystallographic Data and Refinement Details for $[^{oDMP}(NO)^{tBu}]_2MoO_2$, **2.9**

Formula	$C_{26}H_{36}MoN_2O_4$	V (Å^3)	2561.5(3)
M_r	536.51	Z, Z'	4, 1
Cell setting	Monoclinic	D_x (Mg/m^{-3})	1.391
Space group	$P2_1/n$	m (mm^{-1})	0.545
a (Å)	16.2898(9)	T_{min}, T_{max}	0.780, 0.876
b (Å)	8.3409(5)	$R1$[a]	0.0229
c (Å)	18.9997(11)	$wR2$[b]	0.0648
α (°)	90	Goodness-of-fit	1.003
β (°)	97.132(2)	Dr_{max}, Dr_{min} (e Å^{-3})	0.702, -0.388
γ (°)	90		

[a] $R1 = \Sigma \, ||F_o| - |F_c|| \, / \, \Sigma \, |F_o|$; [b] $wR2 = \{ \Sigma \, [w(F_o^2 - F_c^2)^2] \, / \, \Sigma \, [w(F_o^2)^2] \}^{1/2}$

Table 5.3 Crystallographic Data and Refinement Details for $[^{oDMP}(NO)^{Ph}]_2MoO_2$, **2.10**

Formula	$C_{30}H_{28}MoN_2O_4$	V (Å^3)	1298.90(16)
M_r	576.48	Z, Z'	2, 1
Cell setting	triclinic	D_x (Mg/m^{-3})	1.474
Space group	$P\overline{1}$	m (mm^{-1})	0.544
a (Å)	10.7561(8)	T_{min}, T_{max}	0.7459, 0.7145
b (Å)	11.5102(8)	$R1$[a]	0.0223
c (Å)	12.7142(9)	$wR2$[b]	0.0591
α (°)	64.9205(9)	Goodness-of-fit	0.975
β (°)	77.1544(9)	Dr_{max}, Dr_{min} (e Å^{-3})	0.472, -0.424
γ (°)	65.8791(9)		

[a] $R1 = \Sigma \, ||F_o| - |F_c|| \, / \, \Sigma \, |F_o|$; [b] $wR2 = \{ \Sigma \, [w(F_o^2 - F_c^2)^2] \, / \, \Sigma \, [w(F_o^2)^2] \}^{1/2}$

Table 5.4 Crystallographic Data and Refinement Details for $[^{oDMP}(NO)^{PFP}]_2MoO_2$, **2.11**

Formula	$C_{30}H_{18}F_{10}MoN_2O_4$	V (Å^3)	2000.6(3)
M_r	848.54	Z, Z'	2, 1
Cell setting	triclinic	D_x (Mg/m^{-3})	1.409
Space group	$P\overline{1}$	m (mm^{-1})	0.71073
a (Å)	10.4274(8)	T_{min}, T_{max}	0.5830, 0.6467
b (Å)	13.6767(11)	$R1$[a]	0.0346
c (Å)	15.1801(11)	$wR2$[b]	0.0876
α (°)	103.990(3)	Goodness-of-fit	0.994
β (°)	95.055(3)	Dr_{max}, Dr_{min} (e Å^{-3})	0.504, -0.641
γ (°)	105.186(3)		

[a] $R1 = \Sigma \, ||F_o| - |F_c|| \, / \, \Sigma \, |F_o|$; [b] $wR2 = \{ \Sigma \, [w(F_o^2 - F_c^2)^2] \, / \, \Sigma \, [w(F_o^2)^2] \}^{1/2}$

Table 5.5 Crystallographic Data and Refinement Details for $[^{DIPP}(NO)^{tBu}]_2MoO_2$, **2.12**

Formula	$C_{34}H_{52}MoN_2O_4$	V (Å^3)	1.231
M_r	648.71	Z, Z'	8, 1
Cell setting	orthorhombic	D_x (Mg/m^{-3})	1.231
Space group	*Pbca*	m (mm^{-1})	0.411
a (Å)	16.698(2)	T_{min}, T_{max}	0.942, 0.923
b (Å)	17.760(2)	$R1$[a]	0.0685
c (Å)	23.602(3)	$wR2$[b]	0.1326
α (°)	90	Goodness-of-fit	0.934
β (°)	90	Dr_{max}, Dr_{min} (e Å^{-3})	2.207, -1.589
γ (°)	90		

[a] $R1 = \Sigma \, ||F_o| - |F_c|| \, / \, \Sigma \, |F_o|$; [b] $wR2 = \{ \Sigma \, [w(F_o^2 - F_c^2)^2] \, / \, \Sigma \, [w(F_o^2)^2] \}^{1/2}$

Table 5.6 Crystallographic Data and Refinement Details for $[^{DIPP}(NO)^{PFP}]_2MoO_2$, **2.14**

Formula	$C_{38}H_{34}F_{10}MoN_2O_4$	V (Å^3)	1818.7(12)
M_r	868.61	Z, Z'	2, 1
Cell setting	triclinic	D_x (Mg/m^{-3})	1.586
Space group	$P\overline{1}$	m (mm^{-1})	0.456
a (Å)	9.864(4)	T_{min}, T_{max}	0.7462, 0.6907
b (Å)	13.220(5)	$R1$[a]	0.0234
c (Å)	15.416(6)	$wR2$[b]	0.063
α (°)	84.220(6)	Goodness-of-fit	0.994
β (°)	75.291(6)	Dr_{max}, Dr_{min} (e Å^{-3})	0.484, -0.411
γ (°)	69.300(6)		

[a] $R1 = \Sigma \, ||F_o| - |F_c|| \, / \, \Sigma \, |F_o|$; [b] $wR2 = \{ \Sigma \, [w(F_o^2 - F_c^2)^2] \, / \, \Sigma \, [w(F_o^2)^2] \}^{1/2}$

Table 5.7 Crystallographic Data and Refinement Details for [^{oDMP}(NO)^{tBu}]$_2$MoONtBu, **3.3**

Formula	$C_{30}H_{45}MoN_3O_3$	V (Å^3)	9253.8(10)
M_r	591.63	Z, Z'	12, 3
Cell setting	Monoclinic	D_x (Mg/m^{-3})	1.274
Space group	$P2_1/n$	m (mm^{-1})	0.458
a (Å)	8.3513(5)	T_{min}, T_{max}	0.758, 0.853
b (Å)	35.845(2)	$R1$[a]	0.0468
c (Å)	31.159(2)	$wR2$[b]	0.1373
α (°)	90	Goodness-of-fit	1.066
β (°)	97.2000(9)	Dr_{max}, Dr_{min} (e Å^{-3})	0.637, -1.820
γ (°)	90		

[a] $R1 = \Sigma \, ||F_o| - |F_c|| \, / \, \Sigma \, |F_o|$; [b] $wR2 = \{ \Sigma \, [w(F_o^2 - F_c^2)^2] \, / \, \Sigma \, [w(F_o^2)^2] \}^{1/2}$

Table 5.8 Crystallographic Data and Refinement Details for [^{oDMP}(NO)^{PFP}]$_2$MoONtBu, **3.5**

Formula	$C_{34}H_{27}F_{10}MoN_3O_3$	V (Å^3)	1666.6(10)
M_r	811.52	Z, Z'	2, 1
Cell setting	triclinic	D_x (Mg/m^{-3})	1.617
Space group	$P\overline{1}$	m (mm^{-1})	0.49
a (Å)	8.832(3)	T_{min}, T_{max}	0.897, 0.800
b (Å)	13.540(5)	$R1$[a]	0.0471
c (Å)	14.860(5)	$wR2$[b]	0.116
α (°)	102.533(4)	Goodness-of-fit	1.031
β (°)	102.704(4)	Dr_{max}, Dr_{min} (e Å^{-3})	1.599, -0.682
γ (°)	96.744(4)		

[a] $R1 = \Sigma \, ||F_o| - |F_c|| \, / \, \Sigma \, |F_o|$; [b] $wR2 = \{ \Sigma \, [w(F_o^2 - F_c^2)^2] \, / \, \Sigma \, [w(F_o^2)^2] \}^{1/2}$

Table 5.9 Crystallographic Data and Refinement Details for $[^{DIPP}(NO)^{tBu}]_2MoONtBu$, **3.6**

Formula	$C_{38}H_{61}MoN_3O_3$	V (Å^3)	3859.2(13)
M_r	703.83	Z, Z'	4, 1
Cell setting	orthorhombic	D_x (Mg/m^{-3})	1.211
Space group	*Pnq*21	m (mm^{-1})	0.376
a (Å)	23.487(5)	T_{min}, T_{max}	0.950, 0.817
b (Å)	10.453(2)	$R1^a$	0.1084
c (Å)	15.719(3)	$wR2^b$	0.2583
α (°)	90	Goodness-of-fit	1.053
β (°)	90	Dr_{max}, Dr_{min} (e Å^{-3})	1.881, -1.051
γ (°)	90		

$^aR1 = \Sigma \, ||F_o| - |F_c|| \, / \, \Sigma \, |F_o|$; $^bwR2 = \{ \, \Sigma \, [w(F_o^2 - F_c^2)^2] \, / \, \Sigma \, [w(F_o^2)^2] \, \}^{1/2}$

Table 5.10 Crystallographic Data and Refinement Details for $[^{DIPP}(NO)^{Ph}]_2MoONtBu$, **3.7**

Formula	$C_{42}H_{53}MoN_3O_3$	V (Å^3)	7899.4(9)
M_r	743.81	Z, Z'	8, 1
Cell setting	orthorhombic	D_x (Mg/m^{-3})	1.251
Space group	*Pbca*	m (mm^{-1})	0.372
a (Å)	14.5358(10)	T_{min}, T_{max}	0.7459, 0.6640
b (Å)	18.2547(12)	$R1^a$	0.0607
c (Å)	29.770(2)	$wR2^b$	0.1451
α (°)	90	Goodness-of-fit	0.992
β (°)	90	Dr_{max}, Dr_{min} (e Å^{-3})	1.530, -1.046
γ (°)	90		

$^aR1 = \Sigma \, ||F_o| - |F_c|| \, / \, \Sigma \, |F_o|$; $^bwR2 = \{ \, \Sigma \, [w(F_o^2 - F_c^2)^2] \, / \, \Sigma \, [w(F_o^2)^2] \, \}^{1/2}$

Table 5.11 Crystallographic Data and Refinement Details for $[^{tBu}(NO)^{tBu}]_2MoONtBu\text{-}THF$, **3.9**

Formula	C26H53MoN3O4	V (Å^3)	6074.2(8)
M_r	567.65	Z, Z'	8, 2
Cell setting	monoclinic	D_x (Mg/m^{-3})	1.241
Space group	$P21/c$	m (mm^{-1})	0.464
a (Å)	20.40366(15)	T_{min}, T_{max}	0.921, 0.866
b (Å)	10.4939(8)	$R1$[a]	0.0599
c (Å)	29.720(2)	$wR2$[b]	0.1301
α (°)	90	Goodness-of-fit	1.093
β (°)	107.6348(11)	Dr_{max}, Dr_{min} (e Å^{-3})	1.087, -0.437
γ (°)	90		

[a] $R1 = \Sigma \, ||F_o| - |F_c|| \, / \, \Sigma \, |F_o|$; [b] $wR2 = \{ \Sigma \, [w(F_o^2 - F_c^2)^2] \, / \, \Sigma \, [w(F_o^2)^2] \}^{1/2}$

Table 5.12 Crystallographic Data and Refinement Details for $[^{Ph}(NO)^{tBu}]_2Mo(NtBu)_2$, **4.4**

Formula	$C_{30}H_{46}MoN_4O_2$	V (Å^3)	6475.5(8)
M_r	590.65	Z, Z'	8, 2
Cell setting	monoclinic	D_x (Mg/m^{-3})	1.212
Space group	$P21/c$	m (mm^{-1})	0.435
a (Å)	20.1648(15)	T_{min}, T_{max}	0.7460, 0.6960
b (Å)	19.3972(13)	$R1$[a]	0.0299
c (Å)	18.4062(13)	$wR2$[b]	0.0853
α (°)	90	Goodness-of-fit	0.997
β (°)	108.4975(12)	Dr_{max}, Dr_{min} (e Å^{-3})	0.737, -0585
γ (°)	90		

[a] $R1 = \Sigma \, ||F_o| - |F_c|| \, / \, \Sigma \, |F_o|$; [b] $wR2 = \{ \Sigma \, [w(F_o^2 - F_c^2)^2] \, / \, \Sigma \, [w(F_o^2)^2] \}^{1/2}$

Table 5.13 Crystallographic Data and Refinement Details for $[^{oDMP}(NO)^{tBu}]_2Mo(NtBu)_2$, **4.5**

Formula	$C_{34}H_{54}MoN_4O_2$	V (Å^3)	7027(3)
M_r	646.75	Z, Z'	8, 1
Cell setting	Orthorhombic	D_x (Mg/m^{-3})	1.223
Space group	*Pbca*	m (mm^{-1})	0.406
a (Å)	16.066(4)	T_{min}, T_{max}	0.916, 0.984
b (Å)	19.201(5)	$R1^a$	0.0556
c (Å)	22.779(5)	$wR2^b$	0.1585
α (°)	90	Goodness-of-fit	1.006
β (°)	90	Dr_{max}, Dr_{min} (e Å^{-3})	0.888, -1.295
γ (°)	90		

$^aR1 = \Sigma\ ||F_o| - |F_c|| / \Sigma\ |F_o|$; $^bwR2 = \{\ \Sigma\ [w(F_o^2 - F_c^2)^2] / \Sigma\ [w(F_o^2)^2]\ \}^{1/2}$

Table 5.14 Crystallographic Data and Refinement Details for $[^{oDMP}(NO)^{Ph}]_2Mo(NtBu)_2$, **4.6**

Formula	$C_{38}H_{46}MoN_4O_2$	V (Å^3)	3592.4(6)
M_r	686.73	Z, Z'	4, 1
Cell setting	monoclinic	D_x (Mg/m^{-3})	1.27
Space group	*Cc*	m (mm^{-1})	0.402
a (Å)	12.4260(10)	T_{min}, T_{max}	0.938, 0.924
b (Å)	28.161(3)	$R1^a$	0.0189
c (Å)	11.0315(9)	$wR2^b$	0.0469
α (°)	90	Goodness-of-fit	1.003
β (°)	111.4683(11)	Dr_{max}, Dr_{min} (e Å^{-3})	0.315, -0.279
γ (°)	90		

$^aR1 = \Sigma\ ||F_o| - |F_c|| / \Sigma\ |F_o|$; $^bwR2 = \{\ \Sigma\ [w(F_o^2 - F_c^2)^2] / \Sigma\ [w(F_o^2)^2]\ \}^{1/2}$

Table 5.15 Crystallographic Data and Refinement Details for $[^{oDMP}(NO)^{PFP}]_2Mo(NtBu)_2$, **4.7**

Formula	$C_{38}H_{36}F_{10}MoN_4O_2$	V (Å^3)	7547(6)
M_r	866.65	Z, Z'	8, 4
Cell setting	triclinic	D_x (Mg/m^{-3})	1.526
Space group	$P\overline{1}$	m (mm^{-1})	0.437
a (Å)	14.119(6)	T_{min}, T_{max}	0.970, 0.841
b (Å)	19.912(9)	$R1$[a]	0.0661
c (Å)	28.766(13)	$wR2$[b]	0.1341
α (°)	71.177(8)	Goodness-of-fit	0.997
β (°)	81.782(8)	Dr_{max}, Dr_{min} (e Å^{-3})	0.705, -1.170
γ (°)	79.927(7)		

[a] $R1 = \Sigma \, ||F_o| - |F_c|| \, / \, \Sigma \, |F_o|$; [b] $wR2 = \{ \Sigma \, [w(F_o^2 - F_c^2)^2] \, / \, \Sigma \, [w(F_o^2)^2] \}^{1/2}$

Table 5.16 Crystallographic Data and Refinement Details for $[^{DIPP}(NO)^{Ph}]_2Mo(NtBu)_2$, **4.9**

Formula	$C_{46}H_{62}MoN_4O_2$	V (Å^3)	8440(4)
M_r	798.83	Z, Z'	8, 2
Cell setting	Monoclinic	D_x (Mg/m^{-3})	1.258
Space group	$P2_1/n$	m (mm^{-1})	0.352
a (Å)	21.093(6)	T_{min}, T_{max}	0.920, 0.811
b (Å)	16.846(5)	$R1$[a]	0.06
c (Å)	25.994(8)	$wR2$[b]	0.1732
α (°)	90	Goodness-of-fit	1.035
β (°)	113.970(5)	Dr_{max}, Dr_{min} (e Å^{-3})	1.324, -1.733
γ (°)	90		

[a] $R1 = \Sigma \, ||F_o| - |F_c|| \, / \, \Sigma \, |F_o|$; [b] $wR2 = \{ \Sigma \, [w(F_o^2 - F_c^2)^2] \, / \, \Sigma \, [w(F_o^2)^2] \}^{1/2}$

Table 5.17 Crystallographic Data and Refinement Details for $[^{Bn}(NO)^{tBu}]_2Mo(NtBu)_2$, **4.11**

Formula	$C_{32}H_{50}MoN_4O_2$	V (Å^3)	3321.8(6)
M_r	618.7	Z, Z'	4, 0.5
Cell setting	monoclinic	D_x (Mg/m^{-3})	1.237
Space group	$C2/c$	m (mm^{-1})	0.427
a (Å)	18.097(2)	T_{min}, T_{max}	0.886, 0.802
b (Å)	10.2735(12)	$R1$[a]	0.0218
c (Å)	18.286(2)	$wR2$[b]	0.0597
α (°)	90	Goodness-of-fit	0.992
β (°)	102.2871(12)	Dr_{max}, Dr_{min} (e Å^{-3})	0.341, -0.306
γ (°)	90		

[a] $R1 = \Sigma \, ||F_o| - |F_c|| \, / \, \Sigma \, |F_o|$; [b] $wR2 = \{ \Sigma \, [w(F_o^2 - F_c^2)^2] \, / \, \Sigma \, [w(F_o^2)^2] \}^{1/2}$

Table 5.18 Crystallographic Data and Refinement Details for $[^{mDMP}(NO)^{tBu}]_2Mo(NtBu)_2$, **4.12**

Formula	$C_{34}H_{54}MoN_4O_2$	V (Å^3)	3585.8(5)
M_r	646.75	Z, Z'	4, 1
Cell setting	monoclinic	D_x (Mg/m^{-3})	1.198
Space group	$P2_1/c$	m (mm^{-1})	0.398
a (Å)	17.8282(14)	T_{min}, T_{max}	0.958, 0.907
b (Å)	9.9838(8)	$R1$[a]	0.0553
c (Å)	20.1792(15)	$wR2$[b]	0.1469
α (°)	90	Goodness-of-fit	0.998
β (°)	93.2922(12)	Dr_{max}, Dr_{min} (e Å^{-3})	2.501, -1.151
γ (°)	90		

[a] $R1 = \Sigma \, ||F_o| - |F_c|| \, / \, \Sigma \, |F_o|$; [b] $wR2 = \{ \Sigma \, [w(F_o^2 - F_c^2)^2] \, / \, \Sigma \, [w(F_o^2)^2] \}^{1/2}$

Table 5.19 Crystallographic Data and Refinement Details for $[^{PFP}(NO)^{tBu}]_2Mo(NtBu)_2$, **4.13**

Formula	$C_{30}H_{36}F_{10}MoN_4O_2$	V (Å^3)	3440.9(6)
M_r	770.57	Z, Z'	4, 1
Cell setting	monoclinic	D_x (Mg/m^{-3})	1.487
Space group	$P2_1/n$	m (mm^{-1})	0.468
a (Å)	17.7291(18)	T_{min}, T_{max}	0.4322, 0.3473
b (Å)	9.4862(10)	$R1$[a]	0.0499
c (Å)	21.775(2)	$wR2$[b]	0.11
α (°)	90	Goodness-of-fit	1.065
β (°)	110.0207(14)	Dr_{max}, Dr_{min} (e Å^{-3})	1.007, -0.973
γ (°)	90		

[a] $R1 = \Sigma \, ||F_o| - |F_c|| \, / \, \Sigma \, |F_o|$; [b] $wR2 = \{ \Sigma \, [w(F_o^2 - F_c^2)^2] \, / \, \Sigma \, [w(F_o^2)^2] \}^{1/2}$

Table 5.20 Crystallographic Data and Refinement Details for $[[^{oDMP}(NO)^{tBu}]_2Mo(O)]_2(\mu\text{-}O)$, **2.15**

Formula	$C_{52}H_{72}Mo_2N_4O_7$	V (Å^3)	5583(4)
M_r	1057.01	Z, Z'	4, 1
Cell setting	Monoclinic	D_x (Mg/m^{-3})	1.258
Space group	$P2_1/c$	m (mm^{-1})	0.498
a (Å)	12.025(5)	T_{min}, T_{max}	0.907, 0.811
b (Å)	14.880(5)	$R1$[a]	0.0353
c (Å)	31.317(11)	$wR2$[b]	0.0871
α (°)	90	Goodness-of-fit	1
β (°)	94.951(4)	Dr_{max}, Dr_{min} (e Å^{-3})	1.040, -0.470
γ (°)	90		

[a] $R1 = \Sigma \, ||F_o| - |F_c|| \, / \, \Sigma \, |F_o|$; [b] $wR2 = \{ \Sigma \, [w(F_o^2 - F_c^2)^2] \, / \, \Sigma \, [w(F_o^2)^2] \}^{1/2}$